University of Alberta

Probabilistic Analyses of Landslide Hazards and Risks: Bridging Theory and Practice

By

Hassan El-Ramly ©

A thesis submitted to the Faculty of Graduate Studies and
Research in partial fulfillment of the requirements for the
degree of Doctor of Philosophy

in

Geotechnical Engineering

Department of Civil and Environmental Engineering

Edmonton, Alberta

Spring 2001

National Library
of Canada

Acquisitions and
Bibliographic Services

395 Wellington Street
Ottawa ON K1A 0N4
Canada

Bibliothèque nationale
du Canada

Acquisitions et
services bibliographiques

395, rue Wellington
Ottawa ON K1A 0N4
Canada

Your file Votre référence

Our file Notre référence

The author has granted a non-exclusive licence allowing the National Library of Canada to reproduce, loan, distribute or sell copies of this thesis in microform, paper or electronic formats.

L'auteur a accordé une licence non exclusive permettant à la Bibliothèque nationale du Canada de reproduire, prêter, distribuer ou vendre des copies de cette thèse sous la forme de microfiche/film, de reproduction sur papier ou sur format électronique.

The author retains ownership of the copyright in this thesis. Neither the thesis nor substantial extracts from it may be printed or otherwise reproduced without the author's permission.

L'auteur conserve la propriété du droit d'auteur qui protège cette thèse. Ni la thèse ni des extraits substantiels de celle-ci ne doivent être imprimés ou autrement reproduits sans son autorisation.

0-612-60290-7

Canadä

University of Alberta

Library Release Form

Name of Author: Hassan El-Ramly

Title of Thesis: Probabilistic Analyses of Landslide Hazards and Risks: Bridging Theory and Practice

Degree: Doctor of Philosophy

Year This Degree Granted: 2001

Permission is hereby granted to the University of Alberta Library to reproduce single copies of this thesis and to lend or sell such copies for private, scholarly or scientific research purposes only.

The author reserves all other publication and other rights in association with the copyright in the thesis, and except as herein before provided, neither the thesis nor any substantial portion thereof may be printed or otherwise reproduced in any material form whatever without the author's prior written permission.

H. El-Ramly

8515 112 Street
Edmonton, Alberta
Canada, T6G 1K7

Date: January 4, 2001

University of Alberta

Faculty of Graduate Studies and Research

The undersigned certify that they have read, and recommended to the Faculty of Graduate Studies and Research for acceptance, a thesis entitled ***Probabilistic Analyses of Landslide Hazards and Risks: Bridging Theory and Practice*** submitted by **Hassan El-Ramly** in partial fulfillment of the requirements for the degree of Doctor of Philosophy in Geotechnical Engineering.

N.R. Morgenstern, Professor Emeritus
(Supervisor)

D. Cruden, Professor (Co-supervisor)

D. Chan, Professor

C. Deutsch, Associate Professor

Carl Mendoza
C. Mendoza, Associate Professor

for R. Fell, Professor (External
Examiner)

Date: December 11, 2000

ABSTRACT

Slope Engineering is perhaps the geotechnical subject most dominated by uncertainty. The impact of uncertainty on the quality of slope performance predictions is often substantial. Current slope design practice based on the factor of safety cannot directly address uncertainty. Probabilistic slope stability analysis is a rational means to incorporate uncertainty in the design process. It is also the most suitable approach for estimating hazard frequency for site-specific quantitative risk analyses. Unfortunately, the geotechnical profession has been slow in adopting such techniques.

The objective of this work is to integrate probabilistic slope stability analysis into geotechnical practice as a practical design and decision-making tool. A spreadsheet approach for probabilistic slope analysis is developed. The methodology is based on Monte Carlo simulation using the commercial software @Risk and Excel. The analysis accounts for the spatial variability of the input variables as well as the various sources of systematic uncertainty. The output of the analysis is presented as the probability of unsatisfactory performance. It is a measure of the likelihood of the slope failing.

The methodology is tested through the analysis of 10 case studies. It proved practical and flexible in handling a wide variety of real slope problems including effective and total stress analyses, complex stratigraphy, circular and non-circular slip surfaces and different slope analysis methods.

The study indicates that the factor of safety alone can give a misleading sense of safety and is not a sufficient safety indicator. The probability of unsatisfactory performance is a more consistent safety measure. Current slope design practice is calibrated probabilistically through the analysis of case studies of failed and safe slopes. A comparison of the computed probabilities indicates that acceptable slope design practice is equivalent to a probability of unsatisfactory performance not exceeding 2×10^{-2}, which could be regarded as an upper design threshold. Stability assessments based on the results of both deterministic and probabilistic analyses provide greater insight into design reliability and enhance the decision-making process. The study also shows that probabilistic slope analyses ignoring spatial variability of input parameters significantly overestimate the probability of unsatisfactory performance. Other conclusions regarding the implementation and practical value of probabilistic slope analyses are also reached.

ACKNOWLEDGMENT

Thanks are due to many people who, over the course of this study, provided me with enormous help and encouragement. This acknowledgment is but a small appreciation for their priceless support.

The guidance and vision of Professor Norbert Morgenstern, my main supervisor, were instrumental in achieving the goals of this work. I thank him for his enthusiastic support, the unique mentoring environment he provided and the invaluable discussions we had. I also thank Professor David Cruden, my co-supervisor, for his help and advice. His ideas, comments and thorough review of the thesis are greatly appreciated.

The Geotechnical Engineering Group at the University of Alberta, both staff and colleagues, provided an exceptionally cooperative and friendly environment. In particular, thanks are due to Professor David Chan and Sally Petaske. I also thank Tamer El-Kateb, my officemate, for the helpful discussions we had. Appreciation is extended to Dr. Clayton Deutsch, mining group, for his help in geostatistics aspects. Thanks are also due to Syncrude Canada and Geotechnical Engineering Office of Hong Kong for providing the data and technical reports of many of the case studies analyzed in this work.

My brother Mohammad, his wife Aisha and their little boy Mahmoud, have been a very supportive and caring family. I thank them for the wonderful times I had with them. Finally, I am greatly indebted to my parents, Fawzy and Amal, for their continuous support, love and encouragement and to them I dedicate this work.

TABLE OF CONTENTS

CHAPTER 1 1

INTRODUCTION 1

1. RESEARCH PREMISES 1
2. RESEARCH OBJECTIVES 3

CHAPTER 2 6

RISK MANAGEMENT IN SLOPE ENGINEERING: AN OVERVIEW 6

1. INTRODUCTION 6
2. DEFINITIONS 7
3. RISK MANAGEMENT FRAMEWORK 9
   - 3.1 Hazard Identification 10
   - 3.2 Hazard Analysis 10
   - 3.3 Consequence Analysis 11
4. TYPES OF RISK ANALYSIS 12
5. EXAMPLES OF QRA 15
6. CONCLUSIONS 21

CHAPTER 3 23

UNCERTAINTY AND STATISTICAL CHARACTERIZATION OF SOIL PROPERTIES 23

1. SOURCES OF UNCERTAINTY 23
   - 1.1 Parameter Uncertainty 24
     - 1.1.1 Data Scatter 25
     - 1.1.2 Systematic Error 26
   - 1.2 Model Uncertainty 27
   - 1.3 Human Uncertainty 29
2. STATISTICAL ANALYSIS OF SOIL DATA 30
   - 2.1 Data Review 31

2.2 Sample Representativity 32
2.2.1 Sample Size 32
2.2.2 Data Clustering 33
2.3 Statistical Inference 34
2.3.1 Elementary Statistical Analysis 34
2.3.2 Statistical Analysis of Spatial Variability 35
2.3.2.1 Trend Estimation 37
2.3.2.2 Statistical Measures of Spatial Variability 40
2.3.2.3 Methods of Analyzing Spatial Variability 44
2.3.2.4 Size Effect 49
2.3.3 Limitations of Existing Spatial Variability Analyses 51
2.3.3.1 Anisotropy 52
2.3.3.2 Scale of Observations 54
2.3.3.3 Sampling Scheme 55
2.3.3.4 Trend Selection 56
2.3.3.5 Discussion 58
2.3.4 Evaluation of Systematic Error 59
2.3.4.1 Measurement Bias 62
2.3.4.2 Statistical Error in the Mean/Trend 63
2.3.5 Correlation Between Soil Parameters 64
3. SUMMARY 67
CHAPTER 4 69
PROBABILISTIC SLOPE ANALYSIS, MERITS,
CONCEPTS AND METHODS 69
1. DETERMINISTIC VERSUS PROBABILISTIC MODELS 69
2. CONVENTIONAL SLOPE STABILITY ANALYSIS 70
3. PROBABILISTIC SLOPE STABILITY ANALYSIS 73
3.1 Basic Concepts 73
3.2 Methods of Probabilistic Analysis 76
3.2.1 Analytical Methods 76

3.2.2 Approximate Methods 76
3.2.2.1 First Order Second Moment 77
3.2.2.2 Point Estimate Method 77
3.2.3 Monte Carlo Simulation 78
3.3 Limitations of Existing Probabilistic Methods 80
4. SUMMARY 81

CHAPTER 5 83
PROBABILISTIC ANALYSIS METHODOLOGY FOR EARTH SLOPES 83
1. A PRACTICAL PROBABILISTIC SLOPE ANALYSIS 83
1.1 Deterministic Analysis 84
1.2 Outline of the Proposed Methodology 84
1.3 Statistical Characterization of Input Variables 86
1.3.1 Input Random Variables 86
1.3.2 Probability Distributions 87
1.4 Accounting for Random Errors and Spatial Variability 88
1.4.1 Random Measurement Errors 88
1.4.2 Spatial Variability 90
1.4.2.1 Theoretical Background 90
1.4.2.2 Autocorrelation Distance 96
1.4.3 Modeling Uncertainty of Input Variables 101
1.5 Critical Slip Surface 103
1.6 Spreadsheet Modeling 106
1.6.1 Geometry, Stratigraphy and Input Parameters 106
1.6.2 Modeling Spatial Variability 107
1.6.3 Slope Analysis Methods 109
1.6.3.1 Bishop's Simplified Method of Slices 110
1.6.3.2 Spencer's Method of Slices 111
1.7 Issues in Simulation 112
1.7.1 Random Sampling 112
1.7.2 Number of Iterations 115

1.8 Interpretation of the Output 116
1.8.1 Probability of Unsatisfactory Performance 116
1.8.2 Sensitivity Analysis 118
2. ADVANTAGES OF THE PROPOSED METHODOLOGY 118
3. LIMITATIONS OF THE PROPOSED METHODOLOGY 119
4. ESTABLISHING PROBABILISTIC SLOPE DESIGN CRITERIA 121

CHAPTER 6 123
APPLICATION OF THE PROPOSED PROBABILISTIC SLOPE ANALYSIS METHODOLOGY - JAMES BAY CASE STUDY 123
1. JAMES BAY PROJECT 123
2. MONTE CARLO SIMULATION VERSUS FOSM 125
3. IMPLEMENTATION OF THE PROPOSED METHODOLOGY 133
3.1 James Bay Design 1 (H=12m) 133
3.2 James Bay Design 2 (H=6m) 140
4. NAÏVE PROBABILISTIC ANALYSIS 144
5. SUMMARY AND DISCUSSION 147

CHAPTER 7 151
SYNCRUDE TAILINGS DYKE - CELL 23 151
1. INTRODUCTION 151
2. SITE GEOLOGY 151
3. CELL 23 153
3.1 Background 153
3.2 Subsurface Conditions 154
3.2.1 Stratigraphy 154
3.2.2 Shear Strength 154
3.2.3 Pore Water Pressure 162
3.3 Deterministic Slope Stability Analyses 169
3.4 Probabilistic Slope Stability Analysis – Proposed Methodology 170
3.4.1 Input Variables 170
3.4.2 Spatial Variability 171

3.4.3 Probabilistic Analysis 173

3.4.4 Sensitivity of the Analysis to the Autocorrelation Distance 179

3.5 Naïve Analysis 179

4. SUMMARY 183

CHAPTER 8 184

LODALEN SLIDE NORWAY, 1954 184

1. INTRODUCTION 184

2. SUBSURFACE CONDITIONS 185

2.1 Stratigraphy and Soil Properties 185

2.2 Pore Water Pressure 187

3. SLOPE STABILITY ANALYSES 190

3.1 Deterministic Analysis 190

3.2 Probabilistic Analysis – Proposed Methodology 190

3.2.1 Input Variables 190

3.2.2 Critical Slip Surface 191

3.2.3 Spatial Variability 192

3.2.4 Stability Analysis – Geometry Before Failure (2h:1v) 193

3.2.5 Stability Analyses – Slope Geometry Modified 197

3.2.6 Stability Analysis – Acceptable Slope Design (4h:1v) 198

3.3 Naïve Analysis 199

4. SUMMARY 202

CHAPTER 9 203

MUAR TRIAL EMBANKMENT 203

1. INTRODUCTION 203

2. SOIL CONDITIONS 204

2.1 Stratigraphy 205

2.2 Soil Properties 205

2.3 Embankment Material 208

3. SLOPE STABILITY ANALYSES 209

3.1 Deterministic Analysis 209

3.2 Probabilistic Analysis – Proposed Methodology 210
3.2.1 Input Variables 210
3.2.1.1 Soil Parameters 210
3.2.1.2 Bjerrum's Vane Correction Factor 211
3.2.2 Critical Slip Surface 212
3.2.3 Spatial Variability 213
3.2.4 Stability Analysis – Geometry Before Failure (H=4.7m) 214
3.2.5 Stability Analyses – Embankment Geometry Modified 216
3.2.6 Stability Analysis – Acceptable Embankment Design (H=3.3m) 216
3.2.7 Sensitivity of the Analysis to the Autocorrelation Distance 220
3.3 Naïve Analysis 221
4. SUMMARY 224

CHAPTER 10 226
CONGRESS STREET OPEN CUT 226
1. INTRODUCTION 226
2. GEOLOGY OF THE CHICAGO AREA 226
3. SOIL CONDITIONS 228
3.1 Stratigraphy 228
3.2 Soil Properties 229
4. SLOPE STABILITY ANALYSES 230
4.1 Deterministic Analysis 230
4.2 Probabilistic Analysis – Proposed Methodology 231
4.2.1 Input Variables 231
4.2.2 Critical Slip Surface 232
4.2.3 Spatial Variability 233
4.2.4 Stability Analysis – Geometry Before Failure (1.35h:1v) 234
4.2.5 Stability Analyses – Slope Geometry Modified 236
4.2.6 Stability Analysis – Acceptable Cut Design (2.5h:1v) 236
4.3 Naïve Analysis 241
5. SUMMARY 243

CHAPTER 11 244

STABILITY OF GRANITIC SOIL SLOPES IN HONG KONG 244

1. INTRODUCTION 244

2. GRANITIC SOILS OF HONG KONG 245

  2.1 Origin and Formation 245

  2.2 Engineering Properties 246

    2.2.1 Physical Properties 247

    2.2.2 Shear Strength 248

3. SLOPE STABILITY ANALYSES 253

  3.1 Cho Yiu Estate Landslide 255

    3.1.1 Background 255

    3.1.2 Local Geology 256

    3.1.3 Rainfall and Groundwater 257

    3.1.4 Rupture Surface 257

    3.1.5 Shear Strength 258

    3.1.6 Deterministic Stability Analyses 259

    3.1.7 Quantifying Pore Pressure Uncertainty 260

    3.1.8 Spatial Variability of Residual Soil Properties 262

    3.1.9 Probabilistic Stability Analyses 263

  3.2 Tsing Yi (1) Landslide 267

    3.2.1 Background 267

    3.2.2 Local Geology 268

    3.2.3 Rainfall and Groundwater 269

    3.2.4 Rupture Surface 269

    3.2.5 Shear Strength 270

    3.2.6 Deterministic Stability Analyses 270

    3.2.7 Quantifying Pore Pressure Uncertainty 271

    3.2.8 Probabilistic Stability Analyses 273

  3.3 Ching Cheung Road Landslide 277

    3.3.1 Background 277

3.3.2 Local Geology 278

3.3.3 Rainfall and Groundwater 278

3.3.4 Shear Strength 279

3.3.5 Failure Mechanism 280

3.3.6 Deterministic Stability Analyses 280

3.3.7 Quantifying Pore Pressure Uncertainty 281

3.3.8 Probabilistic Stability Analyses 283

3.4 Shek Kip Mei Landslide 287

3.4.1 Background 287

3.4.2 Local Geology 289

3.4.3 Rainfall and Groundwater 290

3.4.4 Rupture Surface 290

3.4.5 Shear Strength 290

3.4.6 Deterministic Stability Analyses 291

3.4.7 Quantifying Pore Pressure Uncertainty 292

3.4.8 Probabilistic Stability Analyses 293

4. SCALE OF FAILURE 297

5. SUMMARY AND DISCUSSION 302

CHAPTER 12 305

PROBABILISTIC SLOPE STABILITY ANALYSIS

SUMMARY AND DISCUSSION 305

1. PROBABILISTIC SLOPE ANALYSIS – WHY? 305

2. PROBABILISTIC SLOPE ANALYSIS METHODOLOGY 306

3. SPATIAL VARIABILITY AND NAÏVE ANALYSIS 307

4. CALIBRATION OF PROBABILISTIC SLOPE ANALYSIS 311

5. PROBABILISTIC SLOPE DESIGN CRITERIA 313

5.1 Probability of Unsatisfactory Performance 313

5.2 Reliability Index 315

6. INSIGHTS OF PRACTICAL VALUE 319

6.1 Probabilistic Versus Deterministic Slope Analyses 319

6.2 Sensitivity Analysis 320
7. PROBABILISTIC SLOPE DESIGN GUIDELINES 321

CHAPTER 13 329

TOWARDS A QUANTITATIVE RISK ANALYSIS
FOR SHEK KIP MEI SLOPE 329
1. OBSERVATIONS RELEVANT TO THE ANALYSIS 329
2. RISK ANALYSIS 330
2.1 Hazard Assessment 332
2.2 Event Tree Development 333
2.2.1 Time Of The Day 333
2.2.2 Signs of Slope Distress/Warning and Response Measures 333
2.2.3 Travel of Displaced Material 333
2.2.4 Effect of Failure on Block 36 336
2.3 Consequence Assessment 336
2.3.1 Number of People at Risk 336
2.3.2 Probability of Death 337
2.4 Risk Estimation 338
3. SUMMARY AND DISCUSSION 340

CHAPTER 14 350

CONCLUSIONS 350

REFERENCES 356

APPENDIX I 382

LIST OF TABLES

Table 3-1 Relationship between range and autocorrelation distance 44

Table 3-2 Assumptions and results of spatial variability analyses for various soil properties 60

Table 5-1 Relationship between scale of fluctuation and autocorrelation distance for exponential models 94

Table 5-2 Autocorrelation distance, r_o, for various soil properties 98

Table 5-3 Scale of Fluctuation, δ, for various soil properties ($\delta \approx 2r_o$) 99

Table 6-1 Input variables and statistical parameters for James Bay dykes (based on Tables 6 and 7; Christian et. al., 1994) 126

Table 6-2 Summary of the results of Monte Carlo simulation and FOSM 130

Table 6-3 Input variables and statistical parameters for James Bay dykes (based on Christian et. al., 1994) 134

Table 6-4 Input variables and statistical parameters for the Naive analysis 145

Table 6-5 Summary of the results of all analyses (based on the results of 25 simulations for each case) 148

Table 7-1 Summary of the physical and mechanical properties of the Kca material 156

Table 7-2 Summary of the of the physical and mechanical properties of the sandy till (Pgs) 159

Table 7-3 Summary of the results of direct shear tests on the tailings sand (TS)..... 161

Table 7-4 Summary of the physical and mechanical properties of the clayey till unit (Pgc) 161

Table 7-5 Summary of the physical and mechanical properties of the clay-shale unit (Kcw) 162

Table 7-6 Statistical parameters of input variables – Proposed Methodology 171

Table 7-7 Comparison of the results of the analysis modeling the spatial variability along slip surface and that based on spatially averaged parameters – Cell 23. 178
Table 7-8 Statistical parameters of the input variables – Naïve Analysis 180
Table 8-1 Summary of results of unconsolidated undrained triaxial tests on the marine clay (Sevaldson, 1956) 186
Table 8-2 Statistical parameters and CDFs of the input variables – Lodalen slide 191
Table 8-3 Comparison of the results of the analysis modeling variability along slip surface and that based on the spatially averaged parameters – Lodalen slide 196
Table 8-4 Sensitivity of the output of probabilistic stability analysis to the presumed value of the autocorrelation distance 199
Table 9-1 Summary of the physical and mechanical properties of the clay layers 205
Table 9-2 Statistical parameters and CDFs of the input variables – Muar Trial Embankment 211
Table 9-3 Statistical parameters of the input variables – Naïve Analysis 222
Table 10-1 Statistical parameters of the unconfined compressive strength of the clay layers 230
Table 10-2 Statistical parameters and CDFs of the input variables – Congress Street Open Cut 232
Table 10-3 Statistical parameters and CDFs of the input variables – Naïve Analysis 241
Table 11-1 Observed and theoretical ratios of the frequencies of occurrence of the different scales of failure 301
Table 12-1 Summary of the results of probabilistic slope stability analyses; Safe Slopes – Proposed Methodology 324
Table 12-2 Summary of the results of probabilistic slope stability analyses; Failed Slopes – Proposed Methodology 326

Table 12-3 Summary of the results of probabilistic slope stability analyses; Safe Slopes – Naïve Analysis 327
Table 13-1 Hazards addressed in risk analysis - Shek Kip Mei slope 332
Table 13-2 Probability of death of occupants of Block 36 – Shek Kip Mei slope 338
Table 13-3 Annual potential loss of life (PLL) as a result of a sliding failure of the Shek Kip Mei Slope 339

LIST OF FIGURES

Figure 2–1 Risk management framework (CSA, 1991) 9

Figure 3–1 Sources of parameter uncertainty (modified from Baecher, 1987) 24

Figure 3–2 Histogram of iron grades; global ore (modified from Journel & Huijbregts, 1978) 35

Figure 3–3 A highly erratic spatial structure (upper right) and a highly continuous structure (lower right), both with similar histograms 36

Figure 3–4 Model of spatial variability; Dilatometer lift-off pressure at the University of Massachusetts Amherst National Geotechnical Experimental Test Site (modified from DeGroot, 1996) 37

Figure 3–5 Model of soil variability (modified from Neter et. al., 1990) 39

Figure 3–6 Components of autocovariance function 41

Figure 3–7 Autocovariance functions: a) Exponential; b) Gaussian (modified from DeGroot and Baecher, 1993) 42

Figure 3–8 Influence of autocorrelation distance on soil variability 42

Figure 3–9 Elements of semivariogram function for a stationary condition 43

Figure 3–10 Method of Moments: estimating random error variance, $C_e(0)$, and autocorrelation distance, r_o 46

Figure 3–11 Variance reduction due to spatial averaging over blocks of sizes 1x1, 5x5 and 10x10 50

Figure 3–12 Spatial structures in different directions for anisotropic data 52

Figure 3–13 Effect of scale of observations on observed variability 54

Figure 3–14 Scatter plot for detecting correlation between soil properties (data from Holtz and Krizek, 1972); a) Negative strong correlation, b) Positive weak correlation 66

Figure 4–1 Muar Embankment : histograms of embankment height predictions. a) all 30 participants; b) four experts (modified from Kay, 1993) 72

Figure 4–2 Concept of probabilistic analysis 74

Figure 4–3 Probabilistic analysis of a pile foundation (modified from Lacasse & Nadim, 1996) 75
Figure 5–1 Monte Carlo simulation procedure using "Excel" and "@Risk" software 86
Figure 5–2 A representation of a random field A with its random variables and deterministic values 91
Figure 5–3 A realization of a one-dimensional random field *X*(t) showing local averages over intervals T and T' 93
Figure 5–4 Variance function versus the averaging interval T normalized with respect to the scale of fluctuation δ for various autocorrelation models 94
Figure 5–5 Estimation of an approximate isotropic autocorrelation distance for an anisotropic random field 96
Figure 5–6 Modeling variability of an input parameter along the failure surface 103
Figure 5–7 Modeling geometry, stratigraphy and slip surface 107
Figure 5–8 Modeling input variables in the spreadsheet 108
Figure 5–9 Accounting for spatial variability in the spreadsheet model 109
Figure 5–10 Notations and symbols used in stability analysis 110
Figure 5–11 Spreadsheet calculations for Bishop's Method of slices (example in Figure 5–7) 111
Figure 5–12 Spreadsheet model for Spencer's method of slices (example in Figure 5–7) 113
Figure 5–13 Latin Hypercube sampling with 10 iterations 114
Figure 5–14 Optimum number of iterations for estimating probability of unsatisfactory performance 116
Figure 6–1 Geometry and stratigraphy of James Bay dykes; Design 1 (H = 12m) 124
Figure 6–2 Geometry and stratigraphy of James Bay dykes; Design 2 (H = 6m) 124
Figure 6–3 Estimating optimum number of iterations for James Bay Design 1 128
Figure 6–4 Estimating optimum number of iterations for James Bay Design 2 128
Figure 6–5 Histogram and CDF of the factor of safety, Design 1 129
Figure 6–6 Histogram and CDF of the factor of safety, Design 2 129

Figure 6–7 Histogram of the probability of unsatisfactory performance: a) Design 1; b) Design 2 130
Figure 6–8 Sensitivity analysis results, Design 1 132
Figure 6–9 Sensitivity analysis results, Design 2 132
Figure 6–10 Proposed approach to account for spatial averaging, Design 1 136
Figure 6–11 Optimum number of iterations - Proposed Methodology; Design 1 137
Figure 6–12 Histogram and CDF of the factor of safety –Proposed Methodology; Design 1 137
Figure 6–13 Histogram of the probability of unsatisfactory performance; Proposed Methodology; Design 1 138
Figure 6–14 Histograms of the average soil parameters – Proposed Methodology; Design 1 139
Figure 6–15 Sensitivity analysis results – Proposed Methodology; Design 1 140
Figure 6–16 Critical slip circles and spatial averaging – Design 2 141
Figure 6–17 Histograms of the factor of safety, Design 2 – Proposed Methodology: a) Deep failure; b) Shallow failure 142
Figure 6–18 Histograms of the probability of unsatisfactory performance, Design 2 – Proposed Methodology; a) Deep failure; b) Shallow failure 143
Figure 6–19 Sensitivity analysis results, Design 2 (deep failure) – Proposed Methodology 143
Figure 6–20 Sensitivity analysis results, Design 2 (shallow failure) – Proposed Methodology 144
Figure 6–21 Histograms of the factor of safety – Naïve analysis : a) Design 1; b) Design 2 146
Figure 6–22 Histograms of the probability of unsatisfactory performance – Naïve analysis : a) Design 1; b) Design 2 146
Figure 6–23 Reliability index versus probability of unsatisfactory performance – James Bay dykes 149
Figure 7–1 Plan of the tailings pond dyke (modified from Nicol, 1994) 152
Figure 7–2 Geometry and soil stratigraphy at Section 53+000E - Cell 23 155

Figure 7–3 Shear box results for the residual strength of the Kca material 157

Figure 7–4 Probability histogram and cumulative distribution function of the residual friction angle of the Kca unit 158

Figure 7–5 Q-Q plot of the experimental residual friction angle of the Kca unit and a parametric LogNormal distribution 158

Figure 7–6 Histogram and CDF of the peak friction angle of the sandy till (Pgs) layer 160

Figure 7–7 Locations of piezometer tips, Section 53+000E – Cell23 163

Figure 7–8 Profile of pore pressure ratio in the Kca layer along dyke cross-section, March 1994..164

Figure 7–9 Histogram and CDF of the residual pore pressure ratio of the Kca unit ...165

Figure 7–10 Histogram of pore pressure ratio in the sandy till, Pgs, in March 1994.....166

Figure 7–11 Profile of pore pressure ratio in the Pgs layer along dyke cross-section, March 1994..166

Figure 7–12 CDF of the pore pressure ratio in the Pgs layer, March 1994 167

Figure 7–13 Phreatic surfaces in the tailing sand and the glacio-fluvial sand, March 1994..168

Figure 7–14 Accounting for spatial variability along the slip surface by the variability of local averages over segments of the surface 172

Figure 7–15 Histogram and CDF of the factor of safety, Cell 23 – Proposed methodology 174

Figure 7–16 Sensitivity analysis results, Cell 23 – Proposed Methodology..................175

Figure 7–17 Histogram of the probability of unsatisfactory performance – Cell 23 176

Figure 7–18 Estimating the spatial average of ϕ'_{Kca} along the slip surface....................176

Figure 7–19 Comparing the estimates of the variances of the average friction angle and the average residual pore pressure ratio using Monte Carlo simulation and the variance reduction factor...177

Figure 7–20 Comparison of the CDFs of the factor of safety from the analysis modeling spatial variability along slip surface and that based on the spatially averaged parameters – Cell 23; a) Probability distribution functions, b) Q-Q plot 178

Figure 7–21 Probability of unsatisfactory performance versus autocorrelation distance 180

Figure 7–22 Histogram and CDF of the factor of safety, Cell 23 – Naïve analysis 181

Figure 7–23 Histogram of the probability of unsatisfactory performance, Cell 23 – Naïve analysis 182

Figure 7–24 Sensitivity analysis results, Cell 23 – Naïve analysis 182

Figure 8–1 Cross-section and stratigraphy of Lodalen slide 185

Figure 8–2 Histogram and CDF of the effective cohesion of the marine clay 187

Figure 8–3 Histogram and CDF of the friction angle of the marine clay 187

Figure 8–4 Scatter plot of C' and tan ϕ' 188

Figure 8–5 Piezometers and pore pressure measurements – Lodalen slide 189

Figure 8–6 Pore pressure versus depth below phreatic surface 189

Figure 8–7 Histogram and CDF of the residual pore pressure – Lodalen slide 190

Figure 8–8 Histogram and CDF of the factor of safety, Lodalen slide (2h:1v) – Proposed Methodology 194

Figure 8–9 Histogram of the probability of unsatisfactory performance; Lodalen slide (2h:1v) – Proposed methodology 194

Figure 8–10 Sensitivity analysis results, Lodalen slide (2h:1v) – Proposed Methodology 195

Figure 8–11 Comparison of the factor of safety from the analysis modeling variability along the slip surface that based on the spatially averaged parameters, Lodalen slide; a) Probability distribution functions, b) Q-Q plot 196

Figure 8–12 Variation of the probability of unsatisfactory performance and the factor of safety with the slope angle, Lodalen slope – Proposed Methodology 197

Figure 8–13 Histogram and CDF of the factor of safety, Lodalen slope (4h:1v) – Proposed Methodology 198
Figure 8–14 Histogram and CDF of the factor of safety; Lodalen slope (4h:1v) – Naïve analysis 200
Figure 8–15 Histogram of the probability of unsatisfactory performance, Lodalen slope (4h:1v) – Naïve analysis 201
Figure 8–16 Sensitivity analysis results, Lodalen slope (4h:1v) – Naïve analysis 201
Figure 9–1 Geometry before failure and soil stratigraphy of Muar trial embankment 204
Figure 9–2 Profile of field vane shear strength 206
Figure 9–3 Histogram and CDF of the residuals of the undrained shear strength of the weathered clay crust 207
Figure 9–4 Histogram and CDF of the residuals of the undrained shear strength of the silty clay layers 208
Figure 9–5 Bjerrum's vane correction factor 212
Figure 9–6 Histogram and CDF of the factor of safety, Muar Embankment (H=4.7m) – Proposed Methodology 215
Figure 9–7 Histogram of the probability of unsatisfactory performance, Muar Embankment (H=4.7m) – Proposed Methodology 215
Figure 9–8 Variation of the probability of unsatisfactory performance and the factor of safety with embankment height, Muar Embankment – Proposed Methodology 217
Figure 9–9 Histogram and CDF of the factor of safety, Muar Embankment (H=3.3m) – Proposed Methodology 217
Figure 9–10 Histogram of the probability of unsatisfactory performance, Muar Embankment (H=3.3m) – Proposed Methodology 218
Figure 9–11 Sensitivity analysis results, Muar Embankment (H=3.3m) – Proposed Methodology 219

Figure 9–12 Comparison of the factor of safety from the analysis modeling soil variability along slip surface and that based on the spatially averaged parameters, Muar Embankment; a) Probability distribution functions, b) Q-Q plot 220
Figure 9–13 Variation of the probability of unsatisfactory performance with the autocorrelation distance, Muar Embankment (H=3.3m) 221
Figure 9–14 Histogram of the probability of unsatisfactory performance, Muar Embankment (H=3.3m) – Naïve Analysis 223
Figure 9–15 Sensitivity analysis results, Muar Embankment (H=3.3m) – Naïve Analysis 224
Figure 10–1 Geometry and soil stratigraphy of the Congress Street open cut 227
Figure 10–2 Histogram and CDF of the factor of safety, Congress Street Cut (1.35:1) – Proposed Methodology 235
Figure 10–3 Histogram of the probability of unsatisfactory performance, Congress Street Cut (1.35:1) – Proposed methodology 235
Figure 10–4 Variation of the probability of unsatisfactory performance and the factor of safety with the slope angle, Congress Street Cut – Proposed Methodology 237
Figure 10–5 Histogram and CDF of the factor of safety, Congress Street Cut (2.5:1) – Proposed Methodology 238
Figure 10–6 Histogram of the probability of unsatisfactory performance, Congress Street Cut (2.5:1) – Proposed Methodology 238
Figure 10–7 Sensitivity analysis results, Congress Street Cut (2.5:1) – Proposed Methodology 239
Figure 10–8 Variation of the probability of unsatisfactory performance with the autocorrelation distance, Congress Street Cut (2.5:1) 240
Figure 10–9 Histogram of the probability of unsatisfactory performance, Congress Street Cut (2.5:1) – Naïve Analysis 242
Figure 10–10 Sensitivity analysis results, Congress Street Cut (2.5:1) – Naïve analysis 243

Figure 11–1 p'-q plots of triaxial tests on granitic soils; a) Based on location, b) Based on weathering grade 250

Figure 11–2 Probability histogram and CDF of the effective friction angle of the granitic soils (HDG and CDG) of Hong Kong 251

Figure 11–3 Q-Q plot of the effective friction angle of the granitic soils of Hong Kong (HDG and CDG) 251

Figure 11–4 Histogram and CDF of the effective cohesion of the granitic soils of Hong Kong (HDG and CDG) 252

Figure 11–5 Scatter plot of tangent of friction angle and effective cohesion, Hong Kong granitic soils (HDG and CDG) 253

Figure 11–6 Geometry, stratigraphy and slip surface of the Cho Yiu landslide 256

Figure 11–7 p'-q plot of the consolidated undrained (single stage) and consolidated drained triaxial tests, Cho Yiu slide 259

Figure 11–8 Histogram and CDF of the pore pressure ratio at failure – Cho Yiu landslide 261

Figure 11–9 Probability distribution of pore pressure ratio at failure – Cho Yiu landslide 262

Figure 11–10 Histogram and CDF of the factor of safety, Cho Yiu slope (acceptable design) – Proposed Methodology 264

Figure 11–11 Sensitivity analysis results, Cho Yiu slope (acceptable design) 265

Figure 11–12 Variation of the probability of unsatisfactory performance with the autocorrelation distance, Cho Yiu slope (acceptable design) 265

Figure 11–13 Histogram of the probability of unsatisfactory performance, Cho Yiu slope (acceptable design) – Proposed Methodology 266

Figure 11–14 Histogram of the probability of unsatisfactory performance, Cho Yiu slope (acceptable design) – Naïve Analysis 267

Figure 11–15 Cross-section and stratigraphy of Tsing Yi: 1 slide 268

Figure 11–16 Histogram and CDF of the pore pressure ratio at failure – Tsing Yi: 1 landslide 272

Figure 11–17 Probability distribution of pore pressure ratio at failure – Tsing Yi: 1 landslide....272
Figure 11–18 Histogram and CDF of the factor of safety, Tsing Yi: 1 slope (acceptable design) – Proposed Methodology....274
Figure 11–19 Sensitivity analysis results, Tsing Yi: 1 slope (acceptable design) – Proposed Methodology....274
Figure 11–20 Variation of the probability of unsatisfactory performance with the autocorrelation distance, Tsing Yi: 1 slope (acceptable design)....275
Figure 11–21 Histogram of the probability of unsatisfactory performance, Tsing Yi: 1 slope (acceptable design) – Proposed Methodology....276
Figure 11–22 Histogram of the probability of unsatisfactory performance, Tsing Yi: 1 slope (acceptable design) – Naïve Analysis....277
Figure 11–23 Cross-section and stratigraphy of Ching Cheung Road landslide....278
Figure 11–24 Histogram and CDF of pore pressure ratio at failure – Ching Cheung Road landslide....282
Figure 11–25 Probability distribution of pore pressure ratio at failure – Ching Cheung Road landslide....282
Figure 11–26 Histogram and CDF of the factor of safety, Ching Cheung Road (acceptable slope) – Proposed Methodology....284
Figure 11–27 Sensitivity analysis results, Ching Cheung Road (acceptable slope) – Proposed Methodology....284
Figure 11–28 Variation of the probability of unsatisfactory performance with the autocorrelation distance, Ching Cheung Road (acceptable design)....285
Figure 11–29 Histogram of the probability of unsatisfactory performance, Ching Cheung Road (acceptable slope) – Proposed Methodology....286
Figure 11–30 Histogram of the probability of unsatisfactory performance, Ching Cheung Road (acceptable slope) – Naïve Analysis....287
Figure 11–31 Geometry and stratigraphy of Shek Kip Mei Estate landslide, Northern Slope....289

Figure 11–32 Histogram and CDF of the pore pressure ratio at failure – Shek Kip Mei landslide 292
Figure 11–33 Probability distribution of pore pressure ratio at failure – Shek Kip Mei landslide 293
Figure 11–34 Histogram and CDF of the factor of safety, Shek Kip Mei slope (acceptable design) – Proposed Methodology 294
Figure 11–35 Sensitivity analysis results, Shek Kip Mei slope (acceptable design) – Proposed Methodology 295
Figure 11–36 Variation of the probability of unsatisfactory performance with the autocorrelation distance, Shek Kip Mei slope (acceptable design) 295
Figure 11–37 Histogram of the probability of unsatisfactory performance, Shek Kip Mei slope (acceptable design) – Proposed Methodology 296
Figure 11–38 Histogram of the probability of unsatisfactory performance, Shek Kip Mei slope (acceptable design) – Naïve Analysis 297
Figure 11–39 Effect of scale of failure on probability of unsatisfactory performance and factor of safety - Tsing Yi: 1 slope (acceptable design) 298
Figure 11–40 Effect of scale of failure on probability of unsatisfactory performance and factor of safety – Ching Cheung Road (acceptable design) 299
Figure 11–41 Effect of scale of failure on probability of unsatisfactory performance and factor of safety – Shek Kip Mei slope (acceptable design) 300
Figure 11–42 Comparison between probability distributions of the pore pressure ratios at failure for all the analyzed case studies 304
Figure 12–1 Probability ratio versus factor of safety for safe slopes 308
Figure 12–2 Probability ratio versus variance reduction factor 309
Figure 12–3 Effect of autocorrelation distance on probability of unsatisfactory performance, Safe Slopes - Soil formations exhibiting continuous spatial variability (solid symbols refer to the analyses based on the most likely r_o values, letter N refers to naïve analysis) 310

Figure 12–4 Effect of autocorrelation distance on probability of unsatisfactory performance, Safe Slopes - Soil formations exhibiting erratic spatial variability (solid symbols refer to the analyses based on the most likely r_o values, letter N refers to naïve analysis) 311

Figure 12–5 Probability of Unsatisfactory performance versus factor of safety for the safe and failed slopes – Proposed Methodology 315

Figure 12–6 Reliability Index versus factor of safety – Proposed Methodology 316

Figure 12–7 Probability of unsatisfactory performance versus reliability index; Safe Slope – Proposed Methodology 317

Figure 12–8 Relationship between probability of unsatisfactory performance and reliability index 318

Figure 12–9 Probability of unsatisfactory performance versus factor of safety; Safe Slopes – Proposed Methodology (data are grouped by the coefficient of variation of the factor of safety in the right plot) 319

Figure 13–1 Limits of landslide debris run-outs for Hazard No. 1 relative to the location of Block 36 335

Figure 13–2 Calculated F-N curves for Hazards Nos. 1 and 2 -Shek Kip Mei slope 340

Figure 13–3 Calculated F-N curve for sliding failure of Shek Kip Mei slope and the ERM (1999) risk acceptance criteria 341

Figure 13–4 Event tree analysis and consequence assessment for Hazard No. 1 – Shek Kip Mei Slope 344

Figure 13–5 Event tree analysis and consequence assessment for Hazard No. 2 – Shek Kip Mei Slope 346

Figure 13–6 Event tree analysis and consequence assessment for Hazard No. 3 – Shek Kip Mei Slope 348

CHAPTER 1
INTRODUCTION

1. RESEARCH PREMISES

The impact of uncertainty on the reliability of design and performance predictions of engineering systems is often significant. Uncertainty arises as a result of inherent natural variability, lack of representative data, deficiencies in our understanding of the causes and effects controlling the physical systems and errors and mistakes of humans operating the system. The concept of uncertainty and its effects on engineering systems was formally introduced in the early seventies. Ang and Tang (1975), probably, made the first notable attempt to discuss uncertainty and its relation to the design and decision-making. They wrote;

"In the development of engineering designs, decisions are often required irrespective of the state of completeness and quality of information, and thus must be formulated under conditions of uncertainty, in the sense that the consequence of a given decision cannot be determined with complete confidence. Aside from the fact that information must often be inferred from similar (or even different) circumstances or derived through modeling, and thus may be in various degrees of imperfection, many problems in engineering involve natural processes and phenomena that are inherently random; the states of such phenomena are naturally indeterminate and thus cannot be described with definiteness. For these reasons, decisions required in the process of engineering, planning and design invariably must be made, and are made, under conditions of uncertainty."

Slope Engineering is perhaps the geotechnical subject most dominated by uncertainty. Geological anomalies, inherent spatial variability of soil properties, scarcity of representative data, changing environmental conditions, unexpected failure mechanisms, simplifications and approximations adopted in geotechnical models and human mistakes in design and construction are all factors contributing to uncertainty. The impact of uncertainty on the quality of performance predictions in geotechnical practice is substantial (Morgenstern, 2000). The deterministic factor of safety cannot directly address uncertainty. The evaluation of the role of uncertainty, necessarily, requires the implementation of probability concepts and methods. Chapter 3 presents a review of the various sources of uncertainty and discusses the statistical and probabilistic techniques to quantify them.

Having quantified uncertainty, probabilistic analyses allow it to be rationally incorporated into the design process. In slope engineering, probabilistic slope stability analysis (PSSA) was first introduced in the 70's. Over the last 3 decades, the concepts and principles of PSSA have developed and are now well established in the literature. Chapter 4 reviews the current state-of-practice of PSSA and expands on the advantages and limitations of the available probabilistic methods.

Probability and risk-based techniques provide valuable insights into the inherent risk level. They are important decision-making tools and valuable supplements to conventional methods. The merits of probabilistic analyses have long been noted by many professionals (e.g. Chowdhury, 1984; Whitman, 1984; Wolff, 1996; Christian, 1996). In spite of the enormous uncertainties involved in slope problems and notwithstanding the benefits gained from a PSSA, the profession has been slow in adopting such techniques.

The reluctance of practicing engineers to apply probabilistic methods is attributed to a number of factors. First, engineers often lack formal training in statistics and probability theory. So, they are less comfortable dealing with probabilities than they are with the deterministic factors of safety. Second, there is a common misconception that probabilistic analyses require significant amounts of data, time and effort and are, thus, not practical. Third, few published studies illustrate the implementation and benefits of probabilistic analysis. Finally, the limits of the acceptable probability of unsatisfactory performance (or failure probability) are ill-defined and the link between a probabilistic assessment and a conventional deterministic assessment is absent. This creates difficulties in comprehending the results of a probabilistic analysis.

Given the appeal of probabilistic slope stability analyses and the advanced state-of-practice of probabilistic techniques, there is a need to facilitate the adoption of PSSA in practice.

2. RESEARCH OBJECTIVES

The global objective of this work is to integrate probabilistic slope stability analysis into geotechnical practice and to convince engineers of its legitimacy as a practical design and decision-making tool. A strategy of a number of specific steps is put forward and implemented to achieve the main goal, as summarized below.

- Most engineers lack a formal background in statistics and probability theory. So, a PSSA methodology, while being consistent with principles of logic and mechanics, should be robust, simple and formulated in a format familiar to engineers. Available techniques and tools that could facilitate the implementation of PSSA are evaluated. Chapter 5 describes a probabilistic slope stability analysis methodology based on Monte Carlo simulation using readily available commercial software (e.g. Excel, @Risk).

- Simplicity and practicality must not, however, alter the rationale of the analysis. The assessment should properly and realistically account for the uncertainty of the input parameters. Issues like the spatial variability of soil properties, the reduction in uncertainty due to spatial averaging and the role of systematic uncertainty should be acknowledged. The probabilistic methodology of Chapter 5 addresses these issues, making use of the principles of statistics and the available models for characterizing soil spatial variability.

- Success in promoting probabilistic analysis among practitioners depends largely on calibrating PSSA with the current design practice to attach meanings to the computed probabilities. This is achieved through the analysis of 10 case studies. Chapters 6 through 11 describe the deterministic and probabilistic analyses undertaken. The analyses also serve as examples illustrating the implementation of PSSA. Because of our limited capabilities in quantifying model and human uncertainties, case studies dominated by these two sources are not addressed.

- In order to use PSSA as a design tool, probabilistic design criteria (in addition to the conventional criteria) should be established. Case studies of both failed and non-failed slopes are analyzed probabilistically. Given the conditions at failure, the failed slopes are re-designed to acceptable geometries based on current design practice. The modified geometry is also analyzed probabilistically. Chapters 6 through 11 detail the analyses undertaken. Comparing the failure probabilities of the failed and the safe slopes provides valuable guidelines for probabilistic slope design, as described in Chapter 12.

- Additional insights provided by PSSA, that are of interest to practicing engineers, are identified. For example, the relative impacts of the various sources of uncertainty on design reliability can be quantified. Hence, resources, whether intellectual or physical, can be rationally allocated towards a better characterization of the inputs whose uncertainties dominate the analysis. Such insights are very appealing to practitioners as they rationalize the decision-making process. Within the context of each case study in Chapters 6 to 11, relevant insights are highlighted. They are further discussed in Chapter 12.

- The adoption of risk management techniques in geotechnical practice is growing. Chapter 2 presents a brief review of a risk management framework with particular emphasis on its application in slope engineering. Risk analysis requires the estimation of hazard frequency. PSSA is the most suitable approach for estimating hazard frequency for site-specific studies, particularly in the absence of representative empirical data. Chapter 13 describes the use of the output of a PSSA, in terms of the probability of unsatisfactory performance, in a quantitative risk analysis for a case study in Hong Kong.

CHAPTER 2

RISK MANAGEMENT IN SLOPE ENGINEERING: AN OVERVIEW

Risk is an inherent element of all engineering systems. It is attributed to our inability to predict future system performance with certainty. As, the population could be exposed to hazards whose occurrence may result in adverse consequences such as injuries, fatalities, economic losses and environmental damage, risk cannot be totally eliminated. It, thus, has to be properly managed. Risk management is a structured systematic approach to assess and control risk (CSA, 1991). It is being formally applied in the chemical industry, the nuclear energy industry and the oil and gas industry, in public health, but only recently in geotechnical engineering. This chapter presents an overview of a risk management framework with particular emphasis on landslide risk assessment. Several case studies of quantitative risk assessment are discussed.

This review is not intended to be a detailed survey of risk assessment and management techniques. Rather, it is a brief summary to introduce the risk analysis presented in Chapter 13. More detailed reviews and references, are provided by Einstein (1988), the Canadian Standards Association (CSA, 1991), Melchers and Stewart (1993), Morgenstern (1995, 1997) and Cruden and Fell (1997).

1. INTRODUCTION

Slope engineering is one of the disciplines where risk management is most needed. Predictions of slope performance are dominated by uncertainty. This includes uncertainty in soil properties, geological setting, environmental conditions, loading and analytical models. Conventional slope practice, based on a deterministic analysis, cannot address uncertainty and relies largely on empiricism, judgment and experience. As a result, the risks associated with slopes cannot be quantitatively assessed. Slopes performing poorly are not rare. Morgenstern (1998) listed 11 major incidents involving mine tailings dams and waste dumps over a period of only 3 years (1995-1998). In his Lumb lecture (Morgenstern, 2000), he added that "Failures associated with landslides and earthquake-induced ground movements remain alarmingly high in many parts of the world indicating that, notwithstanding the success of the past, there is no place for complacency in the future". Geotechnical engineers are making daily decisions under uncertainty using analytical methods not equipped to handle uncertainty. There is an urgent need for more advanced and powerful tools. Risk assessment is one promising option.

In addition to the major role of uncertainty, the implementation of risk management in geotechnical engineering is driven by other factors. For example, regulatory requirements are increasingly being cast in a probabilistic format and limited governmental resources argue for prioritizing expenditure. Comparing the risks of different alternatives is very efficient in this regard. Also, risk communications among professionals and to the public are greatly facilitated by the use of risk-based techniques.

2. DEFINITIONS

The risk management terminologies used in the literature are, unfortunately, inconsistent. The same terms are commonly used with different meanings. The IUGS Working Group on Landslides (1997) published a glossary of the common terms. The committee that undertook that task acknowledged, however, that the published definitions do not represent a complete consensus view of all members. In order to avoid any confusion, the main definitions used in this study are summarized below. They are based on the definitions proposed by CSA (1991), the IUGS Working Group on Landslides (1997) and Fell and Hartford (1997).

Hazard :	A condition with the potential for causing an undesirable consequence.

Elements at risk : The population, buildings and engineering works, economic activities, public service utilities and infrastructures, in the area potentially affected by landslides.

Individual Risk : The risk of fatality or injury to an identifiable (named) individual who lives within the zone exposed to the landslide, or who follows a particular pattern of life that might subject him or her to consequences of the landslide.

Risk : A measure of the probability and severity of an adverse effect to health, property or the environment.

Risk Analysis : The use of available information to estimate the risk to individuals or populations, property, or the environment from hazards.

Risk Assessment: The process of risk analysis and risk evaluation.

Risk Evaluation : The process at which values and judgment enter the decision process, explicitly or implicitly, by including consideration of the importance of the estimated risks and the associated social, environmental, and economic consequences, in order to identify a range of alternatives for managing the risks.

Societal Risk : The risk of multiple injuries or deaths to society as a whole: one where society would have to carry the burden of a landslide accident causing a number of deaths, injuries, financial, environmental and other losses.

Specific Risk : failure probability times the vulnerability of a given element.

Total Risk : The expected number of lives lost, persons injured, damage to property and disruption of economic activity. It is the product of specific risk and elements at risk over all landslides and potential landslides in the study area.

Vulnerability : The degree of loss to a given element or set of elements within the area affected by the landslide(s). It is expressed on a scale of 0 (no loss) to 1 (total loss).

3. RISK MANAGEMENT FRAMEWORK

One of the most widely accepted frameworks for risk management is that produced by the Canadian Standards Association (CSA, 1991). The document sets general requirements and guidelines for the implementation of risk analysis. Figure 2–1 provides an overview of the structure of risk management as proposed by the CSA. Risk management comprises risk assessment and risk control. Risk assessment is concerned with estimating the risk (risk analysis) and assessing whether it is acceptable or not (risk evaluation). Risk control includes the decision-making between risk reduction alternatives, should the estimated risk prove to be unacceptable, and monitoring to observe any deviations from the predicted conditions. This study addresses risk analysis only.

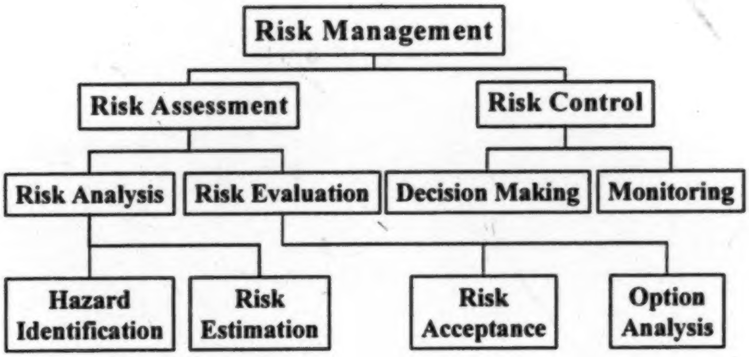
Risk Management
Risk Assessment
Risk Control
Risk Analysis
Risk Evaluation
Decision Making
Monitoring
Hazard Identification
Risk Estimation
Risk Acceptance
Option Analysis

Figure 2–1 Risk management framework (CSA, 1991)

Risk analysis is a structured process that attempts to assess the likelihood of a hazardous event and its consequences. It seeks answers to 3 main questions;

- What can go wrong? (Hazard identification)
- How likely is it? (Hazard Analysis)
- What are the consequences? (Consequence analysis)

The results of the hazard analysis (frequency of occurrence of the hazard) are combined with the results of the consequence analysis (extent of damage/fatalities) for all the identifiable hazards to give a measure of risk.

3.1 Hazard Identification

The first step in risk analysis is to identify potential credible hazards that could result in undesirable consequences. Different procedures can be followed for hazard identification. They could be based solely on experience and/or reviews of historical data. Brainstorming of experts familiar with the problem at hand is another valid alternative. Structured brainstorming techniques such as HAZOP (Hazard and Operability Study) and FMEA (Failure Mode and Effect Analysis) could be used. The Canadian Standard Association guidelines on risk analysis (CSA, 1991) and Neowhouse (1993) provide a convenient overview of hazard identification techniques. In slope engineering, hazards may include the various failure modes (e.g., sliding, debris flow, rock falls) or the instability triggering events (e.g., rainfall, earthquake).

Hazard identification is one of the most crucial elements of risk analysis. Failing to identify a credible hazard may render the results of risk analysis meaningless. Melchers (1993) pointed to the identification of extremely unlikely, but credible, hazardous scenarios as one of the main difficulties affecting risk analysis.

3.2 Hazard Analysis

The probability of the hazard can be evaluated in a number of ways. They include, historical data of slope failures in similar conditions (geology, geomorphology, hydrology, ...etc.), direct subjective assessment, empirical correlations with triggering events (e.g., rainfall) and formal probabilistic methods. Historical records and correlations with triggering events assume that the pattern and frequency of past failures can be extrapolated to the future. This is not true if the current circumstances have changed from those in the past. For example, remedial works and more stringent design criteria can reduce the frequency of failure, as is the case, for example, in Hong Kong. Care should, therefore, be exercised in predicting future performance based on historical records. Subjective assessment of hazard frequencies is necessary where objective data are sparse and statistical techniques can not be applied (e.g., risk mapping of a large area). The task should, however, be undertaken by qualified personnel only and by a team, rather than an individual. Subjective assessment is more reliable in assigning relative failure probabilities to slopes within an area than it is in estimating absolute probability values. Probabilistic slope analysis methods require a lot of details and data and are more useful for site-specific studies. They are the main focus of this work and are covered in detail in Chapters 4 to 12.

3.3 Consequence Analysis

Consequence analysis aims at assessing the extent and nature of damage that can be caused by the hazard. It comprises two main steps; estimating the elements at risk and assessing their vulnerability. The elements at risk are a function of the type of the facilities and the population density in the areas influenced by the landslide. Assessing the vulnerability is much more involved and requires the consideration of many interacting factors. First, the spatial variability of the elements at risk, the probability of the landslide impacting a certain location, has to be addressed. This is a function of debris travel distance. Given a spatial impact, the temporal variability of the exposed elements (i.e., the probability of people being present at the time of the slide) has also to be addressed. This includes the type and degree of usage of the impacted facility (a playground differs from a residential building), the velocity of displaced material, the mobility of the elements at risk and the presence and efficiency of warning systems. Finally, the probability of loss of life or damage, given an impact, has to be quantified. This involves the volume and velocity of the displaced material, the proximity to the landslide and the degree of protection offered by the facility. Fell and Hartford (1997) and Wong et al. (1997) discussed the various components of consequence analysis and provided examples.

Consequence assessment is sometimes based on historical data from similar events. Factors such as population growth, urban development and risk control measures (e.g., zoning requirements) may, however, render extrapolating future trends based on past data unreliable. Direct subjective assessment of the consequences based on judgement and experience is another valid approach. Event tree analysis is, probably, the most common technique for consequence assessment. Starting with the hazard and using inductive reasoning, the structure of the tree identifies all possible scenarios and estimates the probability of the outcome of each scenario. The probabilities of the tree branches are, often, estimated judgmentally. Historical data and analytical/empirical models (e.g., boulder trajectory models, debris runout models) are commonly used to guide the assessment. A consequence model can also be used to quantify landslide consequences. It is an empirical framework based on considerations of the main factors affecting failure consequences (debris velocity and travel distance, spatial and temporal variability of the elements at risk, ... etc.). Wong et al. (1997) developed a consequence model to quantify landslide fatalities in Hong Kong.

4. TYPES OF RISK ANALYSIS

Risk analysis can be classified according to two main criteria. First, distinction is made between qualitative risk analysis and quantitative risk analysis (QRA). In concept, the two approaches are the same and follow the general outlines summarized in Section 3. The difference, however, arises in the extent of usage of probability figures in both analyses. Qualitative studies rely on arbitrary scales (e.g., 1-5) or descriptors (e.g., low to high) to represent the likelihood and the consequences of the landslide. They are more suitable when the available objective data are limited and/or relative ranking of slopes is needed (e.g., zoning purposes). Brand (1988) summarized a qualitative procedure, using instability and consequences scores, to assess the relative risks associated with slopes and retaining walls in Hong Kong. That ranking system was later updated. Pierson (1992) provided another example for managing risks associated with rock slopes along highways. A hazard score was estimated for each slope (based on the conditions of the rock) and combined with a consequence score (based on site conditions) to provide a qualitative measure of risk. Comparison of the scores of different slopes was used to guide and prioritize the mitigation activities.

Quantitative analysis relies largely on computed numeric values such as hazard frequency and estimated number of fatalities in the event of failure. As such, it requires larger amounts of data than the qualitative assessment. It, however, overcomes many of the limitations of the qualitative approach. Quantitative risk values are more easily communicated and are more effective in supporting management strategies. They also allow comparison with other risks affecting the population (e.g., traffic accidents, disease), which greatly facilitate risk communication to the public and help in setting acceptable risk criteria. QRA is a valuable tool for aiding decision-making and has the potential to enhance the balance between safety (or risk) and cost based on rational grounds. This is not to say that QRA is flawless, it has its own limitations. Melchers (1993) and the IUGS Working Group on Landslides (1997) expanded on the difficulties associated with the implementation of QRA. Many of the problems associated with QRA can, however, be avoided through the concept of relative risk. In comparing the risks of design alternatives or courses of action, the unidentified elements of uncertainty (e.g., human error, uncertainty of consequences) are largely the same. As such, the conclusions of the assessment tend to be much more reliable.

One of the main difficulties associated with the implementation of QRA in practice is the high and, often, unrealistic expectations of the outcome of the analysis. Melchers (1993) pointed out the importance of understanding that QRA is not a technique to predict the unknowable. It is merely a structured analytical procedure through which all the relevant facts and foreseeable events are taken into account. Emphasis should not be placed on the precision of the computed numeric risk values, but rather on the insight gained through the analysis.

A second distinction could be made based on the scope and level of detail of the study. This ranges from global risk analysis to site-specific risk analysis. The former focuses on evaluating the overall level of risk affecting the community, mostly on a regional or territorial basis, and is more useful for policy making, resource allocation and land-use and development planning. It, thus, deals with societal risk only. The assessment requires, mainly, general and less quantitative data than the site-specific studies. Such data may include historical landslide frequencies, aerial photos, geological maps, topographic maps and geomorphological data. Depending on the scope of the assessment, the results can be presented in different forms. Hazard or risk maps is one alternative, and the F-N curve or the potential loss of life (PLL) are another.

Hazard maps show the zonal distribution of failure mechanisms with their respective probabilities (either qualitatively or quantitatively) of occurrence. Viberg (1984) and Wu (1992) provide examples of hazard maps. If the consequences of landslides are estimated, they could be combined with hazard maps to produce risk maps. Leiba and Baynes (2000) described the development of risk maps for the Cairns area in Australia. Einstein (1988) presented a convenient overview of landslide hazard and risk mapping techniques with numerous examples. Alternatively, the results can be expressed in the form of the F-N curve or the PLL; both are measures of societal risk. The F-N curve is a plot of the cumulative frequency of N or more fatalities, F, versus the number of fatalities, N, on a log-log scale. The potential loss of life is the annual fatality rate and is equal to the sum of the frequency of the hazard times its consequences (in terms of loss of life) for all identified hazards. It is important, however, to note that the PLL is an average index and cannot distinguish between high-fatality and low-fatality incidents.

Site-specific risk analysis is concerned with evaluating the risk associated with a particular facility, or development, at a specific location. It is useful to owners, designers and regulatory authorities in judging the adequacy of a particular project and whether there is a need for risk reduction measures. That type of assessment, which is considered in this study, requires detailed and site-specific data. DNV (1996) provided examples of site-specific studies applied to actual landslides in Hong Kong.

A screening process prior to the risk analysis is essential to assess the level of detail and the type of analysis most suitable for the objectives of the study. For example, global qualitative analysis is probably more suitable for land-use and development planning studies whereas site-specific quantitative analysis is more suited for evaluating a particular facility.

5. EXAMPLES OF QRA

A literature review is undertaken to assess the state-of-practice of QRA in slope engineering. The search focused entirely on studies involving actual projects, rather than generic examples. A summary of the reviews is presented below.

Over the period 1984-1987, large debris flows, involving several fatalities, took place in the mountainous areas of British Columbia, Canada. As a result of public concern, the local authorities initiated a study to assess the total risk to communities from such events and to guide the planning and design of protective works. Morgan et al. (1992) described the study. The creeks vulnerable to large debris flows were identified and risk maps, in terms of the annual probability of loss of life, were produced. The frequencies of the flows (hazard analysis) were based on an estimated magnitude-recurrence relationship obtained from limited historical data combined with judgment. The consequences were estimated subjectively based on an assessment of the magnitudes of debris flows (in terms of velocity, depth and amount of sediments).

The Montrose area, an outer suburb of Melbourne, Australia, is subject to infrequent but potentially devastating debris flows resulting from landslides. The local government authority commissioned a study of debris flow hazard zoning for development control purposes. Moon et al. (1992) summarized the study. A geological assessment indicated 58 potential landslides in the area. The frequencies of debris flows originating from these potential slides were estimated judgmentally by a team of 4 experts. The estimates were based on assessments of a number of landslide related factors such as topography, relative amount of outcrop and height and proportion of the slope steeper than 26.6 degrees (50% slope). The results were presented in the form of a debris flow hazard map. Finlay (1996) extended the study into a full risk assessment and estimated the total risk to houses in the area and the annual expected loss of life. The consequence analysis was based on a survey conducted by Finlay (1996) in which data regarding the number of houses, their values, type of building construction and occupancy were gathered.

Transportation routes through mountainous terrain are, often, vulnerable to rockfall hazards. In 1982 a rock fall killed a woman and disabled her father in the Argillite Cut of Highway 99 in British Columbia, Canada. Bunce et al. (1995) described a study to quantify the individual and total annual probabilities of loss of life for that highway segment. The frequency of rock falls was based on historical records and an examination of the asphalt for the number of impact marks resulting from falling rocks. The estimates of consequences were entirely subjective. The study did not address the temporal distribution of the elements at risk (e.g., day and night traffic) nor that of the hazard (e.g., higher rockfall frequency during rainy seasons).

Rock falls are also a problem for railway tracks in mountainous terrain. Abbott et al. (1998) discussed the methodology adopted by the Canadian National Railway (CN) for the assessment of rock fall hazards. It was applied for rock slope management along the main track in British Columbia, Canada. The methodology is entirely judgmental and based on field observations. The assessment takes into account the volume of rock detachment, the probability of a rock detaching and reaching the track (based on the geological conditions and the efficiency of the protective and warning measures) and the size of rock present at the track (i.e., rock fragmentation). Train derailment (with no reference to the severity of derailment) is the only consequence considered and is evaluated based on the judgment of CN personnel. The approach does not address the frequency of rock fall due to the lack of representative historical records. It, thus, provides only a relative measure of the danger posed by rock falls to the safe movement of traffic adjacent to a rock slope. The methodology, however, is still in its infancy and is undergoing continuous development and updating.

Landslides in Hong Kong are considered a major hazard to public safety. The Geotechnical Engineering Office of Hong Kong (GEO) adopted risk assessment techniques, particularly QRA, as a means of managing landslide risks. Hardingham et al. (1998) described a study to quantify the landslide risks of the slopes behind the Lei Yue Mun squatter villages. The objective of the study was to assist in the decision-making regarding the re-housing of residents exposed to unacceptable risk levels. Debris slides were identified as the main hazards and the frequencies of their occurrence were estimated based on the landslide database of the area, air-photo interpretations and judgement. Because of insufficient records, the frequencies of major slides, larger than 1000 m^3 in volume, were estimated based on empirical correlations with rainfall. The travel distance of debris was estimated empirically based on the concept of apparent friction angle proposed by Wong and Ho (1996). The failure consequences were evaluated based on a survey of a sample comprising 10% of the villages' population. The survey aimed at defining the number of people in each dwelling, their temporal presence and the degree of protection provided by the dwelling structure. The results were presented as a contour map of the probability of loss of life to any one person, i.e., individual risk. The study concluded that some of the squatters are located within areas of unacceptable individual risk and recommended that they should be re-located as a matter of priority.

Wong and Ho (1998) presented another QRA study to evaluate the global risk of old (prior to the establishment of GEO in 1977) man-made slopes and retaining walls in Hong Kong. For each slope feature (cut slopes, fill slopes and retaining walls), the potential failure mechanisms were identified (e.g., sliding, wash out). Given the failure mechanism, the landslide is classified by the volume of the sliding mass. The global annual landslide frequency for each class was estimated based on historical data coupled with judgment. The database used in the assessment comprised more than 5000 slides that occurred over the period 1984-1996. The failure consequences, in terms of potential loss of life, were evaluated using the consequence model proposed by Wong et al. (1997). The model defines, based on judgement, the expected number of fatalities for a reference landslide (10m wide and 50m^3 in volume) for different types of facilities (buildings, roads, ..etc.) located at the worst possible location. The number of fatalities is then scaled up or down by two factors. The first reflects the size of the actual slide (in terms of the width relative to that of the reference slide) and the second accounts for the vulnerability of the facility taking into the account its location and the mobility and travel distance of the debris. The results of the analyses were presented in terms of the annual potential loss of life for each facility type and slope feature (i.e., cut slope, fill slope, retaining wall) of a given size.

DNV (1996) also described a procedure for site-specific QRA studies for old-man-made slopes in Hong Kong. The approach was applied to quantify the risk associated with a landslide that occurred at the crest of a 15m high cut slope adjacent to Cheung Shan Estate, New Territories. The slide debris hit a bus terminal killing a woman and injuring 5 people. Following a brainstorming session, 6 potential failure modes (e.g., shallow localized failure at the top of the slope with a failure height < 5m) attributed to 11 triggering mechanisms (e.g., saturation by water other than main groundwater table) were identified. The frequency of slope failure due to each triggering mechanism was estimated based on historical data combined with judgement. Each frequency was divided equally between all the relevant failure modes. Thus, the frequency of a particular failure mode due to a specific triggering mechanism was obtained. To reflect the site-specific conditions, these frequencies were adjusted using empirical factors to account for slope angle, soil type, rain intensity and signs of slope instability. The total failure frequency of each failure mode was computed using a fault tree with the failure mode as the top event and the triggering mechanisms as the lower order events. For each failure mode an event tree was constructed to estimate the frequencies of a range of discrete scenarios (e.g., landslide debris impacting a road below the slope). The analysis addressed the mobility of the debris and the scale of failure. For each scenario, the extent of the area affected by the slide debris was estimated based on an empirical estimate of the travel distance (Wong and Ho, 1996) and the slope geometry. The portion of that area occupied by people was multiplied by the population density to obtain the number of individuals at risk. The number of fatalities was evaluated by multiplying the number of people at risk by an empirical factor (between 0 and 1) representing their vulnerability. The results were presented in the form of an F-N curve as well as the potential loss of life. The analysis is comprehensive, but lengthy. It also involves numerous subjective factors, the reliability of which is unclear.

ERM (1996) and Reeves et al. (1998) described a QRA study to evaluate the risk of boulder falls from natural terrain in Hong Kong. Four pilot study areas were considered; east Hong Kong, west Hong Kong, Lei Yue Mun and Tuen Mun highway. Each area was divided into a number of segments (100-500m in length) and a score, based on the percentage of ground covered by boulders and the slope gradient, was assigned for each segment. An empirical correlation was established between the historical rock fall frequency of each study area and the weighted average area score. The correlation was then used to estimate the boulder fall frequency for individual segments using the segment score. Based on an analysis of historic rock fall data, the estimated frequency was divided into a number of categories to address the variation in sizes and starting heights of boulders (boulder travel distance is a function of starting height). Thus, the frequency of a rock of a given size falling from a certain height was obtained. The consequences of each hazard were estimated from considerations of rock fall characteristics (energy, velocity and potential of perforating the impacted facility) and an assessment of the population at risk. The former was computed using boulder trajectory models and target impact models and the latter was estimated from maps of population distribution and traffic data. Event tree analysis was used in the assessment and the results were presented in terms of the potential loss of life as well as the F-N curve for each study area. The authors stated, however, that the developed methodology and the input parameters were coarse and that refinements were needed.

The coastal cliffs of Scarborough, UK, have had a history of slope instability, despite the presence of protective seawalls. The local authority of the area commissioned a study to assess the risks associated with cliff instability and to rationalize a landslide management strategy. Lee et al. (1998) provided a brief overview of the investigation. A geomorphological study identified the unstable cliffs, the likely failure mechanisms, the scales of failure and first-time and pre-existing slides. The failure probabilities (including seawall failure) were estimated from historical records of landslides while the consequences were evaluated subjectively and qualitatively (e.g., minor, partial and total). The failure probability and the consequences were combined qualitatively and 3 risk classes were defined. The cliff sections were categorized accordingly and priority areas were identified. Lee et al. (2000) described a similar study to assess the annual probability of coastal landslides in Lyme Rgis, UK. The probabilities of triggering events (e.g., seawall failure, high groundwater levels) and subsequent responses were estimated subjectively by a team of experts. Event tree analysis was used to estimate the probability of generic consequence scenarios (e.g., loss of property and services in lower zone of the slope).

Leiba et al. (2000) described a study to quantify the landslide risks in the Cairns area, Australia. The study was requested by the Cairns City council for planning and emergency management purposes. Geological and geomorphological studies identified two landslide processes; failure of slopes in weathered bedrock with thin colluvial cover and large debris flows through major gully systems. Based on field observations and historical data, landslide magnitude-recurrence relationships were established for each 10km of escarpment. These relations were the basis for estimating landslide frequencies. The travel distance of the debris was assessed empirically using the concept of apparent friction angle (Wong et al., 1997) with inputs obtained from field observations. The extent of the areas affected by landslide debris was plotted on GIS maps which included comprehensive information on buildings, roads and demography. This allowed a reliable estimation of the elements at risk. The vulnerability of people and facilities was evaluated based on information obtained from the Australian Landslide Database and the Cairns City council coupled with judgment. The results of the assessment were presented in the form of specific and total risk maps for people, buildings and roads.

6. CONCLUSIONS

The cited case studies in Section 5 lead to some important conclusions. First, the number of published site-specific QRA studies is small compared to that of the global QRA studies. Second, hazard frequencies in all of the cited cases are based on historical data (most common), empirical volume or magnitude recurrence relationships, subjective judgement or combinations of two or more. Some of the limitations of these approaches are summarized in Section 3.2. The most important is that reliable frequency estimates based on historic records or volume-recurrence relations require large, high quality databases of failure incidents, seldom available in practice. In consequence, such estimates are general by nature and cannot reflect the specific conditions that may exist at a particular location. As an example, DNV (1996) had to use coarse subjective factors to adjust the historic landslide frequencies to reflect local conditions at the Cheung Shan slope, even though the landslide historic records in Hong Kong are among the most detailed in the world. The adjustment had to cater for inputs as basic as slope angle and soil type. Deducing a site-specific hazard frequency based on historic data or volume-recurrence relations is, thus, unreliable.

Subjective assessment of relative failure frequencies is a well established approach in practice and is based on comparing stability related factors and parameters amongst the investigated slopes. A subjective estimate of absolute site-specific hazard frequency, on the other hand, is based on the undisclosed judgement of the assessor. As such, it tends to be less reliable and is, often, not appealing to practitioners. The difficulty in reliably evaluating hazard frequency at a given site is one of the main reasons behind the rarity of site-specific QRA studies.

In order to encourage the implementation of site-specific QRA in practice, estimates of hazard frequency should be based on well founded, robust and simple techniques. This can be largely achieved through the use of formal probabilistic methods.

Consequence assessment is largely subjective and based on judgement. This is, probably, due to the difficulties associated with the evaluation of many of the input parameters (e.g., debris velocity and impact energy, probability of loss of life given landslide impact). Much of this subjective judgement, however, is not well calibrated, putting some shadow on the reliability of consequence predictions. Recently, there have been some advances in understanding the processes that govern the scale of failure and the velocity and travel distance of the displaced material. This in turn contributed to the development of more rational frameworks for evaluating consequences such as event tree analysis and consequence models. Nevertheless, there is still ample room for further research to improve and advance consequence assessment.

CHAPTER 3

UNCERTAINTY AND STATISTICAL CHARACTERIZATION OF SOIL PROPERTIES

In geotechnical engineering, uncertainty is embedded in all project phases starting from site characterization through analysis and design to decision-making and construction. It is an inherent part of the profession. The influence of uncertainty on the reliability of safety assessment can be significant and is frequently reflected in failures of structures designed to be safe. While such an impact has long been recognized by the pioneers of our profession (Casagrande, 1965; Meyerhof, 1970), the industry always lacked the practical tools to quantify and account for uncertainty. Nearly two decades ago, Einstein and Baecher (1982) wrote "The question is not whether to deal with uncertainty, but how?".

With the growing trend towards applying risk management and reliability-based design in geotechnical engineering, proper understanding and quantification of uncertainty is necessary. While there have been major advances in that direction, there are still many sources of uncertainty that cannot be easily quantified (Lacasse & Nadim 1996). The following sections present an overview of the various sources of uncertainty followed by a discussion of the statistical techniques used for characterizing the uncertainty in soil properties, their merits and their limitations.

1. SOURCES OF UNCERTAINTY

For practical purposes, Morgenstern (1995) divided geotechnical uncertainty into three distinctive categories: parameter uncertainty, model uncertainty and human uncertainty. Parameter uncertainty is the uncertainty in the inputs of the analysis, model uncertainty is due to the limitations of the theories and models used in performance predictions and human uncertainty is related to human errors and mistakes. Due to the inevitable presence of uncertainty in all geotechnical applications, the output of any analysis (e.g., factor of safety, settlement, pile load capacity) is also uncertain. As such, assessing and quantifying uncertainty is a necessity.

1.1 Parameter Uncertainty

Parameter uncertainty is the uncertainty in the input parameters that go into the analysis such as strength, compressibility and pore pressure. Baecher (1987) attributed parameter uncertainty to two sources: data scatter and systematic error. Data scatter is the dispersion of measurements around the mean. It can be further divided into inherent spatial variability and random testing error. Systematic error is the deviation of the observed mean trend from the true unknown one. It can be divided into statistical error and measurement bias. Figure 3–1 illustrates the distinction between the different components.

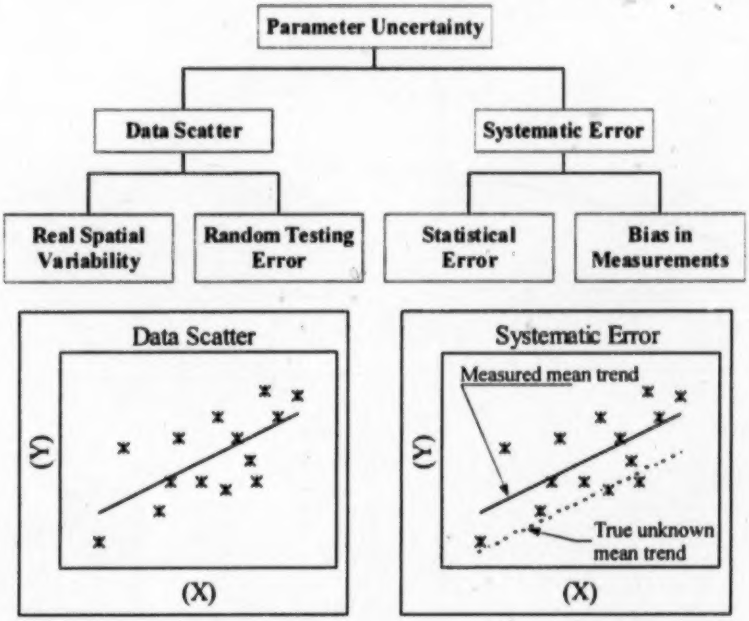
Parameter Uncertainty
Data Scatter
Systematic Error
Real Spatial Variability
Random Testing Error
Statistical Error
Bias in Measurements
Data Scatter
(Y)
(X)
Systematic Error
Measured mean trend
True unknown mean trend
(Y)
(X)

Figure 3–1 Sources of parameter uncertainty (modified from Baecher, 1987)

1.1.1 Data Scatter

Spatial Variation of Soil Properties

Spatial variability is the true variation of soil properties from one point to another, even within a supposedly homogenous layer. It is attributed to factors such as variations in mineralogical composition, conditions during deposition, stress history and physical and mechanical decomposition processes (Lacasse & Nadim, 1996). However, in spite of this expected variability the value of a soil property at one location tends to be close to those at adjacent locations. In other words, spatial variability is not a random process. It is controlled by some form of correlation relating the soil property to location in space. In statistical terms, this phenomenon is known as *spatial structure*. That correlation is expected to diminish as the distance between points increases. Spatial variability is inherent to the soil and cannot be reduced; it must be considered in any analysis of uncertainty. Section 2.3.2 discusses the statistical techniques for analyzing spatial variability.

Random Testing Error

Random testing errors arise from factors related to the measuring process such as operator error or a faulty device. They are independent from one location to another and fluctuate above and below the true unknown magnitude of the soil property. As they do not constitute a true variation in the soil property, random errors should be removed from measurements prior to design. They can be accurately estimated through repeated testing on the same specimen by different operators and/or devices. This is not, however, a viable option for geotechnical applications due to the destructive nature of most geotechnical field and laboratory tests. Section 2.3.2 illustrates the statistical procedures for an approximate estimation of random testing errors.

1.1.2 Systematic Error

Statistical Error

Site investigation programs are almost always controlled by budget constraints which result in a limited number of tests. The mean value of a soil property based on a limited data set is only an estimate of the population mean. The mean of a larger or smaller set of measurements or even another set of the same size is likely to be different. Unless every point within the domain of interest is tested, the estimated mean remains uncertain. The larger the sample size the less uncertain the mean is. Statistical error is the uncertainty in the estimated mean due to limited sample size. Statistical tools for evaluating statistical error are reviewed in Section 2.3.4.2.

Measurement Bias

In soil testing, the measured property can be consistently overestimated or underestimated at all locations. This is known as measurement bias. Several factors may contribute to bias such as the testing device, boundary conditions, soil disturbance or the models and correlations used to interpret the measurements.

Through back-analysis of case studies of slope failures, Bjerrum (1972) observed that the field vane tends to consistently overestimate the undrained shear strength of highly plastic clays. He introduced an empirical correction factor, the ratio of back-calculated to measured undrained shear strength, to correct for bias. Anderson et al. (1984) pointed to the uncertainty associated with the empirical factors used for the conversion of cone penetration resistance into strength parameters. Kulhawy and Mayne (1990) stated that the use of empirical correlations for estimating soil properties introduces additional uncertainty. They emphasized the importance of assessing the effect of this added uncertainty on design reliability. Statistical treatment of measurement bias is discussed in more detail in Section 2.3.4.1.

1.2 Model Uncertainty

Model uncertainty is related to the gap between the theory adopted in prediction models and reality. Analytical models, particularly engineering ones, are usually characterized by simplifying assumptions and approximations. They are imperfect representations capturing some, but not all, of the aspects of the real conditions. Cases of model uncertainty are numerous and can be categorized into numerical and conceptual, with the latter being far more influential. Examples of conceptual uncertainty include progressive failure, time-dependent softening processes, seismic liquefaction triggering, progressive development of internal erosion and undrained versus effective strength characterization (Morgenstern, 1995). Numerical uncertainty includes simplifying computational assumptions (e.g., 2-D versus 3-D models, elastic soil behavior), errors associated with models based on empirical calibrations (e.g., correlations between SPT blow counts and settlement) and mathematical approximations. Model uncertainty is probably the major source of uncertainty in geotechnical engineering (Wu et al., 1987; Morgenstern, 1995; Whitman, 1996). Unfortunately, our capabilities in reliably quantifying model uncertainty are, to date, primitive.

Many researchers pointed out practical problems where model uncertainty is important, yet is being overlooked. Lacasse and Nadim (1996) noted that current methods of predicting capacity of offshore pile foundations are derived from load tests on small piles. The diameter, length and capacity of piles currently used are larger by far. Significant uncertainty may be introduced in design methods due to this different database. Morgenstern (1995) pointed out that the stability of mine waste rock dumps is commonly studied using models based on limit equilibrium. He added that this material is often loose and susceptible to collapse and rapid loss of strength. Analysis must involve assessment of steady state and collapse failure behavior.

The numerical uncertainty in prediction models is commonly accounted for by a global factor that is applied to the equation describing failure (i.e., analytical model). This factor would have a mean and standard deviation and is usually considered to be normally or lognormally distributed (Lacasse and Nadim, 1996). It is commonly evaluated by one or more of the following approaches.

Comparing model predictions with observed performance or predictions of more rigorous and comprehensive models is, probably, the most direct and reliable approach to quantify model uncertainty. As examples, Baecher et al. (1983) compared observed settlement of footings on sand with predictions using Peck and Bazaara's model based on SPT. They concluded that the ratio of observed to predicted settlement has a mean of 1.46 and a standard deviation of 1.32, indicating extreme uncertainty. Yucemen and Tang (1975) compared safety factors computed using the ordinary method of slices with those from rigorous methods in which inter-slice forces are considered and all equilibrium conditions are satisfied. They concluded that the resisting moment in the ordinary method of slices need to be multiplied by a model correction factor with a mean of 1.16 and a standard deviation of 0.053. Azzouz et al. (1983) analyzed the stability of 18 slope case histories using two-dimensional (plain strain) and three-dimensional models. They found that the ratio of 3-D to 2-D factors of safety has a mean of 1.11 and a standard deviation of 0.06. Christian et al. (1994) adopted these values to account for model uncertainty in analyzing the reliability of James Bay hydroelectric dykes. Gilbert et al. (1998) observed significantly higher discrepancies between the 2-D and 3-D factors of safety when assessing the stability of Kettleman Hills landfill. They accounted for the 3-D effect by a correction factor with a uniform probability distribution ranging between a minimum of 0.8 and a maximum of 1.2.

Polling of expert opinions is another way for assessing model uncertainty. Lacasse and Goulois (1989) reported the outcome of polling 30 experts on one of the most commonly used methods for predicting axial capacity of offshore piles, API RP2A method (API, 1993). They indicated the consensus that the method is conservative in medium dense to very dense sand. Engineering judgement could also be applied to assess model uncertainty. Christian et al. (1994) used their judgement to assess the possibility of failing to locate the critical slip surface for James Bay dykes. They assumed that the predicted safety factor is overestimated by a factor of 1.05 with a standard deviation of 0.05. In estimating the axial pull-out capacity of an open ended tubular pile driven into a lightly overconsolidated clay, Ronold (1990) assumed the shaft adhesion factor, α, to be lognormally distributed with a mean of 0.7 and a standard deviation of 0.1.

Another, though less common, approach to account for model uncertainty is to regard the limit state factor of safety as a random variable with a mean, $E[FS_L]$, and a standard deviation, $\sigma[FS_L]$. Based on back-analysis of case studies with minimum parameter uncertainty, Meyerhof (1970) indicated that the factor of safety at failure for earthworks at end of construction in intact clays has a mean of 1.0 and a standard deviation of 0.1. Asaoka and A-Grivas (1981) suggested representing FS_L by a uniform probability distribution ranging between 0.9 and 1.1.

Based on the above discussion, the difficulties in reliably quantifying model uncertainty are evident. The data needed for direct comparison with observed performance are seldom available in practice. Furthermore, the conclusions of the comparison can be blurred by the presence of other sources of uncertainty. Polling of expert opinions and engineering judgement are both subjective. Quantitative estimates are as good as the quality of judgement. What is more important, however, is key features of the problem being overlooked or ignored (conceptual uncertainty) as in the examples provided by Morgenstern in the preceding paragraphs. Commenting on the safety of embankment dams, deMello (1977) in his Rankine lecture wrote: it is "..... not upon the accuracy of our calculations, but upon the adequacy of our hypotheses".

1.3 Human Uncertainty

Human uncertainty is a result of human mistakes. Human errors are often random and unpredictable. Examples include carelessness and ignorance, misleading information, poor construction, inappropriate contractual relationships and lack of communication between parties involved in the project. On many occasions, human mistakes were the reasons for devastating failures. Peck (1973) and Sowers (1991) provided examples of the role of human uncertainty into geotechnical failures. Morgenstern (1995) pointed to the overwhelming contribution of human uncertainty to the failure of the Kwun Lung Lau landslide in Hong Kong which killed 5 people. Basra and Kirwan (1998) complied a large database of human errors in the offshore oil and gas industry.

The nuclear power industry has taken a leading role in quantifying human uncertainty. Samdal et al (1992) pointed to the increasing importance of the human factor in large systems and stated that quantification of probabilities of system failure should not ignore the human component. This has led to the development of the Human Reliability Assessment approach; HRA (Swain and Guttman, 1983; Dhillon, 1986; Dougherty and Fragola, 1988). HRA is a quantitative approach that aims at identifying human errors, assessing their probabilities and seeking ways to reduce or avoid their likelihood of occurrence. In geotechnical engineering, the wide variability and uniqueness of the human contribution from one structure to another create difficulties in identifying potential human errors, not to mention assessing their probabilities.

2. STATISTICAL ANALYSIS OF SOIL DATA

Proper statistical analysis of soil data requires, in addition to the data itself, knowledge about the quality of the data, knowledge about local geology and engineering judgement (Lacasse and Nadim, 1996). Pentz (1982) emphasized the role of judgement, pointing, for example, to the inadequacy of representing rock mass strength by a statistical distribution of laboratory compressive strength tests.

Statistical data analysis comprises a number of stages. Firstly, the available data should be critically reviewed to ensure consistency and detect any anomalies. Secondly, the adequacy of the data to represent the entire population should be assessed. In other words, how reliable are the statistical inferences made about the population on the basis of the available set of observations. Finally, statistical methods are applied to infer the parameters of interest. Issues like errors in observations, spatial correlation and size of the domain of interest are addressed in this stage.

2.1 Data Review

Before starting any formal statistical calculations, it is essential to critically review available data. The first step in data review is to ensure the consistency of data sets (i.e., data belonging to the same population are grouped together) known as *decision of stationarity*. Inconsistency can arise from pooling data belonging to different soil types, stress conditions, testing methods, stress history or patterns of sample disturbance (Lacasse and Nadim 1996).

Secondly, outlier data need to be identified and decisions should be made whether to reject them or accept them as extreme values (Baecher, 1987). Baecher warned that care should be exercised in this process to avoid rejecting a true, important piece of information. An example can be the very low shear strength of a clay-infilled rock joint. This process is often done judgmentally by reviewing testing procedures of odd measurements and the evaluation of the number and range of values of data at nearby locations. Statisticians, however, prefer to use the difference, d_i, given by Equation 3-1.

$$d_i = \frac{x_i - E[x]}{\sigma[x]} \qquad (3\text{-}1)$$

where x_i is the outlier value and $E[x]$ and $\sigma[x]$ are the mean and standard deviation of the entire data set including x_i. If the variable, x, is normally distributed, the quantity, d, would have Student's t-distribution with (n-1) degrees of freedom; n being the number of measurements. The probability of x_i differing that much from $E[x]$ can be estimated from the tables of Student's t-distribution. If the estimated probability is higher than a predetermined criterion (typically 1% or 5%), the outlier is accepted as part of the data. This procedure is exact when the data are normally distributed and is an acceptable approximation as long as the data are not highly skewed.

The next step in data review is to identify the presence of any trends. Trend identification is usually conducted judgmentally by examining the scatter plot of the soil property with depth or distance. Chiasson et al. (1995) pointed to a formal statistical approach for trend identification. Finally, a review of test procedures is also recommended to detect any causes of measurement bias.

2.2 Sample Representativity

Geotechnical engineers are always confronted with the problem of sample representativity. It is not unusual to make decisions based on very little data that may not adequately represent (in a statistical sense) the phenomena being studied. Sample representation has two important characteristics: sample size (number of data) and data clustering. The former being much more common and influential in geotechnical applications

2.2.1 Sample Size

The influence of sample size is expressed in the *confidence interval*. It is defined as the interval within which the unknown statistical parameter of the population, say the mean, is contained with a certain *level of confidence*, say 95% probability. Statistics books (Mace, 1964; Hahn & Shapiro, 1967; Ang & Tang, 1975) have sections on the calculation of confidence intervals for independent, equally-distributed sets of observations. The width of this interval depends on sample size, the parameter being estimated and correlations among observations. For a specified confidence level, the width of the confidence interval decreases as the number of observations increases. In other words, the uncertainty in the estimated statistical parameter (e.g., the mean) is higher for small samples. Statistical techniques for quantifying the uncertainty due to sample size, known as *statistical error,* are discussed in Section 2.3.4.2.

Given a set of observations, the statistical parameters of the population (mean, variance, skewness, ...) can be estimated using different methods, the most common of which is the *method of moments*. According to this method, the mean is referred to as the *first moment* of the random variable, the variance as the *second moment*, and the coefficient of skewness as the *third moment*. For a given level of reliability, the higher the order of the moment being estimated, the larger the number of observations required. For example, a larger number of measurements is needed to estimate the variance compared to that needed for the mean for the same level of accuracy. Also, the stronger the correlation between measurements, the larger the sample size needed to estimate a certain parameter to a given level of confidence. A larger number of correlated measurements is required for a reliable inference of the population covariance, for example, as compared to the variance of non-correlated data.

2.2.2 Data Clustering

The second point of concern is the clustering of data in a limited zone within the spatial domain of interest. In geostatistics, data clustering is of great importance particularly for problems with large areal extent (e.g., mining and reservoir characterization). Different techniques are used to correct histograms for data clustering. In concept, weights are assigned to each data point depending on its closeness to surrounding observations. Data points in densely sampled areas receive less weight than those in sparsely sampled areas. For more details about declustering techniques, the reader is referred to Goovaerts (1997) and Deutsch & Journel (1998). Data clustering is of less importance in geotechnical applications due to the limited data available and the small spatial domain of interest. However, judgmental evaluation to ensure that measurements are evenly distributed within the site is recommended. In a study of the spatial variability of undrained shear strength in James Bay project in Quebec, Soulie et al. (1990) observed higher concentration of vane soundings in a 20m by 50m area at the centre of the site. To avoid any bias in the analysis, they divided the vane data into two subsets corresponding to the central zone and the rest of the site. Each data subset was analyzed separately.

2.3 Statistical Inference

2.3.1 Elementary Statistical Analysis

Before any spatial statistical data treatment, it is advisable to carry out an elementary statistical analysis. The mean and standard deviation are informative simple parameters. The mean is a measure of the central location or best estimate of a soil property, while the standard deviation is a measure of scatter or uncertainty. Statistical expressions for mean and standard deviation are available in all statistics text books.

Besides being a graphical display of data variability, histograms can provide other important pieces of information. A multimodal histogram is an indication of inconsistent data, i.e. non-stationary condition (Section 2.1). In a study of iron deposits in west Africa, Journel & Huijbregts (1978) reported a multimodal, widely-spread histogram of iron grades (Fe) in core samples, Figure 3–2. The histogram indicated a first mode at 67% Fe and several other modes around 50% Fe. A detailed investigation showed the presence of two different ore deposits; a rich shallow hematite and a deeper mixed poorer deposit.

It is important, however, to remember that the visual display of a histogram is affected by the number of cells or intervals used; particularly for a small data set. Manipulating the interval width can distort the shape of the histogram. Baecher (1987) recommended constructing more than one histogram using different numbers of intervals to get a sense of data variability. Because of this dependency on interval width, histograms are not used in statistical calculations. The probability distribution function (cumulative probability histogram), which is independent of interval width, is used instead.

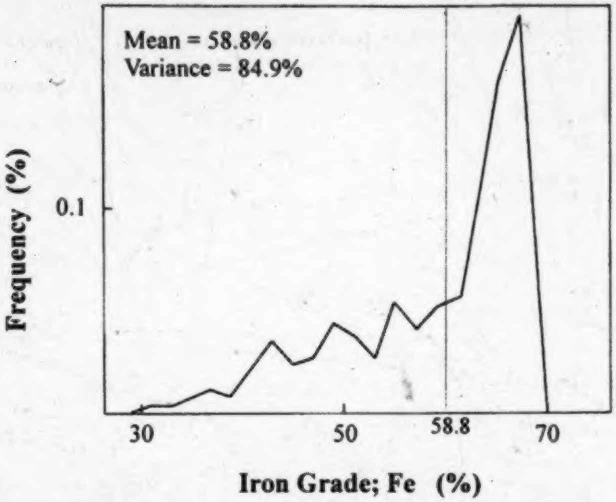

Figure 3–2 Histogram of iron grades; global ore (modified from Journel & Huijbregts, 1978)

2.3.2 Statistical Analysis of Spatial Variability

Measurements of spatial quantities, such as earth data, are intrinsically related to their spatial locations. The magnitudes of a soil property at two adjacent locations are likely to be strongly correlated. As the distance between the two locations increases, the correlation weakens until it vanishes. Lumb (1975) and Vanmarcke (1977a) pointed out that such spatial correlation should not be ignored in modeling soil properties.

Basic statistical parameters described in Section 2.3.1 do not capture the features of soil's spatial structure. Figure 3–3 compares the spatial variability of two artificial sets of data generated using the geostatistics software GSLIB (Deustch and Journel, 1998); both having similar probability distribution functions. The top plot is characterized by highly erratic spatial structure, the data are almost uncorrelated, while the bottom one is characterized by a highly continuous structure. Additional tools are, therefore, needed to deal with spatial variability.

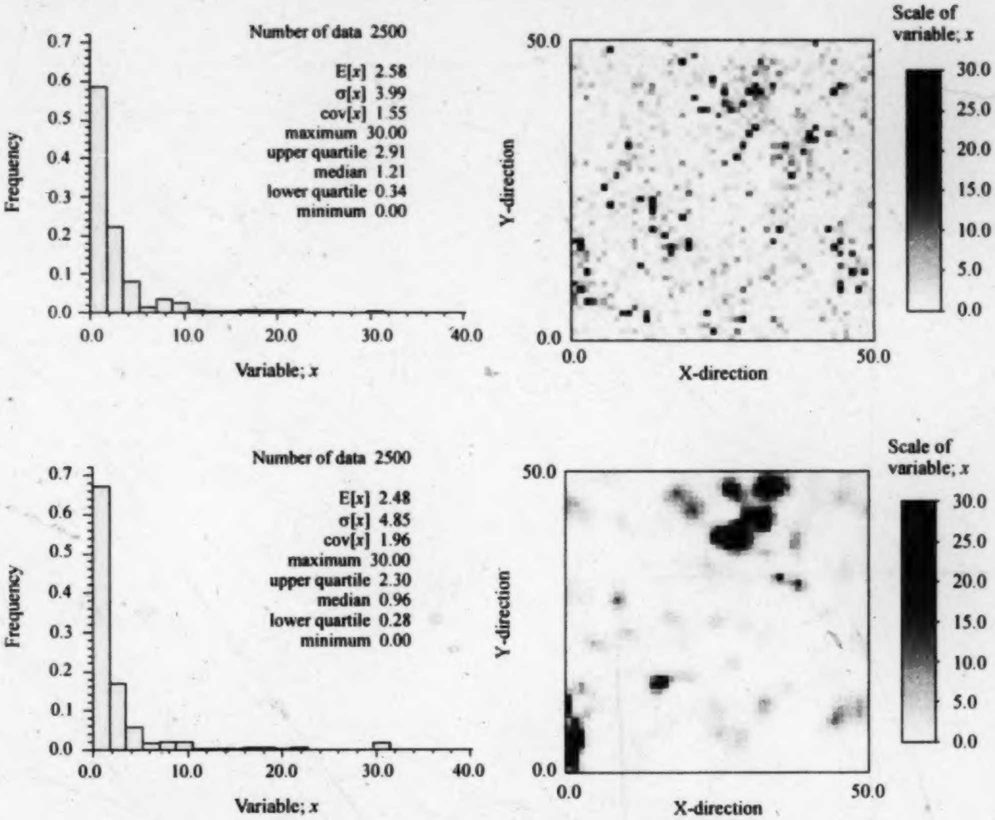

Figure 3–3 A highly erratic spatial structure (upper right) and a highly continuous structure (lower right), both with similar histograms

For practical purposes, a simplified model is commonly used to analyze the spatial structure of soil properties (Vanmarcke, 1977a; Baecher, 1987; DeGroot & Baecher, 1993). The model divides the measured quantity, x_i, at any location, i, into a deterministic trend component, t_i, and a residual component, ε_i, as shown in Figure 3–4. The trend is evaluated deterministically using regression techniques while the residuals are assessed statistically. They are assumed to have a zero mean and a constant standard deviation independent of location. Residuals are further divided into two components; random error, ε_e, and inherent variability, ε_v. The model can, therefore, be written as follows;

$$x_i = t_i + \varepsilon_i \tag{3-2}$$

where; $\varepsilon_i = \varepsilon_{ei} + \varepsilon_{vi}$

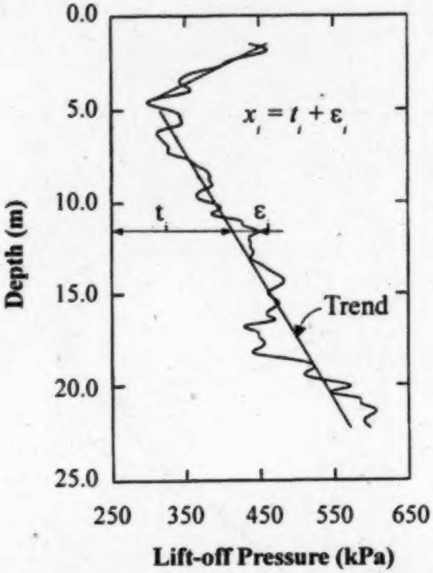

Figure 3–4 Model of spatial variability; Dilatometer lift-off pressure at the University of Massachusetts Amherst National Geotechnical Experimental Test Site (modified from DeGroot, 1996)

2.3.2.1 Trend Estimation

The variability in a soil property frequently follows some trend either in the horizontal direction or with depth. Modeling such a phenomenon with a constant mean leads to an unrealistically high estimate of variability. A trend model should, therefore, be used.

Trend is the mathematical function that best describes the relationship between two correlated variables. The parameters of the function are obtained by regression analysis. The least squares method is the most commonly used technique. Having decided on the functional shape of the trend (e.g., linear, polynomial), the parameters are obtained such that the sum of the squared residuals, ε_i^2, is minimized. Baecher (1987) recommended that trend equations be kept as simple as possible. Complex functions (e.g., high order polynomials) are defined by a large number of coefficients estimated from a limited set of observations. The higher the number of the parameters, the higher the uncertainty in the estimates of these parameters.

Linear models are commonly used to describe soil properties. Equation 3-2 then becomes;

$$x_i = a_o + a_1 z_i + \varepsilon_i \tag{3-3}$$

where; a_o and a_1 are regression coefficients representing the intercept and slope of line, respectively and z_i is the independent variable (e.g., depth). Using method of least squares, regression coefficients can be obtained as follows;

$$a_1 = \frac{\sum(z_i - E[z])(x_i - E[x])}{\sum(z_i - E[z])^2} \tag{3-4}$$

$$a_o = E[x] - a_1 E[z] \tag{3-5}$$

For the special case of linear model through the origin, the intercept is equal to zero and the slope is given by;

$$a_1 = \frac{\sum(z_i x_i)}{\sum z_i^2} \tag{3-6}$$

For both cases, the variance of observations around mean trend is given by the squared difference between measurements and model predictions as follows;

$$V[x] = \frac{\sum(x_i - t_i)^2}{n-2} \tag{3-7}$$

where; $t_i = a_o + a_1 z_i$ is the trend value at location *i*.

At this point, it is important to emphasize the assumptions embedded in the method of least squares. Firstly, the residuals, ε_i, are assumed to have a zero mean and a constant variance given by *V[x]*. Secondly and most importantly, they are assumed to be independent from one location to another. It, thus, follows from the assumptions of the independence of residuals and the deterministic trend component that the soil property, x_i, is an independent random variable; which is seldom the case. Neter et al. (1990) provided a detailed comprehensive discussion of linear regression models.

In summary, the soil property of interest is viewed as a random variable with a mean and a variance. The mean is a function of location and is given deterministically by the trend equation. The variance is estimated from the scatter of observations around the trend and is assumed constant at all locations. Figure 3–5 is a conceptual visualization of the model, where PDF is the probability density function of the residual component.

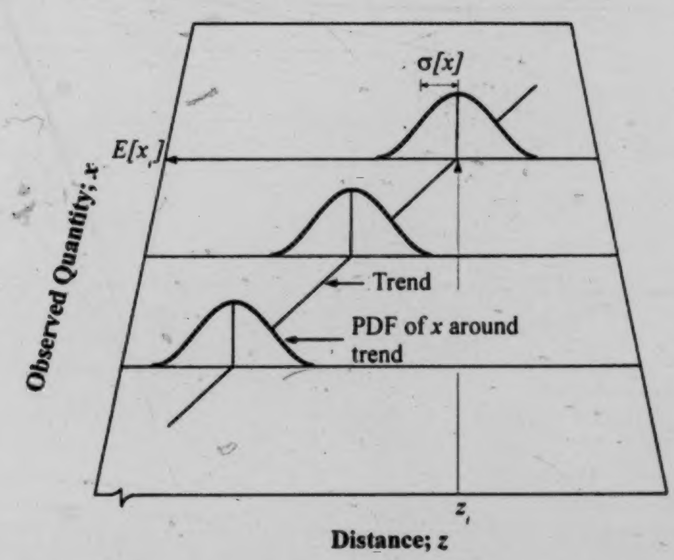

Figure 3–5 Model of soil variability (modified from Neter et al., 1990)

A special case that is sometimes encountered in practice is the one in which the soil property does not indicate a clear trend. The trend is, therefore, a constant given by the mean of observations and the variability around the mean is described by data variance. The trend model (Equation 3-2) then reduces to;

$$x_i = E[x] + \varepsilon_i \tag{3-8}$$

2.3.2.2 Statistical Measures of Spatial Variability

Spatial variability is described by the correlation between soil measurements in space. Since the trend is considered deterministic, spatial variability is concerned with the correlation between residuals. The spatial structure of a spatial quantity can be described by several statistical measures (Deutsch & Journel, 1998). The most common of which are autocovariance, $C_x(r)$, and semivariogram, $\gamma_x(r)$.

Autocovariance

Autocovariance, $C_x(r)$, is a measure of similarity between data of the same type separated by a lag distance r. At small separation distances, the autocovariance is high indicating strong correlation. As r increases, $C_x(r)$ decays gradually till it is equal to zero indicating no correlation; i.e., independent variables. In statistical terms, the autocovariance is defined as the expected value of the residuals at locations r distance apart; as given by Equation 3-9.

$$C_x(r) = E[(x_i - t_i)(x_{i+r} - t_{i+r})] \tag{3-9}$$

where x_i and t_i are the measured and mean values at location i and x_{i+r} and t_{i+r} are the measured and mean values at location $i+r$. The relationship between $C_x(r)$ and r is referred to as *autocovariance function*. It characterizes the degree of spatial continuity of the variable being studied. Figure 3–6 is a schematic illustration of the autocovariance function. At zero separation distance, $r=0$, the autocovariance $C_x(0)$ reduces to the variance of the observations; $V[x]$. Based on the proposed soil model (Equation 3-2), the autocovariance of the measured soil parameter is equal to the sum of the autocovariances of random error, $C_e(r)$, and inherent spatial variability, $C_v(r)$, as given by Equation 3-10 (trend is assumed deterministic). Since random errors are assumed independent from one location to another, $C_e(r)$ is equal to zero for all r values except for $r=0$ (error at location i is perfectly correlated with itself). The values of $C_e(r)$ and $C_v(r)$ at a zero separation distance, are referred to as *random error variance*, $V_e[x]$, and *variance of inherent variability*, $V_v[x]$, respectively. Figure 3–6 illustrates the various components of autocovariance function.

$$C_x(r) = C_v(r) + C_e(r) \tag{3-10}$$

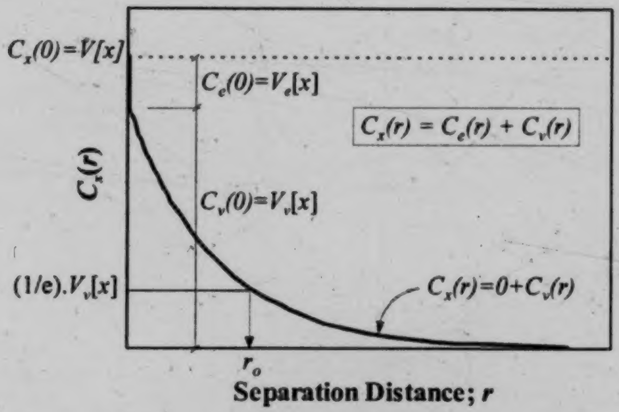

Figure 3–6 Components of autocovariance function

Analytical decay expressions are usually used to describe the autocovariance function. The exponential and gaussian (squared exponential) are the functions most commonly used in practice (Vanmarcke, 1977a; Baecher, 1987; Wu et al., 1987; Christian et al., 1994; DeGroot, 1996; Lacasse and Nadim, 1996), Figure 3–7. Vanmarcke (1977a) pointed out that none of these analytical models can claim any fundamental basis, they only provide a good fit to the autocovariance computed based on observed data (experimental autocovariance).

In exponential and gaussian models, the distance at which $C_x(r)$ decays to 1/e ($\cong 37\%$) of the variance of inherent variability $V_v[x]$, is known as the *autocorrelation* *distance*, r_o, Figure 3–6. It is the model parameter and is interpreted as a measure of the extent of spatial correlation. Observations within a radius r_o are likely to be either all above or all below the mean. Observations more than r_o apart are weakly or no longer correlated. Figure 3–8 illustrates the influence of autocorrelation distance on the variability of soil property (DeGroot & Baecher,1993).

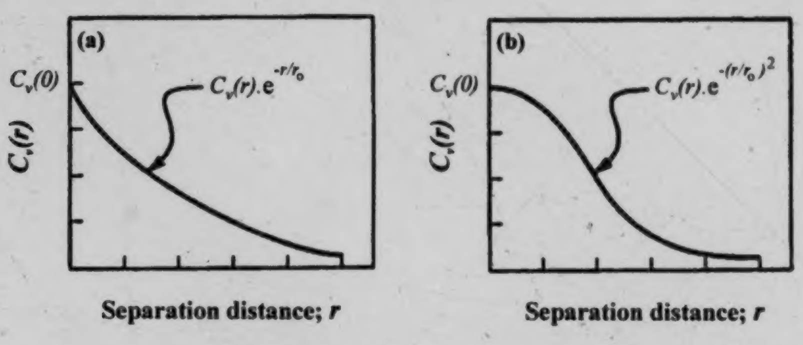

Figure 3–7 Autocovariance functions: a) Exponential; b) Gaussian (modified from DeGroot and Baecher, 1993)

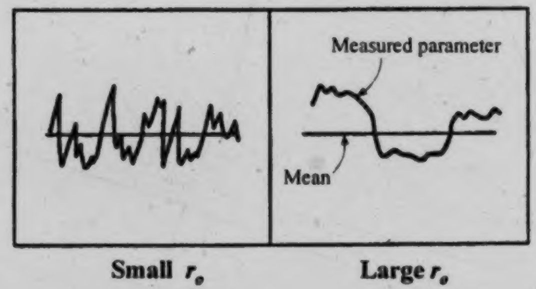

Figure 3–8 Influence of autocorrelation distance on soil variability, both plots have the same horizontal scale

Semivariogram

Unlike the autocovariance, the semivariogram $\gamma_x(r)$ is an average measure of dissimilarity between data separated by distance r. It is defined as half the expected value of the variable $(x_i - x_{i+r})^2$, as indicated by Equation 3-11.

$$\gamma_x(r) = \frac{1}{2} E[(x_i - x_{i+r})^2] \tag{3-11}$$

The use of the semivariogram in studying the spatial structure of spatial quantities is cumbersome for non-stationary problems (observations indicating a clear trend). Therefore, it is often limited to cases where the mean can be assumed constant or the trend can be easily removed from the observations. The use of semivariogram is more common in the context of mining geostatistics (Journel & Huijbregts, 1978). Some recent studies, however, explored its value in geotechnical applications (Kulatilake & Ghosh, 1988; Soulie et al., 1990; Bjerg et al., 1992; Chiasson et al., 1995).

At $r=0$, x_i and x_{i+r} are identical and the semivariogram is equal to zero (unless there is a random measurement error). As r increases the dissimilarity between the measurements increases and the semivariogram gradually increases untill it levels off at a large separation distance indicating total dissimilarity or randomness. Figure 3–9 shows the variation of semivariogram with increasing separation distance. In geostatistical terms, the level off value is referred to as *sill* and is equal to measurements variance $V[x]$. The separation distance at which $\gamma_x(r)$ reaches the sill is known as *range* or *sill distance*, a. It is the separation distance at which the measured data are no longer correlated.

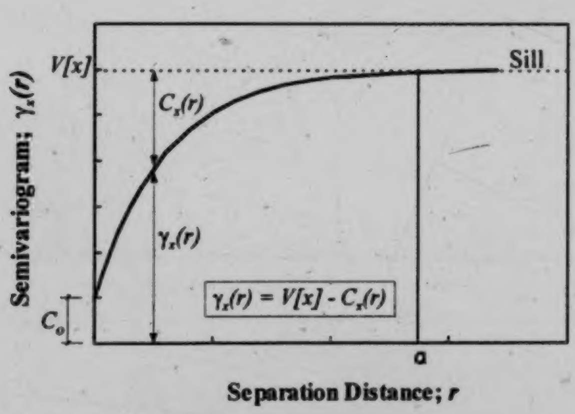

Figure 3–9 Elements of semivariogram function for a stationary condition

Similar to the autocovariance, the semivariogram of a set observations is the sum of two components; random errors plus short scale variability and large scale variability. Random errors and short scale variability appear as a discontinuity at the origin, known in geostatistical literature as the *nugget effect*, C_o, as shown in Figure 3–9. Several analytical functions are used to describe the semivariogram, the most common of which are the spherical, exponential, gaussian (squared exponential) and power models (Goovaerts, 1997). For stationary condition, the autocovariance and semivariogram are related as follows;

$$\gamma_x(r) = V[x] - C_x(r) \qquad (3\text{-}12)$$

The range, a, of exponential models is analytically related to the autocorrelation distance r_o as indicated in Table 3-1. If the data exhibits a trend (non-stationary condition), the semivariogram function does not level off and continues to increase beyond the sill value. Estimating the range becomes highly subjective.

Table 3-1 Relationship between range, a, and autocorrelation distance, r_o

Semivariogram Function	**(a/r_o)**
Exponential	3.0
Gaussian	$\sqrt{3.0}$

2.3.2.3 Methods of Analyzing Spatial Variability

Statistical analysis of spatial variability has two purposes: 1) to separate the random error component from inherent variability, and 2) to estimate the autocorrelation distance. Three methods are commonly used to estimate the autocovariance function based on a set observations. They widely differ in the statistical approach adopted, assumptions, limitations and statistical complexity.

Method of Moments

The method of moments is by far the simplest and most widely used approach (Baecher, 1987; DeGroot, 1996). Sample moments (e.g., mean, variance, autocovariance) are used as estimators of the unknown population moments. The autocovariance, $C_x(r)$, of a set of observations (experimental autocovariance) is;

$$C_x(r) = \frac{1}{N(r)} \sum_{i=1}^{N(r)} (x_i - t_i)(x_{i+r} - t_{i+r}) \qquad (3\text{-}13)$$

where $N(r)$ is the number of data pairs separated by distance r, x_i and t_i are the measurement and the trend values at location i, and x_{i+r} and t_{i+r} are the measurement and the trend values at location $i+r$. Because of the limited number of observations, available data are often grouped into distance classes. That is to say that all data pairs separated by a distance $r \pm \Delta r$ are used to compute $C_x(r)$, where Δr is an arbitrary, constant distance tolerance. The experimental autocovariance is calculated for the different distance classes and a plot of $C_x(r)$ versus r is produced. An appropriate analytical function (Section 2.3.2.2) is fitted to the experimental data as shown in Figure 3–10. Since the autocovariance at $r=0$ is equal to the true spatial variability variance, extrapolating the autocovariance function to the origin divides the total variance into true variability and random error. Baecher et al. (1983) reported that the random error variance of in-situ measurements of soil properties accounts for zero to as high as 70% of observed data scatter. Autocorrelation distance can be obtained as discussed in Section 2.3.2.2. Baecher (1987) and Christian et al. (1994) provided good examples on the application of the method of moments in modeling soil properties.

In spite of its wide application, the method of moments has some limitations. It requires prior knowledge of the trend. Li (1991 & 1994) pointed out that except for the cases of a constant mean, trend estimation is usually done by least squares procedure. As explained in Section 2.3.2.1, the least squares technique implicitly assumes that the residuals off the trend are random or uncorrelated. This is inconsistent with the concept that the portions of residuals representing true variability are autocorrelated. DeGroot and Baecher (1993) also pointed out that the moment estimator of autocovariance is only asymptotically unbiased; meaning that the estimate of autocovariance is only unbiased when the sample size is significantly large. They further added that fitting an analytical function to the experimental autocovariance is often done visually which adds an element of subjectivity to the analysis. Jaksa et al. (1997) indicated that the estimate of the random error variance, $C_e(0)$, based on the method of moments is in fact a combination of short scale variability and random errors. They questioned the reliability of the computed variance. The issue of estimating random measurement errors is discussed in more detail in Chapter 5.

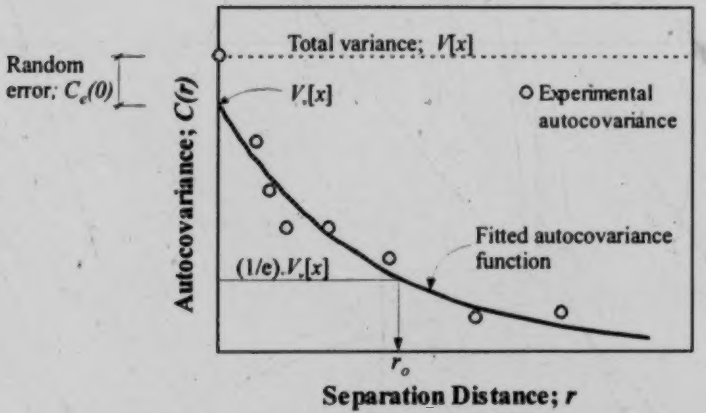

Figure 3–10 Method of Moments: estimating random error variance, $C_e(0)$, and autocorrelation distance, r_o

Method of Maximum Likelihood

Consider the probability density function of a random variable X conditioned on some parameter of interest θ, $f(X|\theta)$. The parameter θ could be data variance, for example. Given a set of observations; $x = \{x_1, x_2, \ldots x_n\}$, the rationale behind the method of maximum likelihood is to estimate the most likely value of θ that will produce the observed data. In other words, among all possible values of θ the maximum likelihood estimator is the one that maximizes the probability of obtaining that set of observations.

The probability of obtaining a particular data value x_i conditioned to θ is given by the magnitude of the probability density function evaluated at x_i; $f(x_i|\theta)$. Assuming a random sample, the joint likelihood function of obtaining $x_1, x_2, \dots x_n$, is given by;

$$f(x_1, x_2, \dots . x_n|\theta) = f(x_1|\theta)\, f(x_2|\theta) \dots . f(x_n|\theta)$$

$$= \prod_{i}^{n} f(x_i|\theta) \qquad (3\text{-}14)$$

The maximum likelihood estimator of θ is the value that maximizes the joint likelihood function. The same concept can be generalized for more than one conditioning parameters: θ_1, θ_2, ... θ_n. Assuming the random variable X to be isotropic Gaussian, Mardia and Marshall (1984) developed a maximum likelihood approach for estimating the trend and autocovariance functions simultaneously, thus, avoiding the problems associated with the method of moments. This technique however, requires the analytical forms of the trend and autocovariance functions (e.g., linear, exponential, …etc) to be known or assumed. DeGroot and Baecher (1993) applied this approach for the analysis of the spatial variability of field vane data of the James Bay project to estimate trend regression coefficients and autocovariance function parameters.

The method of maximum likelihood is statistically superior to the method of moments (DeGroot, 1996), however it also has its own limitations. Li (1994) pointed out that the maximum likelihood function (Equation 3-14) can have a number of local maxima. Thus, the estimators obtained may not necessarily be those associated with the global maximum. He also indicated that the procedure may lead to nonsensical results due to inappropriate assumptions regarding trend and autocovariance functions. For example, ignoring an obvious data trend (i.e., assuming a constant mean) may be reflected in the autocovariance function indicating large scale variability (i.e., large autocorrelation distance) while in reality it is more of a short scale nature. DeGroot and

Baecher (1993) discussed the effect of the assumed form of autocovariance function on maximum likelihood estimators. Using exponential and Gaussian functions for the analysis of field vane data of James Bay project, they reported that trend parameters and variances of spatial variability and random error were very close, however the autocorrelation distances were significantly different: 21.4 m and 37.3 m respectively. To overcome the problems of local maxima and nonsensical results, they suggested using the method of moments to get a general sense of the correlation structure of the data prior to the application of the method of maximum likelihood.

Geostatistical Approach

The application of geostatistics for analyzing the spatial structure of earth data is more common in mining and reservoir characterization problems than it is in geotechnical engineering. However, a number of recent studies investigated its application in studying spatial variability of soil properties in geotechnical applications (e.g. Kulatilake & Ghosh, 1988; Soulie et al., 1990; Bjerg et al., 1992; Chiasson et al., 1995). The semivariogram (Section 2.3.2.2) is the measure of variability commonly used in geostatistics. For a set of observations, the experimental semivariogram is calculated as follows;

$$\gamma_x(r) = \frac{1}{2N(r)} \sum_{i=1}^{N(r)} \left(x_i - x_{i+r}\right)^2 \qquad (3\text{-}15)$$

where *N(r)* is the number of data pairs separated by distance *r*. As in the autocovariance calculations, an arbitrary constant tolerance $\pm\Delta r$ is considered for each separation distance. An appropriate analytical function is fitted to the experimental points and the nugget effect, C_o, and range, a, are obtained, as shown in Figure 3–9. For detailed discussion of the geostatistical approach, the reader is referred to Journel & Huijbregts (1978), Goovaerts (1997) and Deutsch & Journel (1998).

For simplicity, the application of the geostatistical approach is more common in problems where the assumption of stationarity is considered acceptable. Thus, the attribute would have a constant mean and semivariogram function at all locations. In practice, data commonly exhibit some trend. Pinnaduwa et al. (1988) applied a more general methodology to study the spatial variability of cone penetration data showing a polynomial trend with depth. Chiasson et al. (1995) adopted another technique for analyzing the variability of field vane and piezocone data exhibiting linear trends with depth. The idea of both approaches is to filter the trend component from data such that residuals can be modeled as a stationary process. Alternatively, the domain of interest can be divided into zones within which the mean and the semivariogram are assumed constant; a condition of *quasi-stationarity*. Thus the spatial variability would be characterized by different structures depending on location. Both approaches, however, require a large number of observations that are often lacking in practice.

2.3.2.4 Size Effect

So far our discussion of statistical inference has focused on *point statistics*; meaning that observed data and inferred statistical parameters (e.g., mean, variance) refer to discrete points within the domain of interest. Typically, the volumes of soil specimens in geotechnical tests are negligible compared to the volume of the strata and can be regarded as points. However, the performance of a structure is often controlled by the average soil properties within a zone of influence rather than soil properties at discrete locations. Slope failure is more likely to occur when the average shear strength along the failure surface is insufficient rather than due to some local weak pockets. Anderson et al. (1984), Li and Lumb (1987) and Baecher (1987) argued that the uncertainty of the average shear strength along slip surface, not the point strength, is a more appropriate measure of uncertainty. Baecher (1987) warned, however, that depending on performance mode, average properties may not necessarily be the controlling factor. Internal erosion in dams, progressive failure and sliding along a discontinuity are examples of cases where extreme values control performance.

The variance of the strength spatially averaged over some volume/surface is less than the point variance. As the domain over which the soil property is being averaged increases, more local fluctuations tend to average out and the variance of the average property decreases. For quantities averaging linearly, the amount of variance reduction depends on the size of averaging domain and the spatial structure of the soil property. The mean, however, remains almost unchanged. To illustrate this fact, the numerical data in Figure 3-3 (top plot) was discretized based on grids of sizes 1x1, 5x5 and 10x10, respectively. For each scheme, the arithmetic averages within grid squares were calculated and the histogram of the local averages plotted, as shown in Figure 3-11. As the averaging area increases, the coefficient of variation of the local averages dropped from 1.55 to 0.28 and the minimum and maximum values became closer to the mean.

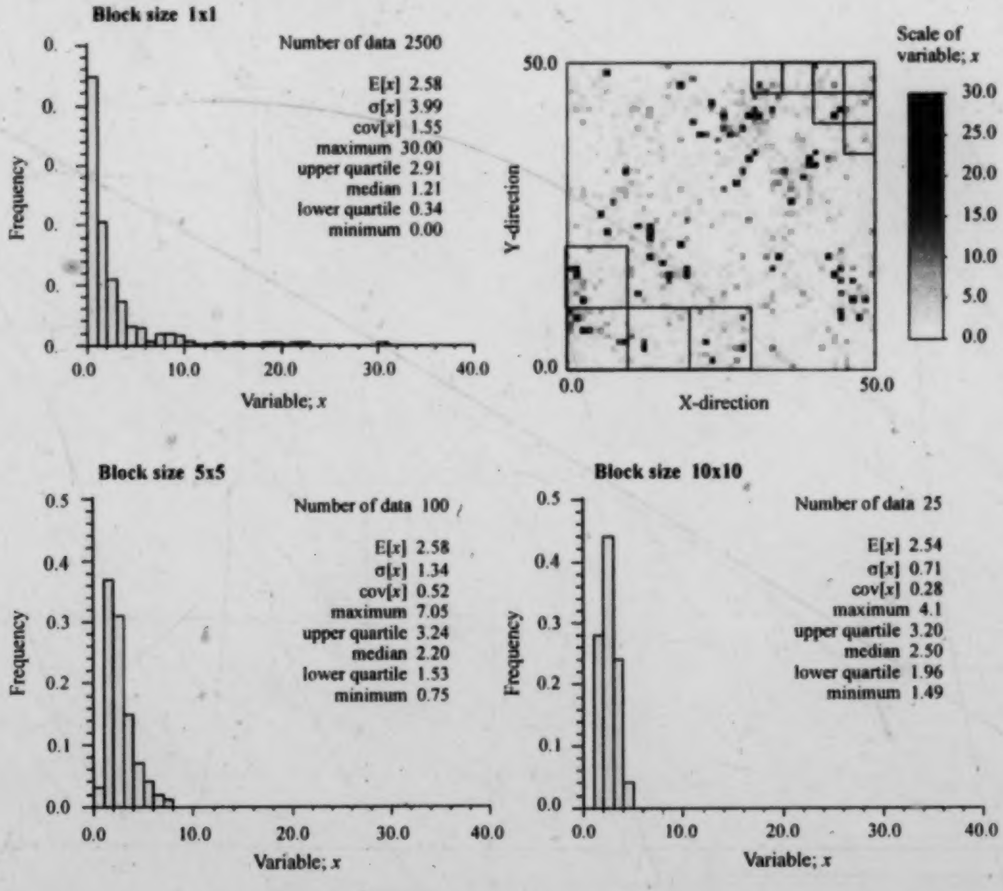

Figure 3–11 Variance reduction due to spatial averaging over blocks of sizes 1x1, 5x5 and 10x10

Data characterized by erratic spatial structure (i.e., short autocorrelation distance) exhibit significant variance reduction, as it is the case in Figure 3–11. Variance reduction in more continuous spatial structures takes place more slowly. The variance of the spatially averaged quantity is expressed as a ratio of the point variance using a *variance reduction factor*, f; Equation 3-16 (Vanmarcke, 1977a).

$$f = \frac{V_{\Delta V}[x]}{V[x]} \qquad (3\text{-}16)$$

where $V_{\Delta V}[x]$ is the variance of the mean soil property averaged over a volume ΔV. In a two dimensional slope configuration, $V_{\Delta V}[x]$ can be replaced by $V_{\Delta L}[x]$; variance of mean strength averaged over the length of the slip surface, L. Vanmarcke (1977a) and Baecher (1987) indicated that the variance reduction factor can be approximated by the ratio of the autocorrelation distance to the length of the slip surface as given by Equation 3-17.

$$f \cong \frac{2r_o}{L} \qquad (3\text{-}17)$$

Vanmarcke (1977b), Li and Lumb (1987) and Christian et al. (1994) applied the variance reduction factor in probabilistic analysis of slope case studies. Lacasse and Nadim (1996) reported that f can be as much as 0.4 to 0.8. Gilbert et al. (1998) estimated f to be around zero for the Kettleman Hills landfill. As a result, they neglected the inherent spatial variability component in assessing uncertainty of shear strength.

2.3.3 Limitations of Existing Spatial Variability Analyses

In spite of the legitimacy of the concept of spatial variability, there are many ambiguities and limitations surrounding the analytical techniques used in evaluating the autocorrelation function and the associated parameters (e.g., autocorrelation distance). The following sections touch on some of these issues.

2.3.3.1 Anisotropy

Soil properties often exhibit some form of anisotropy. Statistical measures used to describe spatial variability are direction-dependent. For example, depending on soil variability, the estimated autocovariance function in the NE direction may be different from that in the NW direction. That difference is reflected in different autocorrelation distances and/or in different spatial variability variances, $V_v(x)$. Figure 3–12 shows semivariogram functions in two directions for a numerically generated anisotropic data (left plot). Spatial continuity in direction "A" is much stronger than "B" as reflected by the larger range, ɑ, and smaller nugget effect and sill values.

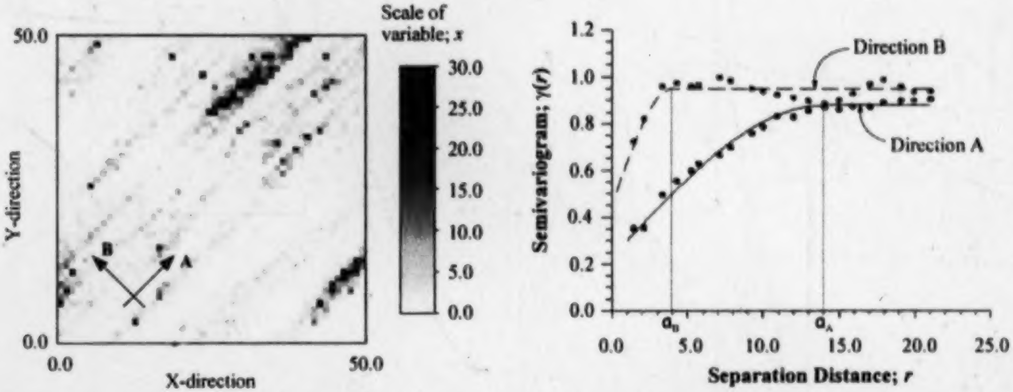

Figure 3–12 Spatial structures in different directions for anisotropic data generated using GSLIB software (Deutsch and Journel, 1998)

Journel & Huijbregts (1978) indicated that the horizontal character of sedimentary processes often leads to larger variability in the vertical direction than in the horizontal direction. Baecher (1987) suggested that the horizontal autocorrelation distance is roughly one order of magnitude larger than the vertical one. Analyzing the spatial variability of vane data in the James Bay project, Soulie et al. (1990) estimated the vertical and horizontal ranges, ɑ, of semivariogram functions to be 3.0m and 30.0m respectively. Honjo and Kuroda (1991) estimated the vertical and horizontal autocorrelation distances of unconfined compressive strength of soft clay to be 2.0m and 40.0m respectively. Table

3-2 (Section 2.3.3.5) provides examples of the range of the autocorrelation distance in the vertical and horizontal directions for different soil properties. Baecher (1987) added that the horizontal autocorrelation distance can also vary with direction depending on geologic history.

As discussed earlier, variance reduction due to size effect is a function of the autocorrelation distance r_o, Equation 3-17. Vanmarcke (1977a) and Kulatilake and Miller (1987) developed 3-dimentional autocovariance models to deal with anisotropy. Both models are complex and require large amounts of data. Alternatively, Vanmarcke (1977b) proposed an approximate procedure to calculate an equivalent autocorrelation distance based on the geometry of the problem and the autocorrelation distances in the horizontal and vertical directions, assuming horizontal isotropy. This approach also requires large amounts of data. Furthermore, site stratigraphy in real projects usually involves a number of soil layers with widely varying characteristics. Estimating autocovariance functions in different directions for each parameter is an extensive and long exercise (Chowdhury and Tang, 1987), requiring significant amounts of data.

In practice, major simplifying assumptions are often adopted. Typically, the autocovariance function in the horizontal plane is assumed to be isotropic. Depending on the geometry of the project, further assumptions can be made. For example, in projects with large extent (e.g., long embankment) soil properties can be averaged vertically in each borehole and the averaged values used to estimate the horizontal autocovariance function. In cases where the vertical function is more important (e.g., compressibility), averages of measurements at the same elevation in different boreholes are used to estimate the vertical autocovariance function. DeGroot (1996) provided examples of both cases. In analyzing the stability of the dykes of the James Bay project, Christian et al. (1994) adopted a single isotropic autocorrelation distance for all soil properties and layers. Simplifying assumptions are essential from a practical point of view. However, there are some concerns over the reliability of autocorrelation distance predictions and their influence on variance reduction factor, f.

2.3.3.2 Scale of Observations

Depending on separation distance, *r*, Journel & Huijbregts (1978) attributed variability between measurements to various causes. There is a variability due to measurement error ($r \cong 0$), variability due to variations in mineralogical composition ($r < 1$ cm), variability due to alteration of properties at strata level ($r < 100$ m), variability due to geologic settings ($r < 100$ km) and possibly variability due to other unknown causes. They added that observing all these variabilities simultaneously requires observations at all ranges of separation distances ($r = 1$ μm-100 km) which is never available in practice. The type(s) of variability that we really observe in practice, thus depend on the scale of observations. Variability due to a major geologic feature cannot be detected by closely spaced observations within a zone of limited extent. Similarly, widely spaced data over a large region may not capture a short scale variability, Figure 3–13.

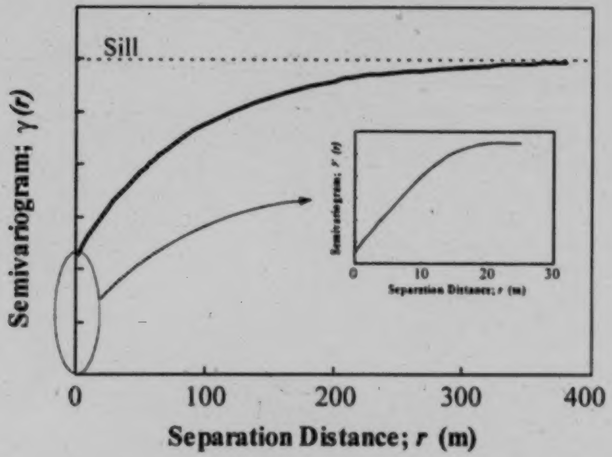

Figure 3–13 Effect of scale of observations on observed variability

Studying the spatial variability of field vane data of the James Bay project, Soulie et al. (1990) observed a high concentration of vane soundings in a central area of the site. The entire site is roughly 1100x450 m (spacing between vane borings > 70 m) while the central zone is about 20x50 m (spacing between vane borings < 10 m). The depth of vane soundings varied between 13 and 19 m in both areas and the vertical spacing between tests was typically 0.5-1.0 m. Soulie and his colleagues divided the data into two subsets corresponding to the central area and the rest of the site and studied their spatial structures separately. They obtained the same vertical semivariogram function for both sets with a range a=3.0 m (note the similarity of vertical scales of observations). The horizontal semivariogram functions, however, were different. The range for the central zone was 7.0 m while for the rest of the site was 30.0 m.

2.3.3.3 Sampling Scheme

The sampling scheme is one of the major difficulties encountered in analyzing spatial variability of soil properties. It refers to both the number of measurements and separation distances between them.

Methods of analyzing spatial variability, discussed in Section 2.3.2.3, provide only estimates of the unknown autocovariance/semivariogram. These estimates are asymptotically unbiased; meaning that stronger inferences can always be obtained with increasing number of observations. Using the method of maximum likelihood, DeGroot & Baecher (1993) showed that uncertainty in the estimates of variance of inherent variability and autocorrelation distance was significantly reduced as the number of observations increased from 36 to 100. They added that the asymptotic property of the method of moments is even inferior to that of maximum likelihood. Russo and Jury (1988) pointed out that the number of observations available in practice is often much less than what is needed for an accurate estimate of the semivariogram. Lacasse and Nadim (1996) indicated that often there are not enough data to reliably assess the autocorrelation distance. Limited data due to budget constraints is a major obstacle facing the implementation of formal spatial variability analyses into geotechnical practice.

In addition to an adequate number of observations, the assessment of spatial variability of soil properties requires the data be located at a wide range of separation distances. Reliable estimates of autocorrelation distance can only be made with data spacing less than the probable autocorrelation distance (DeGroot & Baecher, 1993). Data at very small separation distances are also essential for estimating random error variance (Russo & Jury, 1988). Lack of such data can largely undermine the reliability of spatial variability analyses.

Studying the spatial structures of piezocone and field vane data of a site near Saint-Hilaire in Quebec, Chiasson et al. (1995) concluded that the analysis of horizontal variability for both tests is not possible due to an unfavorable sampling grid. DeGroot (1996) pointed to the Carters dam project where significant amount of SPT data was available, 45 borings, yet few meaningful conclusions could be made about the horizontal spatial structure. The reason was the lack of borings at separation distances in the range of and less than the autocorrelation distance. Benson (1991) analyzed the spatial variability of a large set of measurements of hydraulic conductivity of a clay liner pad performed by Rogowski (1990). He concluded that adequate description of spatial structure was not possible due to lack of data at small separation distances.

Journel & Huijbregts (1978) suggested that estimating experimental semivariogram/autocovariance should only be considered if the number of data pairs for each separation distance is more than 30. DeGroot (1996) drew attention to the limited budget of most site exploration programs and consequently the limited number of tests. Furthermore, boring and testing locations are usually selected judgmentally without regard to the requirements of statistical analysis. As a result, a formal analysis of the spatial variability of soil properties could be, in many cases, fruitless.

2.3.3.4 Trend Selection

As discussed earlier, spatial variability is represented by the scatter of observations around a deterministic trend. Autocovariance and semivariogram estimation is based on the division of observations into a trend component and a random component (residuals). Changing the trend necessarily changes $C_x(r)$ and $\gamma_x(r)$. DeGroot (1996) indicated that the type of trend model selected can have a strong influence on the inferences of the spatial structure of a soil property. Russo and Jury (1988) pointed to the undetected trend or inappropriate trend model as one of the sources of errors in estimating autocovariance and semivariogram functions. In a discussion of the method of maximum likelihood, Li (1994) mentioned that a trend model not conforming to the nature of the spatial structure being studied may lead to nonsensical results. Baecher (1987) explained that the division of observations into a trend and residuals is an artifact of the analysis and it is more of the designer's judgement on how much of the scatter to model deterministically and how much to treat statistically.

DeGroot (1996) investigated the impact of the trend on the inference of the spatial structure of soil properties. He analyzed the spatial variability of dilatometer data (Figure 3–4) assuming constant mean, single linear trend and bilinear trend. Using an exponential autocovariance function, the analysis indicated zero random error for all cases but significantly different estimates of the variance of inherent variability and the autocorrelation distance. The former was estimated to be 6400 kPa^2, 1870 kPa^2 and 630 kPa^2 for the three models, respectively, while the corresponding autocorrelation distances were 3.7 m, 1.1 m and 1.0 m.

Kulatilake and Ghosh (1988) suggested modeling trends using polynomial functions of different orders and computing the semivariogram function of the residuals for each one. The most appropriate model is the one whose corresponding semivariogram function levels off at the sill value of the residuals (refer to Section 2.3.2.2). Analyzing the tip resistance of a cone penetrometer profile, they concluded that a polynomial function of third order is the most appropriate model for that data. Baecher (1987), however, warned that the higher the order of model function, the higher the number of regression coefficients that need to be estimated from the same set of data and the higher the uncertainty in these parameters. Deutsch (2000) also warned of the significant uncertainty associated with extrapolating high order polynomial trends to areas of less data control.

2.3.3.5 Discussion

As discussed in Section 2.3.2, the legitimacy of the concept of spatial variability is not in question. However, the limitations of formal analytical techniques, discussed in Sections 2.3.3.1 through 2.3.3.4, seem substantial. A literature review was conducted to collect results of spatial variability analyses of different soil properties. The search aimed at investigating the influence of different analysis methods, assumptions and simplifications on spatial variability parameters. As such, much focus was put on data whose variability was analyzed using different techniques. Table 3-2 summarizes the results gathered.

Examination of Table 3-2 indicates significant differences in the output of the analyses. Field vane data from the James Bay project are a clear example. Horizontally, estimates of random error variance varied between 0.0 and 10.2 kPa^2, the variance of inherent variability ranged between 12.7 kPa^2 and 50.0 kPa^2 and the horizontal autocorrelation distance ranged between 18.6m and 37.3m. The uncertainty introduced by such scatter challenges the reliability of formal spatial variability analysis techniques. This adds on to the physical limitations imposed by the limited amounts of data, unfavorable sampling plans and complex stratigraphy.

Where data are sparse or absent, engineering judgement can be used to assess uncertainty of soil properties (U.S. Army, 1992). This is a common situation in practice, particularly in embankment design where the in-situ properties of fill material, that is yet to be constructed, are not known. Typical values for the coefficient of variation and the shape of probability density function of various soil properties are available in the literature (Lumb, 1966; Singh, 1971; Chowdhury, 1984; Harr, 1977&1987; Kulhawy et al., 1991; Lacasse and Nadim, 1996). In studying the reliability of James Bay dykes, Christian et al. (1994) applied their judgement for assessing the potential variability of embankment material properties. Friction angle and unit weight were assigned mean values of 30 degrees and 20 kN/m^3 and standard deviations of 2 degrees and 1.4 kN/m^3, respectively. Li and Lumb (1987) judgmentally assumed a coefficient of variation of 10%

for pore pressure ratio when analyzing the stability of Selset landslide. Wolff (1991) adopted a mean of 39 degrees and a coefficient of variation of 8% for the shear strength of the rockfill berm used to stabilize Shelbyville dam. Alternatively, variability can be assumed to follow a triangular probability distribution with estimates of minimum, maximum and most likely values based on expert opinions. For such cases, where there is no data, formal spatial variability analyses cannot be applied.

Li and White (1987) pointed out that ignoring spatial correlation (i.e., assuming soil properties to be perfectly correlated; $r_o = \infty$) would lead to very conservative estimates of the failure probability. However, they commented that analyzing spatial variability requires considerably more data than can be collected in even a "detailed site investigation". Wolff and Harr (1987) shared the same view. Chowdhury and Tang (1987) commented that probabilistic formulation gets very complex when accounting for the autocorrelation of more than one variable. Wolff (1996) stated that spatial correlation theory presents a lot of difficulties for routine analyses in practice.

Based on the discussion in the preceding paragraphs, it seems that empiricism and judgement have to be exercised in order to be able to practically account for spatial variability and spatial averaging processes.

2.3.4 Evaluation of Systematic Error

The concept of systematic error was discussed briefly in Sections 1.1.2 and 2.2.1. As explained, systematic error is divided into measurement bias and statistical error. Its contribution to the uncertainty of the estimates of soil properties is quite different from that of inherent spatial variability. Spatial averaging or size effect tends to reduce the uncertainty due to spatial variability (Section 2.3.2.4). In contrast, systematic error is consistent across the entire domain and propagates unchanged through the analysis. Its contribution to the overall uncertainty can, therefore, be significant.

Table 3-2 Assumptions and results of spatial variability analyses for various soil properties

PROJECT	DATA	DIRECTION	METHOD OF ANALYSIS	TREND	$C(r)$ or $\{\gamma(r)\}$ FUNCTION	$V_e[x]$ {% of $V[x]$}	$V_v[x]$ {% of $V[x]$}	r_o (m)	REFERENCE
James Bay Hydro-electric Dykes (sensitive clay)	Field vane	Horizontal	Moments	Constant	Exponential	9.2 kPa^2	13.8 kPa^2	30.0	Ladd et al., 1983
			Geostatistics	Constant	{Spherical}	0.0 kPa^2	50.0 kPa^2	30.0	Soulie et al., 1990
			Maximum Likelihood	Constant	Exponential	9.6 kPa^2	13.4 kPa^2	21.4	DeGroot and Baecher, 1993
				Surface trend	Exponential	9.1 kPa^2	13.3 kPa^2	23.0	
				Surface trend	Gaussian	10.2 kPa^2	12.7 kPa^2	37.3	
			Moments	Constant	Exponential	6.3 kPa^2	16.7 kPa^2	18.6	DeGroot, 1996
		Vertical	Geostatistics	Constant	{Spherical}	0.0 kPa^2	50.0 kPa^2	3.0	Soulie et al., 1990
Carters Dam	SPT	Horizontal	Moments	Constant	Exponential	0.97 $(bl/ft)^2$	5.03 $(bl/ft)^2$	120.0	DeGroot, 1996
			Maximum Likelihood	Constant	Exponential	0.43 $(bl/ft)^2$	5.57 $(bl/ft)^2$	60.0	
				Linear surface trend	Exponential	0.0 $(bl/ft)^2$	3.0 $(bl/ft)^2$	16.7	
University of Massachusetts Test Site (varved clay)	Dilatometer	Vertical	Moments	Constant	Exponential	0.0 kPa^2	6400 kPa^2	3.7	DeGroot, 1996
				Liner	Exponential	0.0 kPa^2	1870 kPa^2	1.4	
				Bi-linear	Exponential	0.0 kPa^2	630 kPa^2	1.03	
Saint- Hilaire Site (sensitive clay)	CPT tip Resistance	Vertical	Geostatistics	Linear	{Spherical}	0.0 kPa^2	5400 kPa^2	2.0	Chiasson et al., 1995

Table 3-2 Assumptions and results of spatial variability analyses for various soil properties (cont'd)

PROJECT	DATA	DIRECTION	METHOD OF ANALYSIS	TREND	$C(r)$ or $\{\gamma(r)\}$ FUNCTION	$V_e[x]$ {% of $V[x]$}	$V_v[x]$ {% of $V[x]$}	r_o (m)	REFERENCE
Saint- Hilaire Site (sensitive clay)	CPT sleeve friction	Vertical	Geostatistics	Linear	{Spherical}	0.0 kPa^2	4.6 kPa^2	2.0	Chiasson et al., 1995
	Field vane	Vertical	Geostatistics	Linear	{Spherical}	0.0 kPa^2	24.0 kPa^2	2.0	
Oil Exploration Platform (North Sea clay)	CPT tip resistance	Horizontal	Moments	Constant	Gaussian	{0.0 %}	{100 %}	30.0	Tang, 1979
N/A (dense sand)	CPT tip resistance	Horizontal	N/A	N/A	Gaussian	{1.0 %}	{99.0 %}	37.5	Lacasse and Nadim, 1996
N/A (partly laminated clay)	CPT tip resistance	Horizontal	N/A	Constant	Exponential	{0.0 %}	{100.0 %}	9.6	Lacasse and Nadim, 1996
Eglin Air Force Base, Florida (sand)	CPT tip resistance	Vertical	Geostatistics	3rd order polynomial	{Spherical}	0.0 kPa^2	38.7×10^5 kPa^2	1.56	Kulatilake and Ghosh, 1988
Test Embankment, North of Tokyo (soft clay)	unconfined compressive strength	Horizontal	Geostatistics	Constant	{Exponential}	0.0 kPa^2	64.0 kPa^2	40.0	Honjo and Kuroda, 1991
		Vertical	Geostatistics	Constant	{Exponential}	0.0 kPa^2	64.0 kPa^2	2.0	
N/A	SPT	Horizontal	Moments	Constant	Exponential	60.5 $(bl/ft)^2$	60.5 $(bl/ft)^2$	53.5	Baecher, 1986

2.3.4.1 Measurement Bias

Detecting and assessing the magnitude of measurement bias is difficult. The most dependable way is to compare measurements with back-calculated values from observed performance (e.g., failure) or with measurements from a more reliable procedure or device. Bias is often expressed in the form of a factor that is either multiplied or added to the measured value. The soil model discussed in Section 2.3.2, Equation 3-2, then becomes;

$$x_i B = t_i + \varepsilon_{vi} + \varepsilon_{ei} \qquad (3\text{-}18a)$$

or $$x_i + B = t_i + \varepsilon_{vi} + \varepsilon_{ei} \qquad (3\text{-}18b)$$

where B is a bias correction factor. Bjerrum (1972) based his correction factor for field vane data upon a comparison of back-calculated undrained shear strength from slope failures with those obtained from vane measurements. The correction factor is the ratio of the former to the latter and is used with Equation 3-18a.

Analyzing field vane data of the James Bay project, Soulie et al. (1990) observed a systematic shift of about 8 kPa between undrained shear strength from 2 vane soundings 1.0 m apart conducted in 1979 and 1981, respectively. They observed the same shift between other pairs of holes, however they reported that no physical explanation was found. They applied a bias correction factor of 8 kPa using Equation 3-18b. The correction factor can be, however, highly uncertain as is the case, for example, in Bjerrum's factor (Azzouz et al, 1983; Ladd 1983). In addition to the mean value of bias factor, its uncertainty (in the form of standard deviation) should also be considered. Wu (1974) performed a study similar to that of Bjerrum for case histories of slope failures in which the undrained shear strength was based on unconfined compression tests. He concluded that the measured undrained shear strength need to be multiplied by a correction factor with a mean of 1.10 and a standard deviation of 0.33.

2.3.4.2 Statistical Error in the Mean/Trend

So far, the models and analytical techniques adopted were all based on the assumption that the trend component t_i in Equations 3-2 and 3-18 is deterministic (i.e., has zero variance). As a result, the variance of inherent variability is equal to that of the residuals ε_{vi}. Since the trend is estimated based on a limited set of observations, this assumption is somewhat in error, which is referred to as statistical error. It is typically quantified by considering the trend component as a variable with a mean equal to t_i and a non-zero variance. The magnitude of the variance depends on the number of observations n; the larger the number of measurements, the less uncertain the mean trend is. Therefore, the effect of statistical error can be reduced by increasing the number of measurements. The total uncertainty in measurements of a soil property is the sum of uncertainty in the mean trend and that due to the variability of the residuals ε_v around the trend.

Statistical theory allows assessing the magnitude of the statistical error variance. For the case of constant mean and correlated observations, the variance of the mean is given by Equation 3-19, where $C_{ij}(r)$ is the value of autocovariance function evaluated for a separation distance r between locations i and j (Baecher, 1984).

$$V\{E[x]\} = \frac{1}{n^2} \sum_{i}^{n} \sum_{j}^{n} C_{ij}(r) \qquad (3\text{-}19)$$

If measurements are deemed independent (e.g., widely spaced data), Equation 3-19 reduces to Equation 3-20. Baecher (1987) suggested that unless observations are very closely spaced, Equation 3-20 is an acceptable approximation for most practical applications.

$$V\{E[x]\} = \frac{V[x]}{n} \qquad (3\text{-}20)$$

Similarly, the same concept of statistical error applies for a varying trend. Regression coefficients of a linear trend model, a_o and a_1, are inferred from a specific set of measurements. Smaller or larger sets of observations are likely to yield different coefficients. To account for the uncertainty in a_o and a_1, they could be modeled as normally distributed random variables with mean values given by Equations 3-4 and 3-5 and variances given by Equations 3-21 and 3-22 (Neter et al. 1990).

$$V[a_1] = \frac{V[x]}{\Sigma(z_i - E[z])^2} \tag{3-21}$$

$$V[a_o] = V[x]\left\{\frac{1}{n} + \frac{E[z]^2}{\Sigma(z_i - E[z])^2}\right\} \tag{3-22}$$

The estimates a_o and a_1, are usually correlated. The correlation coefficient between them is given by Equation 3-23.

$$\rho(a_o, a_1) = -\frac{E[z]V[a_1]}{\sigma[a_o]\sigma[a_1]} \tag{3-23}$$

For the special case of a linear trend going through the origin, the variance of the slope is given by;

$$V[a_1] = \frac{V[x]}{\Sigma z_i^2} \tag{3-24}$$

2.3.5 Correlation Between Soil Parameters

Correlation between two (or more) parameters is an indication of the association between their values; in other words, how the change in the value of one parameter affects the others. Driven by the appeal of estimating expensive, difficult-to-measure soil parameters based on less expensive easy-to-measure parameters, numerous studies have been conducted to investigate correlations between soil properties. Based on an extensive literature review, Kulhawy and Mayne (1990) prepared a detailed report summarizing correlations between various properties. Most of them were developed empirically and are often highly uncertain.

The correlation between two variables x and y can be easily detected from a scatter plot of their values as shown in Figure 3–14. It is expressed in terms of the correlation coefficient, ρ_{xy}, given by Equation 3-25, where $C(x,y)$ is the covariance of the two variables.

$$\rho_{xy} = \frac{C(x,y)}{\sigma_x.\sigma_y} = \frac{1}{n-1}\left(\frac{\sum(x_i - \mathrm{E}[x]).(y_i - \mathrm{E}[y])}{\sigma_x.\sigma_y}\right) \qquad (3\text{-}25)$$

It is, however, important to note that the correlation coefficient is a measure of only linear association between variables. Two parameters highly dependent in a non-linear form (e.g., sinusoidal function) may have a zero correlation coefficient. The correlation coefficient ranges between +1 and –1. A value of +1 indicates perfect positive linear correlation while –1 indicates perfect negative linear correlation. A zero correlation coefficient indicates no association between the variables (i.e., independence). Figure 3–14a shows strong negative correlation between moisture content and dry density ($\rho_{w\gamma}$= -0.96) while Figure 3–14b implies positive, but poor correlation between dry unit weight and unconfined compressive strength ($\rho_{\gamma q}$= 0.25). Tang et al (1999) pointed, however, to the importance of checking if any functional dependency exists between the soil parameters whose correlation is being investigated (e.g., bulk unit weight and moisture content). If it does, there is a high potential of obtaining a spurious strong correlation between the parameters.

In addition to the probability distributions of input variables, the application of probabilistic methods requires estimating (or assuming) correlation coefficients between variables. In the context of slope design, the parameters that might be cross-correlated are unit weight, friction angle and cohesion. For normal soils, strength parameters are positively correlated to unit weight. The variability in soil unit weight is usually small and the laboratory procedures for unit weight measurements are highly accurate. Furthermore, stability analyses are largely insensitive to variations in unit weight. As a result, unit weight is often taken as a deterministic value and its correlation with strength parameters is ignored. Alonso (1976) and Nguyen and Chowdhury (1984) showed that the contribution of uncertainty in unit weight to the overall uncertainty in slope analysis is insignificant.

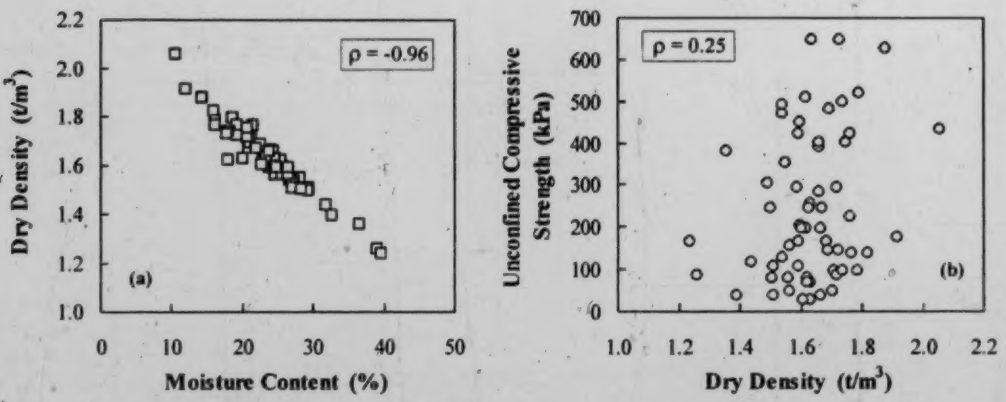

Figure 3–14 Scatter plot for detecting correlation between soil properties (data from Holtz and Krizek, 1972); a) Strong negative correlation, b) Weak positive correlation

Wolff and Harr (1987) and Mostyn and Li (1993) showed that failure probability in slope stability analyses is sensitive to the correlation coefficient between strength parameters C' and ϕ'. The form of this correlation is, however, not very clear. Matsuo and Kuroda (1974) reported strong negative correlation for an unsaturated soil tested in direct shear when sample moisture content was fixed. Holtz and Krizek (1972) also reported negative, but poor, correlation for the impervious borrow material used in constructing Orville dam. Wolff (1985) reported both negative and positive correlations for the borrow materials of Cannon dam. Alonso (1976) presented evidence suggesting the absence of such correlation for natural soils.

3. SUMMARY

The discipline of geotechnical engineering, in general, and the area of slope stability, in particular, are largely dominated by uncertainty. Three categories of uncertainties can be distinguished: parameter uncertainty, model uncertainty and human uncertainty. Parameter uncertainty involves the uncertainty in the input parameters such as soil properties and pore water pressure. Over the past 3 decades major advancements in identifying, quantifying and accounting for parameter uncertainty have been achieved. Model uncertainty is related to the gap between the theories and models used in the analysis and the real conditions. It is one of the major sources of uncertainty in geotechnical engineering, yet our capabilities to quantify it are, to date, primitive. Human uncertainty is due to human mistakes and is very difficult to predict and quantify due to the variability and uniqueness of the human contribution from one project to another

Quantifying parameter uncertainty involves two stages. Firstly, the adequacy of available data (in terms of the amount and clustering of measurements) to represent the entire population is assessed. Secondly, statistical techniques are applied to infer the statistical characteristics of the parameter being studied. This stage involves identifying and estimating the trend function, establishing the histogram and the probability distribution function, quantifying and separating the random error variance, estimating the correlation structure of the data including autocorrelation distance, assessing the impact of spatial averaging on one-point statistics and quantifying statistical uncertainty and bias.

In spite of the significant development in the statistical techniques of quantifying parameter uncertainty, the implementation of such formal analyses into professional practice is still faced with many difficulties. The main obstacles are the amounts of data and the spacing between measurements. Typical geotechnical investigation programs have limited budgets which is reflected in a limited number of tests located at a large spacing. The lack of data and the improper (in a statistical sense) separation distance between measurements can greatly undermine the reliability of the analyses. The matter is further complicated by the directional dependency of the correlation structure of soil properties. Other factors related to the statistical techniques such the subjective selection of the trend and autocorrelation functions add on to the uncertainty of the analyses, however to a much lesser extent. Most engineers lack formal training in statistics and probability theory, which further hinders the implementation of uncertainty analyses in practice. As a result, it seems that an element of judgement and empiricism have to be exercised in order to be able to practically account for uncertainty.

CHAPTER 4

PROBABILISTIC SLOPE ANALYSIS MERITS, CONCEPTS AND METHODS

The assessment of the stability of slopes, particularly natural slopes, is one class of problems that is dominated by uncertainties. Geological anomalies, material properties, environmental conditions and analytical models are all factors contributing to uncertainty. Conventional slope design practices do not account for uncertainty, thus compromising the adequacy of predictions. This limitation is well recognized by researchers as well as practitioners. Bjerrum (1966) and Peck (1967) expressed their concerns about the ability of the profession to make reliable forecasts of slope failure events. In the context of dam slope design, Wolff (1985) also emphasized on the inadequacy of judging a design based on the numerical value of the factor of safety alone.

Probabilistic slope stability analysis offers an efficient framework for logical systematic incorporation of uncertainty, thus providing a more rational basis for design. It is also the first step towards the implementation of quantitative risk assessment in geotechnical engineering; a rapidly growing trend (Whitman, 1984; Morgenstern, 1995). Numerous studies have been undertaken to develop probabilistic slope design methodologies. In the following sections, the concepts of deterministic and probabilistic approaches are explained and the shortcomings of conventional practice are discussed. Then, an overview of existing probabilistic methods, their advantages and limitations is presented.

1. DETERMINISTIC VERSUS PROBABILISTIC MODELS

The concepts of deterministic and probabilistic modeling are significantly different. In the former, available data is assessed, often judgmentally, to come up with a single best estimate for each input parameter. These estimates are then used in analytical (or numerical) models to predict performance. The analysis yields a single output that is thought to be a reasonable representation of reality. The main assumption involved in the deterministic approach is that the estimation errors, the difference between the true unknown values of input parameters and our estimates based on available data, are equal to zero. In earth related sciences where material properties tend to be highly variable and available data are often sparse, there is no real justification for this assumption. Furthermore, the models used for performance prediction and evaluation are assumed flawless and perfect representations of reality which is seldom, if ever, the case.

Probabilistic modeling, on the other hand, recognizes the uncertainty in the input parameters and prediction models. Input parameters are treated as random variables. Each parameter can claim any value, within the observed range, with a given probability of occurrence deduced from available data. Journel (1986, 1994) and Isaaks and Srivastava (1989) provided discussions of the philosophy and practice of modeling earth data. Since the input parameters are variables, the predicted performance is also a variable. A range of possible outputs with respective probabilities of occurrence are obtained. The uncertainty in performance prediction models can also be incorporated into the analysis. Probabilistic modeling is, thus, a reflection of our imperfect knowledge.

2. CONVENTIONAL SLOPE STABILITY ANALYSIS

Analyzing the stability of slopes is usually done using limit equilibrium methods. Over the past four decades these models (e.g., Bishop, 1955; Spencer, 1967; Morgenstern-Price, 1965; Janbu, 1973) have gained wide acceptance and became part of everyday practice. The methodology adopted in conventional practice, however, is of a deterministic nature. Typically, a site characterization program is carried out to collect data regarding geological and hydrological conditions, stratigraphy, material properties and pore water pressures. The data are then assessed to obtain best estimates of parameters of interest (e.g., strength parameters, pore pressure ratio, ...etc). Potential critical failure modes are investigated and appropriate methods of analysis decided upon. Stability analysis is performed to calculate the factor of safety of the slope. Based on experience, an allowable factor of safety is selected. If the calculated safety factor is equal to or greater than the allowable one, the slope is considered safe. If not, design modifications are implemented to attain a higher safety factor. As such, conventional practice attaches significant importance to calculated factors of safety.

The calculated factor of safety obviously depends on the selected input parameters, the postulated failure mode, the reliability of judgmental assumptions and the accuracy of the chosen method of analysis. Therefore, there is no unique value for a given slope problem. Different parameters, assumptions and analysis methods are likely to be adopted by different engineers depending on their judgement and experience. Calculated safety factors are unlikely to be equal. The real meaning of the calculated safety factor is, thus, not clear. The Muar trial embankment is an interesting case study in that regard (Kay, 1993).

Aiming at optimizing the design of a highway embankment on soft marine clay, the Malaysian Highway Authority decided to build a full scale trial embankment in the valley of the Muar river. A detailed site investigation program was conducted, yielding an extensive amount of data. Four reputable geotechnical consultants were invited to predict the performance of the embankment including height at failure. The exercise was later extended to include 30 consultants. Brand and Premchitt (1989) and Polous et al. (1990) provided a discussion of the results and predictions. The embankment was built in 1989 and failed at a height of 4.7m above ground. Figure 4–1a is a histogram of predictions of embankment height above ground surface at failure made by all 30 participants. A significant scatter in predictions is evident, even though all participants had the same site characterization data. Figure 4–1b is the histogram of the predictions of the originally selected four experts. The scatter is significantly less. Kay (1993) pointed out, however, that the detailed level of analysis conducted by those experts is seldom undertaken in normal design activities.

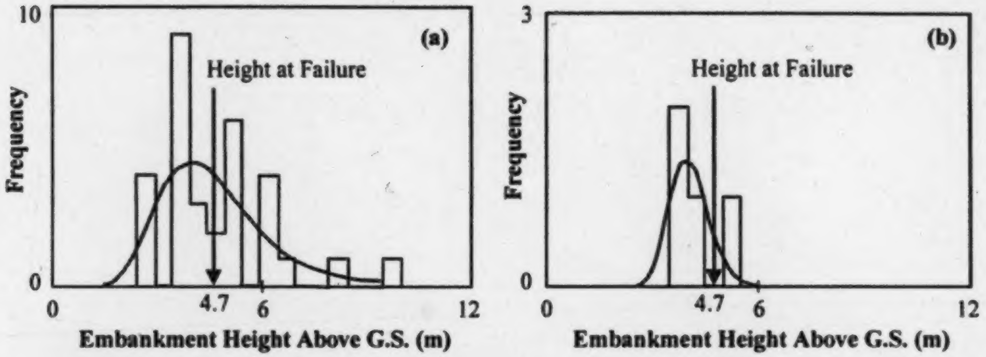

Figure 4–1 Muar Embankment : histograms of embankment height predictions; a) all 30 participants, b) four experts (modified from Kay, 1993)

Based on a number of prediction competitions, Morgenstern (2000) undertook a study into the accuracy of performance predictions in geotechnical engineering. He classified predictions into excellent, good, fair, poor or bad depending on their closeness to the actual performance observed in the field. Predictions within ± 25-50% of the correct answer are classified as "poor" and predictions off by more than ± 50% are classified as "bad". He cited four prediction competitions: the MIT trial embankment; the Muar trial embankment; a spread footing on sand; and, a single driven steel pile. In each case, the participants were asked to predict performance parameters (e.g., embankment height at failure, settlement, pile load capacity, ... etc.) which were compared to the actual field performance. Morgenstern noted that poor to bad prediction amount to 70%, 55%, 90% and 87%, of the total number of predictions, for the 4 cases, respectively. He then commented that this is even an optimistic picture because of the comprehensive data and extensive care in the analysis and design associated with such competitions. While, the findings of this study might be shocking to many practitioners, they truly reflect the significant impact of uncertainty on reliability of geotechnical predictions.

Conventional slope practice accounts for uncertainty very loosely through conservative parameters and designs. The process is often highly subjective and leads to an unknown degree of conservatism in the overall design factor of safety. No explicit consideration of quantified uncertainty is regarded. As a result, failures of slopes evaluated to be safe are not unusual (e.g., Irland, 1954; Insley, 1965; Kaufman & Weaver, 1967; Bjerrum, 1972 & 1973; Lumb, 1975; Vaughan & Walbancke, 1975; Janbu et al., 1977; Skempton, 1977 & 1985; D'Elia et al. 1988; Seed et al. 1990). Tang et al. (1976) stated that in spite of the presumed conservatism in conventional slope design practices, an element of risk is unavoidable. For the sake of objectivity, it should be mentioned that conventional practice has the advantage of being backed up by a large body of experience over decades of practice. Optimally, such experience should be benefited from in the search for a more rational approach.

3. PROBABILISTIC SLOPE STABILITY ANALYSIS

In general terms, probabilistic slope stability analysis methods are based on the same principles as deterministic methods (e.g., failure modes, limiting equilibrium). However, they have the advantage of being able to account quantitatively for the various sources of uncertainty. The output of a probabilistic analysis provides more information about slope performance than does the safety factor. In addition to the most likely condition or performance, it also indicates the potential variability due to uncertainty.

Probabilistic techniques aid greatly in understanding the major sources of risk, enhance engineering judgement and allow for a rational comparison of the reliability of alternative designs. Ultimately this will have the benefit of improving the decision making process. They are a valuable supplement to conventional practice.

3.1 Basic Concepts

Figure 4–2 illustrates the concept of probabilistic analysis in slope design. Available data are first analyzed to obtain a representative probability distribution for each input variable (Chapter 3). Only those parameters whose variability is thought to have a significant effect on the analysis need to be modeled as variables. For example, Alonso (1976) and Matsuo and Kuroda (1974) demonstrated that uncertainty in unit weight has an insignificant effect compared to those of pore pressure and strength parameters. Failure mode is then assessed and appropriate slope models and methods of analysis are selected. Input distributions are integrated into stability analysis to estimate the probability distribution of the factor of safety. Model uncertainty (refer to Chapter 3) can be accounted for by either applying statistical factors to the input distributions or, more commonly, by applying a global factor to the analytical model used as shown in Figure 4–2 (Lacasse & Nadim, 1996).

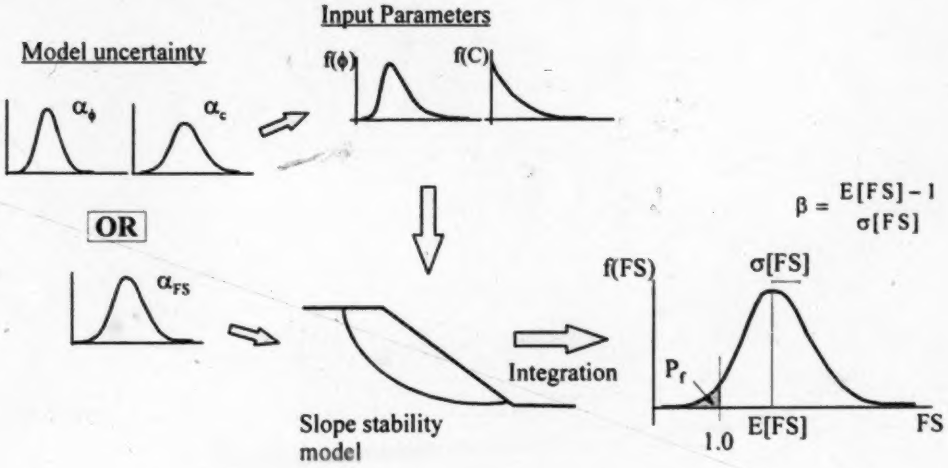

Figure 4–2 Concept of probabilistic analysis

Failure probability (P_f) is the probability of having a safety factor less than one. United States Corps of Engineers (U.S. Army, 1992) uses the term *probability of unsatisfactory performance* (P_u) instead of failure probability. It is defined as the probability of the value of performance function (i.e., factor of safety) exceeding the limit state. In slope problems, the limit state is typically a factor of safety of one. In some cases, different limits could also be used such as, for example, the factor of safety associated with excessive deformations. Safety can also be expressed in terms of reliability index, β. It is defined as the distance between the best estimate of the factor of safety (i.e., mean) and the failure threshold, FS =1.0, expressed in units of standard deviation of factor of safety as shown in Figure 4–2.

In conventional practice, it is believed that the higher the calculated safety factor the higher the level of safety. This is, however, not always the case depending on the level of uncertainty involved. Lacasse and Nadim (1996) showed the results of the re-examination of the safety of a pile foundation installed in 1976. The pile was originally designed based on limited information to a safety factor of 1.79. The re-examination, which was based on new detailed information about soil parameters and loading, yielded a safety factor of 1.40. The failure probability associated with the latter analysis was found to be significantly less than that associated with the original design as shown in Figure 4–3. The added new information reduced the safety factor, however it also reduced the uncertainty in soil and load parameters. The analysis concluded that the pile had a higher level of reliability or safety than it was originally thought. A major advantage of probabilistic analyses is that they provide a consistent measure of safety. Designs with equal probabilities of failure or equal reliability indices would have a more consistent level of safety than designs with equal factors of safety.

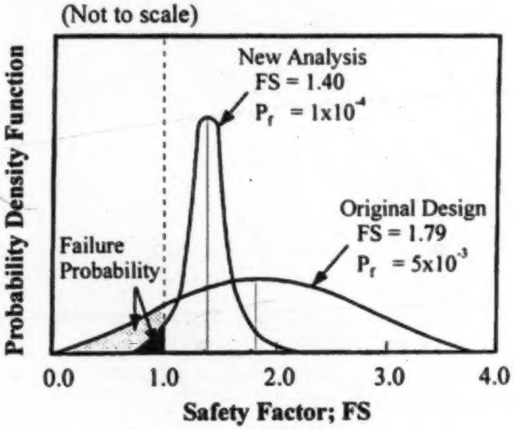

Figure 4–3 Probabilistic analysis of a pile foundation (modified from Lacasse & Nadim, 1996)

3.2 Methods of Probabilistic Analysis

During the past three decades there have been numerous attempts to devise probabilistic procedures for slope stability analysis (Matsuo, & Kuroda 1974; Alonso, 1976; Tang et al., 1976; Vanmarcke, 1977b; Kim, et al. 1978; Priest & Brown, 1983; Nguyen & Chowdhury, 1984; Li & Lumb, 1987; Wolff & Harr, 1987; Li, 1992a, 1992b; Low & Tang, 1997). These methods vary in terms of assumptions, limitations, capability to handle complex problems and mathematical complexity. Most of them, however, fall into one of three categories: analytical methods, approximate methods or Monte Carlo simulation.

3.2.1 Analytical Methods

In analytical methods, the probability density functions of input variables are expressed mathematically. They are then integrated analytically into the adopted slope model to derive a mathematical expression of the density function of the factor of safety. Failure probability is obtained by multiple integrals of that expression over the entire failure domain. The mathematical complexities involved in this approach are enormous rendering it impractical for most users and uses. Few attempts have been made to apply analytical methods (Tobutt & Richards, 1979; McMahon, 1975; Marek & Savely; 1978). Moreover, in all of these studies the problems analyzed were too ideal and involved major simplifying assumptions.

3.2.2 Approximate Methods

The majority of approximate methods are modified versions of either the First Order Second Moment method or the Point Estimate method. Thus, only these two techniques will be covered here. Both approaches require knowledge of the mean and variance of all input variables as well as the performance function $g(x_1, x_2, \ldots x_n)$ that defines safety factor (e.g., Bishop equation), where $x_1, x_2, \ldots x_n$ are input variables (e.g., soil properties).

3.2.2.1 First Order Second Moment

First order second moment (FOSM) is based on Taylor's series expansion of a $g(x_1,x_2,...x_n)$ around its mean value. For simplicity, only the linear terms of the series are usually retained. The mean and variance of the safety factor are given by Equations 4-1 and 4-2.

$$E[FS] = g(E[x_1], E[x_2], ...E[x_n]) \qquad (4\text{-}1)$$

$$V[FS] \cong \sum_{i=1}^{k} \sum_{j=1}^{k} \left(\frac{\partial g}{\partial x_i} \frac{\partial g}{\partial x_j} \right) C(x_i, x_j) \qquad (4\text{-}2)$$

where $E[FS]$ and $V[FS]$ are the mean and variance of the safety factor, respectively, and $C(x_i,x_j)$ is the covariance between input variables x_i and x_j. Detailed description of FOSM is available in many text books such as Ang and Tang (1984) and Harr (1977 and 1987).

According to Equation 4-1, the mean safety factor is equal to the safety factor calculated using mean values of input variables. If the input variables are uncorrelated, $C(x_i,x_j)$ is equal to zero except when $i=j$ where it is reduced to the data variance $V[x_i]$. Equations 4-1 and 4-2 are exact only if $g(x_1,x_2,...x_n)$ is a linear function, which is not the case in slope problems. However, they still provide an acceptable approximation provided that the performance function is not highly non-linear. For most geotechnical models, evaluating the derivatives $(\partial g/\partial x_i)$ can be cumbersome. A finite difference approach can be used to approximate the partial derivatives. Because of its simplicity, FOSM is commonly used in probabilistic slope stability analyses (Cornell, 1972; Yucemen and Tang, 1975; Alonso, 1976; Tang et al., 1976; Anderson, et al., 1984; Li and White, 1987; Christian et al., 1994).

3.2.2.2 Point Estimate Method

The point estimate method is an approximate numerical integration technique that was originally developed by Rosenblueth (1975, 1981). It is based on replacing the continuous probability distribution of each input variable x_i with a discrete distribution having only two values, x_{i+} and x_{i-} with two associated probability concentrations, p_+ and p_-. The values and probability concentrations are selected such that the first and second moments (mean and variance) of the discrete distribution are the same as those for the original distribution.

The mean and variance of the safety factor are evaluated by adding 2^n estimates of the performance function, where n is the number of input variables. These estimates constitute the values of safety factor calculated for all possible combinations of x_+ and x_- for all input variables. Commonly, x_+ and x_- are taken one standard deviation above and one standard deviation below the mean (U.S. Army, 1992). Before summing, the individual terms are multiplied by corresponding probability concentrations which are functions of correlation coefficients between variables. As the number of input variables increases, the number of terms to be evaluated increase by a power law and the analysis gets more cumbersome. The mathematical details of the technique can be found in Rosenblueth (1975, 1981) and Harr (1987). While the method is shown to be reasonably accurate for a wide range of practical problems, it can be seriously in error in some cases. Christian and Baecher (1999) provided detailed discussions of the accuracy and the limitations of the point estimate method. The technique was modified and implemented by many researchers for slope stability analyses (McGuffey et al., 1982; Nguyen and Chowdhury, 1984; Wolff, 1985; Wolff & Harr 1987; Li, 1992a).

3.2.3 Monte Carlo Simulation

Monte Carlo simulation is, often, an efficient way to deal with problems that are mathematically complex. In the context of slope design, Monte Carlo simulation was adopted by many researchers (Kim, et al. 1978; Major et al., 1978; Tobutt, 1982; Priest & Brown, 1983; Nguyen & Chowdhury, 1984). Prior to the simulation process, an appropriate deterministic performance function should be selected and the probability distribution functions of input variables are to be defined. Monte Carlo simulation uses a pseudo random number generator to select a random value for each input variable based on the corresponding probability distribution. The selected values are then used to solve the performance function and calculate a safety factor. The process is repeated a large number to times to build up a statistical distribution of the performance variable (i.e., safety factor). The mean safety factor and failure probability can be inferred from the resulting probability distribution.

Monte Carlo simulation has a number of advantages over analytical and approximate methods. Firstly, it does not require the comprehensive statistical and mathematical background needed for other methods; something most practicing engineers unfortunately lack (Whitman, 1984). Secondly, it provides the shape of the probability distribution of the factor of safety and, consequently, the failure probability, thus eliminating the need to assume the shape of the distribution. Thirdly, unlike the other approaches, the complexity of the analysis is not amplified by the increase in number of input variables.

Depending on number of variables and their variances, conventional Monte Carlo techniques may require significant number of iterations (up to tens of thousands) for solution convergence, particularly when estimating events of low probabilities of occurrence. Because of the extensive computational effort involved in the iteration process, the implementation of Monte Carlo techniques in geotechnical engineering was limited (Anderson et al., 1984; Chowdhury, 1984; Mostyn & Li, 1993; Christian el. al., 1994). In fact, not so long ago the economics of running a Monte Carlo simulation was considered marginal (Tobutt, 1982; Priest & Brown, 1983). However, with the recent advancements in random sampling techniques (e.g., stratified sampling, Latin Hypercube) and the rapid development in software engineering this picture is significantly changing. The increasing number of commercial simulation software, the continuous improvement in their capabilities and the consequent reduction in cost is encouraging a wider implementation of simulation techniques in practical problems.

3.3 Limitations of Existing Probabilistic Methods

In spite of the significant advancement in probabilistic slope design techniques over the past three decades there are still many shortcomings that limit their integration into routine practice. Analytical methods are mathematically demanding to the extent that they are seldom applied even at research level. Approximate methods are much less complex and are widely adopted by many researchers and practitioners. However they involve various simplifying assumptions that often limit their application to specific classes of problems. For example, some researchers used very simple slope models such as Janbu's stability charts (Claes, 1996), ordinary method of slices (Yucemen and Tang, 1975; Tang et al., 1976; Harr, 1977; Vanmarcke, 1980; Honjo and Kuroda, 1991; Bergado et al., 1994) and force equilibrium methods (Priest & Brown, 1983; Wolff & Harr, 1987; Wolff, 1991). Others dealt with frictionless soils only (Cornell, 1972; Matsuo & Kuroda, 1974; Vanmarcke, 1977b; McGuffey et al., 1982; Bergado et al., 1994). A restriction to circular (or cylindrical) slip surface is common in many studies (Alonso, 1976; Vanmarcke, 1977b; Anderson et al., 1984; Yucemen & Al-Homoud, 1990; Bergado et al., 1994). The spatial variability of soil properties and pore water pressure is often ignored, assuming perfect autocorrelation (Tobutt and Richards, 1979; Nguyen and Chowdhury, 1984; Wolff and Harr, 1987; Tejchman et al., 1996; Duncan, 2000). Correlation between input variables such as that between cohesion and friction angle (if it exists) are commonly discarded (Tang et al., 1976; Alonso, 1976; Tobutt and Richards, 1979; Vanmarcke, 1980; Anderson et al., 1984; Li, & Lumb, 1987; Christian et al. 1994).

While approximate methods do not require prior knowledge of the shape of probability distributions of input variables, most of them (e.g., methods based on FOSM) assume zero coefficients of skewness which implies symmetric probability density functions. Various studies (Lumb, 1970; Chowdhury, 1984; Wolff, 1985; Lacasse and Nadim, 1996) showed that soil properties can have skewed distributions. Studying the stability of Clarence Cannon dam, Wolff and Harr (1987) reported that ignoring the skewness of the density function of cohesion resulted in a 50% underestimation of failure probability. Furthermore, a symmetric distribution with a low mean and a high standard deviation (e.g., effective cohesion) could imply negative values associated with the low probability tail of the distribution which is not admissible for most parameters.

In terms of ease of application, approximate methods can be reasonably handled for a limited number of input variables. As the number of variables increases (above say 4 or 5), the computations become cumbersome. More importantly, approximate methods do not provide any information about the shape of the probability density function of the factor of safety. They provide only estimates of mean and variance. An estimate of the failure probability can only be obtained by assuming a parametric shape for the density function of the factor of safety. Estimates of low probabilities, the typical case of safe structures, become very sensitive to the assumed shape (Chowdhury, 1984; Chowdhury and Tang, 1987; Mostyn and Li, 1993; Wolff, 1996).

Monte Carlo simulation is seldom applied with correlated random variables (e.g., Kim et al., 1978; Tobutt, 1982; Priest & Brown, 1983; Nguyen and Chowdhury, 1984). This is attributed, at least in the past, to the difficulties associated with generating random values in a way that preserves the correlation between variables. Also, spatial variability of soil properties is rarely addressed in studies applying Monte Carlo technique (Major et al., 1978; Tobutt, 1982; Nguyen and Chowdhury, 1985). Because of the computational effort involved in the iterative process of simulation, the use of computers is unavoidable. In most of the cited cases in Section 3.2.3, researchers had to develop software specifically tailored towards solving slope stability problems. While this might be justifiable for a research project, it is certainly not suitable for professional practice.

4. SUMMARY

Slope engineering is one of the disciplines most dominated by uncertainty. The conventional deterministic slope analysis does not account for quantified uncertainty and relies on conservative parameters/designs to deal with uncertain conditions. The impact of such subjective conservatism cannot be evaluated and past experience shows that an apparently conservative design is not a safeguard against failure. Probabilistic slope analysis, on the other hand, explicitly accounts for uncertainty. The output of the analysis, in terms of failure probability or reliability index, is a measure of the reliability of the design. Probabilistic analysis provides greater insight into design reliability, thus, enhancing the engineering judgement and improving the decision making process. It is, inevitably, the next stage in the progress of slope engineering.

To date, the impact of probabilistic techniques on professional practice is, however, trivial. The limitations, and sometimes the complexity, of the current probabilistic methods and the poor education of most engineers in statistics and probability theory are major obstacles in the face of the integration of such techniques into geotechnical practice. Clarity, simplicity and cost/time effectiveness are essential elements in order to effectively convey and communicate a probabilistic methodology to practicing engineers.

CHAPTER 5

PROBABILISTIC ANALYSIS METHODOLOGY FOR EARTH SLOPES

The awareness of the value of probabilistic analyses in geotechnical engineering, particularly in slope problems, is progressively increasing among practitioners and professional organizations. For example, probabilistic assessment is currently a requirement of the US Corps of Engineers in planning studies for the rehabilitation of hydraulic structures. Dam safety boards in most hydropower corporations (e.g., B.C. Hydro, USBR) adopted risk and probability concepts in their practice. Unfortunately, the development of resources and techniques needed to undertake this task is not adequate. Available data from site characterization programs are often scarce, probabilistic methods and techniques are either too simplified to deal with real problems or too complex for practical use, and engineers still lack proper education in statistics and probability theory. Geotechnical engineers are faced with the challenge of performing probabilistic and risk analyses with little data, limited tools and little experience (Wolff, 1996).

One of the objectives of this research is to develop a practical probabilistic slope analysis methodology that allows practicing engineers to combine statistical quantification of uncertainty together with conventional practice, experience and judgement to meet an acceptable criterion. This chapter describes the proposed methodology and the approach followed to establish a probabilistic slope design criteria.

1. A PRACTICAL PROBABILISTIC SLOPE ANALYSIS

Probabilistic slope design comprises two main stages: 1) Statistical characterization of uncertainty, and 2) Probabilistic slope stability analyses for estimating a probabilistic safety measure. A comprehensive review of the concepts and techniques commonly used in characterizing parameter uncertainty is presented in Chapter 3 and some points are further touched upon in the following sections. Model uncertainty can be a dominant factor in many classes of geotechnical problems. Several examples were cited in Chapter 3, including progressive failure, time dependent softening processes, seismic liquefaction triggering and undrained versus effective strength characterization (Morgenstern, 1995). Since our ability to reliably quantify model uncertainty is, to date, limited, this study is focused mainly on classes of problems where model uncertainty is not a significant source of uncertainty. This includes slopes of unstructured coarse grained soils, unstructured saturated fine grained soils, sliding along preexisting shear planes at residual strength, and properly compacted fills.

The recent advances in random sampling techniques and software engineering have led to the development of commercial simulation software. For example, a number of Monte Carlo simulation packages that work interactively with spreadsheet programs are commercially available; e.g., @Risk (Palisade, 1996), Crystal Ball (Decisioneering, 1996). The proposed probabilistic slope analysis methodology makes use of such advanced, yet simple, tools. The following sections detail the concepts and procedures of the proposed approach.

1.1 Deterministic Analysis

In spite of the limitations of conventional slope design practice, the body of experience attached to it is significant and should not be ignored. Exercising engineering judgement in deciding upon representative soil properties, pore pressures, failure modes and an appropriate method of analysis helps greatly in understanding the problem. Performing a deterministic slope analysis prior to any probabilistic analyses is of great value in guiding the probabilistic analysis and in the interpretation of the results.

1.2 Outline of the Proposed Methodology

The proposed probabilistic methodology is based on Monte Carlo simulation using the familiar spreadsheet program "Excel" in conjunction with @Risk (Palisade,

1996) software. Firstly, the slope problem (geometry, stratigraphy, soil properties and slip surface) and the selected method of analysis are modeled in an Excel spreadsheet. Available data are examined and uncertainties in input parameters are identified and described statistically by representative probability distributions. Only those parameters whose uncertainty is deemed crucial to the analysis need to be treated as random variables.

The simulation procedure is shown schematically in Figure 5–1. @Risk draws, at random, a value for each input variable from within the defined probability distributions. These values form input set #1 that is placed by @Risk into the spreadsheet. The spreadsheet calculates the corresponding value of the factor of safety which is stored by @Risk. The process is repeated a large number of times, *m*, to estimate the statistical distribution of the factor of safety. Statistical analysis of the output distribution allows estimating the mean and variance of the factor of safety. The failure probability, probability of the factor of safety being less than one, can also be easily estimated. The various elements of the proposed approach are discussed in more detail in the following sections.

The main probabilistic safety measure used in this study is the failure probability. However, the term "Failure Probability" is likely to raise many concerns with clients, particularly non-professional clients. Kulhawy (1996) correctly stated "..... a FS of 2 or 2.5 sounds better to the average person than a probability of failure of 1 or 2 percent. The former suggests a healthy cushion in the design, while the latter states directly that it could fail". Furthermore, the term "failure" implies that the catastrophic collapse of the slope is the only event of concern to the designer, which is not necessarily the case. The serviceability of the slope is as important as slope collapse and requires thorough evaluation and assessment. Serviceability issues may include slope movement and cracking (without the slope collapsing), high water seepage and surface erosion. In my view, different terminology needs to be adopted. The US Army (1992, 1995) used *Probability of Unsatisfactory Performance*, P_u, instead of failure probability. The same terminology, probability of unsatisfactory performance, is adopted in this study to address failure mechanisms. Another terminology, *Probability of Unsatisfactory Serviceability*, is proposed to address the serviceability criteria. The evaluation of slope serviceability is, however, beyond the scope of this study.

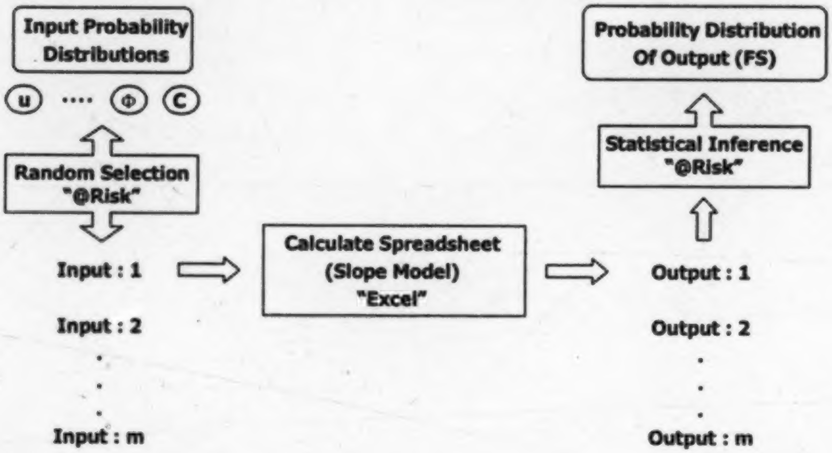
Input Probability Distributions
u ···· Φ c
Random Selection "@Risk"
Input : 1
Input : 2
Input : m
Calculate Spreadsheet (Slope Model) "Excel"
Probability Distribution Of Output (FS)
Statistical Inference "@Risk"
Output : 1
Output : 2
Output : m

Figure 5–1 Monte Carlo simulation procedure using "Excel" and "@Risk" software

1.3 Statistical Characterization of Input Variables

The statistical techniques described in Section 2 of Chapter 3 are considered, in general, adequate for the statistical characterization of the input data. The main concepts discussed in Chapter 3 are adopted in analyzing the case histories in the following chapters. However, for practicality and for simulation purposes some guidelines and simplifications are introduced as discussed below.

1.3.1 Input Random Variables

Identifying which parameters to treat as random variables is the first important step in modeling input variables. The decision depends on the observed variability in the measured values of each parameter and the sensitivity of the output (e.g., factor of safety) to variations in the magnitude of that parameter. Strength parameters and pore pressure are, typically, prime candidates. However, if judged necessary any other parameters could be treated as variables (e.g., thickness of a soft layer, Bjerrum's vane correction factor).

1.3.2 Probability Distributions

Depending on the amount of data available, different approaches can be adopted to infer the probability distribution of each parameter. Where there are significant amounts of data, greater than, say, 1000 (Deutsch, 1996), the observed distribution is considered adequate and can be used directly in the simulation. In cases where fewer data are available, a typical case in practice, the observed histogram may show spikes that would not appear were more data available. An appropriate parametric distribution can be fitted to the sample data, *histogram smoothing*, and the fitted distribution is then used instead of the original distribution. Deutsch (1996) showed that this is often a satisfactory approach provided that the data follow a parametric distribution and that the form of that distribution (e.g., normal or lognormal) is known. Unfortunately, this is seldom the case in practice. More advanced techniques for histogram smoothing (e.g., Gaussian kernel approach, simulated annealing) can be used. However, the effort involved in these techniques in relation to the gains acquired from histogram smoothing, particularly with limited data, is deemed excessive for slope stability analyses. In this study, the experimental probability distributions are used directly in the simulation process provided that a reasonable amount of data is available. The cumulative distribution function is obtained by resetting the probability associated with each data value to the average of its cumulative probability and that associated with the next lowest data (Deutsch and Journel, 1998). This eliminates, to some extent, unrealistic spikes in the probability distribution function and allows finite probabilities for data values less than data minimum and more than data maximum. The minimum and maximum limits of the distribution are assigned judgmentally.

Where data are scarce or absent, parametric distributions are assumed. Guidelines for selecting appropriate distributions for different soil parameters are available in the literature. The normal and lognormal are the most widely used distributions. In assigning a parametric distribution, care should be exercised to ensure that the minimum and maximum values of the selected distribution are consistent with the physical limits of the parameter being modeled. For example, shear strength parameters cannot take negative values. If the selected distribution implies negative values, then either a truncation limit (e.g., a practical minimum threshold) is imposed on the distribution or another distribution that does not allow negative values (e.g., lognormal) is adopted. Where no data are available, a triangular distribution based on expert opinions (minimum, maximum and most likely values) is commonly used.

@Risk built-in functions allow a great flexibility in modeling input variables. Nearly 20 parametric probability distributions (including symmetric and skewed distributions) are available in the @Risk library. Non-parametric distributions (e.g., observed cumulative distribution function, CDF) can also be modeled using special functions. Desired truncation limits can be easily imposed on any distribution either through @Risk functions or using Excel functions.

1.4 Accounting for Random Errors and Spatial Variability

As discussed in Chapter 3, current spatial variability analysis techniques are difficult to implement in practice. Some approximations guided by judgement are needed in order to account for spatial variability and spatial averaging processes in a practical manner. A simplified empirical approach is discussed below.

1.4.1 Random Measurement Errors

The reliability of the analytical quantification of random testing errors (Chapter 3) is in question. Reducing the observed data variance by an unreliable quantity that is assumed to represent the random error variance may not be sensible. Hence, random errors are not considered in this study. Instead, a critical review of the exploration program should ensure that sound engineering is being practiced. This review would include the personnel, the equipment and testing procedures. Available standards and specifications (e.g., British Standards, ASTM) greatly facilitate this task. The rationale behind this decision is explained in the following paragraphs.

Firstly, separating random testing errors (noise) from soil measurements requires data at very small separation distances ($r \approx 0$) which is never available in practice. As a result, the distinction between noise and real short scale variability (variability at distances less than data spacing) is not possible. Hence, the analytically calculated random errors (Chapter 3, Section 2.3.2.2) are, in fact, composed of random errors and short scale variability. Unfortunately, the geotechnical engineering literature often gloss over that concept and do not recognize short scale variability.

Secondly, the analytical estimates of random measurement errors greatly depend on data spacing. The smaller the spacing, the better the data reflect short scale variability and the more reliable are the estimates of random errors. Jaksa et al. (1997) analyzed the spatial variability of CPT data from two case studies in relatively homogenous clays. In the first study, the vertical spatial variability of the data was analyzed, whereas the horizontal variability was the focus of the second study. Using the method of moments, they showed that the random error variance, as a percentage of data variance, varied between 3% and 62% for the vertical data and between 3% and 50% for the horizontal data as the spacing between measurements varied between 5mm and 200mm. Using geostatistics, the estimates varied between 7% and 100% for the vertical data and between 0% and 100% for the horizontal data. They, however, demonstrated that the variability was not significant for data spacing less than 20mm. In practice, this optimum spacing is not known prior to the completion of the site investigation and it is not, usually, economically feasible to take measurements at intervals less than 20mm.

Furthermore, in a typical site investigation the spacing in the horizontal direction, between borings, is in the order of tens of metres while that in the vertical direction, between tests, is in the order of decimetres. As a result, the computed random error variance when analyzing the variability in the vertical direction may differ from that estimated through analyzing the variability in the horizontal direction, even though the data are the same. Finally, the random error variance is estimated by extrapolating an analytical function fitted, often visually, to the experimental autocovariance (or semivariogram) to a zero separation distance; a process that involves an element of subjectivity.

In addition to that, random errors are characterized by a zero mean and fluctuate in magnitude above and below the zero. In a spatial averaging process over an area or a volume, random errors tend to cancel each other thus reducing, if not eliminating, the overall random error in the averaged quantity.

1.4.2 Spatial Variability

1.4.2.1 Theoretical Background

So far, the discussions of the various aspects of spatial variability (Chapters 3 and 4) were oriented mainly towards the practical implementation of the concept. In contrast, the following sections present a more fundamental and theoretical background needed for the development of the proposed spreadsheet approach to account for spatial variability. It is thought that presenting that background in this chapter, rather than in the literature review chapters, will better illustrate the logic behind the proposed methodology.

Studies concerned with analyzing the spatial variability of geotechnical data are based, in most cases, on the theory of random fields which is also the basis of the proposed methodology. The theory of random fields is a mathematical approach that aims at modeling complex patterns of variation and interdependence of an attribute in space and/or time. The implementation of the theory in engineering practice was pioneered by the work of Vanmarcke (1977a, 1977b, 1980, 1983) which became the main references for most studies accounting for the spatial variability of geotechnical properties (e.g., Lumb, 1983; Anderson et al., 1984; Chowdhury, 1984; Tang, 1984; Li and Lumb, 1987; Wu et al., 1987; Ronold, 1990; Yucemen and Al-Homoud, 1990; Mostyn and Li, 1993; Christian et al., 1994; Lacasse and Nadim, 1996; Phoon and Kulhawy, 1999). A brief review of some of the concepts related to the proposed methodology is presented in the following paragraphs.

Within an n-dimensional space **A**, Figure 5–2, a parameter X is defined by a location vector **u** and the magnitude of the parameter $x(u)$. At a given location u_α, Figure 5–2, the parameter $X(u_\alpha)$ is an uncertain quantity to be observed or a *random variable*. Each random variable is characterized by a probability distribution and is usually correlated with the random variables at adjacent locations. The set of random variables at all locations within the space **A** is referred to as a *random field* and is characterized by the joint probability distribution of all random variables. Thus, a random variable $X(u)$ is the value of the random field at location u. Once the value of the parameter at a specific location is accurately measured, its magnitude is no longer uncertain and it becomes *deterministic*, e.g., (u_1,x_1) in Figure 5–2. Unfortunately, sampling all locations is usually impractical and unfeasible and predictions, analyses and decision-making are based on a limited number of deterministic observations (i.e., incomplete information about the random field).

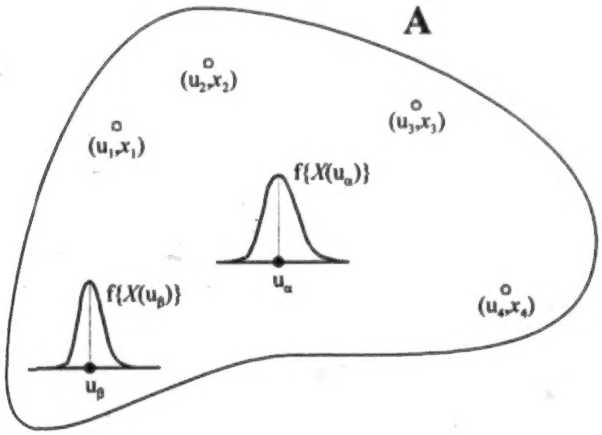

Figure 5–2 A representation of a random field **A** with its random variables and deterministic values

Several assumptions regarding the properties of the random field are often made to facilitate the inference of its characteristics based on little data. Commonly, the random field is assumed *homogenous*, *isotropic* and *ergodic*. A random field is called *homogenous* (or stationary) if the probabilistic laws, i.e. joint probability distributions, that govern the field are invariant when translated over the parameter space. This implies that all probabilities and statistical parameters depend on the relative, not the absolute, locations of the points. As a consequence, the one-point CDF, the mean and the variance are constant for any location within the domain **A** and the covariance of two random variables r distant apart is also constant regardless of their absolute locations. When the data imply a trend (i.e., non-constant mean), the trend component is removed from the observations and the residuals are modeled as a stationary random field. Once the analysis of the residuals is complete, the trend is added to the estimated parameters. The random field is *isotropic* if its probabilistic laws are the same for any direction. The field is said to be *ergodic* if the statistics of its joint probability distribution can be obtained from a single realization of the random field.

A thesis central to Vanmarcke's (1983) work on random fields is that the local point-to-point variation of the field is very difficult (if not impossible) to obtain in practice and is often of no real interest. Local averages over a spatial or temporal local domain are of much greater value. For example, the hourly or the daily rainfall depth is of interest to hydrologists rather than the instantaneous depth. Similarly, the average shear strength of a soil over a local area is of interest to geotechnical engineers rather than the point-to-point variation over the entire layer. With this view point, Vanmarcke focused on estimating the statistical characteristics of local averages including their inter-correlation as well as their correlation with point processes.

Figure 5–3 shows a one-dimensional stationary ergodic random field, e.g., a time series, with a mean E[x] and a variance σ^2 (the same process could be the variation along a line in the parameter space of a homogenous ergodic n-dimensional random field). The family of the moving local averages $X_T(t)$ over a time interval T has a mean equal to E[x]

and a variance σ_T^2 which is less than σ^2 (note; $\sigma_T^2=\sigma^2$ for T=0). Vanmarcke (1983) defined the dimensionless variance function Γ(t) which measures the reduction in the point variance σ^2 under local averaging, Equation 5-1. He showed that Γ(t) is related to the correlation function $\rho(r)$ through Equation 5-2, where r is the separation distance (or time) between data points. Vanmarcke also noted that Γ(t) decays to zero as $T \rightarrow \infty$, which is the condition of ergodicity in the mean.

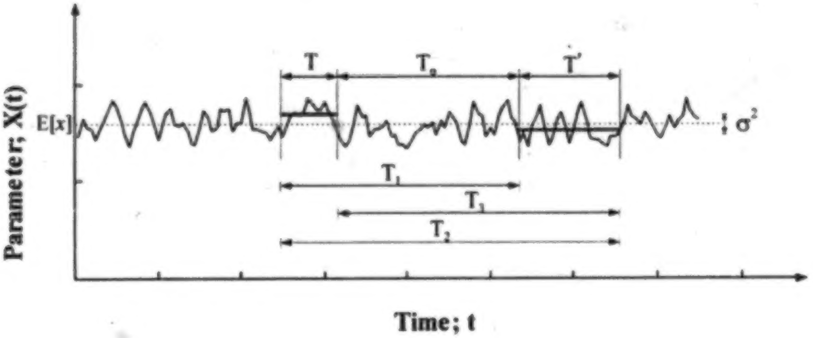

Figure 5–3 A realization of a one-dimensional random field *X*(t) showing local averages over intervals T and T'

$$\Gamma(t) = \frac{\sigma^2}{\sigma_T^2} \tag{5-1}$$

$$\Gamma(t) = \frac{2}{T}\int_0^T \left(1 - \frac{r}{T}\right)\rho(r)\,dr \tag{5-2}$$

For most correlation functions commonly used in practice (e.g., exponential, Gaussian and spherical), Vanmarcke (1983) showed that Γ(t) is inversely proportional to T at large values of T as shown in Figure 5–4. He thus introduced the *scale of fluctuation*, δ, which equals the proportionality constant and is given by Equation 5-3. It is interpreted as the interval over which the attribute shows strong correlation from point to point. The scale of fluctuation is related to the autocorrelation distance as indicated in Table 5-1.

$$\delta = \lim_{T \to \infty} T\,\Gamma(T) \qquad (5\text{-}3)$$

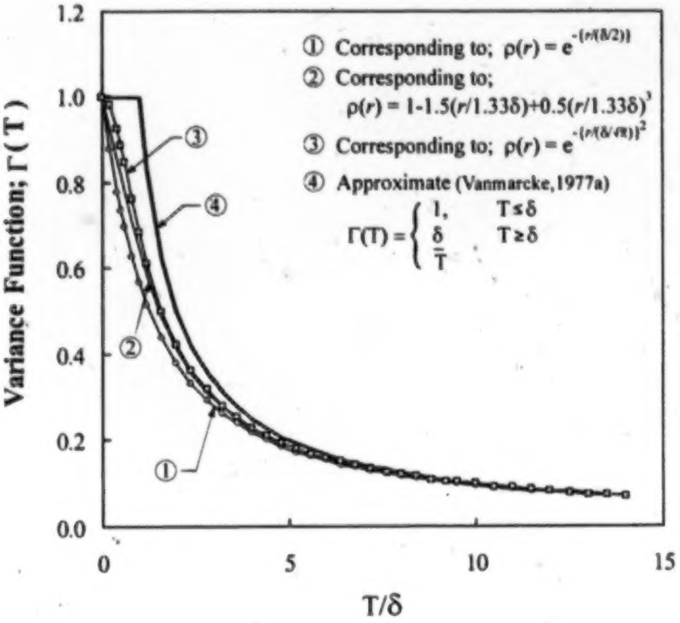

Figure 5–4 Variance function versus the averaging interval T normalized with respect to the scale of fluctuation δ for various autocorrelation models

Table 5-1 Relationship between scale of fluctuation and autocorrelation distance for exponential models

Correlation Function; $\rho(r)$	**Scale of Fluctuation; δ**
Exponential	$2r_o$
Gaussian	$\sqrt{\pi}\, r_o$

Based on Figure 5–4, Vanmarcke (1983) suggested that the variance function of a stationary ergodic one-dimensional random process could be approximated by a unique function regardless of the underlying autocorrelation function. He then proposed the approximate function given by Equation 5-4 and shown in Figure 5–4 (Vanmarcke, 1977a). The model indicates no variance reduction, $\Gamma(t)=1$, due to local averaging up to a characteristic averaging interval equal to δ. This implies that the attribute is perfectly correlated, i.e. $\rho(r)=1$, within intervals less than δ. Vanmarcke (1983) argued that trying to model a random phenomenon at a level of aggregation more detailed than the way the information about the phenomenon is acquired or processed is impractical and unnecessary. For a wide range of practical applications, the spacing or the time interval between observations is large. Characterizing the correlation structure at small intervals becomes highly unreliable, thus justifying the approximation by a perfect correlation.

$$\Gamma(T)=\begin{cases}1, & T\leq\delta\\ \dfrac{\delta}{T} & T\geq\delta\end{cases} \tag{5-4}$$

Vanmarcke (1983) also derived an expression for the correlation coefficient between a pair of local averages $X_T(t)$ and $X_T'(t)$ over time intervals T and T', Figure 5–3. The correlation coefficient, Equation 5-5, is a function of the size of the two intervals, the separation distance between them (refer to Figure 5–3) and the variance function of the parameter.

$$\rho(X_T,X_{T'})=\frac{T_o^2\Gamma(T_o)-T_1^2\Gamma(T_1)+T_2^2\Gamma(T_2)-T_3^2\Gamma(T_3)}{2TT'\{\Gamma(T)\Gamma(T')\}^{0.5}} \tag{5-5}$$

where;

T_o = distance from the end of the first interval to the beginning of the second interval.

T_1 = distance from the beginning of the first interval to the beginning of the second interval.

T_2 = distance from the beginning of the first interval to the end of the second interval.

T_3 = distance from the end of the first interval to the end of the second interval.

1.4.2.2 Autocorrelation Distance

As discussed in Chapter 3, the amounts and spacing of data from a typical site investigation program in geotechnical engineering rarely allow reliable estimates of the autocorrelation distance. In such cases, an empirical approach is proposed to account for spatial variability.

As indicated also in Chapter 3, the autocorrelation distance varies with direction. In this study, the common assumption of horizontal isotropy is adopted. The variation of the autocorrelation distance in a vertical plane is represented by an ellipse (Journel and Huijbregts, 1978) as shown in Figure 5–5. The radius of the ellipse in the horizontal direction is the horizontal autocorrelation distance, r_{oh}, and the radius in the vertical direction is the vertical autocorrelation distance, r_{ov}.

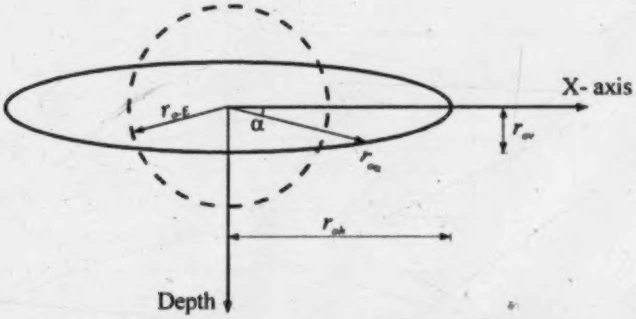

Figure 5–5 Estimation of an approximate isotropic autocorrelation distance for an anisotropic random field

As shown in Table 5-1, the scale of fluctuation, δ, is related to the autocorrelation distance, r_o, depending on the autocorrelation function. The exponential and gaussian are the functions most commonly used to describe the autocorrelation of soil properties (Vanmarcke, 1977a; Baecher, 1987; Wu et al., 1987; Christian et al., 1994; DeGroot, 1996; Lacasse and Nadim, 1996). Thus, based on Table 5-1 it can be stated that the scale of fluctuation is approximately equal to $2r_o$ in most cases.

Fenton and Vanmarcke (1991), suggested that the scale of fluctuation is largely dependent on "the geotechnical process of layer deposition" rather than the specific soil property being studied. Thus, the various properties of a soil layer could have comparable autocorrelation distances. A literature search undertaken to examine the range of the autocorrelation distance for different soils and properties forms Table 5-2. In order to reflect practice, the search focused on studies based on real projects, in which reasonable amounts of data were available and formal analyses of spatial variability were undertaken. Table 5-2 indicates that the variation in autocorrelation distances is small in spite of the different soil types, properties and testing techniques. Most values of the horizontal autocorrelation distance fall within a range of 20-40m, while the vertical distance is within 1-3m. Based on a similar review by Phoon et al. (1995), Table 5-3, Phoon and Kulhawy (1999) also noted that the vertical scale of fluctuation ranges between 1-6m while the horizontal scale of fluctuation is typically between 40-60m (note: $\delta \approx 2r_o$).

Considering the large uncertainties surrounding the analytical estimation of the autocorrelation distance using sparse or improperly-spaced (in a statistical sense) data, it is reasonable to empirically assign a value (or values) for the autocorrelation distance from within the ranges reported in the preceding paragraph. The selection of the empirical value involves two steps. Firstly, the soil data are examined to assess the likely pattern of soil variability, i.e. continuous smooth variability or erratic variations. This assessment will indicate whether the autocorrelation distance is towards the upper or lower ends of the typical ranges reported above. Such assessment would allow a subjective estimate, or a range, of the autocorrelation distance. Experience with the soil being dealt with could be of great value in that regard. For example, marine sediments tend to be homogenous with a continuous pattern of variability whereas tills and residual soils tend to be more erratic.

Table 5-2 Autocorrelation distances, r_o, (Figure 5–5) for various soil properties

Measured Soil Property	Soil Type	r_{ov} (m)	r_{oh} (m)	Reference
Field Vane Strength	Organic soft clay	1.21 3.11	- -	Asaoka and A-Grivas, 1982.
	Sensitive clay	3.0	30.0	Soulie et al., 1990
	Very soft clay	1.05	22.10	Bergado et al., 1994
	Sensitive clay	2.0	-	Chiasson et al., 1995
Unconfined Compressive Strength	Chicago clay	0.4	-	Wu, 1974
	Soft clay	2.0	40.0	Honjo and Kuroda, 1991
Normalized Undrained Shear Strength	Offshore soil (Triaxial)	3.57	-	Keaveny et al., 1989
	Offshore soil (DSS)	1.39	-	Keaveny et al., 1989
Cone Penetration Resistance	North sea clay	-	30.0	Tang, 1979
	Clean sand	1.56	-	Kulatilake and Ghosh, 1988
	North sea soil	-	13.89	Keaveny et al., 1989
	North sea soil	-	37.51	Keaveny et al., 1989
	Silty clay	1.0	-	Lacasse and de Lamballerie, 1995
	Sensitive clay	2.0	-	Chiasson et al., 1995
	Laminated clay	-	9.6	Lacasse and Nadim,1996
	Dense sand	-	37.5	Lacasse and Nadim,1996
Lift-off pressure of Flat Dilatometer	Varved clay	1.03	-	DeGroot, 1996

DSS Direct simple shear test

Table 5-3 Scale of Fluctuation, δ, for various soil properties ($\delta \approx 2r_o$)

Data	Direction	Soil Type	No. of Studies	Scale of Fluctuation δ (m)		Reference
				Range	Mean	
Cone Penetration Resistance	Vertical	Sand, Clay	7	0.1-2.2	0.9	Source: Phoon et al., 1995, pp 4-20
	Horizontal	Sand, Clay	11	3.0-80.0	47.9	
Field Vane	Vertical	Clay	6	2.0-6.2	3.8	
	Horizontal	Clay	3	46.0-60.0	50.7	
Undrained shear strength (lab. tests)	Vertical	Clay	5	0.80-6.1	2.5	
Compressibility Index	Horizontal	Sand	1	-	55.0	Vanmarcke, 1977a

The second step is to evaluate the problem being studied to decide whether the variability along a particular direction is likely to dominate the analysis. For example, the earth pressure in retaining structures is controlled by the variability of the coefficient of earth pressure with depth. Spatial variability in the vertical direction is likely to be more important to the analysis. In contrast, failure surfaces in flat cohesionless slopes tend to be superficial with a shallow dip. Since stability is controlled by the average shear strength along the failure surface, the horizontal spatial structure is likely to be more critical to the analysis. Where both the vertical and horizontal spatial structures are deemed equally important, soil variability can be roughly approximated by an isotropic spatial structure with an equivalent isotropic autocorrelation distance $r_{o\text{-}E}$. An estimate of $r_{o\text{-}E}$ can be obtained by approximating the ellipse defining the variation of the autocorrelation distance with direction by a circle of equal area as shown in Figure 5–5. Thus, $r_{o\text{-}E}$ can be calculated using Equation 5-6, where r_{oh} and r_{ov} are the autocorrelation distances in the horizontal and vertical directions, respectively.

$$r_{o\text{-}E} = \sqrt{r_{oh}\, r_{ov}} \qquad (5\text{-}6)$$

The reliability of such empirical estimates of the autocorrelation distance would improve greatly with larger soil specific and property specific databases. A parametric study using different selected values could also be very insightful. It should be noted that the impact of the autocorrelation distance on the stability analysis will vary from case to case depending on the relative contributions of systematic uncertainty and uncertainty due to soil variability. Problems dominated by systematic uncertainties are largely insensitive to the value of r_o compared to problems dominated by spatial variability. If the output of the analysis is sensitive to variations in r_o to the extent that could impair the decision-making, a rigorous estimate of the autocorrelation distance may be worth the effort. A special exploration program could be designed (in terms of the number and spacing of tests) and conducted to estimate the site and soil specific autocorrelation distances. It should be mentioned, however, that this could be an expensive solution for the typical site investigation budget of many projects.

In modeling pore water pressure, its pattern of spatial variability (e.g., autocorrelation distance) is assumed similar to that of the soil properties. The spatial structure of pore pressure is not a characteristic soil property. Rather, it is a response to the spatial variability of the flow parameters of the soil mass (e.g., hydraulic conductivity, porosity, …). It is, thus, likely that the pattern of variability of pore pressure is largely controlled by the pattern of soil variability. In other words, if the soil is uniform the variability of the pore pressure from one point to another is likely to be smooth and continuous whereas if the soil variability is erratic, the pore pressure would vary significantly over very short distances. Consequently, the smaller the autocorrelation distance, the more erratic the variability of the pore pressure and the less uncertain is the average pore pressure over an area or a surface (refer to Chapter 3). The results of Bergado and Anderson (1985) and Griffiths and Fenton (1993) confirm this hypothesis. Both conducted stochastic finite element analyses to study the variability of pore pressure due to the spatial variability of soil permeability assuming a steady-state flow through a porous medium. Bergado and Anderson (1985) reported less uncertainty in predicting the phreatic surface of water flow through an earth dam as the autocorrelation distance of permeability is decreased. Similarly, Griffiths and Fenton (1993) noted smaller standard deviation of the uplift force beneath a water retaining structure as the autocorrelation distance of permeability is reduced.

1.4.3 Modeling Uncertainty of Input Variables

Based on the review presented in Chapter 3 and the discussions in the previous sections, the uncertainty surrounding an input parameter is modeled as follows. The measured parameter at any location, u, is divided into a trend component, $t(\mathrm{u})$, and a residual value off the trend, $\varepsilon_v(\mathrm{u})$. The spatial variability of the parameter is represented by the correlation structure of the residuals. The measured quantity, $X(\mathrm{u})=t(\mathrm{u})+\varepsilon_v(\mathrm{u})$, is corrected for bias (if any) by a bias factor, B. Equation 5-7 summarizes the model adopted.

$$Z(\mathrm{u}) = B[t(\mathrm{u})+\varepsilon_v(\mathrm{u})] \qquad (5\text{-}7)$$

where $Z(\mathrm{u})$ is the random variable (corrected for bias) representing the input parameter at location u. The trend, $t(\mathrm{u})$, is estimated using the method of least squares. In cases of a linear trend, the slope and the intercept are given by Equations 3-4 and 3-5. The variances of the slope and intercept due to the limited amounts of data (statistical error) and the correlation coefficient between them are estimated using Equations 3-21, 3-22 and 3-23, respectively. In cases of a constant mean, the variance of the mean is estimated using Equation 3-20. In both cases, linear trend and constant mean, the variance estimates are based on the assumption that the residuals, $\varepsilon_v(u)$, are independent. This approximation is acceptable for most practical applications unless the measurements are very closely spaced (Baecher, 1987). Having removed the trend, the residuals are regarded as a stationary ergodic random field. The variability of an input parameter along the slip surface is then approximated by a one-dimensional random field having the statistical characteristics of the residuals.

Typically, site investigation programs in geotechnical engineering practice aim at minimizing redundant measurements by locating tests and boreholes at a large spacing. As a result, reliable assessment of the point-to-point variability of soil properties is often not possible. Numerous published studies failed in characterizing the spatial structure of soil properties in real projects due to the lack of enough data and/or the improper spacing of the available data (Wu et al., 1987; Benson, 1991; Fenton and Vanmarcke, 1991; Chiasson et al., 1995; DeGroot, 1996). In addition, all the methods of analyzing the stability of earth slopes do not require the point-to-point variability of soil properties, but rather the average operational properties over the slip surface. Therefore, it is proposed to account for soil variability along the slip surface by the variability of local averages over segments of the surface. Vanmarcke's model (Equation 5-4) is adopted for the analysis of the random fields.

Based on Vanmarcke's model, the process of local averaging a stationary ergodic one-dimensional random field over an interval not exceeding δ has the same mean and variance as the point process; $\Gamma(T) = 1$. Therefore, if the portion of the slip surface within each layer is divided into a number of segments of length $l = \delta$ plus a residual segment, the average parameter, $X(l)$, over any of these segments can be represented by the cumulative distribution function of the point measurements, $F(x)$. The correlation coefficients between any of these local averages can be estimated using Equation 5-5. For adjacent segments of equal length δ, the correlation coefficients are equal to zero which greatly simplifies the computations. The correlation coefficients between the average over the residual portion of the failure surface, of length less than δ, and those of the contiguous segments are greater than zero and can be calculated using Equation 5-5. Figure 5–6 is a schematic illustration of the model.

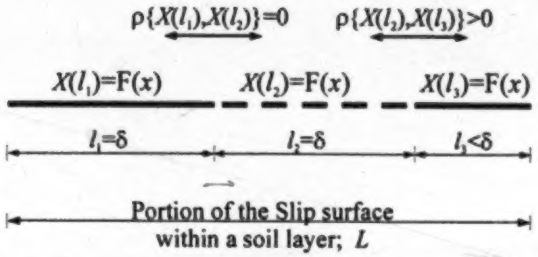

Figure 5–6 Modeling variability of an input parameter along the failure surface

In summary, the uncertainty due to the variability of an input parameter along the slip surface is accounted for by a number of correlated variables. Each of these variables represents the local average of the input parameter over a segment of the failure surface. Choosing the length of the segments equal to δ eliminates the correlation between most of the variables and greatly simplifies the simulation. Statistical uncertainty and bias are represented by random variables independent of those characterizing spatial variability. The overall uncertainty of any input parameter is a function of the three sources of uncertainty combined in accordance with the adopted model, Equation 5-7.

1.5 Critical Slip Surface

It is well established that the location and radius of critical slip circles in stability analyses depend on strength parameters. Ideally, a probabilistic analysis using Monte Carlo simulation should involve a search for the critical slip circle for each set of the randomly generated inputs. In this way, the uncertainty in the location of the critical slip surface is incorporated into the evaluation of the performance function and the estimated probability of unsatisfactory performance is associated with the slope as a whole and not with a specific surface. The computational effort and the computer time needed to search a few hundred circles for each input data set (a simulation run may involve from 10,000 up to 100,000 data sets) are, however, significant.

In practice, the problem is usually simplified by analyzing fixed slip surface(s) regardless of the values of the input data. The question, is which surface(s) to consider?

Most published studies (e.g., Vanmarcke, 1977b; Wolff, 1985; Honjo and Kuroda, 1991; Christian et al., 1994) dealt with the critical slip surface from a deterministic analysis (minimum factor of safety) using the mean values of input variables. Many researchers, however, (Tobutt and Richards, 1979; Chowdhury and Tang, 1987; Hassan and Wolff, 1999) indicated that the deterministic critical slip surface is not always the most critical surface in a probabilistic analysis. In cases where the uncertainties in the input variables contribute equally to the overall uncertainty in safety factor, the two surfaces tend to coincide. On the other hand, if one variable contributes much more than the others the two surfaces can be significantly different. For example, a slip surface with a higher deterministic factor of safety (compared to the minimum), but with a larger portion going through a layer of highly uncertain strength is likely to have a higher probability of unsatisfactory performance. This decrease in reliability is due to the increased contribution of the uncertainty in the shear strength which is not reflected in a deterministic analysis.

In a recent study Hassan and Wolff (1999) proposed a search algorithm for locating the slip circle with the minimum reliability index. The idea is to search for the slip surface dominated by the input variable whose uncertainty contributes the most to the overall uncertainty in the safety factor. They suggested performing a series of deterministic analyses with each variable, in turn, assigned a value of the mean either plus or minus one standard deviation while the other variables are kept to their mean values. Therefore, a number of deterministic analyses equal to the number of variables needs to be performed. The sign (plus or minus) is determined such that a destabilizing effect is imposed on the slope. For example, strength parameters are assigned values of the mean minus one standard deviation while the pore pressure ratio is assigned the mean plus one standard deviation. Out of these surfaces, the one with the lowest factor of safety is shown to have the lowest reliability index.

The Hassan and Wolff (1999) algorithm, however, does not directly account for a trend in the data nor for the spatial variability of soil properties and pore water pressure along the slip surface. Taking spatial variability into account could cause the increase in the variance of the factor of safety, due to the longer portion within the highly uncertain layer, to be offset by the variance reduction due to spatial averaging. Thus, in slopes dominated by the uncertainty due to spatial variability, the deterministic critical slip surface is likely to have higher probability of unsatisfactory performance than the Hassan and Wolff surface. An essential part of the analysis is to consider also any other slip surfaces that may seem hazardous. Examples may include surfaces through a weak bentonitic layer and joint controlled surfaces.

For any slope, there is an unlimited number of potential slip surfaces. The slope fails, or performs unsatisfactorily, if any of these surfaces fails. Failure is more likely, but not necessarily, to occur along the surface with the maximum computed probability of unsatisfactory performance. The total probability of unsatisfactory performance of a slope is, thus, the joint probability of the failure occurring along any of the admissible slip surfaces. As such, the probability associated with the most critical surface is a lower bound to the total probability of unsatisfactory performance of the slope. The mathematics for estimating the total probability of unsatisfactory performance are not yet developed (Wolff, 1996). However, the probability estimate based on the most critical failure surface is considered an adequate representation of slope reliability (Vanmarcke, 1977b; Alonso, 1976; Yucemen and Al-Homoud, 1990). This approximation is based on the fact that all surfaces are analyzed using the same input variables and the same analytical model. As a result, they tend to be highly correlated which significantly reduces the difference between total probability of unsatisfactory performance and that of the most critical surface (Mostyn and Li, 1993). In addition, potential critical slip surfaces tend to be close to one another. This introduces additional element of spatial correlation which further reduces the difference between total probability and that of the most critical surface.

In this study, the probability of unsatisfactory performance is obtained by independently analyzing a number of fixed slip surfaces. The highest estimated probability of unsatisfactory performance is considered representative of the total probability of unsatisfactory performance of the slope. The failure surfaces are selected to reflect: the engineer's judgement of potentially critical failure modes (e.g., non-circular joint controlled surfaces); the deterministic critical slip surface; and, the minimum reliability index surface according to Hassan and Wolff (1999).

1.6 Spreadsheet Modeling

Modeling a slope problem in a spreadsheet follows, more or less, the same sequence as hand calculations. It comprises three main steps as follows.

1.6.1 Geometry, Stratigraphy and Input Parameters

To facilitate experimenting with the input parameters and the different potential slip surfaces, the spreadsheet is designed to largely automate the computations. The geometry of the slope, the slip surface and the stratigraphy are modeled using the principles of analytical geometry. The equations describing the various boundaries (lines and circles) with reference to a coordinate system are established, Figure 5–7, and modeled in the spreadsheet. The coordinates of the points of intersection between the boundaries (e.g., points 1-5 in Figure 5–7) can be easily obtained within the spreadsheet and used in calculating the slice information (e.g., width, coordinates of mid base point, total height and thickness in each soil type).

The input parameters (e.g., soil properties, pore pressure ratio, vane correction factor) are then added to the spreadsheet, Figure 5–8. @Risk functions are used to assign appropriate probability distributions for the input variables (shaded cells). The total uncertainty of any input parameter is modeled in accordance to Equation 5-7. It is regarded as the sum of two variables representing soil variability and statistical errors multiplied by a third variable representing bias. For example, the spatial variability of the effective cohesion of the silty sand layer in Figure 5–7 is described by a lognormal distribution with a 5.0 kPa mean and a 1.5 kPa standard deviation {@Risk function: RiskLognorm(5,1.5) in Figure 5–8}. The uncertainty in the mean (i.e., statistical uncertainty) is represented by a normal distribution with a zero mean and a standard deviation of 0.23 kPa and is added to the variable representing spatial variability.

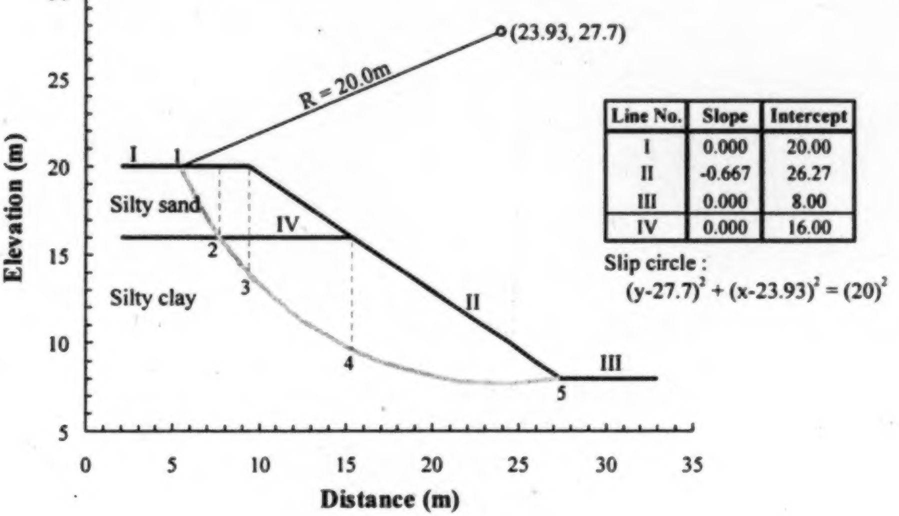

Line No.	Slope	Intercept
I	0.000	20.00
II	-0.667	26.27
III	0.000	8.00
IV	0.000	16.00

Slip circle :
$(y-27.7)^2 + (x-23.93)^2 = (20)^2$

Figure 5–7 Modeling geometry, stratigraphy and slip surface

1.6.2 Modeling Spatial Variability

The proposed scheme to account for spatial variability, Section 1.4.3, can be easily modeled in a spreadsheet. The failure surface within each soil layer is divided into segments of length δ and a segment of length equal to the residual portion as shown in Figure 5–9. The variability of a soil property along the failure surface is represented by a number of variables equal to the number of segments. Each variable is assigned the point CDF of the measurements and represents the local average of the soil parameter over the length of the corresponding segment. All variables are uncorrelated except for the residual segment and that contiguous to it (e.g., segments 3 and 4, Figure 5–9). The correlation coefficient is modeled using @Risk functions "IndepC" and "DepC". In any simulation iteration, a value is sampled for each variable such that the correlation coefficients between the variables are preserved. Thus, the soil parameter along the slip surface is represented by a number of values corresponding to the different segments. For example, the friction angle along the failure surface within the silty clay layer (Figure 5–9) is represented by 4 values (corresponding to segments 1 to 4) sampled from four probability distributions with the same mean and standard deviation; N(25,2.5).

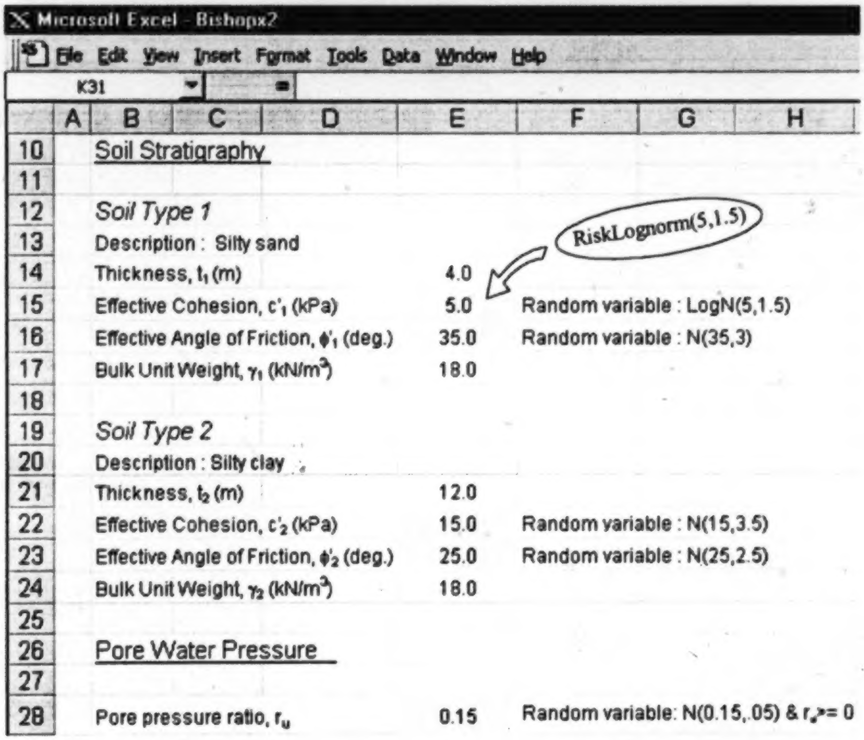
Microsoft Excel - Bishopx2
File Edit View Insert Format Tools Data Window Help
K31
=

	A	B	C	D	E	F	G	H
10		Soil Stratigraphy						
11								
12		*Soil Type 1*						
13		Description : Silty sand						
14		Thickness, t_1 (m)			4.0			
15		Effective Cohesion, c'_1 (kPa)			5.0	Random variable : LogN(5,1.5)		
16		Effective Angle of Friction, ϕ'_1 (deg.)			35.0	Random variable : N(35,3)		
17		Bulk Unit Weight, γ_1 (kN/m^3)			18.0			
18								
19		*Soil Type 2*						
20		Description : Silty clay						
21		Thickness, t_2 (m)			12.0			
22		Effective Cohesion, c'_2 (kPa)			15.0	Random variable : N(15,3.5)		
23		Effective Angle of Friction, ϕ'_2 (deg.)			25.0	Random variable : N(25,2.5)		
24		Bulk Unit Weight, γ_2 (kN/m^3)			18.0			
25								
26		Pore Water Pressure						
27								
28		Pore pressure ratio, r_u			0.15	Random variable: N(0.15,.05) & r_u>= 0		

RiskLognorm(5,1.5)

Figure 5–8 Modeling input variables in the spreadsheet

Alternatively, the probability distribution of the average soil parameter along the entire length of the failure surface can be estimated and used directly in the stability analysis. The probability distribution of the average property is the weighted sum, in terms of length, of the correlated variables representing the local averages over the segments of the failure surface. Monte Carlo simulation could be used in a separate spreadsheet to estimate the CDF of the average property prior to the stability analysis. The variance of the average property using this simulation scheme is the same as that obtained by the common approach of the variance reduction factor, *f*. Using the CDF of the average property in the stability analysis simplifies spreadsheet modeling and Monte Carlo simulation. However, it introduces some approximation by smoothing the variability along the failure surface into a single average variable. A comparison of the two approaches is presented in the following chapters.

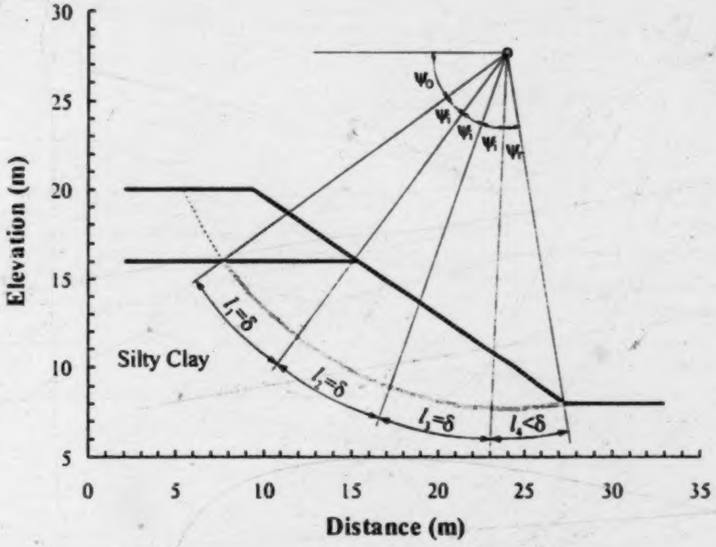

Figure 5–9 Accounting for spatial variability in the spreadsheet model

1.6.3 Slope Analysis Methods

Many of the slope analysis methods commonly used in practice (e.g., Bishop, Janbu, Spencer) can be easily modeled in a spreadsheet. In this study the Bishop and Spencer methods are used for analyzing the case studies in the following chapters. The notations and symbols used are illustrated in Figure 5–10. The force Q is the resultant of the inter-slice forces Z_k and Z_{k+1} and has an angle ξ with the horizontal; x and y are the coordinates of the points of interest; W is the weight of the slice; P, τ and u are the total normal stress, shear stress and pore water pressure at the base of the slice, respectively.

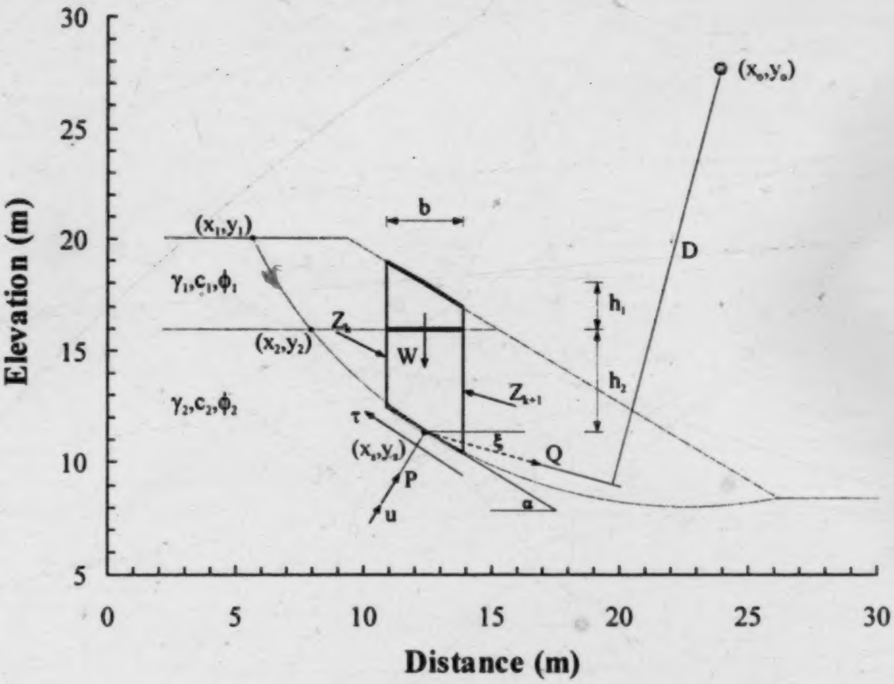

30
25
20
15
10
5
0
5
10
15
20
25
30
Elevation (m)
Distance (m)
(x_o,y_o)
b
(x_1,y_1)
D
γ_1,c_1,ϕ_1
h_1
Z_k
(x_2,y_2)
W
h_2
Z_{k+1}
γ_2,c_2,ϕ_2
τ
ξ
Q
(x_s,y_s)
P
u
α

Figure 5–10 Notations and symbols used in stability analysis

1.6.3.1 Bishop's Simplified Method of Slices

Bishop's method of slices is based on moment equilibrium only assuming that the summation of the vertical components of Z_k and Z_{k+1} is equal to zero. The spreadsheet model is built by creating a calculation table similar to that proposed by Bishop (1955) for hand computations, Figure 5–11. The appropriate soil parameters for each slice are automatically chosen by a series of nested 'IF' statements (an Excel function) that compares the x-coordinate of the mid-base point (x_s) with the coordinates of the key points established in Section 1.6.1 (points 1-5 in Figure 5–7). Excel 'circular reference' feature is used for the iteration process untill the difference between the assumed and the calculated factors of safety is within the user-specified range (≤ 0.002 in the example problem). Initially, the values of the factor of safety "F" in column 'O' (Figure 5–11) are set to an arbitrary value, say F=1. The equation in cell: M66 is established (the division of the resisting and driving moments: P64/L64), then the arbitrary value in column 'O' is replaced by cell: M66.

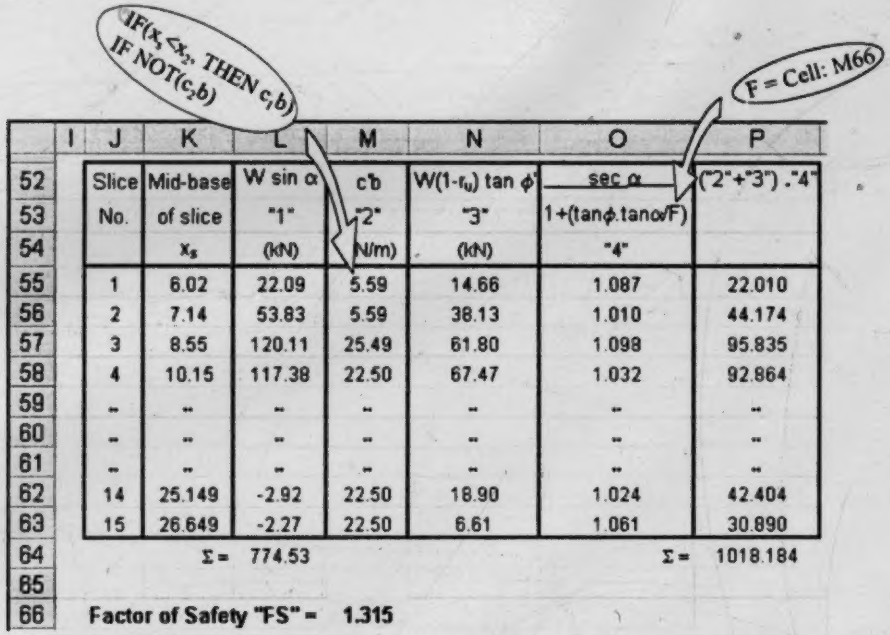
IF(x_s<x_2, THEN c_1b) IF NOT(c_2b)

F = Cell: M66

	I	J	K	L	M	N	O	P
52		Slice	Mid-base	W sin α	c'b	W(1-r_u) tan ϕ'	$\sec\alpha$	("2"+"3") ."4"
53		No.	of slice	"1"	"2"	"3"	$1+(\tan\phi.\tan\alpha/F)$	
54			x_s	(kN)	N/m)	(kN)	"4"	
55		1	6.02	22.09	5.59	14.66	1.087	22.010
56		2	7.14	53.83	5.59	38.13	1.010	44.174
57		3	8.55	120.11	25.49	61.80	1.098	95.835
58		4	10.15	117.38	22.50	67.47	1.032	92.864
59		--	--	--	--	--	--	--
60		--	--	--	--	--	--	--
61		--	--	--	--	--	--	--
62		14	25.149	-2.92	22.50	18.90	1.024	42.404
63		15	26.649	-2.27	22.50	6.61	1.061	30.890
64			Σ =	774.53			Σ =	1018.184
65								
66		Factor of Safety "FS" =			1.315			

Figure 5–11 Spreadsheet calculations for Bishop's Method of slices (example in Figure 5–7)

1.6.3.2 Spencer's Method of Slices

Spencer's method (Spencer, 1967) satisfies both moment and force equilibrium and is based on the assumption that the resultant inter-slice force, Q, has a constant angle with the horizontal, ξ, throughout the slope. As in Bishop's model, the appropriate soil parameters for each slice are automatically chosen by a series of nested 'IF' statements. The spreadsheet is established by rearranging the force and moment equilibrium equations in a tabular form, as shown in Figure 5–12. The solution for the factor of safety involves three simultaneous iterative processes using the Excel circular reference feature as shown in Figure 5–12. For an assumed value of the angle ξ, the spreadsheet solves the moment equilibrium equation by iteration untill the difference between the assumed and calculated moment factors of safety, F_m (cell: H92), is within the user-defined range ($\leq$ 0.005 in the example problem). Simultaneously, another iterative process is performed to calculate the force equilibrium factor of safety, F_f (cell: K92). The absolute difference between the two factors of safety (cell: I93) is calculated in percent and compared with the user specified acceptable limit. If the difference exceeds the limit, another value of the angle ξ is assumed and the whole process is repeated. To minimize the iteration time the angle ξ is changed by fixed increments defined by the user (0.2 degrees in Figure 5–12) such that ξ increases when $F_m > F_f$ and decreases when $F_m < F_f$ (Spencer, 1967).

1.7 Issues in Simulation

1.7.1 Random Sampling

Monte Carlo simulation requires the generation of random numbers, between 0 and 1, which are used in sampling the cumulative distribution functions (CDFs) of the input variables. @Risk allows two sampling techniques namely; Monte Carlo sampling (or random sampling) and Latin Hypercube sampling. A problem often encountered with Monte Carlo sampling is the clustering of the randomly selected values at the central part of the CDF, thus missing the low and high probability portions of the curve which correspond to the extreme values at the upper and lower tails of the distribution. Failure occurs mainly because of these extreme values (e.g., very low shear strength, very high pore pressure ratio). Unless an enormous number of iterations is used, Monte Carlo sampling could miss these extremes resulting in a misleadingly low probabilities of unsatisfactory performance.

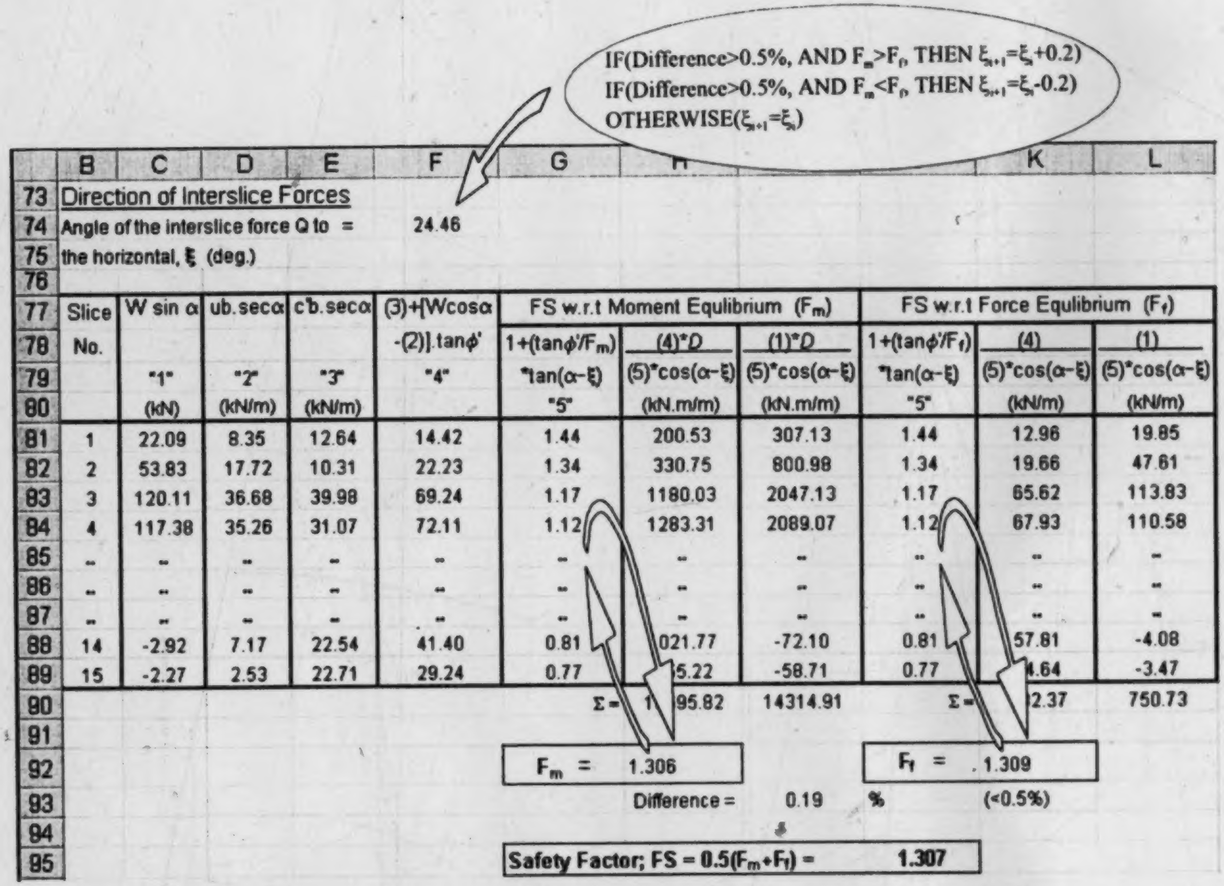

IF(Difference>0.5%, AND $F_m>F_f$, THEN $\xi_{s+1}=\xi_s+0.2$)
IF(Difference>0.5%, AND $F_m<F_f$, THEN $\xi_{s+1}=\xi_s-0.2$)
OTHERWISE($\xi_{s+1}=\xi_s$)

	B	C	D	E	F	G	H			K	L
73	Direction of Interslice Forces										
74	Angle of the interslice force Q to =				24.46						
75	the horizontal, ξ (deg.)										
76											
77	Slice	W sin α	ub.secα	c'b.secα	(3)+[Wcosα	FS w.r.t Moment Equlibrium (F_m)			FS w.r.t Force Equlibrium (F_f)		
78	No.				-(2)].tanφ'	1+(tanφ'/F_m)	(4)*D	(1)*D	1+(tanφ'/F_f)	(4)	(1)
79		"1"	"2"	"3"	"4"	*tan(α−ξ)	(5)*cos(α−ξ)	(5)*cos(α−ξ)	*tan(α−ξ)	(5)*cos(α−ξ)	(5)*cos(α−ξ)
80		(kN)	(kN/m)	(kN/m)		"5"	(kN.m/m)	(kN.m/m)	"5"	(kN/m)	(kN/m)
81	1	22.09	8.35	12.64	14.42	1.44	200.53	307.13	1.44	12.96	19.85
82	2	53.83	17.72	10.31	22.23	1.34	330.75	800.98	1.34	19.66	47.61
83	3	120.11	36.68	39.98	69.24	1.17	1180.03	2047.13	1.17	65.62	113.83
84	4	117.38	35.26	31.07	72.11	1.12	1283.31	2089.07	1.12	67.93	110.58
85	--	--	--	--	--	--	--	--	--	--	--
86	--	--	--	--	--	--	--	--	--	--	--
87	--	--	--	--	--	--	--	--	--	--	--
88	14	-2.92	7.17	22.54	41.40	0.81	021.77	-72.10	0.81	57.81	-4.08
89	15	-2.27	2.53	22.71	29.24	0.77	5.22	-58.71	0.77	4.64	-3.47
90						Σ =	1 95.82	14314.91	Σ =	2.37	750.73
91											
92						F_m =	1.306		F_f =	1.309	
93							Difference =	0.19	%	(<0.5%)	
94											
95						Safety Factor; FS = 0.5(F_m+F_f) =			1.307		

Figure 5–12 Spreadsheet model for Spencer's method of slices (example in Figure 5–7)

Latin Hypercube sampling is adopted in this study. It was first proposed by McKay et al. (1979) and is shown to be efficient in dealing with events of low probabilities. The probability range of the CDF (0 to 1) is divided into a number of intervals (or layers) equal to the number of iterations, *m*. All layers would have equal probabilities of 1/*m* (i.e., equal weights). Sampling proceeds by randomly selecting an interval and then randomly sampling a value from within this interval, Figure 5–13. The process is performed without replacement (i.e., each interval is sampled only once) thus ensuring that the full range of the CDF is represented. Sampling of each input variable is conducted independently of other variables to ensure complete randomness, unless otherwise desired.

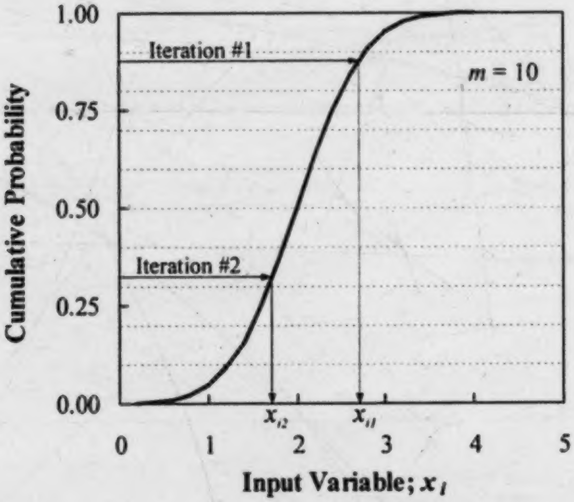

Figure 5–13 Latin Hypercube sampling with 10 iterations

An important feature of @Risk is the ability to handle correlated input variables. The correlations are expressed using the Spearman Rank Correlation Coefficient. It is calculated using the "rank" of data values, not the actual values themselves. The rank of a data point is its position within the observed minimum to maximum range. The rank correlation coefficient has the advantage of being more reliable than the traditional correlation coefficient when the data exhibit a non-linear relationship and/or the input variables are not normally distributed. Walpole and Myers (1978) pointed, however, that the two coefficients are usually very close.

@Risk generates correlated sets of random numbers (between 0 and 1) such that the input rank correlation coefficient matrix is preserved. These numbers are then used in sampling the input distributions of the correlated variables. The recreated distributions, by sampling, reflect the input CDFs as well as the correlation between the variables.

1.7.2 Number of Iterations

The output of a simulation process is sensitive to the number of iterations, m. When m is large, the number of random samples drawn for each input variable is also large and the match between the distribution recreated by sampling and the original input distribution is more accurate. As a result, the output quantity becomes more stable at the expense of increasing computer time. By sampling every portion of the CDF, the Latin Hypercube technique helps reduce the number of iterations needed to attain a stable solution. The optimum number of iterations depends on the variability in the input parameters (i.e., standard deviation) and the output parameter being estimated (e.g., mean safety factor, probability of unsatisfactory performance). A simple practical way to optimize the simulation process is to run the simulation a few times using a constant seed value and an increasing number of iterations. The number of iterations m is then plotted versus the output of interest (e.g., probability of unsatisfactory performance), Figure 5–14. When the number of iterations is small, the scatter of the estimated probability of unsatisfactory performance is significant. As m increases, the level of noise in the output diminishes and the sensitivity of the estimated probability to the number of iterations decreases. The minimum number of iterations at which the desired output quantity stabilizes, Figure 5–14, is the optimum number of iterations.

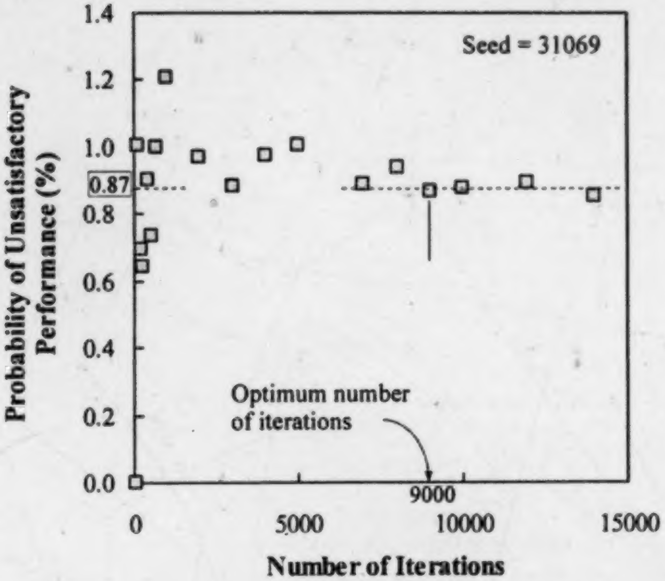

Figure 5–14 Optimum number of iterations for estimating probability of unsatisfactory performance

1.8 Interpretation of the Output

1.8.1 Probability of Unsatisfactory Performance

The main output of the simulation is the probability density function of the factor of safety from which the mean and standard deviation can be inferred. The probability of unsatisfactory performance is the probability of the factor of safety being less than one, or simply the number of iterations with FS ≤ 1.0 relative to the total number of iterations, *m*. It is commonly interpreted as the percentage of *m* identical structures that could fail. The physical meaning of this interpretation is, however, not appealing. In reality there would never be *m* identical structures and there is no assurance that failure will occur even with a non-zero probability of unsatisfactory performance. It is probably more meaningful to interpret it as the probability of the demand on the slope, i.e. the destabilizing forces, exceeding its capacity, or the resisting forces.

An important point to keep in mind is that the computed probability of unsatisfactory performance is an indication of whether the slope is likely to perform satisfactorily or not without any consideration of time effects. If, for example, soil strength degrades or improves throughout the service life of the structure, the impact of time on stability can only be assessed by other analyses using revised strength probability distributions. The same concept applies when accounting for temporal changes in pore water pressure.

Since the simulation process is based on random sampling of input variables, the calculated probability of unsatisfactory performance is also a variable. The value estimated from a single simulation could differ, for that particular simulation, from the true value. Law and McComas (1986) described relying on the results of a single simulation run as one of the most common and potentially dangerous simulation practices. It is, therefore, essential to repeat the simulation a few times using different seed values to ensure consistency in the estimates. In fact, it is even desirable to run the simulation many times to estimate the histogram of the probability of unsatisfactory performance. Estimates of the mean probability and the 95% confidence interval around the mean are revealing. Using @Risk "Macro" functions, the process of running a number of simulations can be fully automated. A simple Macro file can be designed to run a number of simulations and save the output of each simulation in a separate file without any human involvement.

While there is a strong desire to estimate the actual probability of unsatisfactory performance, we are still unable to do so. In spite of the effort by the designer to address all sources of uncertainty, there is always the possibility of undetected uncertainties (e.g., human mistakes) affecting the slope performance. The contribution of these unknown uncertainties to the probability of unsatisfactory performance is not considered and the computed probability could be a lower bound to the actual probability. That is why the comparison between computed probabilities of different designs is believed to be of greater value. This, however, should not be an excuse to delay or avoid the implementation of probabilistic and risk analysis techniques that require absolute values while awaiting a complete flawless approach that may never be achieved. It is our responsibility, as professionals, to continuously search for more advanced tools to better understand and control the influence of the various sources of uncertainty on safety, at least those sources that we can control.

1.8.2 Sensitivity Analysis

Through @Risk, a sensitivity analysis can be performed to assess the relative significance of the input variables to the determination of the output variable. In other words, the relative contributions of each input variable to the overall uncertainty in the factor of safety. This contribution reflects the physical impact the parameter has on the slope performance as well as its uncertainty. For example, a highly uncertain unit weight may still contribute little to the uncertainty of the safety factor. On the contrary, a large portion of the slip surface going through one layer may cause the factor of safety to be highly sensitive to the uncertainty in the shear strength of this layer even though it may not be the highest among input variables. The results of the sensitivity analysis are extremely useful in practice as they identify the most critical variable(s) in the analysis. Resources can, therefore, be rationally allocated towards reducing the uncertainty of these variables.

Two different techniques are used by @Risk for sensitivity analysis: multivariate stepwise regression analysis and rank order correlation analysis. The former is less reliable when the inputs are non-linearly related to the output. The rank correlation analysis is used in this study. The value of the rank order correlation coefficient (Spearman Coefficient) varies between 1 and –1. A value of zero indicates no correlation between the input variable and the output. A value of 1 indicates a complete positive correlation and a value of –1 indicates a complete negative correlation.

2. ADVANTAGES OF THE PROPOSED METHODOLOGY

The proposed methodology, as described in the preceding sections, overcomes many limitations of the existing techniques (Chapter 4). Firstly, and probably most importantly, it is simple, intuitive and compatible with conventional slope design practice. The procedures and concepts are transparent and understandable requiring only fundamental knowledge of statistics and probability theory. No computer programming is needed, only familiarity with spreadsheet programs. This is likely to make it more appealing to practicing engineers. In addition, by having to actually model the slope problem in a spreadsheet and to experiment with the input variables the engineer gains significant insight into the analysis and gets to appreciate the critical parameters. This greatly enhances understanding of the problem and improves the decision-making process.

The methodology is very flexible in handling a wide variety of slope problems. These include various loading conditions, complex stratigraphy, c-ϕ soils, a large number of input variables, almost any input probability distribution function (including non-parametric distributions), slip surfaces of any shape and many of the slope analysis methods. The rapidly developing features of spreadsheet programs are promising further capabilities in handling even more complex problems. In addition, the analysis can be very easily updated upon obtaining any new information by simply changing few cells in the spreadsheet and running a new simulation. Spatial variability and correlation between input variables can be readily and transparently accounted for. Furthermore, the analysis yields the probability distribution function of the factor of safety thus eliminating the need to assume a parametric shape. Finally, the economics of the analysis, in terms of computer system requirements and time, are reasonable.

3. LIMITATIONS OF THE PROPOSED METHODOLOGY

While the proposed probabilistic methodology overcomes most of the shortcomings of the current methods, it is has some limitations. First, modeling spatial variability in the proposed approach is based on the approximate variance function proposed by Vanmarcke (1977a). The function implies a perfect correlation, $\rho(r) = 1.0$, for separation distances, r, less than the scale of fluctuation, δ, and no correlation, $\rho(r) = 0$, for *r* values greater than δ. This sudden drop from a perfect correlation to a total lack of correlation is, clearly, an approximation. In reality, the correlation between soil properties at two locations decreases gradually as the separation distance increases. The impact of that approximation on the output of a slope analysis is on the conservative side. More rigorous models accounting for the gradual decay of the autocorrelation function (e.g., Vanmarcke, 1983) could be incorporated in the spreadsheet. This, however, would result in a drastic increase in the number of correlated variables requiring advanced computing capabilities beyond those of a commercial spreadsheet-based simulation software. Also, the application of the proposed methodology is governed by the capabilities of spreadsheet programs. Some of the more advanced and complex slope stability methods (e.g., Morgenstern-Price method, 3-D methods) are, for now, cumbersome to model in a spreadsheet. The rapid development in software, however, will soon overcome these limitations.

Second, spatial averaging of the pore water pressure along the failure surface is based on the assumption that the spatial structure of the pore pressure ratio is similar to that of the soil properties. Qualitatively, this assumption is thought to be true. However, the quantitative relationship between the spatial variability of soil properties and that of the pore pressure is not known. Unfortunately, there are very few studies addressing the spatial variability of pore water pressure. In fact, the author is aware of only 3 such studies (Hachich and Vanmarcke, 1983; Bergado and Anderson, 1985; Griffiths and Fenton, 1993). The three studies tried to quantify the variability of the piezometric head (or phreatic surface) due to the spatial variability of soil permeability assuming a steady-state laminar flow through a porous saturated incompressible medium. The problem is, however, much more complex. The spatial variability of pore water pressure is a response to a number of highly variable and interacting phenomena. These include rainfall intensity, rate of infiltration, regional and local flow patterns, spatial variability of hydraulic conductivity and state of stress. The problem is further complicated with time being a pertinent dimension. Pore pressures tend to vary over relatively short periods of time; the variations can be significant and rapid in tropical areas, for example. The enormous complexity of the problem and the often sparse data available are the main reasons behind the scarcity of studies. More research is certainly needed in that area.

4. ESTABLISHING PROBABILISTIC SLOPE DESIGN CRITERIA

Having estimated the probability of unsatisfactory performance, the next step is to assess whether it is acceptable or not. This is achieved through comparing the computed values with acceptable limits, or probabilistic slope design criteria. Establishing these criteria is, however, not easy. One option is to estimate them based on the actual failure rate from a comprehensive survey of case histories combined with judgement and experience. Typical values in the literature are in the range of 10^{-3} to 10^{-4} (e.g., Meyerhof, 1970; US Army, 1995). A major drawback to this approach is that the site/case specific features are not considered. In other words, the geometry, site conditions and sources and levels of uncertainty (e.g., soil variability, depth of investigation, adequacy of design models, quality of construction) of the case histories constituting the database are not addressed. Applying such a global criterion to any slope is a very crude generalization.

Another common approach is to calibrate the computed probabilities with experience and observed performance of existing structures. In addition to building upon the available body of experience in slope design, this approach helps maintain the compatibility between probabilistic and conventional design methods (Kulhawy, 1996). In this research, a major study is undertaken to calibrate current, acceptable slope design practice in probabilistic terms. Case histories of slope failures are redesigned based on conventional practice (deterministic analysis combined with judgement) and accounting for the fact that the slope failed. The revised designs are then analyzed probabilistically using the proposed methodology. The probabilities of unsatisfactory performance of other slopes performing adequately (e.g., Syncrude tailings dyke) are also estimated. The computed values from both categories (failed and safe) are assessed and an upper limit of the acceptable probability of unsatisfactory performance is proposed.

The calibration process is also repeated with the probabilistic stability analyses based directly on the probability distributions of the measured data with minimal statistical analysis. Statistical treatment of the data is limited to excluding outlier values and redundant measurements due to clustering, calculating means and standard deviations and constructing the probability distribution functions (CDFs). The issues of spatial variability, spatial averaging and statistical uncertainty are not addressed. It should be mentioned that some geostatisticians consider this a "naïve" approach. In the light of the increasing complexity of the more rigorous probabilistic analyses, it is thought that investigating whether such a simple and common approach could be of any value, even as a preliminary assessment, is worth the effort.

CHAPTER 6

APPLICATION OF THE PROPOSED PROBABILISTIC SLOPE ANALYSIS METHODOLOGY
JAMES BAY CASE STUDY

To illustrate the implementation and capabilities of the proposed probabilistic approach (Chapter 5) the well documented case study of the James Bay hydroelectric project is analyzed. The project was never built, however, the design was the subject of extensive studies including quantifying the various sources of uncertainty (Ladd et al., 1983; Soulie et al., 1990) and the probabilistic analysis of dykes' stability (Christian et al., 1994). The probabilistic stability analysis of Christian and his colleagues was performed using the FOSM method. Although the FOSM method is an approximate technique, the results should not differ significantly from Monte Carlo simulation. This case study, thus, provides a useful test of the proposed methodology.

1. JAMES BAY PROJECT

The proposed James Bay hydroelectric project required the construction of nearly 50 km of earth dykes in the James Bay area of Quebec, Canada. Among various design options investigated were single stage construction of the embankment to a height of either 12.0 m or 6.0 m, hereafter referred to as Design 1 and Design 2, respectively. The embankment had side slopes of 3h:1v and the 12.0 m high design included a 56 m wide berm at mid height. The subsurface investigation indicated the presence of a surface layer of peat overlying a clay crust. The crust thickness ranges between 1.0 and 6.0 m with an average of 4.0 m. The clay is of low plasticity and has an undrained shear strength that decreases with depth from about 82 kPa at surface to 35 kPa at the bottom of the crust. To account for the potential of fissures reducing the operational strength of the crust, the average strength over the bottom half of the crust, 41 kPa, is adopted for the entire thickness.

The crust is underlain by a sensitive marine clay overlying a lacustrine clay. The total thickness of the two layers varies between 8 m and 23 m with a poorly defined boundary between them. On average, the marine clay is about 8m thick and the lacustrine clay is about 6.5 m. Both clays have low plasticity. The undrained shear strength of both clays was measured by field vane tests at 1.0 m depth intervals. The data indicated a large scatter in the shear strength of both layers. The mean undrained shear strength is about 35 kPa for the marine clay and 31 kPa for the lacustrine clay. The lacustrine clay is underlain by a stiff layer of till. Figure 6–1 and Figure 6–2 show the stratigraphy and the geometry of both designs.

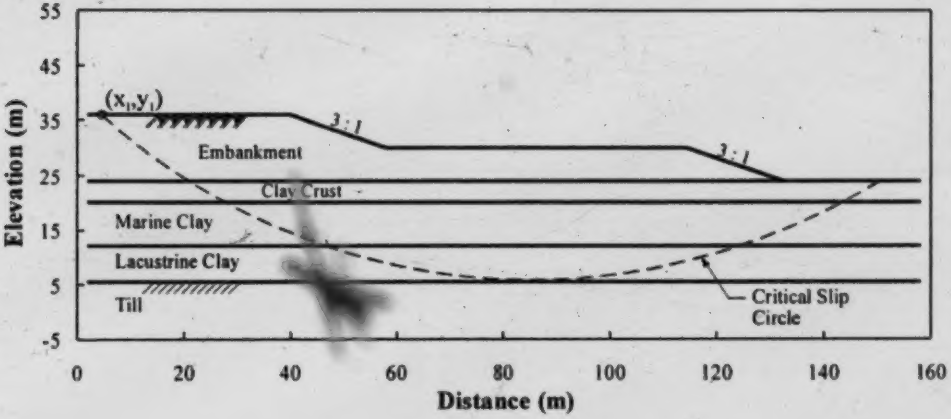

55
45
35
25
15
5
-5
Elevation (m)
(x_1,y_1)
3 : 1
3 : 1
Embankment
Clay Crust
Marine Clay
Lacustrine Clay
Till
Critical Slip Circle
0
20
40
60
80
100
120
140
160
Distance (m)

Figure 6–1 Geometry and stratigraphy of James Bay dykes; Design 1 (H = 12m)

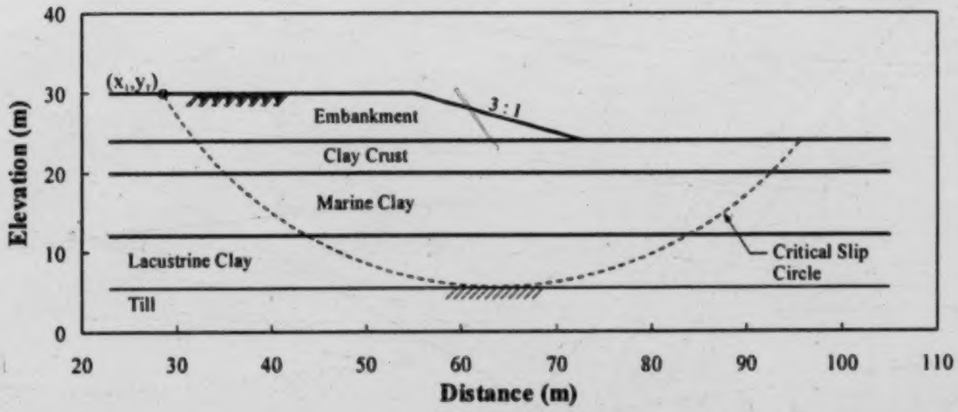

40
30
20
10
0
Elevation (m)
(x_1,y_1)
3 : 1
Embankment
Clay Crust
Marine Clay
Lacustrine Clay
Till
Critical Slip Circle
20
30
40
50
60
70
80
90
100
110
Distance (m)

Figure 6–2 Geometry and stratigraphy of James Bay dykes; Design 2 (H = 6m)

2. MONTE CARLO SIMULATION VERSUS FOSM

In order to reliably reflect on the conclusions of the proposed probabilistic approach in relation to those from the FOSM method, the differences between the Monte Carlo technique and the FOSM method are first investigated. A Monte Carlo analysis is performed to assess the stability of the dykes using the exact input variables and probability distributions defined by Christian et al. (1994), hereafter referred to as M.C.-Christian analysis. Six variables were considered as summarized in Table 6-1. All variables are assumed normally distributed. The standard deviations shown in Table 6-1 were the end result of a detailed statistical analysis of the measured data by Christian and his colleagues. The analysis included the removal of random measurement errors, estimation of statistical errors due to sample size, accounting for bias due to Bjerrum's vane correction factor and variance reduction due to spatial averaging. The differences in the standard deviations of the same variables from Design 1 to Design 2 is a result of the spatial averaging process and the difference in the lengths of the critical slip circles. Bishop's method of slices was used in the FOSM analysis (Christian et al., 1994) and Monte Carlo simulation. Deterministic slope stability analyses using Slope/W software and the mean values of input variables resulted in minimum factors of safety of 1.455 and 1.527 for Design 1 and Design 2, respectively. Figure 6–1 and Figure 6–2 show the critical slip circles for both cases.

The uncertainty in the depth of the till layer, D_{till}, is entirely systematic uncertainty due to the limited number of borings. Because of the low strength of the lacustrine clay, the depth of the till layer greatly controls the location of the critical slip circle. The uncertainty in D_{till}, thus, introduces uncertainty in the location of the slip circle. To examine the impact of this uncertainty, a series of deterministic stability analyses were performed varying D_{till} incrementally between 15.5m and 21.5m (± 3 standard deviations). For Design 1, the minimum factor of safety varied between 1.69 and 1.3 and the critical slip circles were always tangent to the top of the till, daylight within a short distance at the top of embankment (x_1 = 2.9 - 7.1 m, Figure 6–1) and have a narrow range of the x-coordinate for the centres (x_o = 85.6 - 86.5 m). For Design 2, the factor of safety varied between 1.56 and 1.51 and the critical slip circles were also tangent to the till with the coordinates of the centres varying within a narrow range (x_o = 63.5 - 63.9m, y_o = 38.7 - 43.7m). These results indicate that the uncertainty of D_{till} will have a greater impact on Design 1 than it would on Design 2. It also shows that the variations in the location of the centres of the slip circles and the daylight points at the top of the embankment are small in spite of the variations in the depth of the till layer.

Table 6-1 Input variables and statistical parameters for James Bay dykes (based on Tables 6 and 7; Christian et al., 1994)

Input Variable		Design 1① (H = 12m)	Design 2② (H = 6m)
Fill unit weight; γ_{fill} (kN/m^3)	$E[\gamma_{fill}]$	20.0	20.0
	$\sigma[\gamma_{fill}]$	1.10	1.30
Fill friction angle; ϕ_{fill} (deg.)	$E[\phi_{fill}]$	30.0	30.0
	$\sigma[\phi_{fill}]$	1.79	1.92
Thickness of clay crust; t_{cr} (m)	$E[t_{cr}]$	4.0	4.0
	$\sigma[t_{cr}]$	0.48	0.84
Strength of marine clay; S_{uM} (kPa)	$E[S_{uM}]$	34.5	34.5
	$\sigma[S_{uM}]$	3.95	5.97
Strength of Lacustrine clay; S_{uL} (kPa)	$E[S_{uL}]$	31.2	31.2
	$\sigma[S_{uL}]$	6.31	8.79
Depth of till layer; D_{till} (m)	$E[D_{till}]$	18.5	18.5
	$\sigma[D_{till}]$	1.00	1.00

① Based on a variance reduction factor, *f*, of 0.20

② Based on a variance reduction factor, *f*, of 0.70

Spreadsheet models were prepared for both designs. Since the depth of the till is considered a variable, a different value is sampled for each simulation iteration and consequently the critical slip circle varies from one iteration to another. To minimize computer time, some restrictions were imposed on the geometry of the slip circles based on the results of the parametric study in the preceding paragraph. For Design 1, the slip circles are assumed tangent to the till layer, daylight at a fixed point at the top of the embankment (x_l=4.9, y_l=36.0) and have a common x-coordinate for the centers (x_o=85.9). For Design 2, the circles were assumed tangent to the till and have a common center (x_o=63.7, y_o=42.0). The search for the critical slip circle is thus limited to one circle per iteration. The geometry of the circle is controlled by the sampled value of D_{till}.

A number of @Risk simulations were performed using a seed value of 31069 (an arbitrary value) and an increasing number of iterations to assess the optimum number of iterations needed for a stable estimate of the probability of unsatisfactory performance, Figure 6–3 and Figure 6–4. Based on these plots 14,000 iterations are needed for Design 1 and 35,000 iterations for Design 2. The increase in the number of iterations for Design 2 is attributed to the larger uncertainty of the input variables. In subsequent simulations 20,000 and 38,000 iterations were used for Design 1 and Design 2, respectively. Using a PC machine (Pentium II, 233 MHz), the computer time for the simulation was approximately 11 minutes for Design 1 and 22 minutes for Design 2.

Using a seed value of 31069, Monte Carlo simulation for Design 1 resulted in a mean factor of safety of 1.46, a standard deviation of 0.17 and a probability of unsatisfactory performance of 0.27%. For Design 2, the mean factor of safety is 1.53, the standard deviation is 0.26 and the probability of unsatisfactory performance is 1.76%. Figure 6–5 and Figure 6–6 show the histograms and the CDFs of the factor of safety. Twenty four additional simulations were run for both designs using different seed values to build up the histogram of the probability of unsatisfactory performance, Figure 6–7. The mean value of P_u for Design 1 is estimated to be 0.24% with a 95% confidence interval (assuming t-distribution) of 0.23-0.25 %. For Design 2, the mean P_u is 1.76% and the 95% confidence interval is 1.73-1.78%. Table 6-2 summarizes the results of Monte Carlo simulation and the FOSM method.

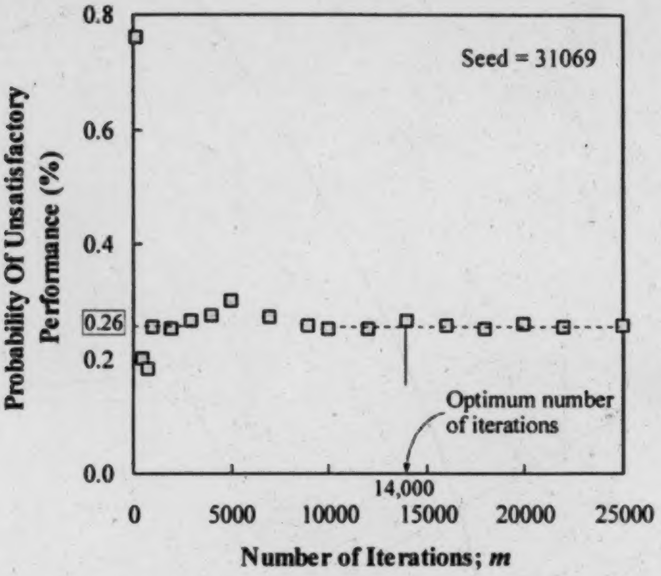

Figure 6–3 Estimating optimum number of iterations for James Bay Design 1

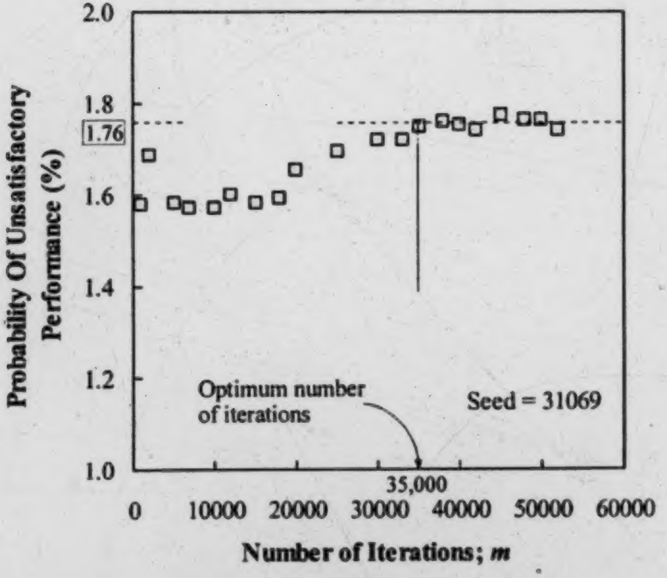

Figure 6–4 Estimating optimum number of iterations for James Bay Design 2

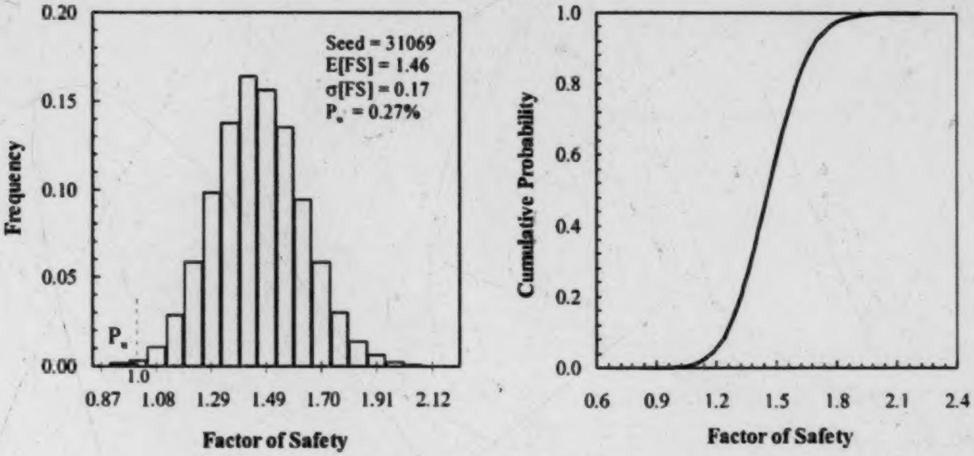

Figure 6–5 Histogram and CDF of the factor of safety, Design 1

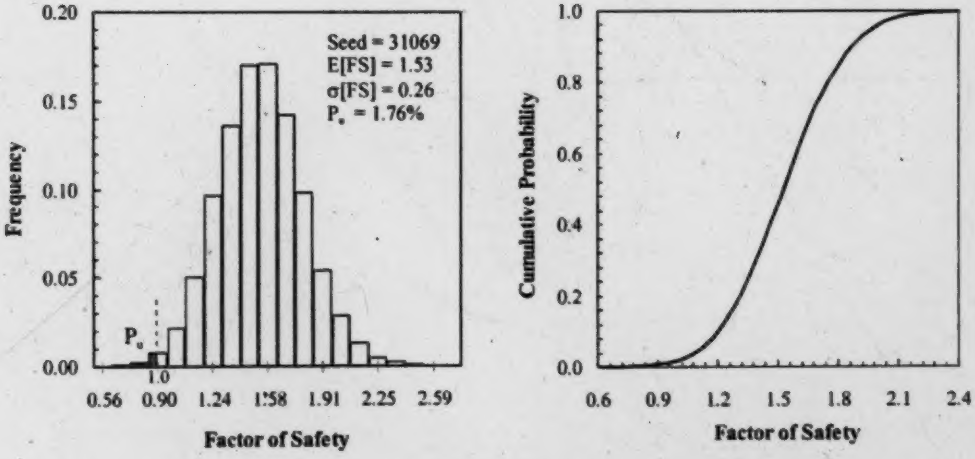

Figure 6–6 Histogram and CDF of the factor of safety, Design 2

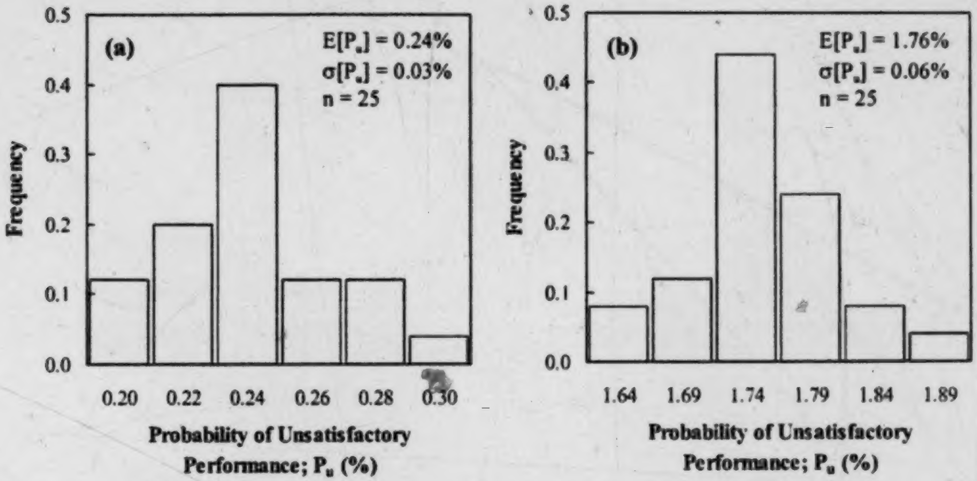

Figure 6–7 Histogram of the probability of unsatisfactory performance: a) Design 1; b) Design 2

Table 6-2 Summary of the results of Monte Carlo simulation and FOSM

	Design 1 (H = 12m)		**Design 2** (H = 6m)	
	Monte Carlo	**FOSM**①	**Monte Carlo**	**FOSM**①
E[FS]	1.46	1.45	1.53	1.50
σ[FS]	0.17	0.17	0.26	0.27
P_u (%)	0.24	0.40②	1.76	3.25②
β③	2.75	2.66	2.06	1.84

① Analysis by Christian et al. (1994)

② Assuming the factor of safety is normally distributed

③ $\beta = \frac{E[FS]-1}{\sigma[FS]}$

As discussed in Chapter 4, the FOSM is an approximate technique because it is based on the linear terms only of Taylor's series expansion. Solutions based on Taylor's series are exact only if the performance function is linear which is not the case with the factor of safety. Also, the partial derivatives of the performance function are approximated by numerical techniques. The results in Table 6-2 show, however, that the FOSM method is accurate in estimating the first two moments (mean and the variance) of the performance function. Nonetheless, the lack of any information about the shape of the probability density function of the factor of safety, particularly at the tails, combined with the minor deviations in the mean and variance can introduce some errors in estimating the probability of unsatisfactory performance as shown in Table 6-2. The magnitude of the error is likely to be higher in estimating very low probabilities.

A sensitivity analysis was performed to identify the main variables affecting the uncertainty of the factor of safety. Figure 6–8 and Figure 6–9 show Spearman rank correlation coefficients for both designs. The uncertainty in the undrained shear strength of the lacustrine clay is by far the most influential source of uncertainty in both cases. Therefore, any extra spending to improve the reliability of the design should be directed towards a better characterization of the shear strength of the lacustrine clay. The uncertainty in the unit weight of the fill comes second. As expected, the uncertainty in the depth of till has a large influence on Design 1 while it has practically no effect on Design 2. Both of the uncertainties in the thickness of the clay crust and the friction angle of the fill have a minimal impact on either design. Based on the FOSM analysis (Christian et al., 1994), the relative contributions of the various sources of uncertainty to the overall uncertainty of the factor of safety are in good agreement with the results of the sensitivity analysis.

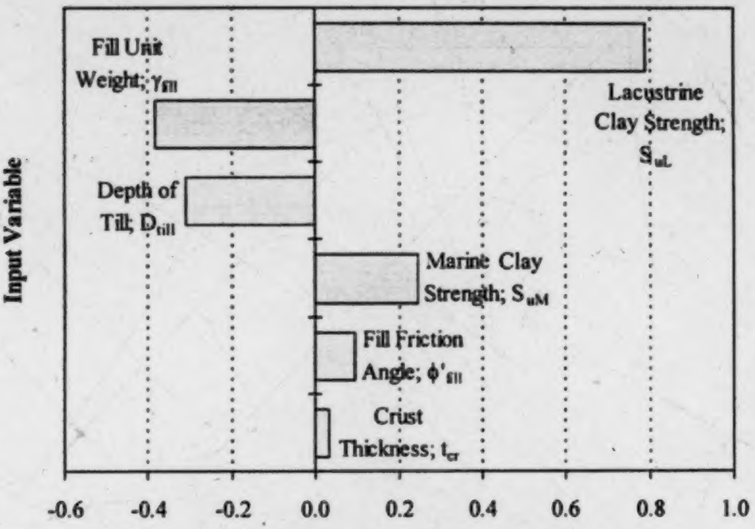

Figure 6–8 Sensitivity analysis results, Design 1

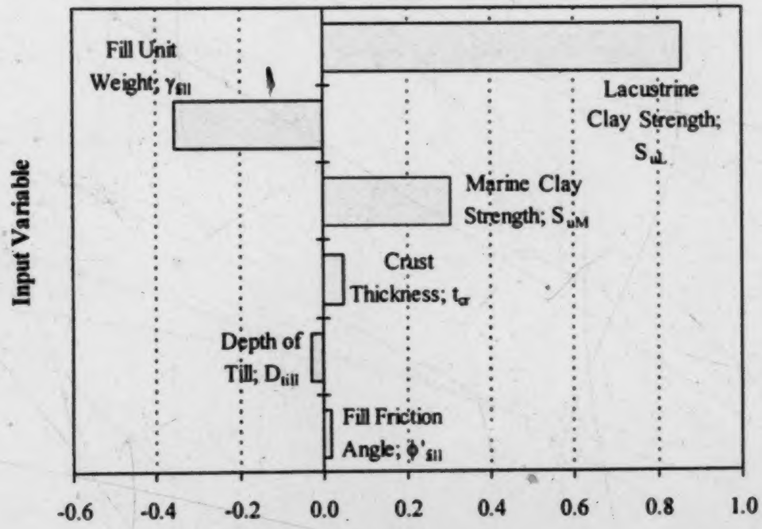

Figure 6–9 Sensitivity analysis results, Design 2

3. IMPLEMENTATION OF THE PROPOSED METHODOLOGY

3.1 James Bay Design 1 (H=12m)

The stability of James Bay dykes Design 1, is analyzed probabilistically using the proposed methodology (Chapter 5). The input variables defined by Christian et al. (1994) are adopted. However, the statistical parameters describing the uncertainty of these variables are approached and combined differently. Three sources of parameter uncertainty are considered: soil variability, statistical errors and measurement bias. Soil variability is described by the mean and variance of the measured data. Statistical errors due to the limited number of measurements are estimated using Equation 3-20 (Chapter 3). The bias in the measurements of the undrained shear strength of the marine and lacustrine clays is accounted for through Bjerrum's vane correction factor using the same mean and variance proposed by Christian and his colleagues. Table 6-3 summarizes the statistical parameters of the various sources of uncertainty. In principle, these uncertainties are combined using the following model;

$$y = B(x + \mathrm{SE}) \tag{6-1}$$

where y is the corrected input variable, B is the bias correction factor, x is the measured variable and SE is the statistical error. All variables are assumed normally distributed. Due to the large standard deviation of the measured shear strength of the marine and the lacustrine clays and the potential of sampling negative values, a zero truncation limit is imposed on both distributions (i.e., $x \geq 0$). Alternatively, a practical minimum strength threshold may be used instead. The use of a zero truncation limit may result in the shear strength at discrete locations along the slip surface being equal to zero. The average shear strength over the length of the slip surface, however, will be higher than zero. In addition, a zero truncation limit is imposed on the sum of the measured strength and the statistical error (i.e., $x + \mathrm{SE} \geq 0$).

To simplify the spreadsheet model, the uncertainty in soil stratigraphy is dealt with as a systematic uncertainty. In other words, the thickness of a soil layer can vary from one iteration to another, however within one iteration the thickness is not allowed to vary along the slope profile. Thus, to account for the effect of spatial averaging on the uncertainty of the mean thickness of the clay crust, a variance reduction factor of 0.20 is applied to the point variance, Table 6-3.

Table 6-3 Input variables and statistical parameters for James Bay dykes (based on Christian et al., 1994)

Input Variable	Soil Variability①		Statistical Error②		Measurement Bias	
	E[--]	σ[--]	E[--]	σ[--]	E[--]	σ[--]
Fill Friction Angle; ϕ_{fill} (deg.)	30.0	1.00	0.0	1.73	--	--
Fill Unit Weight; γ_{fill} (kN/m^3)	20.0	1.00	0.0	1.00	--	--
Thickness of Clay Crust; t_{cr} (m)	4.0	0.48③ 0.84④	--	--	--	--
Shear Strength of Marine Clay; S_{uM} (kPa)	34.5	8.14	0.0	0.95	--	--
Bjerrum Vane Correction Factor for S_{uM} ; μ_M	--	--	--	--	1.0	0.075
Shear Strength of Lacustrine Clay; S_{uL} (kPa)	31.2	8.65	0.0	1.73	--	--
Bjerrum Vane Correction Factor for S_{uL} ; μ_L	--	--	--	--	1.0	0.150
Depth of Till; D_{till} (m)	--	--	18.5	1.00	--	--

① Mean and standard deviation of the measured data without any alteration

② Based on Equation 3-20

③ Uncertainty due to spatial variability ($f = 0.2$) plus statistical error, Design 1

④ Uncertainty due to spatial variability ($f = 0.7$) plus statistical error, Design 2

A spreadsheet model is prepared and a print out is attached in Appendix I. The critical slip circles are assumed tangent to the till layer, daylight at a fixed point (4.9, 36.0) and have the same x-coordinate for the centres (x_o=85.9), as outlined in Section 2. For each iteration, different value of D_{till} is sampled and a different slip circle is analyzed.

In accounting for spatial averaging, Christian et al. (1994) used a variance reduction factor of 0.20 which implied an autocorrelation distance in the order of 15m. The same distance is adopted in this study. The procedure outlined in Chapter 5 is followed to model the spatial variability of soil properties in the spreadsheet. The portion of the slip surface within each layer is divided into a number of segments depending on the geometry of the slip surface and the autocorrelation distance. The average soil property over the length of each segment (i.e., local average) is modeled as a random variable having the probability distribution of the point measurements, Table 6-3. The correlation coefficients between local averages are calculated using Equation 5-5. Thus, each iteration in the simulation process involves sampling a number of correlated variables (for each soil parameter); each represents the local average over the length of the corresponding slip surface segment.

The length of the slip surface cutting through the embankment is less than 30m (i.e., $<2r_o$). The friction angle of the fill material is, thus, modeled by one variable. The undrained shear strength of the marine clay is modeled by two variables representing the average strength over the two segments of the slip surface within the clay layer, Figure 6–10. The correlation coefficient between the two local averages is equal to zero.

Depending on the geometry of the slip surface, the portion within the lacustrine clay is divided into 2-4 segments. In most cases, however, 3 segments are used as shown in Figure 6–10. The undrained shear strength is represented by a number of variables equal to the number of segments. The correlation coefficients between the local averages are estimated based on the geometry of the slip surface associated with the mean values of the crust thickness and the depth to the till layer. The embankment cross-section is divided into 5 zones, Figure 6–10. The average unit weight within each zone is regarded as a variable with the point probability distribution. The correlation coefficients between all variables are equal to zero except for those representing zones 4 and 5 where the correlation coefficient is calculated to be 0.37.

Statistical errors and bias are both sources of systematic uncertainty. As such, they have a constant impact all across the slope. Each source of these uncertainties (Table 6-3) is modeled by a single variable. In total, 19 variables are defined and used to account for the various sources of uncertainty.

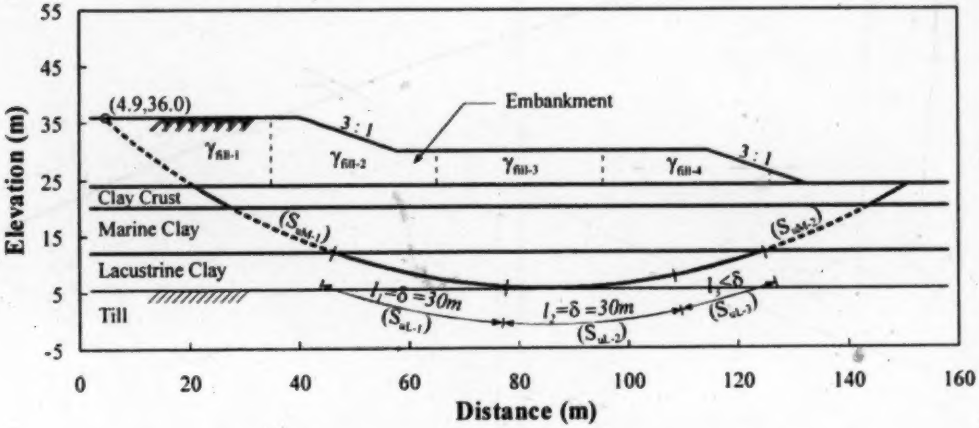

Elevation (m)
55
45
35
25
15
5
-5
(4.9,36.0)
Embankment
3 : 1
3 : 1
γ_{fill-1}
γ_{fill-2}
γ_{fill-3}
γ_{fill-4}
Clay Crust
Marine Clay
Lacustrine Clay
Till
(S_{uM-1})
(S_{uM-2})
$l_1=\delta=30m$
(S_{uL-1})
$l_2=\delta=30m$
(S_{uL-2})
$l_3<\delta$
(S_{uL-3})
0
20
40
60
80
100
120
140
160
Distance (m)

Figure 6–10 Proposed approach to account for spatial averaging, Design 1

The optimum number of iterations is estimated to be 30,000 as shown in Figure 6–11. In the subsequent analyses 32,000 iterations were used which corresponded to about 25 minutes of computer time using a Pentium II, 233 MHz. Figure 6–12 shows the frequency histogram and the CDF of the factor of safety using a seed value of 31069. The mean factor of safety is estimated to be 1.46 with a standard deviation of 0.20. The probability of unsatisfactory performance is calculated to be 0.47%. Close examination of the histogram indicates that it is slightly right skewed, coefficient of skewness = 0.29. This is expected, as a corollary of the central limit theorem, since the performance function involves the multiplication of a number of independent normally distributed variables. Based on 25 simulations the mean probability of unsatisfactory performance is 0.47% and the 95% confidence interval is 0.45-0.49%. Figure 6–13 shows the histogram of the probability of unsatisfactory performance.

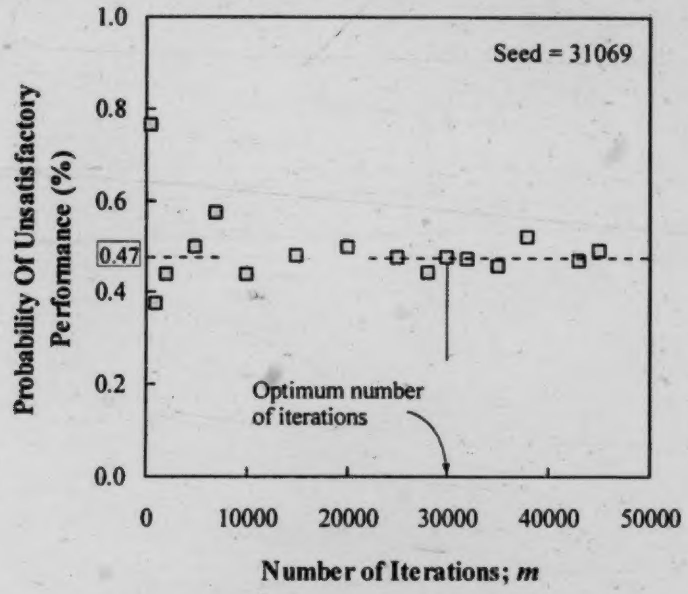

Figure 6–11 Optimum number of iterations - Proposed Methodology; Design 1

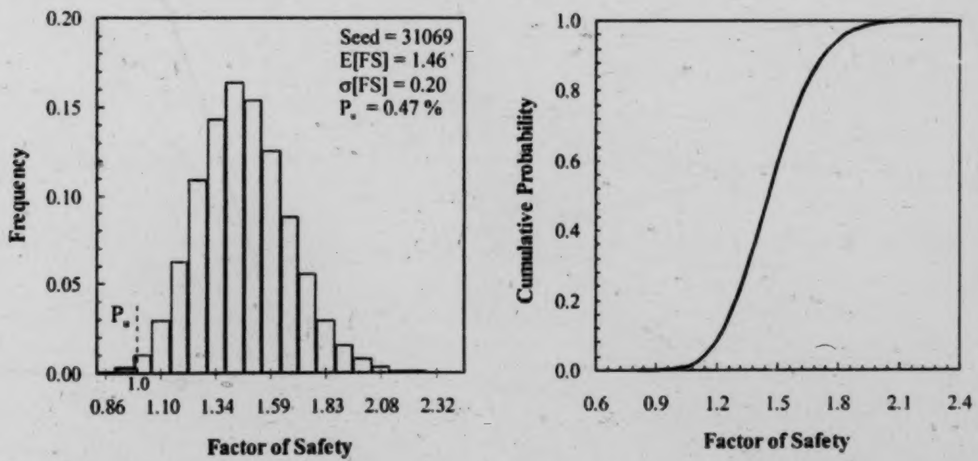

Figure 6–12 Histogram and CDF of the factor of safety –Proposed Methodology; Design 1

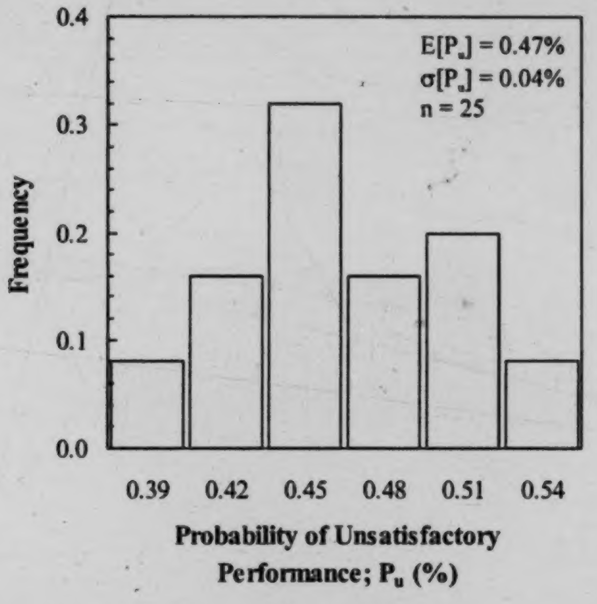

Figure 6–13 Histogram of the probability of unsatisfactory performance; Proposed Methodology; Design 1

Figure 6–14 shows the histograms of the spatially averaged soil parameters corrected for bias and statistical errors. For simplicity, Christian et al. (1994), accounted for spatial averaging through a single variance reduction factor regardless of the spatial contribution of each input variable. One of the advantages of the proposed methodology is that it accounts for spatial averaging in a more realistic and transparent way. The variance of the average soil parameter is reduced based on its spatial contribution to the analysis rather than by a constant collective factor. For example, the unit weight of the fill contributes to the analysis across the entire spatial domain of the slope as shown in Figure 6–10. As a result, the reduction in the uncertainty of the *average* unit weight is significant. The standard deviation of the average unit weight is 1.12 kN/m^3 (Figure 6–14, top right) which is similar to the value estimated by Christian et al. (1994) through applying the variance reduction factor (Table 6-1). In contrast, the friction angle of the fill material contributes to the analysis only along the small section of the slip surface within the embankment which is smaller than the scale of fluctuation, δ. Consequently, the uncertainty of the average friction angle has not undergone any reduction and is equal to the point variance. The undrained shear strength of the marine and lacustrine clays are averaged over a number of slip surface segments and have, therefore, undergone variance reduction proportional to their spatial contributions.

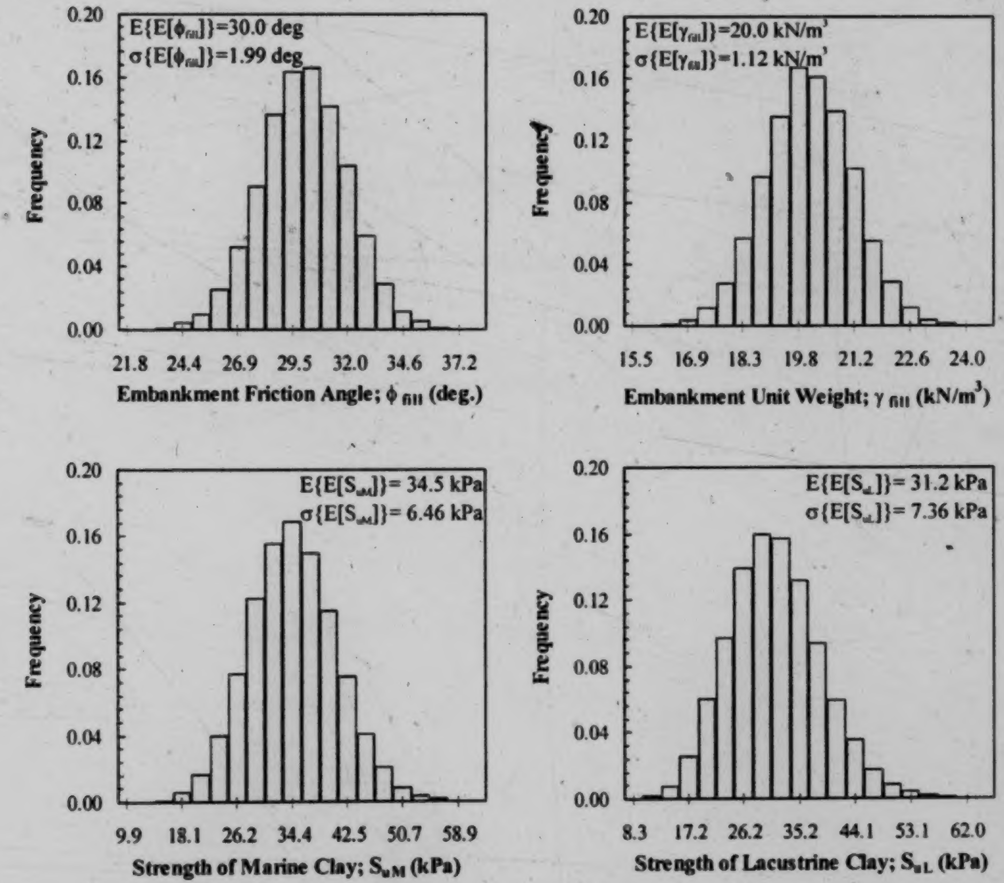

Figure 6–14 Histograms of the average soil parameters – Proposed Methodology; Design 1

A sensitivity analysis is performed and Figure 6–15 shows Spearman rank correlation coefficients for all 19 input variables. It is interesting to note that many of the factors with major contributions to the uncertainty of the safety factor are not related to the measured data. For example, Bjerrum's correction factor for the undrained shear strength of the lacustrine clay, the statistical error in the unit weight of the fill and the statistical error in the depth of the till layer are among the main factors affecting the reliability of the design.

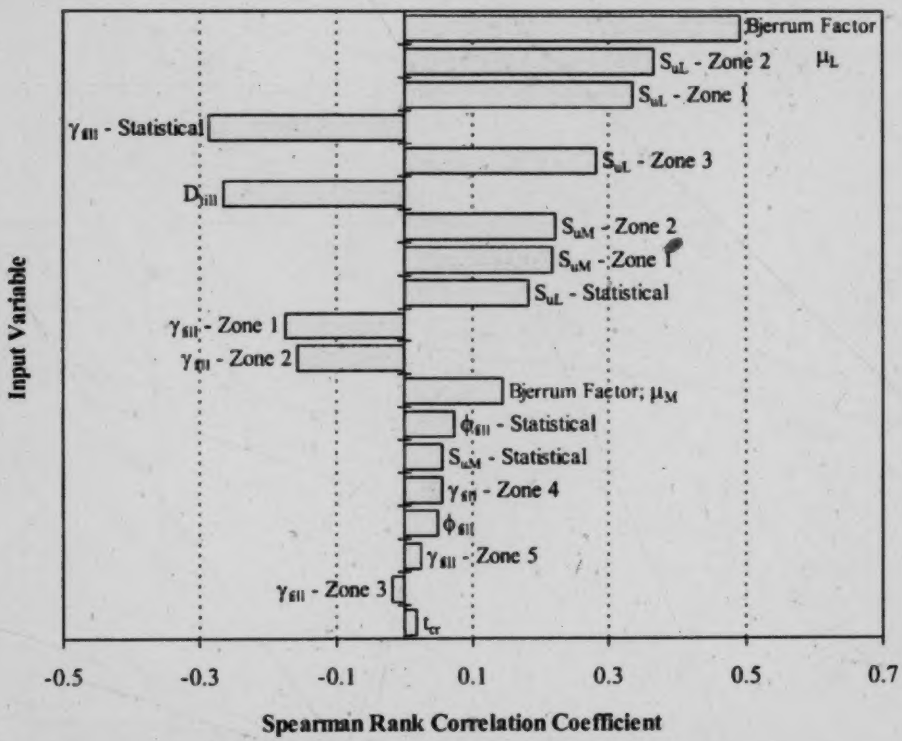

Figure 6–15 Sensitivity analysis results – Proposed Methodology; Design 1

3.2 James Bay Design 2 (H=6m)

The proposed methodology is also applied to study the stability of Design 2 following the same approach as for Design 1. The input variables and the statistical parameters are summarized in Table 6-3. A variance reduction factor of 0.7 (Christian et al., 1994) is applied to estimate the standard deviation of the mean thickness of the clay crust. Similar to the analysis described in Section 2, the slip circles are assumed tangent to the till layer and have a common center (63.7, 42.0). The geometry of the slope and the nearly equal strength of the marine and lacustrine clays indicated, however, the potential of a shallow failure should the sampled strength of the latter be higher than that of the former. Another analysis is performed assuming a shallow slip surface tangent to the bottom of the marine clay as shown in Figure 6–16. An autocorrelation distance of 30m is assumed which is equivalent to the 0.7 variance reduction factor adopted by Christian and his team. The spatial variability of soil properties is modeled following the same approach used for Design 1 (Figure 6–16). Because the domain of the slope is relatively small compared to the autocorrelation distance, the number of slip surface segments and embankment zones is much less than Design 1. In total, 13 and 8 variables are used to model the various sources of uncertainty for the deep and shallow slip circles, respectively.

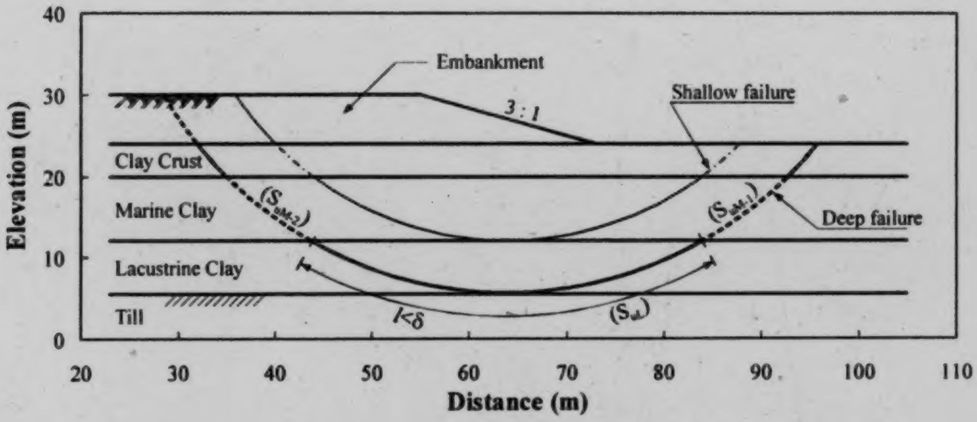
Embankment
3 : 1
Shallow failure
Clay Crust
Marine Clay
Lacustrine Clay
Till
(S_{uM_2})
(S_{uM_1})
Deep failure
$l<\delta$
(S_{uL})
Elevation (m)
0
10
20
30
40
Distance (m)
20
30
40
50
60
70
80
90
100
110

Figure 6–16 Critical slip circles and spatial averaging – Design 2

Spreadsheet models prepared for both cases (deep failure and shallow failure) are analyzed using Monte Carlo simulation with 38,000 iterations. Figure 6–17 shows the histograms of the factors of safety for the deep and shallow slip surfaces. Both histograms are slightly right skewed with coefficients of skewness of 0.34 and 0.23, respectively. The mean factor of safety and probability of unsatisfactory performance are estimated to be 1.54 and 2.38% for the deep failure and 1.67 and 1.61% for the shallow failure.

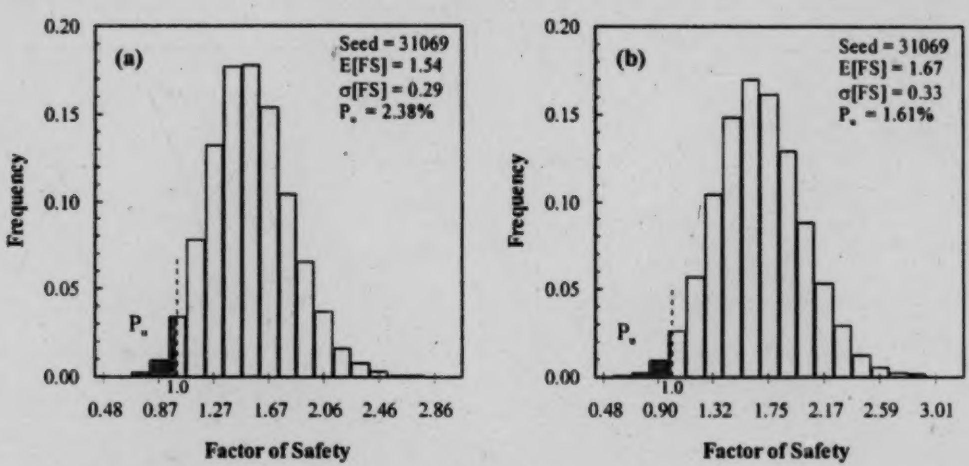

Figure 6–17 Histograms of the factor of safety, Design 2 – Proposed Methodology: a) Deep failure; b) Shallow failure

Based on the results of 25 simulations, the mean probability of unsatisfactory performance is estimated to be 2.33% for deep failure and 1.58% for shallow failure as shown in Figure 6–18. The 95% confidence intervals are 2.30-2.35% and 1.56-1.60%, respectively. Deep failure is, thus, more critical and the probability of unsatisfactory performance of the slope is approximately 2.30%. A sensitivity analysis is performed and Spearman rank correlation coefficients for both failure modes are shown in Figure 6–19 and Figure 6–20. Similar to Design 1, the uncertainty of the factor of safety is strongly influenced by sources not related to the measured data (e.g., Bjerrum's factor and statistical errors), however to a lesser extent. This is mainly due to the larger contribution of the uncertainty of soil variability as a result of the smaller impact of spatial averaging.

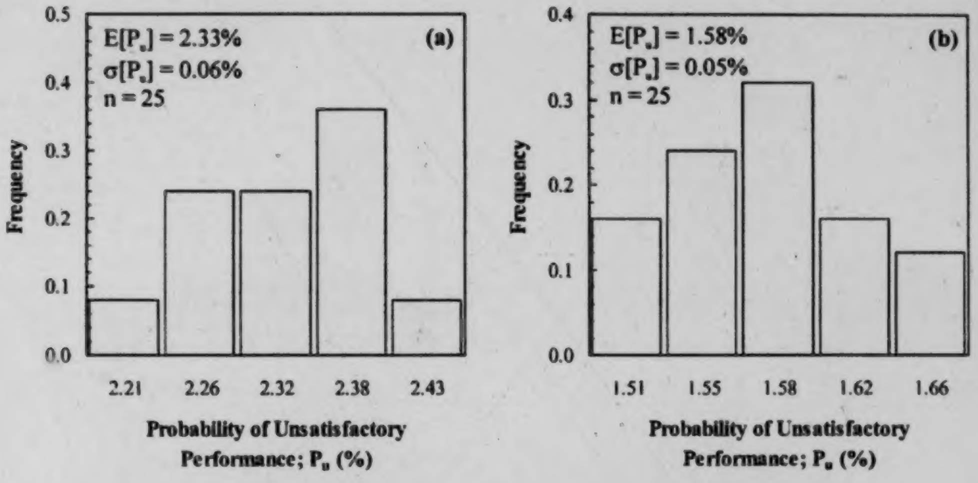

Figure 6–18 Histograms of the probability of unsatisfactory performance, Design 2 – Proposed Methodology; a) Deep failure; b) Shallow failure

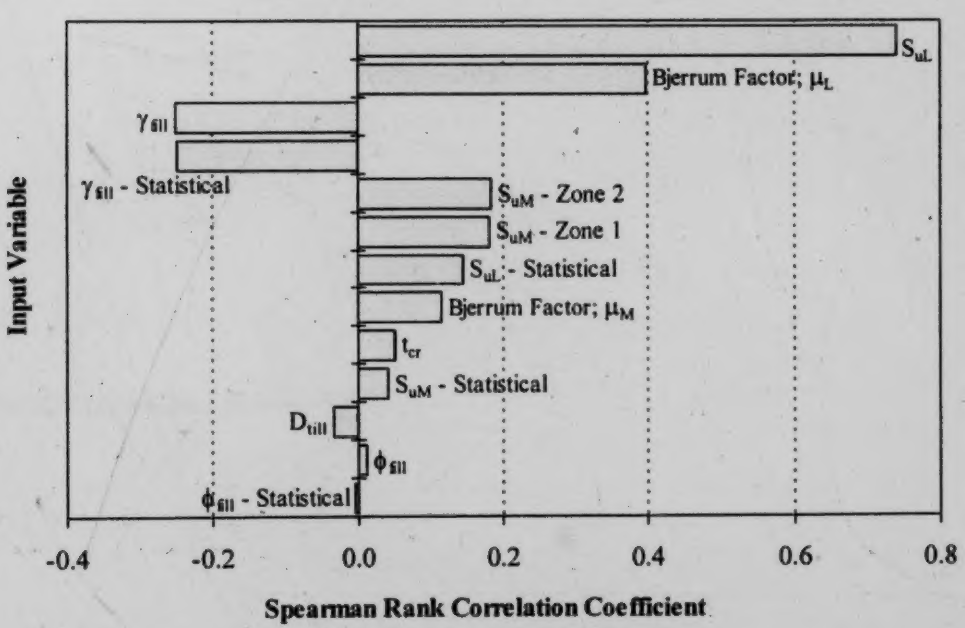

Figure 6–19 Sensitivity analysis results, Design 2 (deep failure) – Proposed Methodology

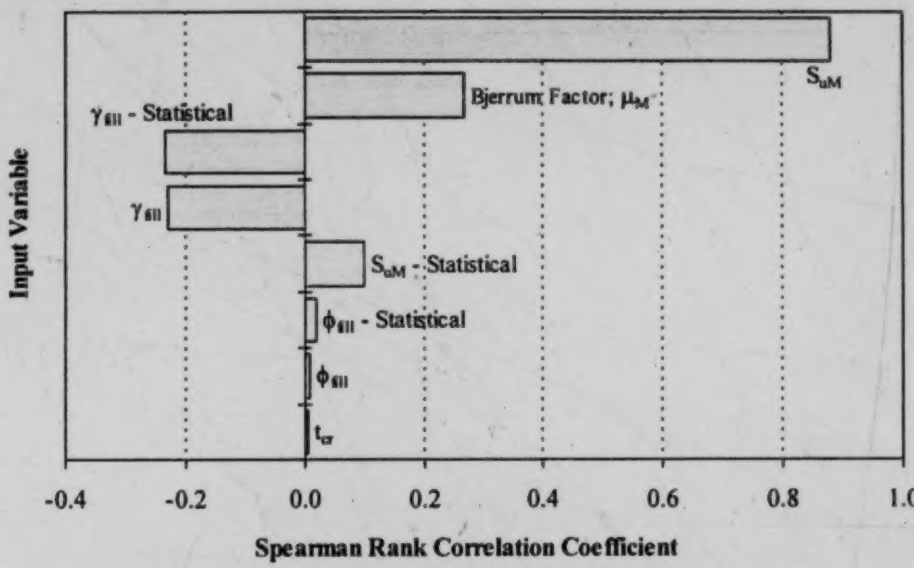

Figure 6–20 Sensitivity analysis results, Design 2 (shallow failure) – Proposed Methodology

4. NAÏVE PROBABILISTIC ANALYSIS

As discussed in Chapter 5, the value of a primitive and quick probabilistic analysis (hereafter referred to as "Naïve Analysis") is investigated. The approach follows closely the footprints of a conventional analysis. Uncertainty is based on the observed variability of the measured data (with minimal statistical treatment) and the well established sources of systematic uncertainty such as the uncertainty in Bjerrum's vane correction factor. Table 6-4 summarizes the input variables and the statistical parameters used in the analysis (Christian et al., 1994). All variables are assumed normally distributed. The mean and standard deviation of the thickness of the clay crust, the strength of the marine clay and the strength of the lacustrine clay are obtained directly from the site investigation results. Zero truncation limits are imposed on the three distributions to prevent sampling negative values. The uncertainties in the properties of the fill (unit weight and friction angle) are assigned judgmentally to account for the potential variability in the properties of the borrow material and the construction techniques. The uncertainty in Bjerrum's correction factors is also assigned judgmentally to account for the scatter of the database from which these factors were obtained.

Table 6-4 Input variables and statistical parameters for the Naive analysis

Input Variable	Soil Variability		Measurement Bias	
	E[--]	σ[--]	E[--]	σ[--]
Fill Friction Angle; ϕ_{fill} (deg.)	30.0	2.00	--	--
Fill Unit Weight; γ_{fill} (kN/m^3)	20.0	1.41	--	--
Thickness of Clay Crust; t_{cr} (m)	4.0	0.99	--	--
Shear Strength of Marine Clay; S_{uM} (kPa)	34.5	8.14	--	--
Bjerrum Vane Correction Factor for S_{uM} ; μ_M	--	--	1.0	0.075
Shear Strength of Lacustrine Clay; S_{uL} (kPa)	31.2	8.65	--	--
Bjerrum Vane Correction Factor for S_{uL} ; μ_L	--	--	1.0	0.150

The Hassan and Wolff (1999) algorithm for minimum reliability index is applied to locate the probabilistic critical slip surface for each design. The case with the lacustrine shear strength equal to "$E[S_{uL}]-\sigma[S_{uL}]$" yielded the most critical slip circles for both designs. They were subsequently used in Monte Carlo analysis. These surfaces, however, almost coincided with the deterministic critical slip circles shown in Figure 6–1 and Figure 6–2. Monte Carlo simulation is performed using 32,000 iterations for Design 1 and 38,000 iterations for Design 2. Figure 6–21 shows the histograms of the factor of safety based on a seed value of 31069. Figure 6–22 shows the histograms of the probability of unsatisfactory performance based on 25 simulations. The mean probability for Design 1 is estimated to be 2.37% with a 95% confidence interval of 2.34-2.41%. For Design 2, the mean probability of unsatisfactory performance is 2.70% with a 95%

confidence interval of 2.68-2.73%. Clearly, the naïve analysis (i.e., ignoring soil spatial variability and spatial averaging) overestimates the probability of unsatisfactory performance.

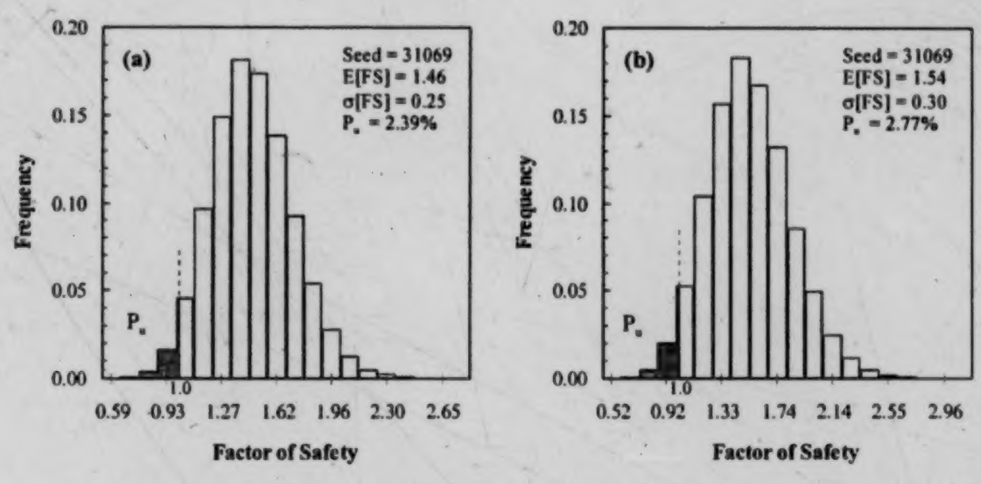

Figure 6–21 Histograms of the factor of safety – Naïve analysis : a) Design 1; b) Design 2

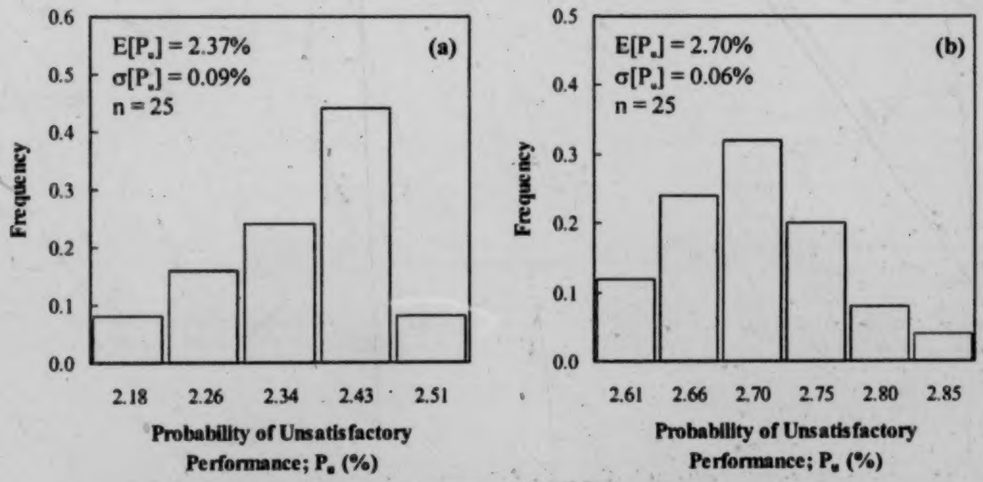

Figure 6–22 Histograms of the probability of unsatisfactory performance – Naïve analysis : a) Design 1; b) Design 2

5. SUMMARY AND DISCUSSION

The results of all the analyses are summarized in Table 6-5. Since the mean factor of safety is dependent on the mean values of the input variables, all analyses yielded almost the same mean factor of safety in spite of the differences between the various approaches. The standard deviation, which greatly controls the probability of unsatisfactory performance, varied however depending on the assumptions and the analytical technique adopted.

The techniques of Monte Carlo simulation and FOSM method are compared using exactly the same input variables. The results (M.C.-Christian and FOSM, Table 6-5) indicate good agreement in the estimates of the mean and standard deviation of the factor of safety. However, the estimates of probability of unsatisfactory performance using FOSM method and based on an assumed parametric shape for the density function of the factor of safety could be in error particularly when estimating low probabilities.

The results of the proposed methodology indicate a slightly higher uncertainty in the factor of safety, and consequently higher probability of unsatisfactory performance, than the M.C.-Christian analysis for both designs. The differences arise mainly from the way spatial averaging is accounted for in the analyses. In the M.C.-Christian analysis, spatial averaging is taken into account through a collective variance reduction factor for all variables regardless of the size of the domain over which each parameter is averaged. This limitation is overcome in the proposed methodology by allowing the variance reduction to be proportional to the size of the domain over which each soil parameter is averaged. Another factor that contributed to the difference but to a lesser extent, is the reduction in the variance of the strength of the marine clay in the M.C.-Christian analysis to account for random measurement errors. The reliability of the amount of reduction is, however, in question as discussed in Chapter 5.

Table 6-5 Summary of the results of all analyses (based on the results of 25 simulations for each case)

Type of Analysis	**Design 1** (H=12m)				**Design 2** (H=6m)							
					Deep Failure				**Shallow Failure**			
	E[FS]	**σ[FS]**	**P_u (%)**	**β①**	**E[FS]**	**σ[FS]**	**P_u (%)**	**β①**	**E[FS]**	**σ[FS]**	**P_u (%)**	**β①**
Deterministic Analysis	1.46	--	--	--	1.53	--	--		1.66	--	--	--
FOSM②	1.45	0.17	0.40	2.66	1.50	0.27	3.25	1.84	--	--	--	--
M.C.–Christian analysis	1.46	0.17	0.23	2.76	1.53	0.26	1.76	2.06	--	--	--	--
Proposed Methodology	1.46	0.20	0.47	2.32	1.54	0.29	2.33	1.82	1.67	0.33	1.58	2.03
Naïve Analysis	1.46	0.25	2.37	1.84	1.54	0.30	2.70	1.78	--	--	--	--

① $\beta = \dfrac{E[FS]-1}{\sigma[FS]}$

② Christian et al. (1994)

The results of the naïve analysis are in good agreement with the results of the other probabilistic techniques for Design 2. However, the probability of unsatisfactory performance for Design 1 is approximately one order of magnitude higher. This is a direct result of the significant reduction in the uncertainty of soil variability due to spatial averaging which is taken into account in all analyses but the naïve analysis. Thus, the naïve analysis could largely overestimate the probability of unsatisfactory performance for slope problems dominated by the uncertainty due to soil spatial variability.

The reliability index is calculated for all cases using the simple definition in Chapter 3 and is summarized in Table 6-5. Figure 6–23 shows the relation between the reliability index and the probability of unsatisfactory performance for all Monte Carlo analyses. The relation appears linear, however there is no reason to believe that it should be linear. What is important to note, is that the slope of the line is steep, implying that the probability of unsatisfactory performance is more sensitive to any changes in the analysis than the reliability index.

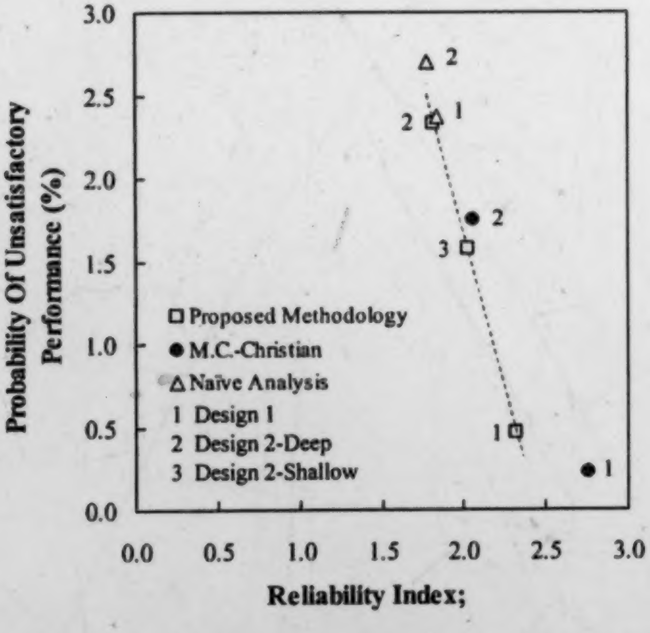

Figure 6–23 Reliability index versus probability of unsatisfactory performance – James Bay dykes

The results of sensitivity analyses illustrated that the systematic sources of uncertainty could influence the reliability of the design more than the uncertainty due to soil variability. Most of these systematic uncertainties are estimated either judgmentally or using approximate statistical relations. Seldom are they based on measured data. It is, therefore, important to exercise care and avoid conservatism in assigning quantitative values for systematic uncertainties.

CHAPTER 7

SYNCRUDE TAILINGS DYKE CELL 23

The probabilistic methodology proposed in Chapter 5 is applied to examine the stability of one section of the Syncrude tailings dyke. The site of the dykes is 40 km north of Fort McMurray, Canada, and is part of the oil sands mining operations run by Syncrude Canada Limited. The following sections provide a brief description of the project and detail the analyses undertaken to characterize the uncertainty in soil parameters and assess the stability of the dykes.

1. INTRODUCTION

The Syncrude project is one of the main operations for mining oil sands in Canada. The bitumen is recovered from the McMurray Formation (oil sands) by surface mining and processing through an extraction plant. The process required the construction of a tailings pond (Mildred Lake Settling Basin) to store the mining tailings. The pond has a storage capacity of 350 hm^3 and is formed by constructing a sand dyke with circumference of about 18 km, an average height of about 40 m and a maximum height of 88 m. The dyke is constructed using the tailings sand from the bitumen extraction process. For ease of reference, the dyke is divided into 30 cells, each of roughly 700 m length. Figure 7–1 shows a plan of the tailings pond and dyke cells. The stability of the dykes of Cell 23 is the focus of this chapter.

2. SITE GEOLOGY

The pond area is covered at surface with Holocene deposits composed primarily of aeolian sands (Hae), lacustrine clayey deposits (Hl), alluvial sediments (Hf) and highly organic deposits (Ho). The total thickness of the Holocene deposits varies from 0-4 m.

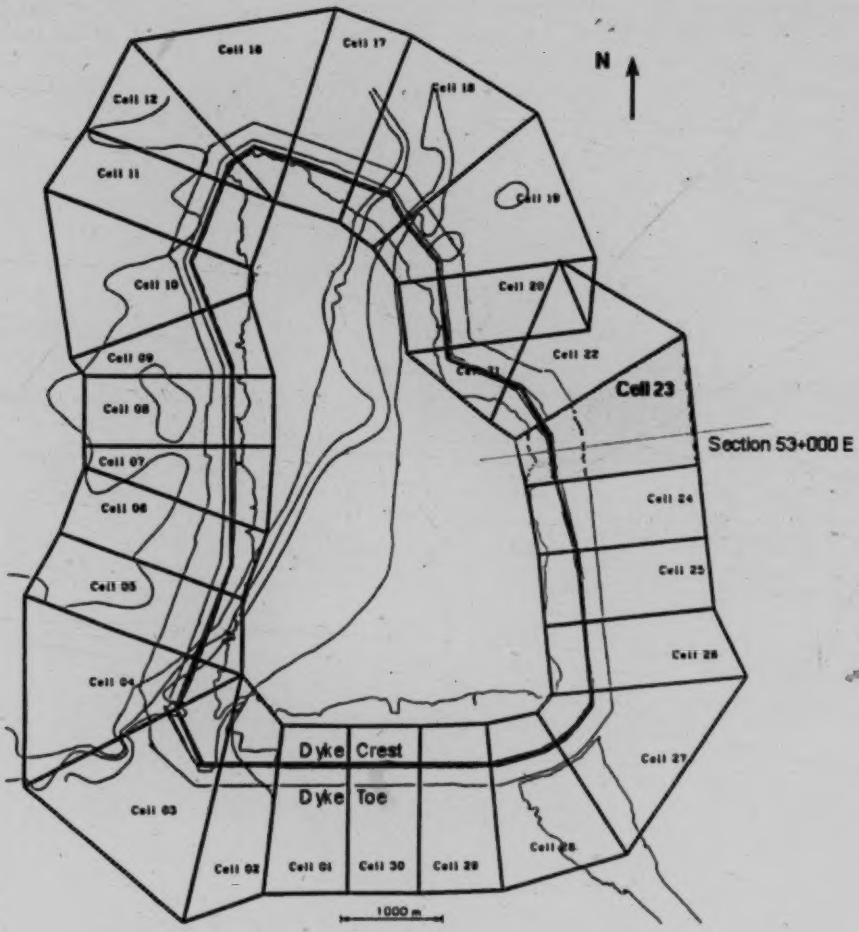
N
Cell 16
Cell 17
Cell 18
Cell 12
Cell 11
Cell 19
Cell 10
Cell 20
Cell 09
Cell 22
Cell 21
Cell 08
Cell 23
Section 53+000 E
Cell 07
Cell 24
Cell 06
Cell 25
Cell 05
Cell 26
Cell 04
Dyke Crest
Dyke Toe
Cell 27
Cell 03
Cell 28
Cell 02
Cell 01
Cell 30
Cell 29
1000 m

Figure 7–1 Plan of the tailings pond dyke (modified from Nicol, 1994)

The Holocene unit is underlain by Pleistocene glacial deposits that vary in thickness between 5 and 15 m. These deposits comprise glacio-lacustrine sands and clays (Pl) overlying glacio-fluvial sands (Pf) which, in turn, overly unconsolidated lodgement and ablation tills (Pg). Two till deposits can be distinguished based on the composition of the till materials; sandy till (Pgs) and clayey till (Pgc).

The marine Clearwater Formation underlies the Pleistocene deposits and belongs to the Upper Cretaceous age. It consists of a succession of bedded clays, silts, and sands with occasional thin indurated siltstones and has been divided into a sequence of units denoted by; Kcg, Kcf, Kce, Kcd, Kcc, Kca and Kcw. Most of these units have been eroded on the east side of the pond except for Kca and Kcw. Geological evidence suggests that the formation was prone to thrusting and transportation by glacial ice. The Cretaceous McMurray Formation is composed of dense oil bearing sands and silty sands (ore zone) and underlies the Clearwater Formation. Glacial disturbance and erosion processes have altered the described stratigraphic column at some locations within the pond area. Fair and Handford (1986) provides a more detailed description of the geology at the pond site.

3. CELL 23

3.1 Background

The dyke height at Cell 23 is 44 m with the down stream slope originally designed to a slope of 4h:1v. Slope inclinometers were installed to monitor slope movements. Since 1981, localized movements along the Kca/Kcw contact were observed. By the time the fill height was 23 m (1984), up to 19 cm of displacement had been measured. It was, therefore, decided that a complete design review was needed. A detailed investigation program was conducted which included boring and sampling, laboratory testing and installation of slope indicators and pneumatic and standpipe piezometers.

The investigation indicated the presence of a raft of glacially-disturbed clay-shale (Kca) with distinctive shear planes under much of the downstream slope. The movements were noted to be mainly along discrete shear planes in the Kca immediately above the overconsolidated clay-shale (Kcw), with very little movements in the overlying till. A substantial increase in pore water pressure was also observed close to the Kca/Kcw interface. Based on the observed foundation performance and the geological data, Section 53+00 E (refer to Figure 7–1) was considered the most critical dyke section in Cell 23.

A design review indicated that the original geometry (slope 4:1) was unacceptable, FS = 1.09 at ultimate dyke height, and design modifications were needed. Targeting a safety factor of 1.30, the downstream slope above elevation 331 m was flattened to 8.5 :1 thus reducing the overall slope to 6.8:1. Cell 23 was completed to the final design elevation of 352 m in 1993. During construction, the dyke was heavily instrumented and monitored till completion. The maximum movement recorded was 43.7 cm under elevation 319 m in section 53+000 E. The movement has almost ceased since 1996 and the performance of the dyke is deemed adequate. Figure 7–2 shows a cross-section of the completed dyke at section 53+000 E. The probabilistic analyses presented in this chapter are focused entirely on the stability of section 53+000 E.

3.2 Subsurface Conditions

3.2.1 Stratigraphy

The stratigraphy at section 53+000E comprises an upper layer of glacio-fluvial sand (Pf4) with an average thickness of 3.0 m overlying a sandy till (Pgs) layer of a thickness varying from 3.0 m at the centre of the dyke to about 10.0 m at the toe. A composite foundation horizon consisting of clayey till (Pgc) and pre-sheared laminated clay-shale (Kca) underlies the sandy till. The clayey till is found under the crest of the dyke and extends upstream whereas the clay-shale is encountered under the downstream slope. Both layers had an average thickness of about 6.0 m. A layer of heavily over-consolidated clay-shale (Kcw) underlies this composite horizon. The Kcw unit is about 2.0m thick and overlies a very dense interlocked bitumen rich sand (Km). Figure 7–2 shows the soil stratigraphy at section 53+000 E.

3.2.2 Shear Strength

The main focus of the laboratory programs, as of 1984, was to reassess the peak and residual shear strength of the clay-shale unit Kca. Unconsolidated undrained triaxial

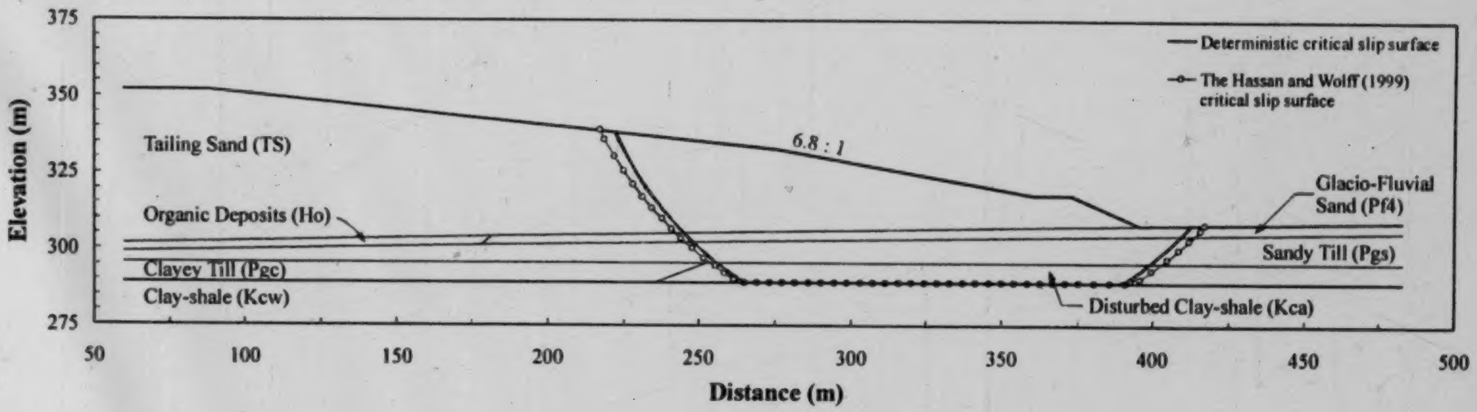

Figure 7–2 Geometry and soil stratigraphy at Section 53+000E - Cell 23

tests with pore pressure measurements and drained direct shear tests were conducted on intact samples as well as samples with pre-existing shear planes. Tests were also conducted on samples from the clayey and sandy till layers, the tailings sand and the clay-shale unit Kcw. No testing results were available for the strength of glacio-fluvial sand (Pf4).

Pre-sheared Clay-shale (kca)

Because previous studies (Thurber, 1989; Nicol, 1994; Alencar et al., 1994) concluded that the stability of the dyke is controlled by the residual strength of the disturbed clay-shale, only tests with residual shear strength measurements (drained direct shear tests) were considered. Testing results of 82 shear box specimens were collected from within Cell 23 and surrounding locations within the Syncrude mining site. Table 7-1 provides a summary of the physical and mechanical properties of the Kca material.

Table 7-1 Summary of the physical and mechanical properties of the Kca material

Soil Parameter	**Range**		**Mean**
	Minimum	Maximum	
Moisture content (%)	17	40	26.4
Liquid limit (%)	59	162	110.0
Plastic limit (%)	16	30	23.8
Bulk unit weight (kN/m^3)	18.1	20.7	19.5
Residual friction angle (deg.)	3.8	13.8①	7.5
Peak friction angle (deg.)	6.8	36.7②	18.6

① The results of 2 tests were unjustifiably high (18.7 and 19.8 degrees) and were excluded.

② The results of 2 tests were unjustifiably high (40.3 and 44.0 degrees) and were excluded.

Figure 7–3 is a plot of the normal stress versus the residual shear strength of all 82 specimens. The failure envelope corresponding to the mean residual friction angle, 7.5

degrees, and a zero effective cohesion is also plotted. The scatter of data points around the mean trend is obvious indicating high uncertainty in the value of the residual friction angle. The standard deviation of ϕ'_{Kca} is calculated to be 2.1 degrees. The shape of the probability histogram of ϕ'_{Kca}, Figure 7–4, implies a lognormal probability density function. The density function of a parametric lognormal distribution with a mean of 7.5 degrees and a standard deviation of 2.1 degrees is also plotted on the same graph. The figure (right plot) also compares the cumulative distribution functions of the experimental data and that of the parametric distribution.

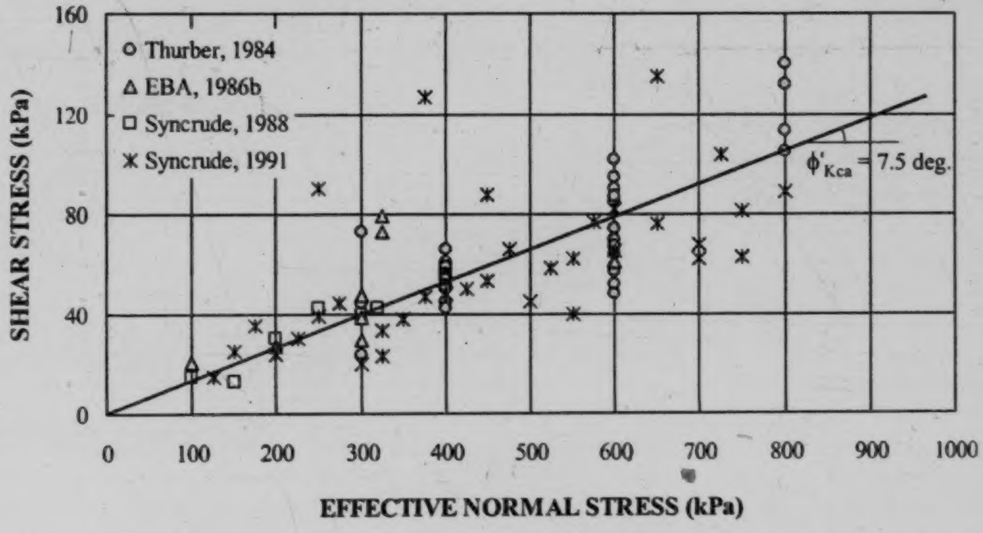

Figure 7–3 Shear box results for the residual strength of the Kca material

The Q-Q plot, Figure 7–5, is used to examine the goodness of fit between the experimental histogram and the postulated parametric distribution. It is a plot of the quantiles of the first distribution versus the quantiles of the second distributions for the same probability values. Identical distributions (in terms of shape, mean and variance) plot as 45-degree line. When the points fall on any straight line, the shapes of the distributions are similar, but the means and/or the variances are different. A non-linear plot indicates two different distributions. Figure 7–5 indicates a good match between the experimental distribution and the parametric lognormal distribution with a mean of 7.5 degrees and a standard deviation of 2.1 degrees.

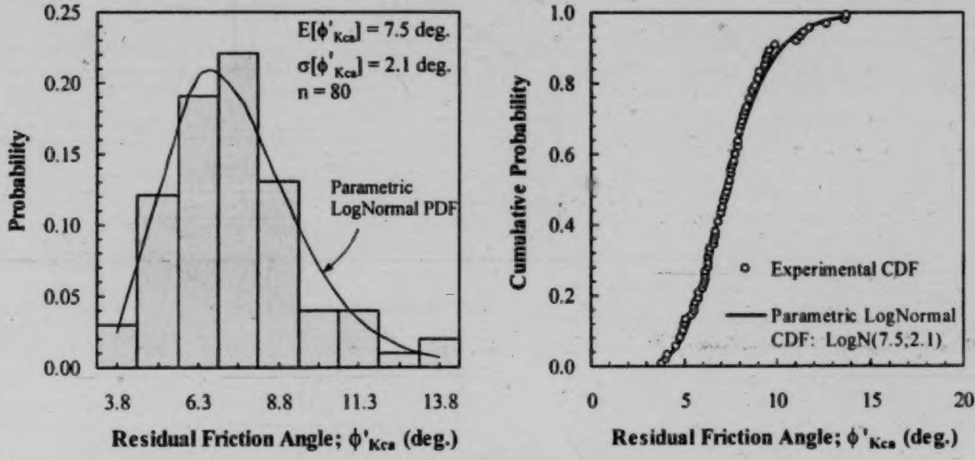

Figure 7–4 Probability histogram and cumulative distribution function of the residual friction angle of the Kca unit

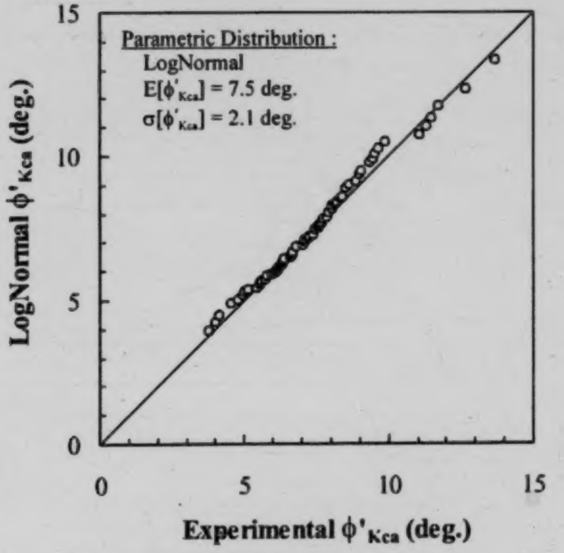

Figure 7–5 Q-Q plot of the experimental residual friction angle of the Kca unit and a parametric LogNormal distribution

Sandy Till (Pgs)

An important factor contributing to the stability of the dyke is the shear strength of the sandy till (Pgs) at the toe. Unfortunately, only 5 shear strength tests were available; 4 triaxial tests and 1 direct shear test. Furthermore, the triaxial tests were performed following different techniques; 1 isotropically consolidated undrained test, 2 anisotropically consolidated undrained tests and 1 isotropically consolidated drained test. The measured peak friction angles (assuming zero cohesion), thus, belong to different statistical populations. Grouping them together will increase the uncertainty in the shear strength of the Pgs. However, it is judged that the uncertainty from assuming a single deterministic value of ϕ'_{Pgs} or assuming a parametric density function based on one subgroup of the data could be even higher. All measurements were, thus, lumped together for an approximate statistical analysis. The measured values (16 specimens) ranged between 33.3 and 39.2 degrees with a single extreme value of 44.4 degrees that was excluded from the analysis. Table 7-2 summarizes the physical and mechanical properties of the tested samples. The mean and standard deviation of the peak friction angle are calculated to be 35.7 and 2.0 degrees, respectively. Figure 7–6 shows the histogram and the cumulative distribution function of the data.

Table 7-2 Summary of the of the physical and mechanical properties of the sandy till (Pgs)

Soil Parameter	**Range**		**Mean**
	Minimum	Maximum	
Fines content (%)	34	76	46.1
Atterberg limits	Non-plastic to low plasticity		
Bulk unit weight (kN/m^3)	21.3	22.6	22.1
Peak friction angle (deg.)	33.3	39.2	35.7

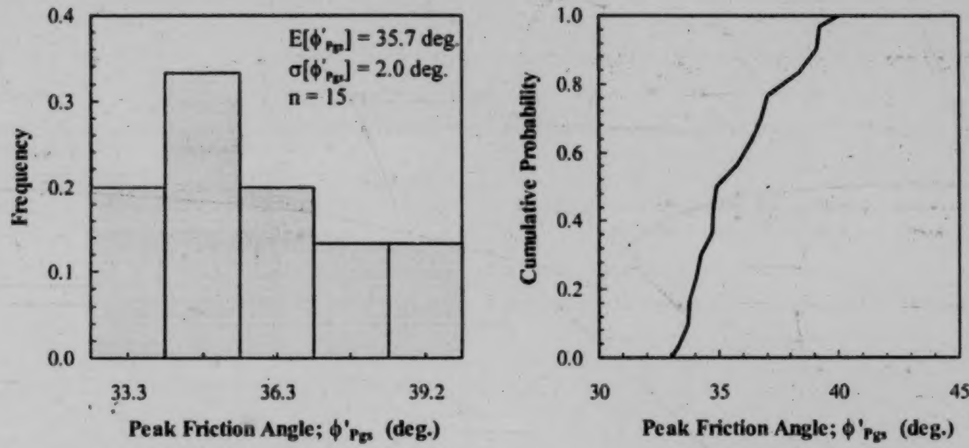

Figure 7–6 Histogram and CDF of the peak friction angle of the sandy till (Pgs) layer

Tailing Sand (TS)

Compared to the other formations, very limited amounts of data were available to characterize the shear strength of the tailings sand. Table 7-3 summarizes the results of few direct shear tests conducted in 1984 by different organizations. A parametric study to examine the effect of the variability of the shear strength of the tailings sand on the stability of the dykes indicated that the strength of the sand has very little impact on stability. The strength of the tailing sand is, thus, considered a deterministic quantity. Since the dyke has experienced large movements, the operating shear strength along the slip surface is likely to be less than the peak strength. A zero effective cohesion and a friction angle of 34 degrees were selected to represent the strength of the sand. These values are also consistent with previous stability studies (Thurber, 1989; Syncrude, 1992).

No laboratory results were available to assess the strength of the glacio-fluvial sand (Pf4) underlying the tailings sand. The impact of the strength of the Pf4 unit on the stability of the dykes is, however, minimal. It was, thus, assigned the same strength parameters as the tailings sand ($C' = 0$, $\phi' = 34$ deg.) which is the same assumption reported in Thurber (1989) and Syncrude (1992) studies.

Table 7-3 Summary of the results of direct shear tests on the tailings sand (TS)

Shear Strength		Range		Mean
		Minimum	Maximum	
Peak	Cohesion (kPa)	16	51	33.8
	Friction angle (deg.)	34.8	45.2	38.7
Residual	Cohesion (kPa)	0	32	19.5
	Friction angle (deg.)	27	32.5	30.4

Clayey Till (Pgc) and Clay-shale (Kcw)

As discussed in the following sections, the critical slip surface does not cut through either the clayey till or the clay-shale (Kcw). Thus, the shear strength of these two units is not of any importance to the stability analyses. However, for the sake of completeness a summary of the physical and mechanical properties of both layers is presented in Table 7-4 and Table 7-5. The shear strength of both layers was obtained mainly through direct shear tests and very few triaxial tests. The triaxial tests for the clayey till layer resulted in much higher strength than the direct shear tests. The results from the Kcw unit indicate that its shear strength is somewhat higher than the overlying Kca unit.

Table 7-4 Summary of the physical and mechanical properties of the clayey till unit (Pgc)

Soil Parameter	Range		Mean
	Minimum	Maximum	
Moisture content (%)	10	18	14.9
Liquid limit (%)	19	39	30.5
Plastic limit (%)	16	23	19.3
Bulk unit weight (kN/m^3)	20.7	23.0	21.6
Peak friction angle (deg.)	Direct Shear		22.5
Peak friction angle (deg.)	Triaxial		35.8

Table 7-5 Summary of the physical and mechanical properties of the clay-shale unit (Kcw)

Soil Parameter	Range		Mean
	Minimum	Maximum	
Moisture content (%)	12	32	19.8
Liquid limit (%)	30	121	65.7
Plastic limit (%)	16	35	22.8
Bulk unit weight (kN/m^3)	19.2	22.7	21.0
Residual friction angle (deg.)	5.9	35.7	15.5
Peak friction angle (deg.)	10.6	47.6	26.3

3.2.3 Pore Water Pressure

Following the redesign of the dyke slopes in 1984, Syncrude adopted an observational approach to closely follow the dyke performance. Tens of pneumatic and standpipe piezometers were installed during construction within the different geologic units with particular emphasis on the Kca unit. The piezometers are being monitored regularly leading to a wealth of measurements. Figure 7–7 shows the locations of piezometer tips at section 53+000 E.

The construction of Cell 23, both dyke and beaches, was completed to the design elevation in 1993. This study is concerned with the final dyke geometry, thus only those records after dyke completion were considered. Since the pore water pressure varies with time, the records were divided into time intervals of 1-2 months long. All data falling within one interval are considered as belonging to the same statistical population. The time interval corresponding to the highest pore pressure recorded after the completion of the dykes (March, 1994) is the only interval considered in this study.

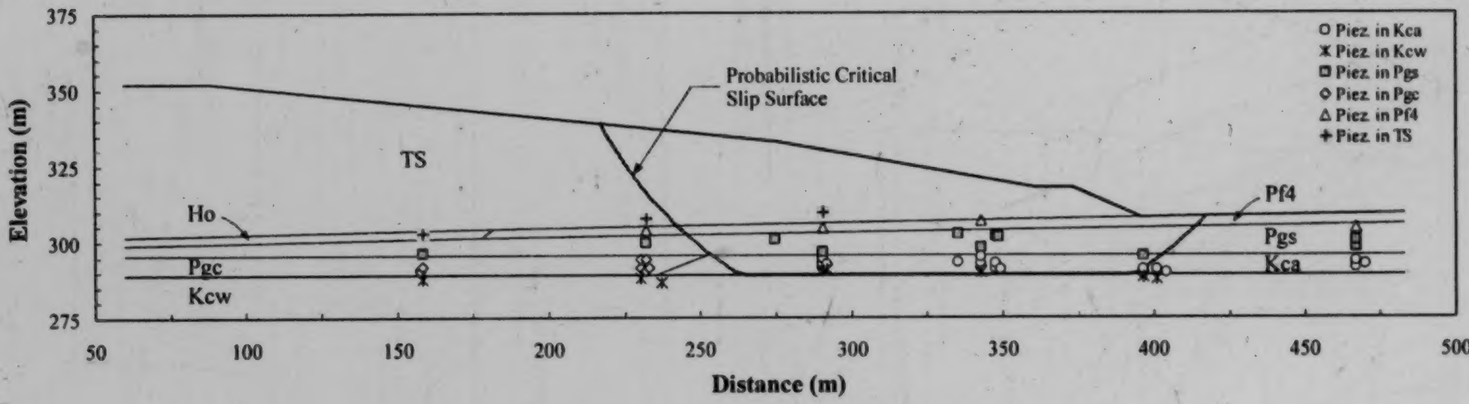

Figure 7–7 Locations of piezometer tips, Section 53+000E – Cell23

Pre-sheared Clay-shale (kca)

Measurements from 18 piezometeric tips along section 53+000E were considered for assessing the pore pressure conditions. Figure 7–8 shows a plot of the pore pressure ratio along Section 53+000E in March of 1994. The measurements are scattered. They range between 0.20 and 0.72 with an average of 0.45. A value of 0.17 was recorded below the dyke crest, where the pore pressure is presumably the highest. It was judged unreasonable and was excluded from the analysis. Examining Figure 7–8 indicates that the pore pressure ratio tends to decrease towards the dyke toe. Using the method of least squares, a linear trend is fitted to the data as shown in the plot. The slope and the intercept of the fitted trend are estimated to be -0.001 and 0.859, respectively. The standard deviation around the mean trend is calculated to be 0.12.

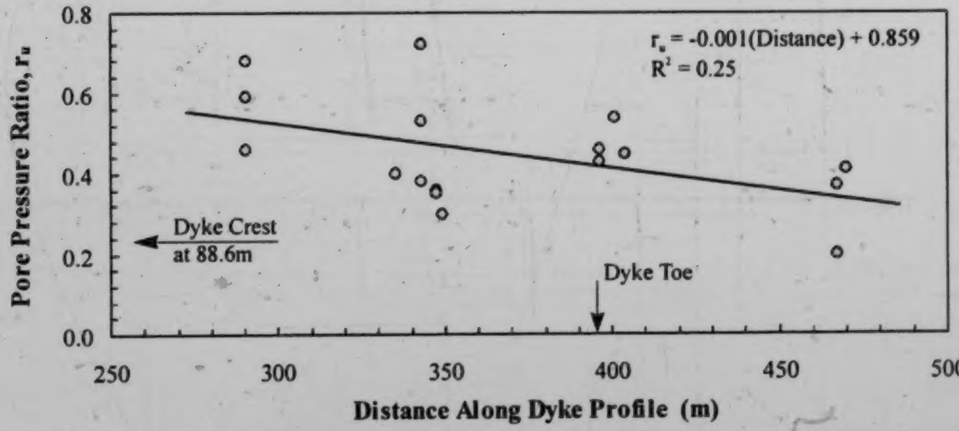

Figure 7–8 Profile of pore pressure ratio in the Kca layer along dyke cross-section, March 1994

Since the pore pressure ratio is exhibiting a linear trend and the mean varies with location, the process is non-stationary. The random field is transformed to a stationary field by removing the trend component at each location from the observed pore pressure value. The residuals, ε_{ru}, are modeled as a stationary random process with a zero mean and a standard deviation of 0.12. Figure 7–9 shows the histogram and the CDF of the residual pore pressure ratio.

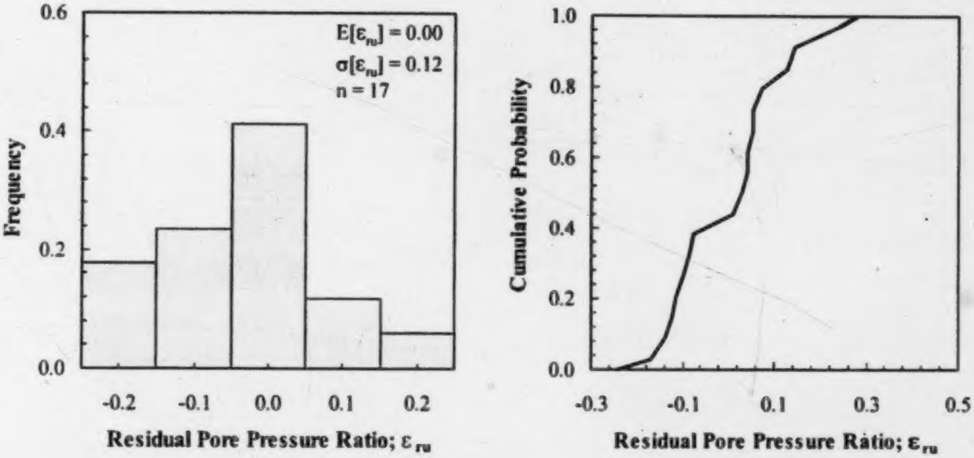

Figure 7–9 Histogram and CDF of the residual pore pressure ratio of the Kca unit

Sandy Till (Pgs)

The pore pressure in the sandy till layer is assessed based on data from 14 piezometers at different depths and locations along Section 53+000E. The pore pressure ratio varied between 0.10 and 0.46 with a mean of 0.30. Figure 7–10 shows the histogram of the pore pressure ratio in March, 1994. The histogram exhibits two peaks, at pore pressure ratios of 0.24 and 0.39, implying that the data might belong to different statistical populations. Figure 7–11 is a plot of the pore pressure ratio along the dyke cross-section. The plot indicates a sudden and large increase in pore pressure ratio towards the dyke toe. The same phenomenon is also observed in the pore pressure records at later dates. It was, therefore, decided to divide the data into two subgroups and the pore pressure ratio is modeled by two random variables. The first variable, corresponding to the middle portion of the slope, varies between 0.10 and 0.26 with a mean of 0.21 and a standard deviation of 0.06. The second variable, corresponding to the toe area, varies between 0.35 and 0.46 with a mean of 0.40 and a standard deviation of 0.03. Figure 7–12 shows the CDFs of the two variables.

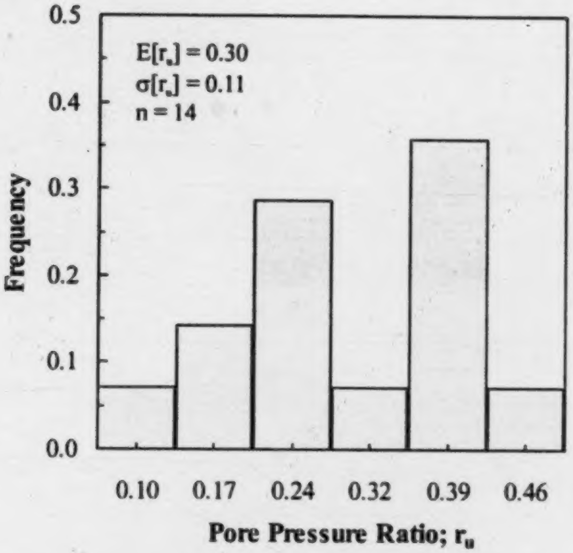

Figure 7–10 Histogram of pore pressure ratio in the sandy till, Pgs, in March 1994

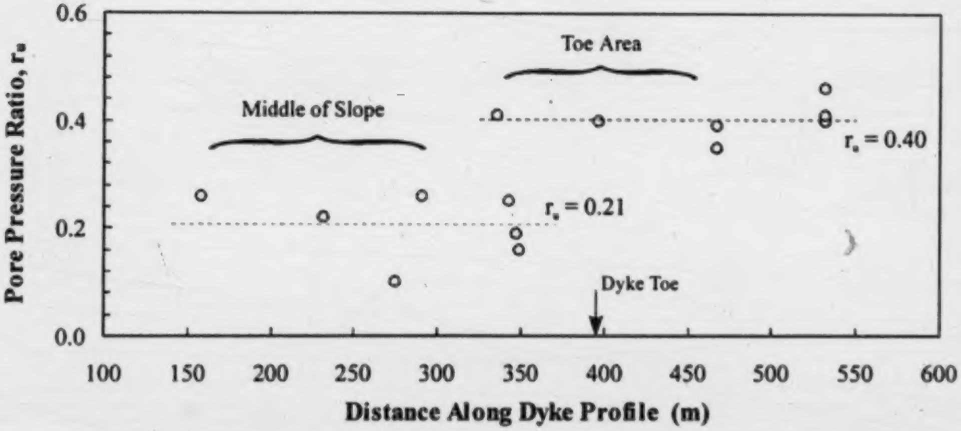

Figure 7–11 Profile of pore pressure ratio in the Pgs layer along dyke cross-section, March 1994

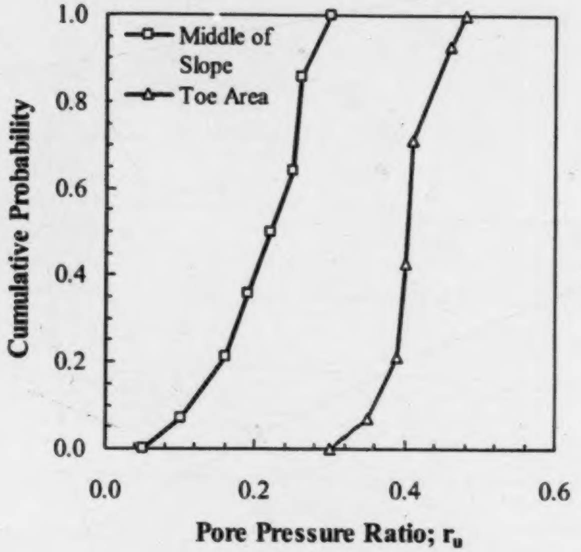

Figure 7–12 CDF of the pore pressure ratio in the Pgs layer, March 1994

Tailing Sand (TS) and Glacio-Fluvial Sand (Pf4)

Measurements from few piezometers were available for assessing the pore water pressure conditions in the tailings sand and the underlying glacio-fluvial sand. Based on total head data from 3 piezometers, the phreatic surface within the tailing sand is inferred as indicated in Figure 7–13. Similarly, the phreatic surface in the glacio-fluvial sand is obtained based on data from 4 piezometers, Figure 7–13. As would be expected, the two surfaces are very similar. Due to the limited extent of the failure surface within either layer and the little scatter of the measurements, the pore water pressure in both layers is considered deterministic and represented by the corresponding phreatic surface as shown in Figure 7–13.

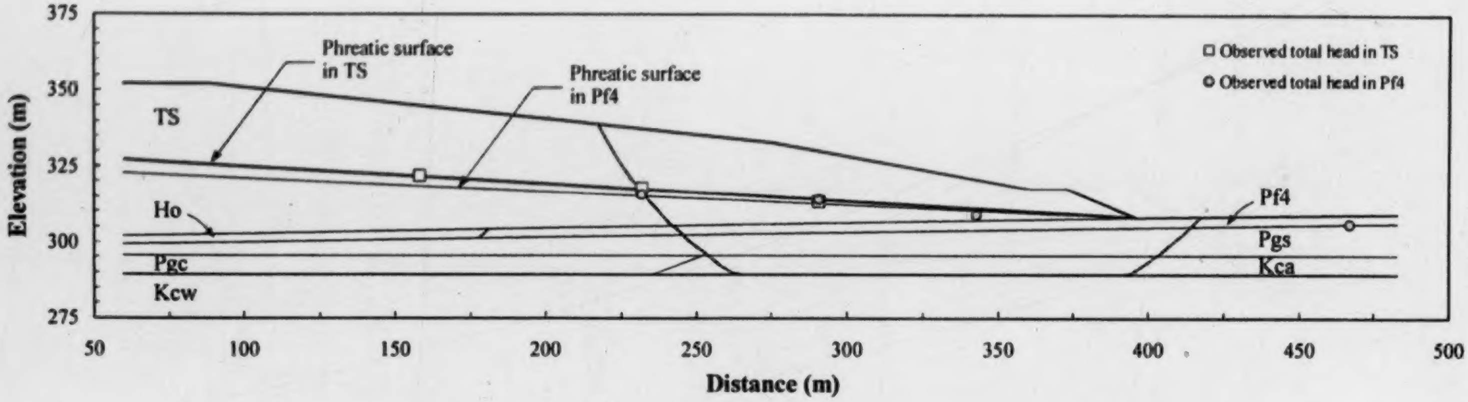

Figure 7–13 Phreatic surfaces in the tailing sand and the glacio-fluvial sand, March 1994

Clayey Till (Pgc) and Clay-shale (Kcw)

As the critical slip surface does not extend through either the clayey till or the clay-shale Kcw, the pore water pressure within the two layers is not of particular interest. Only preliminary assessment of the available data is undertaken

The pore pressure data in the clayey till layer were significantly scattered. Based on measurements from 8 piezometers, the pore pressure ratio in March of 1994 ranged between 0.20 and 0.77. The mean is estimated to be 0.47 with a standard deviation of 0.22. The clustering of the measurements at 2 locations (Figure 7–7) casts some doubt on the representativity of these estimates. Data from 7 piezometers were examined to assess the pore pressure conditions in the Kcw unit. Measurements taken in March of 1994 indicated the pore pressure ratio ranging between 0.24 and 0.49 with a mean of 0.36 and a standard deviation of 0.10.

3.3 Deterministic Slope Stability Analyses

A deterministic slope stability analysis is performed using Slope/W software to assess the factor of safety for Section 53+000E and to locate the critical slip surface. The mean values of the shear strength parameters and pore water pressures (Sections 3.2.2 and 3.2.3) are used in the analysis. Based on the observed movements during construction (Section 3.1), the critical slip surface is taken horizontal at the interface between the Kca and the Kcw units. Beyond the interface the slip surface is assumed circular. Bishop's method of slices is used in the analysis. The minimum factor of safety is calculated to be 1.30. Figure 7–2 shows the critical slip surface.

The slip surface with the minimum reliability index, according to the Hassan and Wolff (1999) algorithm, is also located. Two deterministic analyses are performed. Firstly, the residual friction angle of the Kca material is reduced by one standard deviation, then the pore pressure ratio in the Kca unit is increased by one standard deviation. The two analyses yielded factors of safety of 1.17 and 1.19, respectively. The surface corresponding to the reduced friction angle is considered the critical slip surface based on the Hassan and Wolff criterion. The deterministic and the Hassan and Wolff critical slip surfaces, Figure 7–2, are regarded as candidate surfaces for the probabilistic stability analysis. They are examined in Section 3.4.3 to identify the surface with the maximum probability of unsatisfactory performance. As is the case with the James Bay dykes, the two surfaces are very similar. It should be noted that neither of the surfaces cuts through the clayey till layer Pgc. The outcome of the probabilistic analysis is, thus, not affected by the uncertainties in the properties and pore pressures of the Pgc unit.

3.4 Probabilistic Slope Stability Analysis – Proposed Methodology

3.4.1 Input Variables

Based on the discussions in Sections 3.2.2 and 3.2.3, five input parameters were treated as variables: the peak friction angle and the pore pressure ratios at the middle and at the toe of the dyke for the sandy till and the residual friction angle and pore pressure ratio of the pre-sheared clay-shale, Kca. The observed (i.e., experimental) CDFs of all parameters are used in Monte Carlo simulation except for the residual friction angle of the Kca unit whose CDF is approximated by a lognormal distribution. This approximation is intended to reduce the simulation time since the observed CDF closely approximates a lognormal shape, Figure 7–4 and Figure 7–5, (simulation time is largely reduced when input variables are parametric distributions). Table 7-6 summarizes the statistical parameters and the CDFs of all variables.

The statistical uncertainty due to the limited amounts of data available is assessed using the procedures described in Chapter 3. These uncertainties are then added to those of soil variability. The uncertainty in the linear trend of the pore pressure ratio of the Kca material is accounted for by regarding the intercept and the slope of the trend as variables. Both are assumed normally distributed with means equal to the best estimates obtained from the regression analysis, Section3.2.3. Using Equations 3-21 and 3-22 of Chapter 3, the standard deviations of the slope and the intercept are estimated to be $5\text{x}10^{-4}$ and 0.187, respectively. A zero truncation limit is imposed on the probability distribution of the slope to prevent sampling positive values, i.e., increasing pore pressure ratio towards the toe of the dyke. The correlation coefficient between the two variables is calculated to be –0.998 (Equation 3-23). The uncertainties in the mean values of all other variables are also assumed normally distributed with zero means and variances estimated using Equation 3-20. Table 7-6 summarizes the mean, standard deviation and CDF of statistical errors. A total of six input variable are used to account for the statistical uncertainty.

Table 7-6 Statistical parameters of input variables – Proposed Methodology

Soil Unit	**Input Variable**			**Soil Variability**			**Statistical Error**		
				E[--]	**σ[--]**	**CDF**	**E[--]**	**σ[--]**	**CDF**
Pre-sheared clay-shale; Kca	Friction angle; ϕ'_{Kca} (deg.)			7.50	2.09	LogN.	0.000	0.233	N.
	Pore Pressure ratio	Trend	Slope	--	--	--	-0.001	$5x10^{-4}$	TN.
			Intercept	--	--	--	0.859	0.187	N.
		Residuals; ε_{ru}		0.00	0.12	Exper.	--	--	--
Sandy Till; Pgs	Friction angle; ϕ'_{Pgs} (deg.)			35.74	1.97	Exper.	0.000	0.509	N.
	Pore pressure ratio	Middle of slope; r_{u-M}		0.21	0.06	Exper.	0.000	0.023	N.
		Toe area; r_{u-T}		0.40	0.03	Exper.	0.000	0.012	N.

LogN. - LogNormal distribution; N. - Normal distribution; TN. - Truncated normal distribution; Exper. - Experimental (or observed) distribution

3.4.2 Spatial Variability

The first step to account for spatial variability is to decide on an estimate of the autocorrelation distance. As discussed in the preceding section, the uncertain parameters are the properties and pore pressures of the sandy till, Pgs, and the clay-shale, Kca. Examination of the critical slip surfaces, Figure 7–2, indicates that more than 70% of the portion cutting through the Pgs and the Kca layers is horizontal. Thus, the stability analysis is largely controlled by the spatial variability of soil properties in the horizontal, rather than the vertical, direction. Based on the survey presented in Chapter 5, the horizontal autocorrelation distance ranges between 20 and 40m. The spatial variability of the properties of the clay-shale unit Kca, the main unit affecting dyke stability, is known to be continuous rather than erratic. As such, it is likely that the spatial structure of this formation is characterized by a large autocorrelation distance. A range of 28-38m is postulated as a possible range for the autocorrelation distance. The probabilistic analysis is based on an intermediate value of 33m. The sensitivity of the probability of unsatisfactory performance to other values within the aforementioned range is investigated in Section 3.4.4.

The spatial variability of the sandy till and the clay-shale are dealt with separately. For the sandy till, the slip surface intersects the layer at two locations as shown in Figure 7–14. The lengths of the two segments within the sandy till are much smaller than the scale of fluctuation; $\delta \cong 2r_o$. The probability distribution of the local average of the friction angle over either segments is, therefore, the same as the point CDF. Since the spacing between the two segments is large, the correlation coefficient between the two averages (Equation 5-5, Chapter 5) is equal to zero. In summary, the variability of the friction angle of the sandy till is modeled by two uncorrelated variables representing the average friction angles at the middle of the slope and at the toe area. Both variables are assigned the point CDF of the observations.

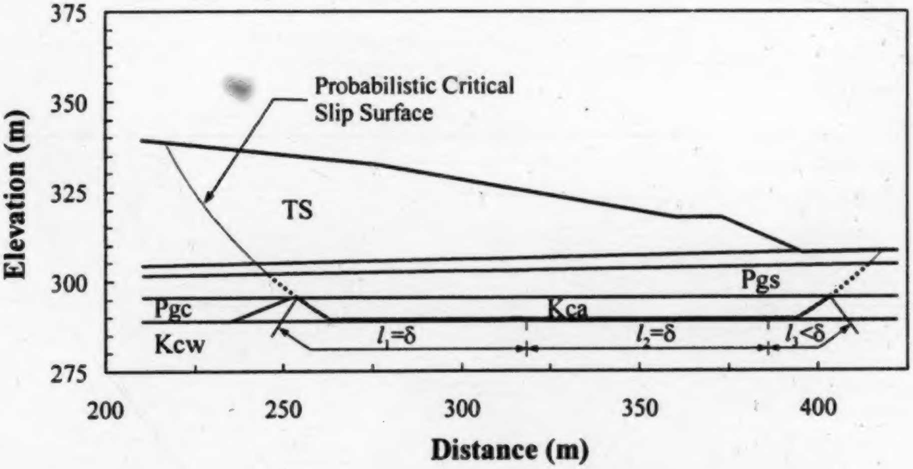

Figure 7–14 Accounting for spatial variability along the slip surface by the variability of local averages over segments of the surface

The portion of the slip surface within the clay-shale is divided into two segments of length δ and a third segment equal to the residual length, Figure 7–14. Thus, the variances of the average friction angle and the average residual pore pressure ratio over any of the segments are equal to the corresponding point variances. The correlation coefficients between the averages of segments 1 and 2 and segments 1 and 3 are equal to zero and that between segments 2 and 3 is equal to 0.35. The variability of the residual friction angle of the Kca material is, thus, modeled by three variables representing the average friction angle over three segments of the slip surface. All variables are longnormally distributed with statistical parameters as indicated in Table 7-6. The variables are uncorrelated, $\rho = 0$, except for segments 2 and 3 where the correlation coefficient is estimated to be 0.35. Similarly, the residual pore pressure ratio is represented by three variables all having the experimental CDF, Figure 7–9. Only variables 2 and 3 are correlated with a correlation coefficient of 0.35. In total, ten input variables are used to account for the spatial variability of input parameters along the slip surface.

3.4.3 Probabilistic Analysis

A spreadsheet model mimicking the geometry, stratigraphy, soil properties and pore pressures is prepared to assess the stability of the dyke at Section 53+000E. Bishop's method of slices is used in the model. The equilibrium equations were re-arranged to account for the non-circular portion of the slip surface. A total of 16 input variables, some of them are correlated, are used to account for soil spatial variability and statistical uncertainty. Recognizing a small probability of sampling negative values of the pore pressure ratios during simulation, the model is designed to replace negative values with a zero.

Based on a few trial simulations, the optimum number of iterations is estimated to be 34,000. Using a seed number of 31069, the probability of unsatisfactory performance associated with the deterministic critical slip surface is 0.13% and that of the Hassan and Wolff surface is 0.16%. The latter is, thus, considered the probabilistic critical slip surface and is used in the subsequent analyses. The mean factor of safety is computed to be 1.31 with a standard deviation of 0.14. Figure 7–15 shows the histogram and the CDF of the factor of safety. Since the correlation coefficients used in the analysis are the conventional coefficients, rather than Spearman coefficients required by @Risk software, the generated input data are examined to ensure that the proper correlations are reproduced. Using Equation 3-25 (Chapter 3), the conventional correlation coefficients between the slope and the intercept of the linear trend of Kca: r_u, between ϕ'_{Kca} of segments 2 and 3, and Kca: ε_{ru} of segments 2 and 3 are calculated to be –0.99, 0.34 and 0.33, respectively. These values compare very well with the input values of –0.99, 0.35 and 0.35.

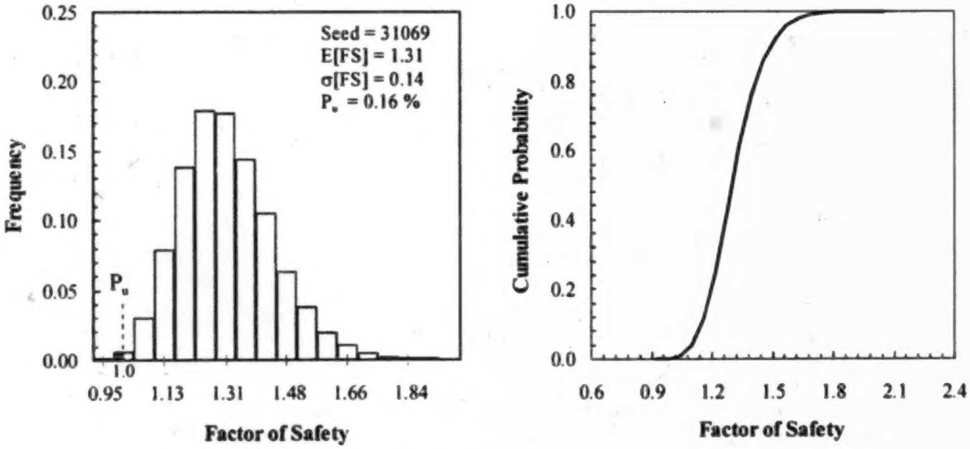

Figure 7–15 Histogram and CDF of the factor of safety, Cell 23 – Proposed methodology

A sensitivity analysis was performed and Figure 7–16 shows Spearman rank correlation coefficients for all 16 variables. As expected, the uncertainties in the residual friction angle and the pore pressure ratio of the Kca material are, by far, the largest contributors to the uncertainty in the factor of safety. Unlike the James Bay case study, systematic uncertainty contributes little compared to the uncertainty due to spatial variability. This is mainly due to the large amounts of data available particularly for the strength of the Kca material. Such a large role of soil variability could increase the sensitivity of the output (i.e., probability of unsatisfactory performance) to the assumption of the autocorrelation distance. The uncertainty in the strength of the sandy till at the toe area ranks third followed by the pore pressure ratio of the Pgs at the middle of the slope.

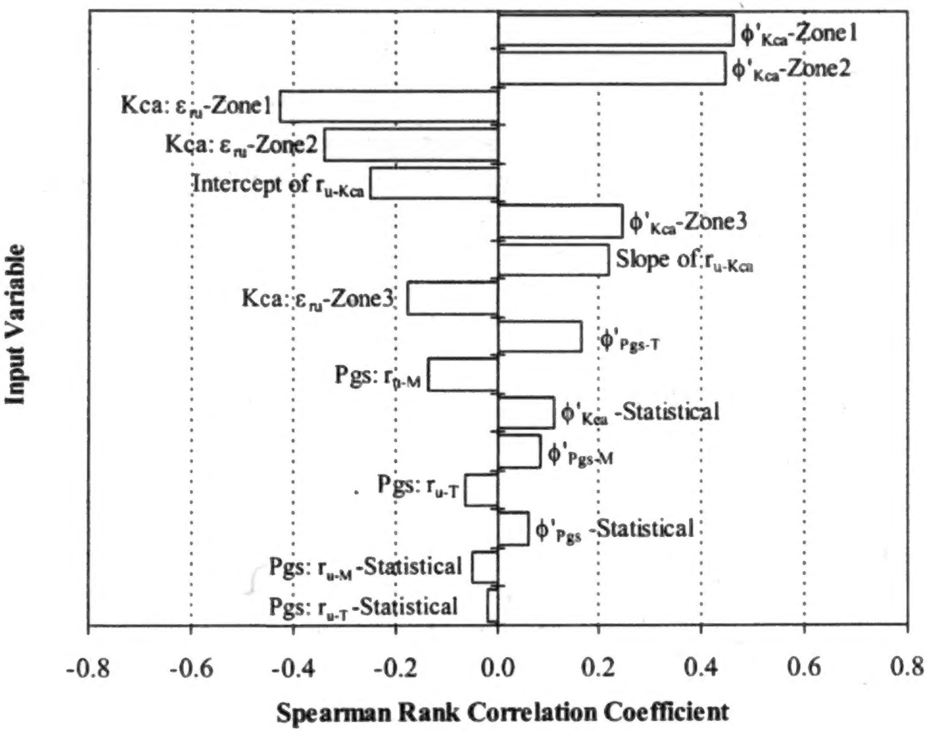

Figure 7–16 Sensitivity analysis results, Cell 23 – Proposed Methodology

From the results of 25 simulations, the mean probability of unsatisfactory performance is estimated to be 0.16% with the 95% confidence interval ranging between 0.15 - 0.17%. Figure 7–17 shows the histogram of the probability of unsatisfactory performance.

As discussed in Chapter 5, the analysis can be, alternatively, performed using the spatially averaged parameters along the entire failure surface within each layer. Only the variables representing soil variability are included in this averaging process, i.e., no systematic uncertainty. For example, the average friction angle $E[\phi'_{Kca}]$ along the failure surface is the weighted sum of the variables representing the local averages along segments 1 to 3 as illustrated in Figure 7–18. The averaging process can be easily conducted by simulation in a separate spreadsheet prior to the stability analysis.

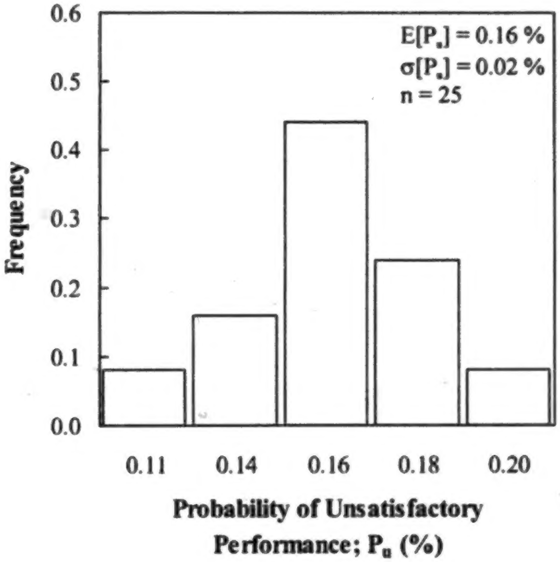

Figure 7–17 Histogram of the probability of unsatisfactory performance – Cell 23

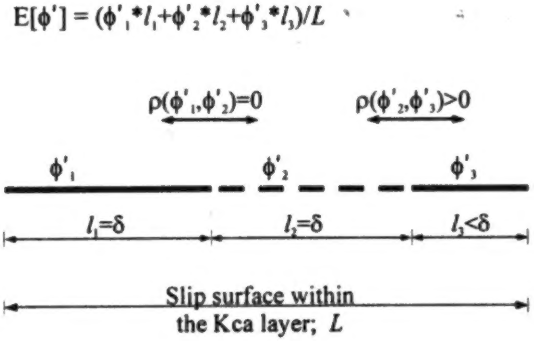
$E[\phi'] = (\phi'_1 * l_1 + \phi'_2 * l_2 + \phi'_3 * l_3)/L$
$\rho(\phi'_1, \phi'_2)=0$
$\rho(\phi'_2, \phi'_3)>0$
ϕ'_1
ϕ'_2
ϕ'_3
$l_1=\delta$
$l_2=\delta$
$l_3<\delta$
Slip surface within the Kca layer; L

Figure 7–18 Estimating the spatial average of ϕ'_{Kca} along the slip surface

Using @Risk software, Monte Carlo simulation is performed to estimate the CDFs and the variances of the *average* friction angle ϕ'_{Kca} and the *average* residual pore pressure ratio Kca: ε_{ru} over the length of the failure surface. The simulation time using 50,000 iterations was nearly 1 minute. The estimated variances are almost identical to those obtained using the variance reduction factor *f* (Equation 3-17) as shown in Figure 7–19 for different values of the autocorrelation distance.

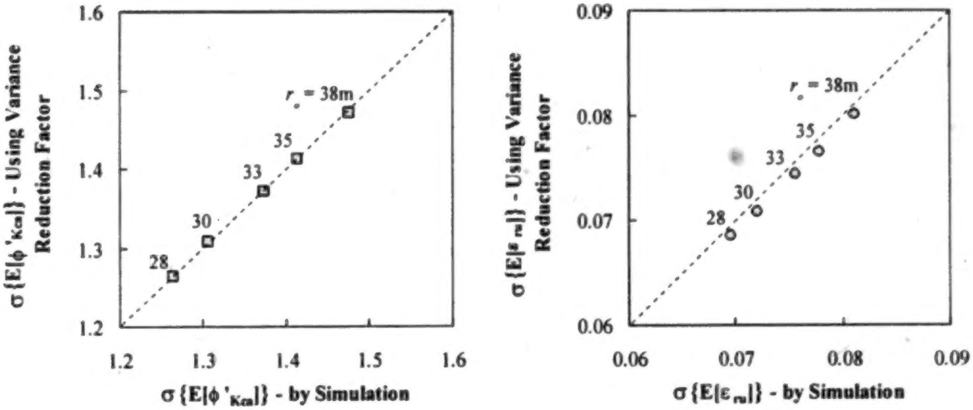

Figure 7–19 Comparing the estimates of the variances of the *average* friction angle and the *average* residual pore pressure ratio using Monte Carlo simulation and the variance reduction factor

A probabilistic stability analysis is undertaken using the probability distributions of the spatially averaged parameters E[ϕ'_{Kca}] and E[Kca:ε_{ru}]. The output of the analysis, using 34,000 iterations, is almost identical to the analysis accounting for the variability along the failure surface in Figure 7–15. Figure 7–20 compares the probability distributions of the factor of safety from both analyses, whereas Table 7-7 compares the statistical parameters of the two distributions.

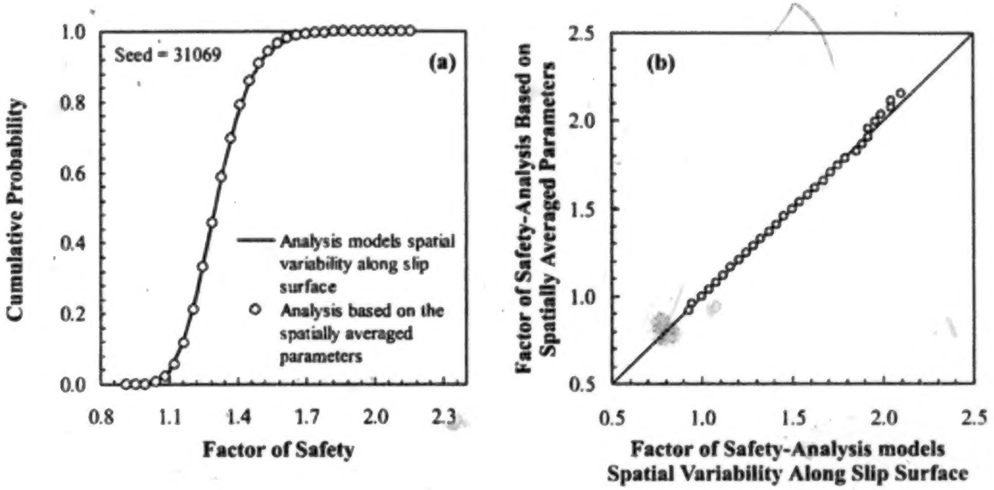

Figure 7–20 Comparison of the CDFs of the factor of safety from the analysis modeling spatial variability along slip surface and that based on the spatially averaged parameters – Cell 23; a) Probability distribution functions, b) Q-Q plot

Table 7-7 Comparison of the results of the analysis modeling the spatial variability along slip surface and that based on spatially averaged parameters – Cell 23.

Parameter	Analysis Characteristics	
	Models Variability Along Slip Surface	**Based on Spatially Averaged Parameters**
E[FS]	1.31	1.31
σ[FS]	0.14	0.13
Skewness	0.58	0.55
P_u (%)	0.16	0.17

Simulation is performed using a seed number of 31069 and 34,000 iterations

3.4.4 Sensitivity of the Analysis to the Autocorrelation Distance

The judgmental assessment of the autocorrelation distance is probably the most critical assumption made in the previous analyses, particularly since the stability of the dykes is largely controlled by the uncertainty due to spatial variability, Figure 7–16. It is, therefore, essential to examine the sensitivity of the output to the value of the autocorrelation distance.

As discussed in Section 3.4.2, the range 28-38m is perceived as a reasonable range for the autocorrelation distance. The probabilistic stability analysis is repeated using different values of the autocorrelation distance within the previous range. For each analysis, the failure surface is divided into segments and the correlation coefficients between the local averages over these segments are calculated in a way similar to the analysis outlined in the previous section. Figure 7–21 shows the estimated probability of unsatisfactory performance for different assumptions of the autocorrelation distance. The estimates vary between 0.08% for r_o=28m and 0.27% for r_o =38m.

In absolute terms, the range of P_u might seem substantial. However, in a practical sense, stating that the probability of unsatisfactory performance is somewhere in between 0.10% and 0.25% is not unreasonable. This is particularly true given the large uncertainty surrounding the analytical estimation of a single value of the autocorrelation distance.

3.5 Naïve Analysis

The stability of Section 53+000E is also assessed using the naïve approach. The uncertainties in the input variables are based solely on the observed variability as reflected by the testing and monitoring results. Statistical treatment of the data is limited to excluding few outlier values, that are judged unrepresentative, and calculating the means, variances and CDFs (Sections 3.2.2 and 3.2.3). Table 7-8 summarizes the statistical parameters and probability distributions used in the analysis.

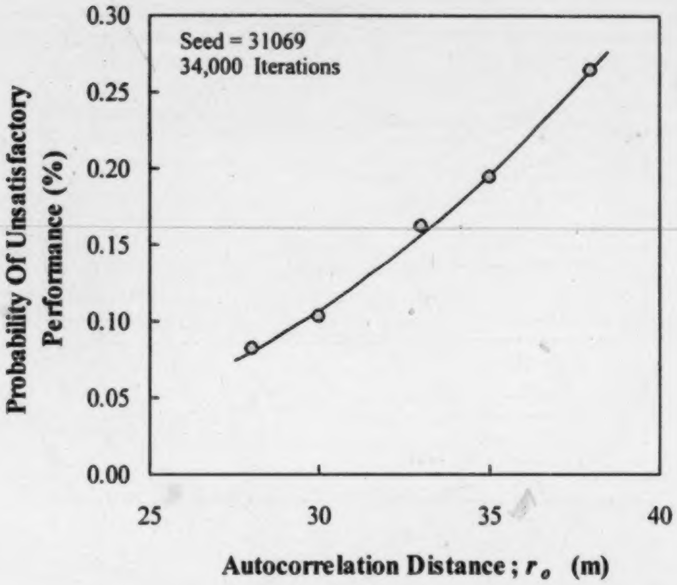

Figure 7–21 Probability of unsatisfactory performance versus autocorrelation distance

Table 7-8 Statistical parameters of the input variables – Naïve Analysis

Input Variable	Mean	Standard Deviation	Probability Distribution
Residual friction angle of Kca unit; ϕ'_{Kca} (deg.)	7.50	2.09	LogNormal
Residual pore pressure ratio of the Kca unit; ε_{ru}	0.00	0.12	Observed CDF
Friction angle of Pgs unit; ϕ'_{Pgs} (deg.)	35.74	1.97	Observed CDF
Pore pressure ratio of Pgs unit at middle of slope; $r_{u\text{-}M}$	0.21	0.06	Observed CDF
Pore pressure ratio of Pgs unit at toe of slope; $r_{u\text{-}T}$	0.40	0.03	Observed CDF

Bishop's method of slices and the failure surface from the Hassan and Wolff (1999) algorithm, Figure 7–2, were used in preparing the spreadsheet model. A Monte Carlo simulation using 34,000 iterations and a seed value of 31069 was performed. The analysis yielded a mean factor of safety of 1.31, a standard deviation of 0.18 and a probability of unsatisfactory performance of 1.66%. Figure 7–22 shows the histogram and the probability distribution of the factor of safety. Based on the results of 25 simulations, the mean probability of unsatisfactory performance is estimated to be 1.6% with a 95% confidence interval of 1.57-1.63%. Figure 7–23 shows the histogram of the probability of unsatisfactory performance.

A sensitivity analysis is performed and Figure 7–24 shows Spearman rank correlation coefficients for all input variables. The results match those of the previous analyses, emphasizing the significance of the uncertainties in the friction angle and pore pressure ratio of the Kca material. The shear strength of the sandy till ranks third whereas the pore pressure in the Pgs unit does not seem to have a large impact on the stability.

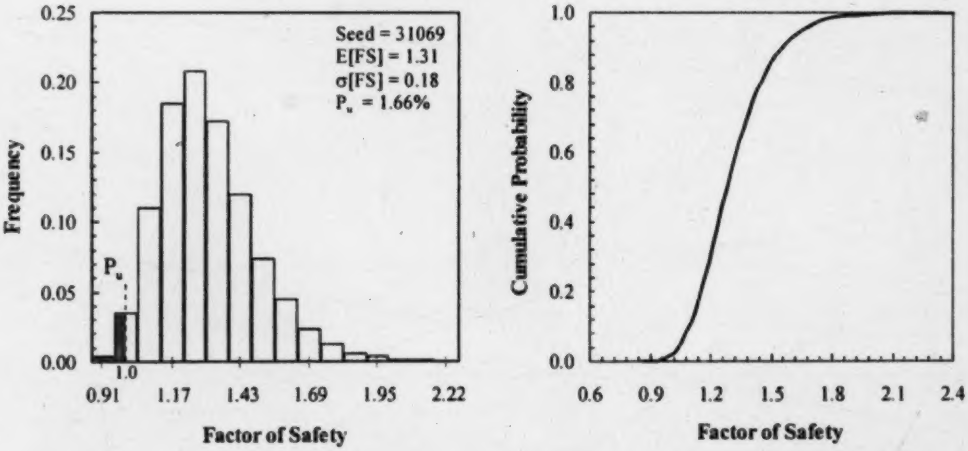

Figure 7–22 Histogram and CDF of the factor of safety, Cell 23 – Naïve analysis

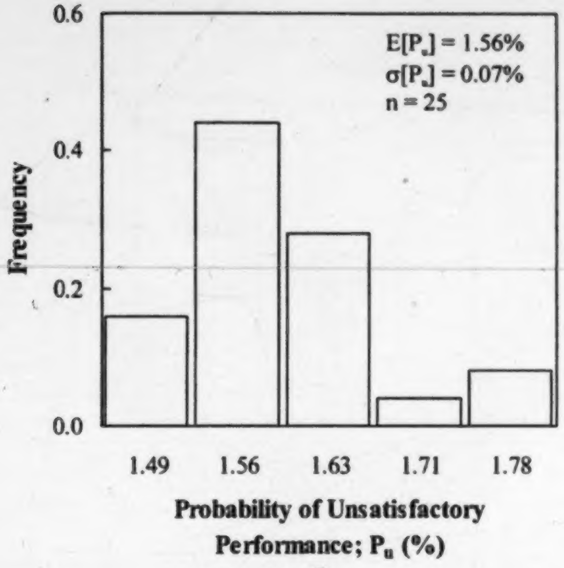

Figure 7–23 Histogram of the probability of unsatisfactory performance, Cell 23 – Naïve analysis

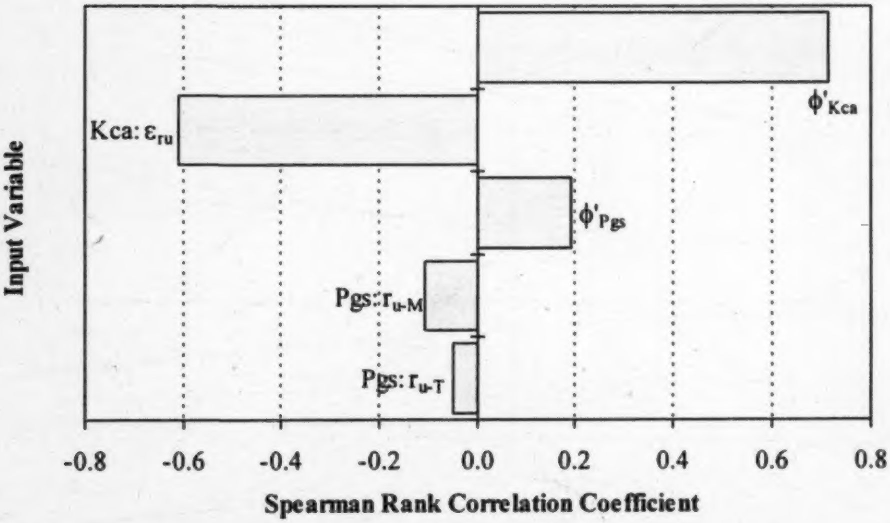

Figure 7–24 Sensitivity analysis results, Cell 23 – Naïve analysis

4. SUMMARY

The new methodology is applied to study the stability of Section 53+000E at Cell 23 of Syncrude tailings dyke. The various analyses undertaken illustrate the great flexibility the spreadsheet approach can offer in terms of handling input variables, accounting for spatial variability, or spatial averaging, and conducting stability analyses.

Unlike the James Bay dykes, systematic uncertainty contributed little to the overall design reliability. This is attributed mainly to the significant amounts of data available, particularly for the strength of the clay-shale Kca, and the absence of any indications of bias. This, however, is not the norm in geotechnical practice. Systematic uncertainties could have a large impact on the design of many projects.

Because of the modest contribution of systematic uncertainty, the uncertainty due to soil variability has a large impact on the reliability of the design. As a result, the output of the analysis is sensitive to the value of the autocorrelation distance. The probability of unsatisfactory performance varied between 0.082% and 0.265% as the autocorrelation distance varied between 28m and 38m. From a practical point of view, such variability does not seem substantial. However, a large number of case studies need to be analyzed before concluding that the autocorrelation distance has, practically, insignificant impact on the probability of unsatisfactory performance. As with the James Bay dykes, the estimate of the probability of unsatisfactory performance from the naïve analysis is approximately one order of magnitude higher than the analysis accounting for spatial variability.

CHAPTER 8

LODALEN SLIDE NORWAY, 1954

The probabilistic methodology is applied to the Lodalen slide that occurred in Norway in 1954. The geometry immediately before failure is first analyzed. The slope angle is then reduced to various values and the modified geometries are analyzed to establish the relationships between the slope angle, the factor of safety and the probability of unsatisfactory performance. These relations allow estimating the probability associated with an acceptable design based on conventional deterministic practice. Such estimates are of great value in setting guidelines for the allowable probability of unsatisfactory performance. The following sections present a brief description of the slide and detail the deterministic and probabilistic analyses undertaken.

1. INTRODUCTION

The slide occurred in 1954 in the area of the Lodalen marshalling yard near Oslo railway station, Norway. Failure occurred in a clay slope excavated 30 years earlier to expand the marshalling yard. Over this period, the slope was back excavated and steepened a few times. At the time of failure the slope was about 17m high with a 2h:1v inclination. Figure 8–1 shows a cross-section of the slope before failure. Field evidence indicated that the slide was mainly rotational. As a result of the rotation, a 5m main scarp was formed and the toe of the slope moved forward about 10m. The width of the displaced mass was about 50m and its volume was estimated to be 10,000 m^3.

The slide was thoroughly investigated by, among others, the Norwegian Geotechnical Institute in a study that aimed at verifying the methods of analyzing the stability of slopes then available. Sevaldson (1956) provided a detailed description of the slide and the investigation into its causes.

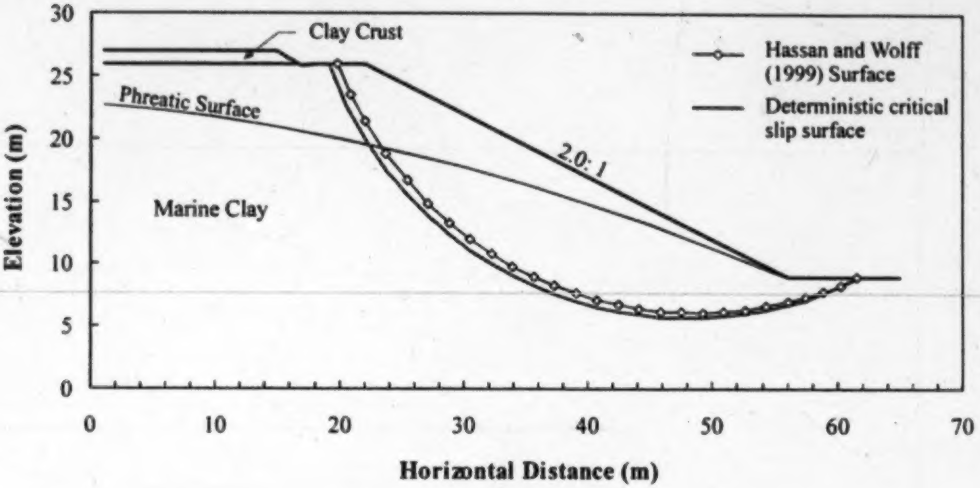

Figure 8–1 Cross-section and stratigraphy of Lodalen slide

2. SUBSURFACE CONDITIONS

Shortly after the slide, the Norwegian Geotechnical Institute carried out a field investigation program. The program included 7 boreholes, 2 test pits and 4 piezometers with moving measuring points to allow pore pressure measurements at various depths. Three boreholes and one piezometer were located within the slide area. The subsurface conditions at the site of the slide are assessed based on the data gathered through this investigation.

2.1 Stratigraphy and Soil Properties

The stratigraphy at the slide location is simple, comprising a clay crust about 1 m thick, overlying a firm homogenous marine clay extending to the end of borings. Some thin silt layers intercalate the marine clay. The clay has a moisture content of about 30%, liquid limit of about 35%, plastic limit of about 20% and a sensitivity ranging from 3 to 15. Figure 8–1 shows the soil stratigraphy at the slide area.

The strength of both the clay crust and the marine clay is measured by a number of unconsolidated undrained triaxial tests with pore pressure measurements. Based on the results of 2 tests, the effective cohesion and the friction angle of the crust are estimated to be 11.8 kPa, and 32 degrees, respectively. The effective shear strength parameters of the marine clay are assessed based on the results of 10 tests, each comprising 3 or 4 specimens. Table 8-1 summarizes the results of the 10 tests. The mean effective cohesion is estimated to be 10.0 kPa with a standard deviation of 2.2 kPa. The mean friction angle is 27.1 degrees with a standard deviation of 1.7 degrees. Figure 8–2 and Figure 8–3 show the histograms and the CDFs of the effective cohesion and the friction angle, respectively. The data are also examined to assess the correlation between the cohesion, C', and the tangent of the friction angle ϕ' (the intercept and slope of the strength envelope), if any. Figure 8–4 is a scatter plot of C' versus tan ϕ'. The two parameters are apparently uncorrelated with a near zero correlation coefficient, $\rho = -0.06$.

Table 8-1 Summary of results of unconsolidated undrained triaxial tests on the marine clay (Sevaldson, 1956)

Test No.	Cohesion; C' (kPa)	Friction Angle; ϕ' (deg.)
1	9.8	27.5
2	7.8	24.9
3	9.8	28.1
4	9.8	27.7
5	7.8	26.6
6	12.8	24.0
7	9.8	26.3
8	6.9	29.4
9	11.8	27.2
10	13.7	29.2

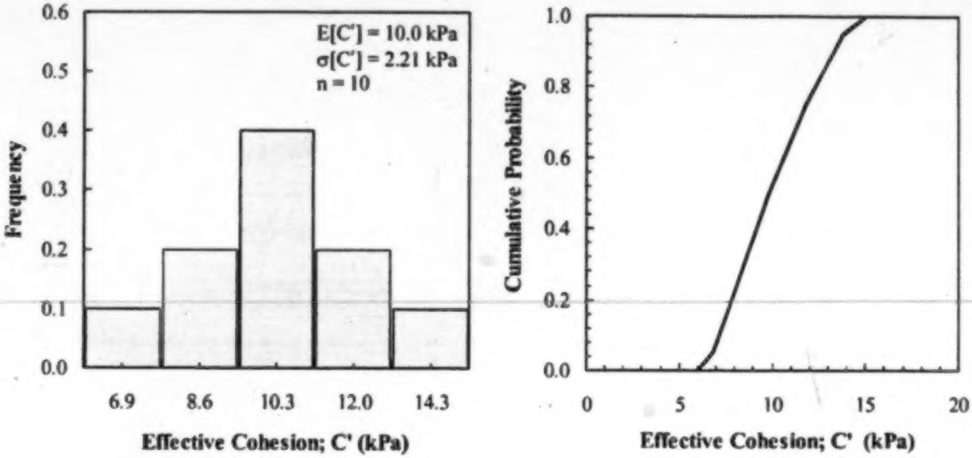

Figure 8–2 Histogram and CDF of the effective cohesion of the marine clay

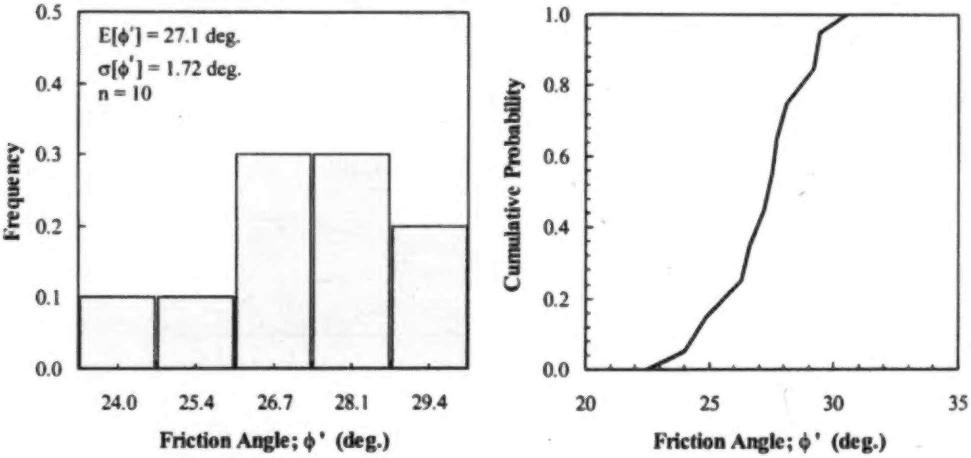

Figure 8–3 Histogram and CDF of the friction angle of the marine clay

2.2 Pore Water Pressure

Following the slide, the Norwegian Geotechnical Institute installed 4 piezometers (A, B, C and D) in and around the slide area to assess the pore water pressure. Measurements were taken at various depths in each piezometer. Piezometer D was located within the slide area and the reported pore pressure measurements are most likely affected by the remolding of the sliding mass. The data from piezometer D were excluded from the analysis. Figure 8–5 shows the locations of the piezometers and the pore pressure measurements along the profile of the slope.

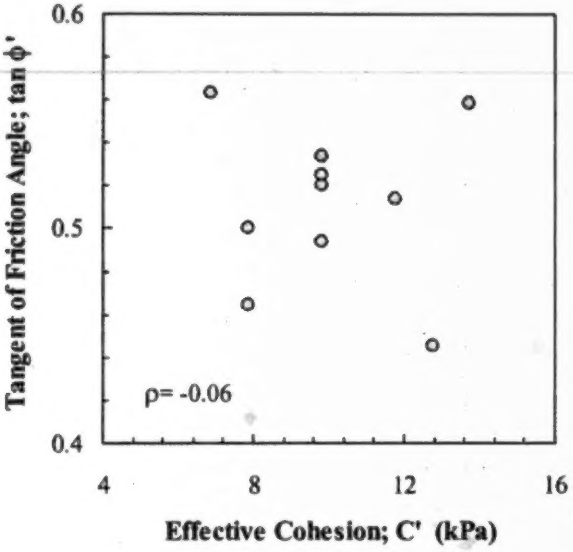

Figure 8–4 Scatter plot of C' and tan ϕ'

Based on the reported pore pressure data, the phreatic surface is inferred as shown in Figure 8–5. The pore pressure measurements are plotted versus the depth below the phreatic surface in Figure 8–6. All measurements plot above the hydrostatic pressure line indicating artesian conditions. Using the method of least squares, a linear trend is fitted to the data. Surprisingly, the measurements show minimal scatter around the trend. Since the data exhibit a clear trend with depth, the process is non-stationary. The pore pressure is transformed into a stationary process by removing the trend component from all measurements. The residual pore pressure (in terms of pressure head) is then modeled as a stationary random field with zero mean and a standard deviation equal to 0.34m. Figure 8–7 shows the histogram and the CDF of the residual pore pressure.

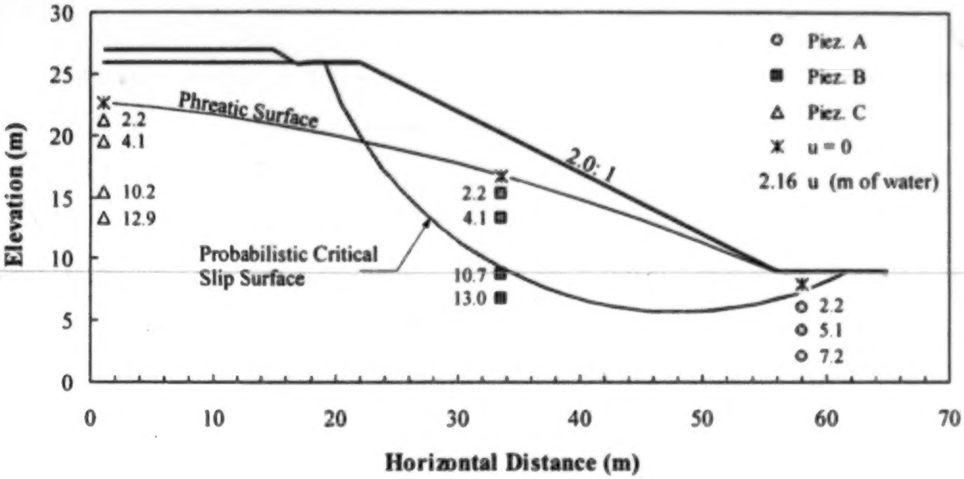

Figure 8–5 Piezometers and pore pressure measurements – Lodalen slide

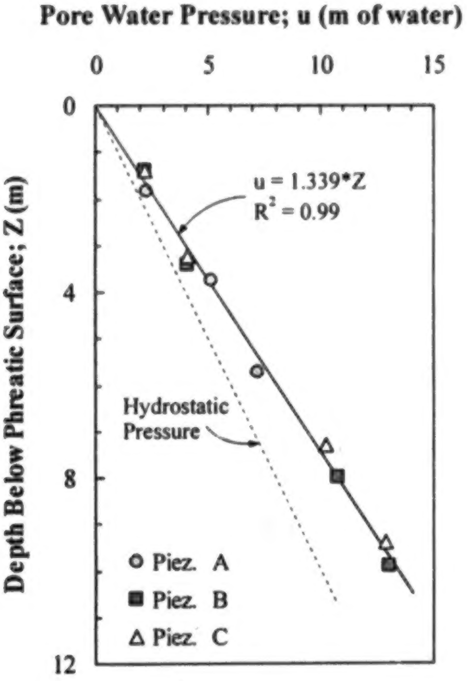

Figure 8–6 Pore pressure versus depth below phreatic surface

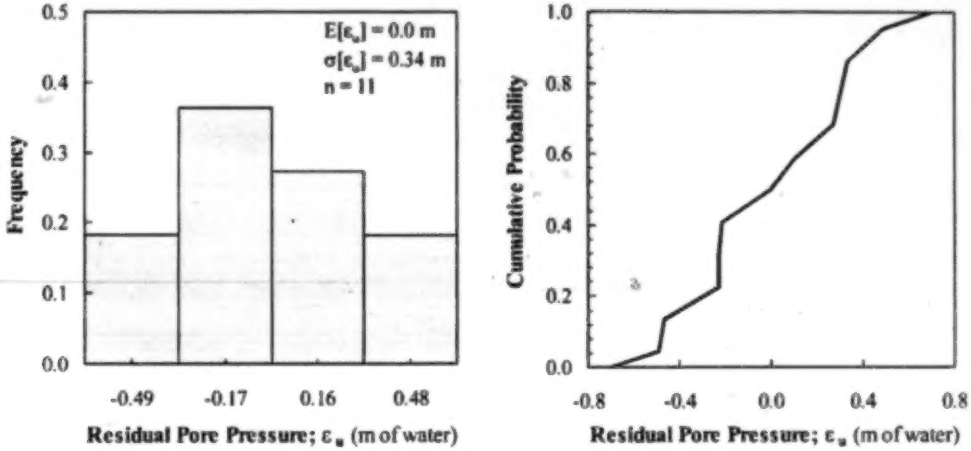

Figure 8–7 Histogram and CDF of the residual pore pressure – Lodalen slide

3. SLOPE STABILITY ANALYSES

3.1 Deterministic Analysis

The stability of the slope is assessed deterministically using Slope/W software and the Bishop method of slices, assuming a circular slip surface. The mean values of the shear strength parameters and the deduced phreatic surface (taking into account the artesian conditions, Figure 8–6) are used in the analysis. The minimum factor of safety is calculated to be 0.96. Figure 8–1 shows the critical slip surface.

3.2 Probabilistic Analysis – Proposed Methodology

3.2.1 Input Variables

Based on the discussions in Section 2, three parameters are considered as random variables; the effective cohesion, the friction angle and the pore water pressure of the marine clay. The uncertainties due to soil variability are represented by the observed CDFs, Figure 8–2, Figure 8–3 and Figure 8–7. Since there are no indications of any correlation between the three parameters, they are treated independently. Statistical uncertainties in the mean values of the cohesion and friction angle are represented by normal distributions with zero means and standard deviations estimated using Equation 3-20. The uncertainty in the slope of the linear trend of the pore pressure is also represented by a normal distribution. The mean of the distribution is the best estimate obtained from the regression analysis using the method of least squares and is equal to 1.34. Using Equation 3-24, the standard deviation of the slope is estimated to be 0.017. Table 8-2 summarizes the statistical parameters and the probability distributions of all variables.

Table 8-2 Statistical parameters and CDFs of the input variables – Lodalen slide

Input Variable		**Soil Variability**			**Statistical Error**		
		E[--]	**σ[--]**	**CDF**	**E[--]**	**σ[--]**	**CDF**
Effective Cohesion; C' (kPa)		10.0	2.21	Exper.	0.0	0.70	N.
Friction angle; ϕ' (deg.)		27.1	1.72	Exper.	0.0	0.54	N.
Pore Pressure	Slope of the trend	--	--	--	1.339	0.017	N.
	Residuals; ε_u (m)	0.0	0.34	Exper.	--	--	--

N. - Normal distribution; Exper. - Experimental (or observed) distribution

3.2.2 Critical Slip Surface

In locating the probabilistic critical slip surface, two candidate surfaces are considered; the deterministic critical slip surface and the slip surface based on the Hassan and Wolff (1999) algorithm. The latter is determined by performing three deterministic analyses with the effective cohesion reduced by one standard deviation, then the friction angle reduced by one standard deviation and, finally, with the pore pressure increased by one standard deviation. The failure surface corresponding to the reduced cohesion yielded the least factor of safety and is considered the critical surface based on the Hassan and Wolff criterion. The deterministic surface and the Hassan and Wolff surface are, however, very similar as shown in Figure 8–1.

Preliminary probabilistic stability analyses (using the proposed methodology) of the slope geometry before failure indicated that the probability of unsatisfactory performance associated with the deterministic surface is 77.49%, whereas that associated with the Hassan and Wolff surface is 76.21%. The former is considered the probabilistic critical slip surface and is used in the subsequent analyses. It should be mentioned that as the slope geometry is modified (Section 3.2.5), the deterministic critical surface was not always the most critical in probabilistic terms. For each slope geometry, the two surfaces are examined to determine the surface that yields a higher probability of unsatisfactory performance.

3.2.3 Spatial Variability

The first step to account for the spatial variability of the input variables is to estimate the autocorrelation distance. In his assessment of the subsurface conditions at the slide area, Sevaldson (1956) described the marine clay as "comparatively homogeneous". This conclusion is backed by the relatively small coefficients of variation of the cohesion and friction angle; 0.22 and 0.06, respectively. In addition, the depositional process in an offshore marine environment tends to produce materials of similar characteristics over large areas as well as with depth. As a result, marine deposits are, in general, characterized by continuous, rather than erratic, pattern of spatial variability. Also, the scatter of the pore pressure measurements around the mean trend, Figure 8–6, is unusually small. Such observations imply that the variability of the marine clay and the pore pressure is small and of a continuous nature. The autocorrelation distance is likely to be at the upper end of the typical ranges reported in Chapter 5. A range of 30-40m is postulated as a possible range for the horizontal autocorrelation distance and 1-3m as a possible range for the vertical autocorrelation distance.

Since the critical slip surface, Figure 8–1, is almost a quarter of a circle the analysis is not dominated by the spatial structure in a specific direction. The variability is, thus, approximated by an equivalent isotropic spatial structure with an equivalent autocorrelation distance. Based on the presumed ranges of the horizontal and vertical autocorrelation distances and using Equation 5-6, the equivalent autocorrelation distance is in the range of 5-15m. The probabilistic analyses in the following sections are based on an intermediate value of 10m. The sensitivity of the output of the analysis to other values within the postulated range is investigated in Section 3.2.5.

In analyzing the slope geometry before failure (2h:1v), the spatial variability of the strength parameters and the residual pore pressure are accounted for by dividing the probabilistic critical slip surface, Figure 8–1, into two segments of length $l_1=l_2=\delta=20$m and a residual segment of length $l_3<\delta$. The local average of each parameter over any of the three segments is modeled by the observed point CDF (Figure 8–2, Figure 8–3 and Figure 8–7). Thus, the variability of each of the uncertain parameters is represented by three variables corresponding to the local averages over the three segments of the slip surface. A total of 9 variables are used to account for spatial variability. The correlation coefficients between the variables are calculated using Equation 5-5. In analyzing other slope geometries (Section 3.2.5), the same approach is applied with the difference that the number of segments, and consequently the number of variables, varies depending on the length of the slip surface.

3.2.4 Stability Analysis – Geometry Before Failure (2h:1v)

A spreadsheet model mimicking the slope geometry before failure and the probabilistic critical slip surface is prepared. Bishop's method of slices is used in the model. The model includes 3 uncertain parameters (cohesion, friction angle and residual pore pressure of the marine clay) represented by a total of 12 variables. Three variables account for statistical uncertainty and 9 variables account for spatial variability.

Based on a few trial simulations, the optimum number of iterations is estimated to be 15,000. Using a seed number of 31069, the mean factor of safety is 0.95 with a standard deviation of 0.06. The probability of unsatisfactory performance is estimated to be 77.49%. Figure 8–8 shows the histogram and the CDF of the factor of safety. Based on the results of 25 simulations, the mean probability of unsatisfactory performance is estimated to be 77.38% with the 95% confidence interval ranging between 77.28-77.48%. Figure 8–9 shows the histogram of the probability of unsatisfactory performance.

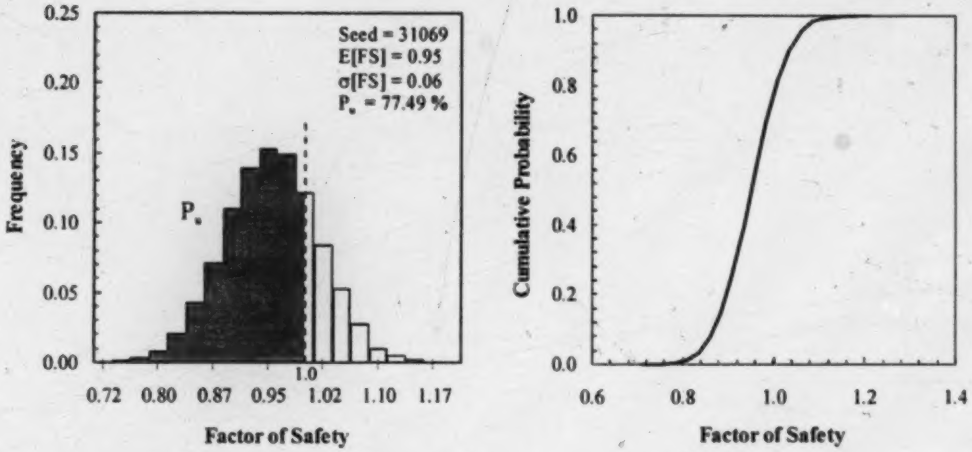

Figure 8–8 Histogram and CDF of the factor of safety, Lodalen slide (2h:1v) – Proposed Methodology

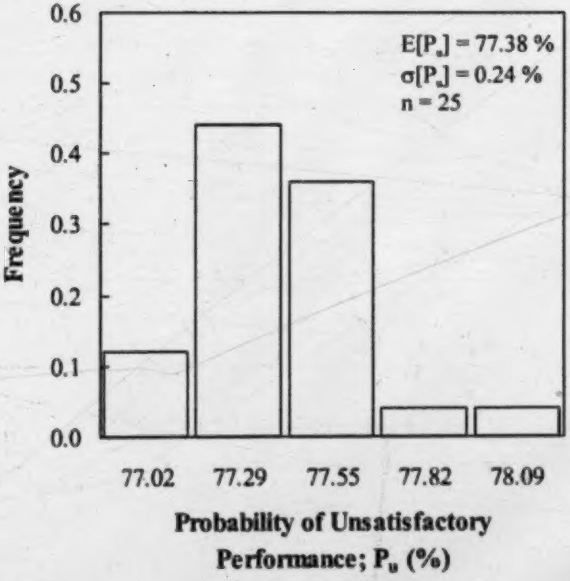

Figure 8–9 Histogram of the probability of unsatisfactory performance; Lodalen slide (2h:1v) – Proposed methodology

A sensitivity analysis is also performed and Figure 8–10 shows Spearman rank correlation coefficients for all 12 variables. The plot implies that the reliability of the slope is not dominated by the uncertainty of one parameter in particular. However, if the three input parameters are ranked based on their contributions to the uncertainty of the factor of safety, the cohesion ranks first followed by the friction angle and the pore water pressure. Even though, the amount of data available is not significant, statistical uncertainty contributes little to the overall uncertainty. This is attributed to the homogeneous nature of the marine clay and the exceptionally small scatter in the pore water pressure measurements (Section 2).

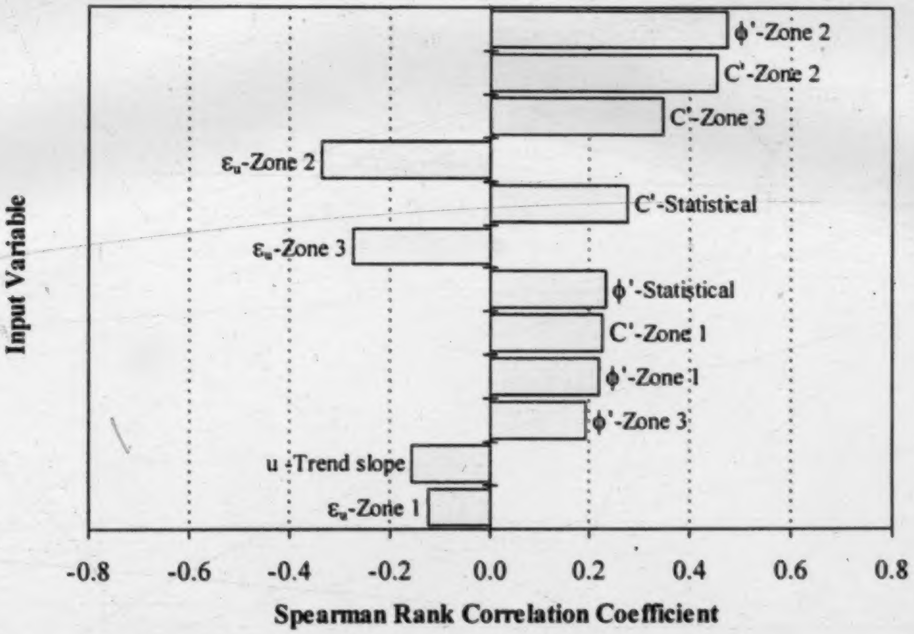

Figure 8–10 Sensitivity analysis results, Lodalen slide (2h:1v) – Proposed Methodology

The stability analysis is repeated using the alternative approach based on the probability distributions of the spatially averaged parameters over the length of the slip surface. In a separate spreadsheet, the probability distribution of the average cohesion is estimated by simulation following the same approach outlined in Chapter 7. Using 50,000 iterations, the simulation time was less than 1 minute. The probability distributions of the average friction angle and the average residual pore pressure are estimated similarly. The stability analysis yielded almost the same results as the analysis modeling variability along the failure surface. Figure 8–11 compares the CDFs of the factors of safety from both analyses while Table 8-3 compares the statistical parameters of both distributions.

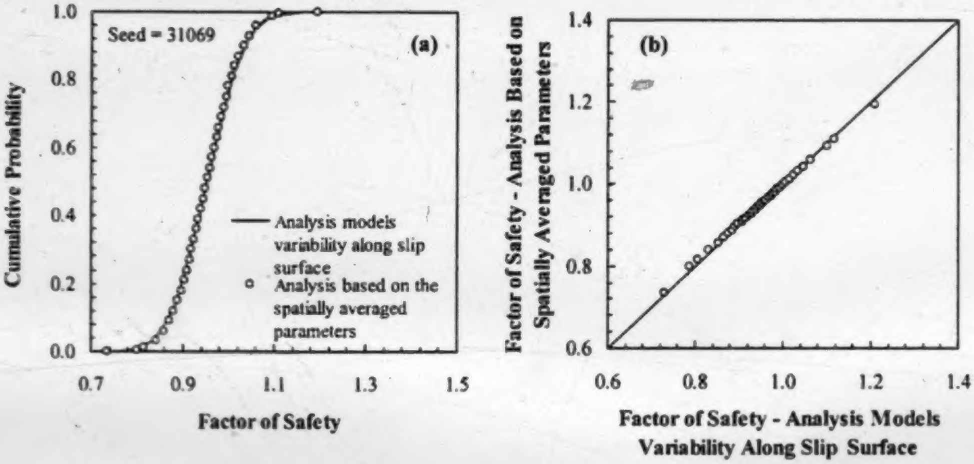

Figure 8–11 Comparison of the factor of safety from the analysis modeling variability along the slip surface that based on the spatially averaged parameters, Lodalen slide; a) Probability distribution functions, b) Q-Q plot

Table 8-3 Comparison of the results of the analysis modeling variability along slip surface and that based on the spatially averaged parameters – Lodalen slide

Parameter	Analysis Characteristics	
	Modeling Variability Along slip Surface	Based on Spatially Averaged Parameters
E[FS]	0.95	0.95
σ[FS]	0.06	0.06
Skewness	0.01	0.05
P_u (%)	77.49	78.59

3.2.5 Stability Analyses – Slope Geometry Modified

The probabilities of unsatisfactory performance associated with acceptable slope designs based on the current state of practice are of great value in setting guidelines for a probabilistic acceptance criterion for earth slopes. The slope geometry of the Lodalen case is modified to various inclinations (2.5:1, 3.0:1, 3.5:1 and 4.0:1) and each geometry is analyzed to estimate the probability of unsatisfactory performance. The analysis of each case involved locating the probabilistic critical slip surface, accounting for spatial variability and statistical uncertainty and determining the optimum number of iterations. For each geometry, 10 simulation runs are performed and the outputs are averaged. Figure 8–12 shows the change of the probability of unsatisfactory performance and the factor of safety with the slope angle. The plot indicates minimal increase in the probability of unsatisfactory performance as the slope angle increases from 14 degrees (4h:1v) to 17 degrees (3.3h:lv). A slope angle of 18 degrees marks the beginning of a significant increase in the probability of unsatisfactory performance. The factor of safety associated with that angle is about 1.12.

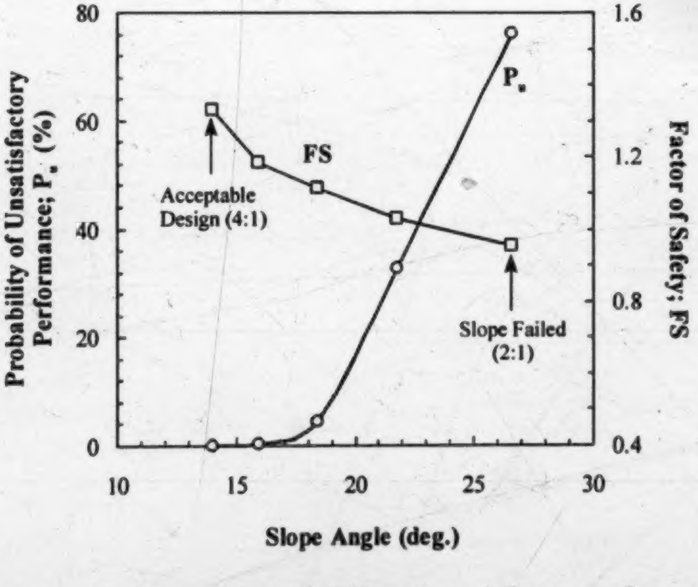

Figure 8–12 Variation of the probability of unsatisfactory performance and the factor of safety with the slope angle, Lodalen slope – Proposed Methodology

3.2.6 Stability Analysis – Acceptable Slope Design (4h:1v)

Conventional slope design practice is based on an allowable factor of safety, typically, in the range of 1.3-1.5. The decision on a specific value is left to the judgement of the designer. Based on experience and judgement, the current practice is to adopt design factors of safety at the upper end of that range (e.g., FS=1.4-1.5) for slope problems involving long-term stability, such as the Lodalen case. A slope of 4h:1v has a factor of safety of 1.33 (Figure 8–12) and would, therefore, be regarded by many practitioners as somewhat non-conservative. Figure 8–13 summarizes the output of the probabilistic assessment of the stability of the 4h:1v slope. The slope has a mean factor of safety of 1.33 with a standard deviation of 0.07 and a near zero probability of unsatisfactory performance. Such a low probability is attributed to the small uncertainty in the input parameters. Because of the high reliability of the inputs, the probabilistic approach gives higher credibility to the calculated factor of safety (a coefficient of variation of only 5%) compared to the deterministic approach whose account of uncertainty is subjective. Combining the conclusion of the probabilistic analysis with conventional practice may well lead to the acceptance of the 4.0:1 slope as an adequate design.

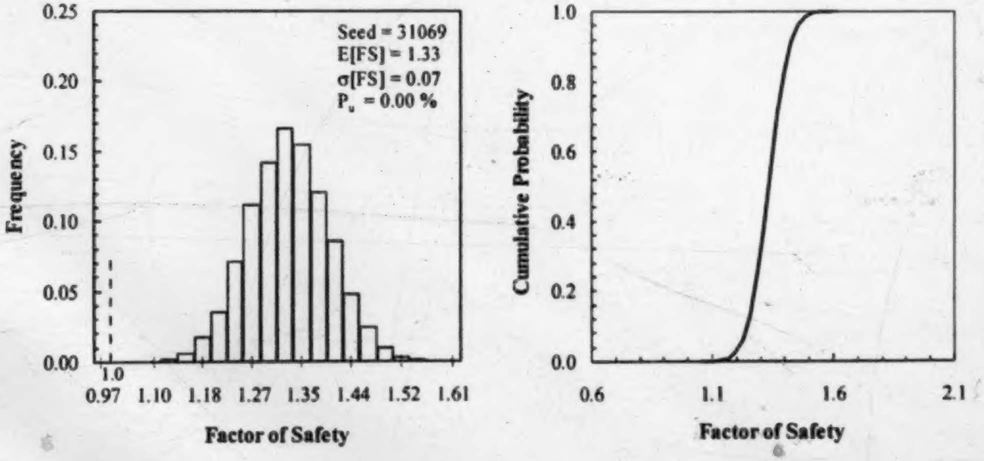

Figure 8–13 Histogram and CDF of the factor of safety, Lodalen slope (4h:1v) – Proposed Methodology

The sensitivity of the near zero probability of unsatisfactory performance of the 4:1 slope to the autocorrelation distance is assessed. As discussed in Section 3.2.2, the range 5-15m is perceived as a reasonable range for an equivalent isotropic autocorrelation distance. The probabilistic stability analysis is repeated assuming different autocorrelation distances. Table 8-4 summarizes the outputs of the analyses. As the autocorrelation distance increases (i.e., spatial variability becomes less erratic), the variances of the spatially averaged input parameters increase leading to a higher uncertainty in the factor of safety (i.e., higher standard deviation). The impact of such increases on the probability of unsatisfactory performance (rounded to 4 decimal places) is, however, not visible as shown in Table 8-4.

Table 8-4 Sensitivity of the output of probabilistic stability analysis to the presumed value of the autocorrelation distance

	Autocorrelation Distance; r_o (m)					
	5.2	**8.0**	**10.0**	**12.0**	**15.0**	**20.0**
E[FS]	1.33	1.33	1.33	1.33	1.33	1.33
σ[FS]	0.057	0.063	0.068	0.074	0.079	0.088
Skewness	0.02	0.02	0.02	0.04	0.01	0.02
P_u (%)	0.00	0.00	0.00	0.00	0.00	0.00

3.3 Naïve Analysis

The stability of the 4h:1v slope is assessed following the naïve approach. A spreadsheet model mimicking the slope geometry and the probabilistic critical slip surface is prepared. The Bishop method of slices is used in the spreadsheet. Each of the uncertain input parameters (cohesion, friction angle and pore pressure) is modeled as a random variable having the experimental distribution function, Figure 8–2, Figure 8–3 and Figure 8–7.

Using a seed value of 31069 and 25,000 iterations, Monte Carlo simulation yielded a mean factor of safety of 1.33 with a standard deviation of 0.11. The probability of satisfactory performance is estimated to be 0.03%. Figure 8–14 shows the histogram and the CDF of the factor of safety. Based on the results of 25 simulations, the mean probability of unsatisfactory performance is estimated to be 0.04% with the 95% confidence interval ranging between 0.04-0.05%. Figure 8–15 shows the histogram of the probability of unsatisfactory performance. As with the James Bay and Cell 23 cases, the probability of unsatisfactory performance is nearly one order of magnitude larger than that of the analyses accounting for spatial variability. A sensitivity analysis is also performed and Figure 8–16 shows Spearman rank correlation coefficients for the three input variables. The results confirm the conclusion in Section 3.2.4 that none of the uncertain input variables has a dominant impact on the reliability of the design.

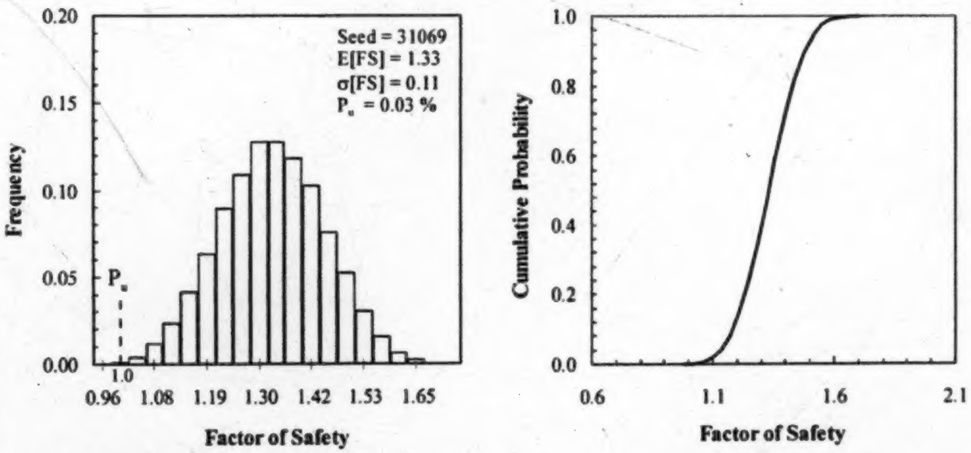

Figure 8–14 Histogram and CDF of the factor of safety; Lodalen slope (4h:1v) – Naïve analysis

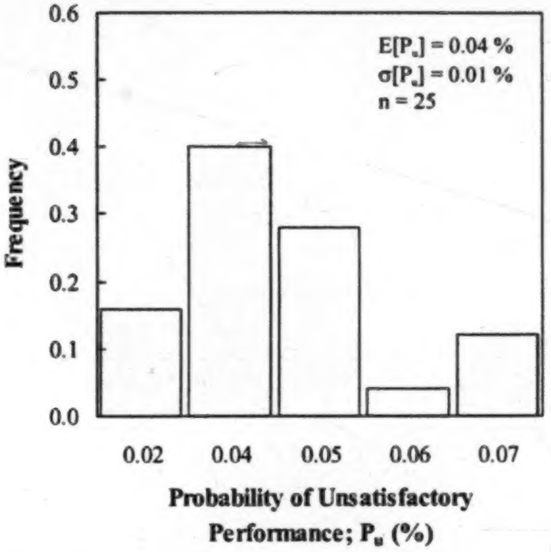

Figure 8–15 Histogram of the probability of unsatisfactory performance, Lodalen slope (4h:1v) – Naïve analysis

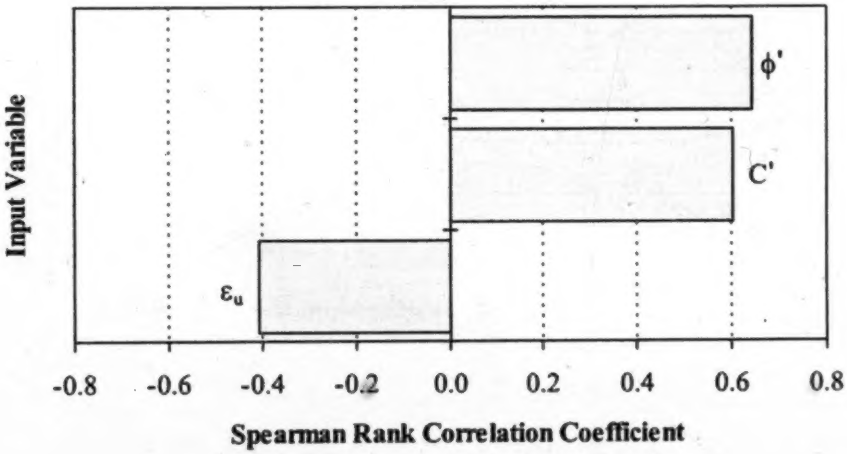

Figure 8–16 Sensitivity analysis results, Lodalen slope (4h:1v) – Naïve analysis

4. SUMMARY

The proposed methodology is applied to analyze the stability of the Lodalen slide. The probability of unsatisfactory performance is estimated to be 76% indicating that failure was imminent. As the inclination of the slope is reduced to 4.0h:1v the factor of safety, based on the conventional deterministic practice, is estimated to be 1.33 and the probability of unsatisfactory performance is almost zero. Such low probability is attributed to the small uncertainty in the input parameters. It should not be interpreted as a no failure condition, but rather as a high level of reliability. A deterministic factor of safety of 1.33 might be regarded as not being conservative enough to address the long-term stability of an excavated clay slope. However, the results of the probabilistic analyses grant high credibility to the calculated factor of safety which, if taken into consideration, may well lead to the acceptance of the 4.0:1 slope as an adequate design.

This case study clearly illustrates the large impact probabilistic analyses could have on conventional slope design practice. If the outcome of the probabilistic analysis indicates high reliability of the computed factor of safety we may be able to adopt a lower design factor of safety than normal provided that the serviceability (or performance) of the slope is not compromised.

CHAPTER 9

MUAR TRIAL EMBANKMENT

The proposed probabilistic methodology is applied to the Muar trial embankment in Malaysia. Sections 1 and 2 present a brief background about the embankment and the subsurface conditions. Then, in Section 3 the stability of embankment geometry before failure is analyzed deterministically and probabilistically. The analysis is repeated to assess the stability of the embankment at various stages during construction (i.e., different embankment heights). Emphasis is put on estimating the probability of unsatisfactory performance associated with the embankment height whose safety is deemed acceptable from the conventional practice point of view.

1. INTRODUCTION

Aiming at optimizing the design of an express highway on a very soft marine clay, the Malaysian Highway Authority decided to construct a large-scale field trial embankment at a section of the highway in the valley of the Muar River, Malaysia. A subsurface investigation was conducted between 1985 and 1987 to characterize the soil conditions at the location of the trial embankment. The Malaysian Highway Authority invited 30 geotechnical practitioners to predict the behavior of the embankment at different stages of construction up to failure. Each participant was provided with a detailed soil profile, the in-situ and laboratory testing results and the embankment geometry.

The embankment had a base area of about 55x90m and side slopes of 2h:1v. It was constructed using a compacted clayey sand to sandy clay material of a granitic origin. The soft clay layers beneath and around the embankment were heavily instrumented to monitor the deformations and excess pore water pressures during construction. The embankment failed when the thickness of the fill material reached 5.4m. At the time of failure the average settlement of the embankment was about 0.70m, thus the height of the embankment above ground surface was 4.70m. Figure 9–1 shows a cross-section of the embankment before failure. The construction time up to failure was 100 days. Failure occurred rapidly, one day after the development of a longitudinal crack along the centreline of the embankment. The predictions of all participants as well as the actual field data were discussed in a special symposium on Trial Embankments on Malaysian Marine Clays held in Kuala Lumpur in November of 1989. Brand and Premchitt (1989) provided a summary of the predictions and the conclusions drawn from the comparison with field performance.

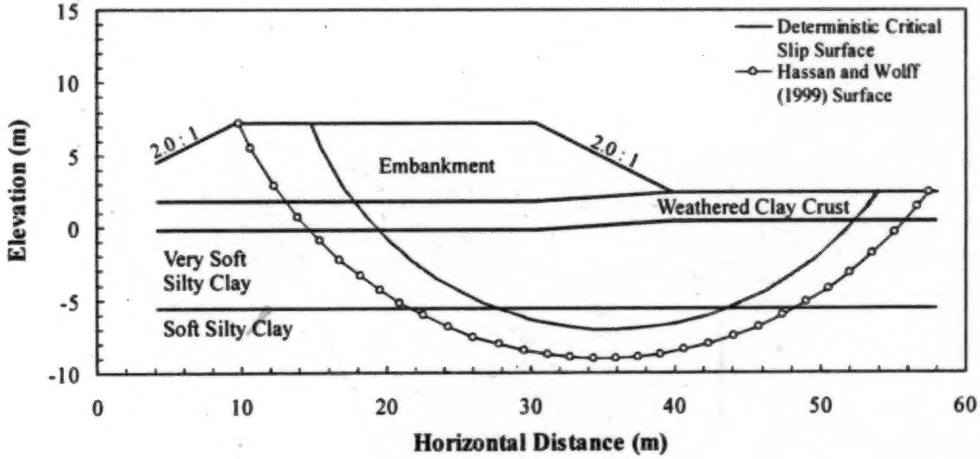

Figure 9–1 Geometry before failure and soil stratigraphy of Muar trial embankment

2. SOIL CONDITIONS

The Malaysian Highway Authority conducted a comprehensive investigation program to characterize the subsurface conditions at the site of the test embankment. The investigation included 2 deep boreholes with SPT tests, piston sampling, 9 field vane soundings and numerous laboratory tests including classification, compressibility, permeability and shear strength measurements. The following assessment of the subsurface conditions is based on the data gathered throughout that investigation. A more detailed description of the geology and the soil conditions is given in the report prepared by the Asian Institute of Technology (AIT, 1989) and the summary paper by Brand and Premchitt (1989).

2.1 Stratigraphy

The stratigraphy at the site of the embankment comprises a surface crust of weathered clay, about 2.0m thick, overlying a very soft silty clay. The silty clay is about 6m in thickness and is highly compressible. The strength of the clay increases almost linearly with depth. Below this, a layer of soft silty clay, 9.5m thick, is encountered. Its shear strength is slightly higher than the overlying very soft clay and also increases with depth. A highly compressible layer of peat, 0.7m thick, underlies the soft clay. The peat is underlain by a medium dense to dense clayey silty sand. The sand extends to the end of borings at 40m below ground surface. Figure 9–1 and Figure 9–2 show the soil stratigraphy at the embankment location.

2.2 Soil Properties

A summary of the physical and mechanical properties of the three clay layers is presented in Table 9-1. As indicated by Atterberg limits, all layers are of highly plastic clays. The very soft and the soft silty clay layers are slightly overconsolidated with liquidity indices above one and low bulk unit weights. Both layers, particularly the upper very soft layer, are highly compressible with high void ratios and compressibility indices.

Table 9-1 Summary of the physical and mechanical properties of the clay layers

Layer	Liquid Limit (%)	Plastic Limit (%)	Liquidity Index	Void Ratio	Compression Index	Bulk Unit Weight (kN/m^3)
Weathered clay crust	90	30	0.6	1.85	---	15.5
Very Soft silty clay	80	27	1.5	2.60	1.75	14.0
Soft silty clay	55	23	1.4	1.65	1.05	16.0

Because the construction of the embankment took only 100 days, undrained conditions prevail. As so, emphasis is put on assessing the undrained shear strength of the clay layers. Figure 9–2 is a plot of the field vane measurements versus elevation. The plot shows that the undrained shear strength of the surface crust is much higher than that of the underlying very soft clay. Close to ground surface the undrained strength is about 50kPa and decreases to as low as 8 kPa at the top of the very soft layer. A linear trend is fitted to the data as shown in Figure 9–2. The measurements show some scatter around the trend. The strength of the crust may, thus, be regarded as a random variable. By removing the trend component from all measurements, the residuals can be modeled as a stationary random field with a zero mean and a standard deviation equal to 4.55 kPa. Figure 9–3 shows the histogram and the CDF of the residuals, $\varepsilon_{Su\text{-}cr}$.

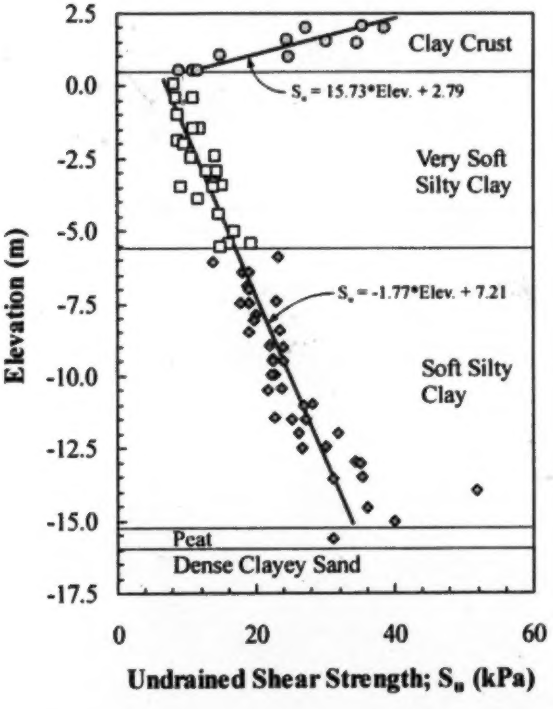

Figure 9–2 Profile of field vane shear strength

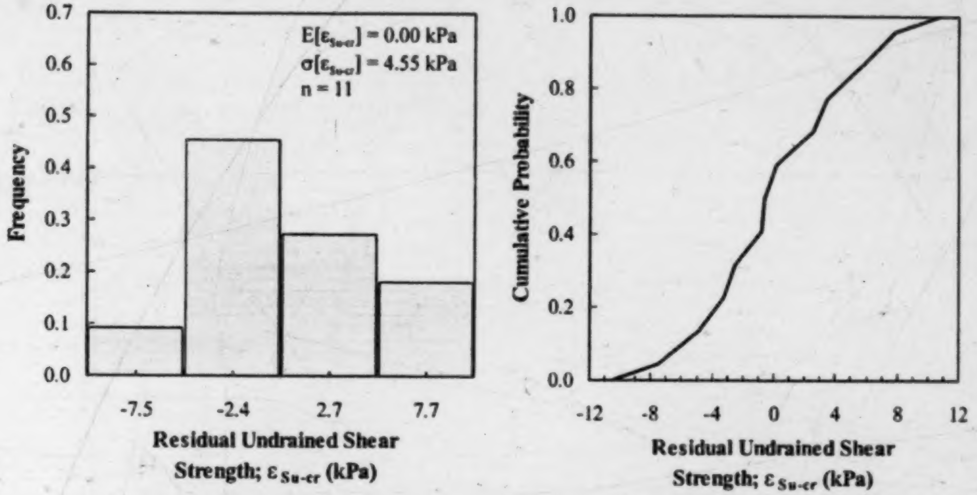

Figure 9–3 Histogram and CDF of the residuals of the undrained shear strength of the weathered clay crust

Figure 9–2 indicates that the undrained shear strength of the very soft and the soft clay deposits is not sensitive to stratigraphic layering. In other words, there is hardly any distinction between the two layers in terms of the trend and scatter of shear strength measurements. The data of the two deposits are thus combined and the shear strength is treated as a single random process. One exceptionally high measurement (at elevation -14.0, Figure 9–2) is judged unreasonable and is discarded. A linear trend is fitted to the measurements as shown in Figure 9–2. The data show some scatter around the trend. Since the strength of the silty clay layers is likely to have a major impact on the stability of the embankment, addressing its uncertainty in the probabilistic analysis is important. In the stability analyses in the following sections, it is regarded as a variable. The trend component is removed from all measurements and the residuals are modeled as a stationary random field with a zero mean and a standard deviation equal to 2.45 kPa. Figure 9–4 shows the histogram and the CDF of the residuals of the undrained shear strength; $\varepsilon_{Su\text{-}C}$. The histogram has a single peak, thus implying that the two data groups (the very soft and the soft silty clay layers) are consistent in a statistical sense. It should be stated, however, that this model does not reflect the geology on site as indicated by the different physical properties of the two layers, Table 9-1. Rather, it is intended to simplify the statistical treatment of the data.

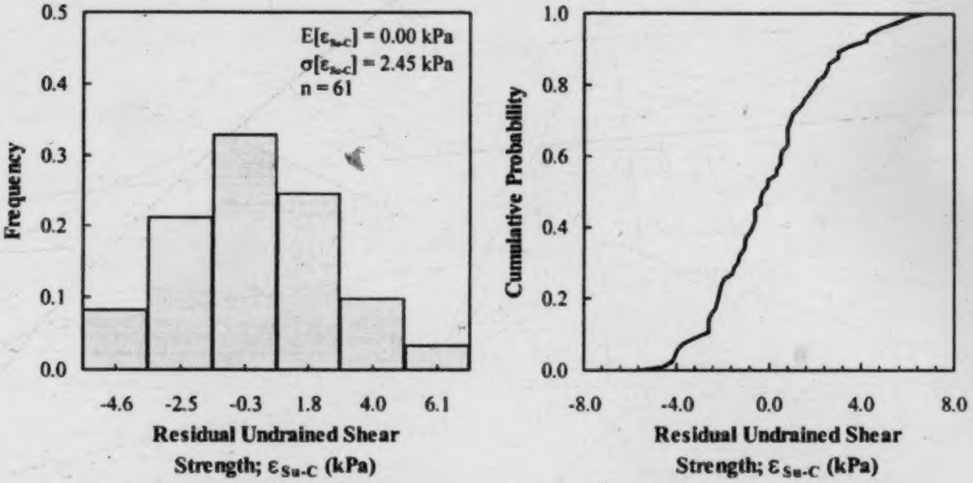

Figure 9–4 Histogram and CDF of the residuals of the undrained shear strength of the silty clay layers

2.3 Embankment Material

The embankment was constructed using a compacted decomposed granite that is described as clayey sand to sandy clay. The shear strength of the embankment material was assessed based on the results of 3 unconsolidated undrained triaxial tests and 2 drained triaxial tests. From the drained tests, the effective friction angle and the effective cohesion were estimated to be 31 degrees and 14 kPa, respectively. The undrained tests showed the strength to vary from C_u= 64 kPa, ϕ_u=12 degrees to C_u =19 kPa, ϕ_u =26 degrees. Based on the results of the undrained tests, the shear strength of the embankment material is roughly approximated by the average strength of the 2 envelopes at mid height of the embankment. It is estimated to be 60 kPa. Uncertainty in this estimate arises firstly from the rough approximation scheme, particularly as the initial stresses within the embankment are not geostatic and largely depend on the compaction energy. Then, from the incompatibility of the strains needed to mobilize the peak strength of the compacted stiff fill material and the underlying soft ductile clays which makes the operational shear strength of the fill very difficult to assess. As such, accounting for the uncertainty of fill strength in the probabilistic stability analyses is essential.

If the fill material exhibits a strain-softening behaviour, cracks may develop within the embankment. This further complicates the assessment of the operational strength of the embankment material. This issue of the fill cracked is, however, better handled as a matter of model uncertainty.

3. SLOPE STABILITY ANALYSES

3.1 Deterministic Analysis

The stability of the embankment before failure is analyzed deterministically using Slope/W software and the Bishop method of slices assuming a circular slip surface. The average strength of the embankment material and the linear trends of the undrained shear strength of the weathered crust and the underlying clays (corrected for bias using Bjerrum's vane correction factor, Section 3.2.1.2) are used in the analysis. The minimum factor of safety is estimated to be 1.11. Figure 9–1 shows the critical slip surface.

It should be noted that the field vane may overestimate the operational strength of the overconsolidated clay crust due to the presence of preexisting fissures (Tavenas et al., 1980; Lefebvre et al., 1987). Some researchers (e.g., Ferkh and Fell, 1994) recommended the use of a reduced strength for the crust. When an upper strength threshold of 13.9 kPa at the lower quarter of crust thickness is imposed on the vane profile (corrected using Bjerrum's factor) within the crust and another stability analysis is performed, the factor of safety is computed to be 1.07. So, the scenario of reduced crust strength has only a small impact on this design and is not considered in the subsequent probabilistic analyses.

3.2 Probabilistic Analysis – Proposed Methodology

3.2.1 Input Variables

3.2.1.1 Soil Parameters

Based on the discussions in Section 2, three soil parameters are considered as variables; the strength of the embankment, the strength of the surface crust and the strength of the underlying silty clays.

The undrained shear strength of the embankment is estimated to be 60 kPa as outlined in Section 2.3. Because of the high uncertainty surrounding the operational fill strength, the average strength along the slip surface is judgmentally assigned a standard deviation of 12 kPa which is equivalent to a coefficient of variation of 20%. It is assumed to have a normal probability density function.

The uncertainty of the undrained shear strength of the surface crust is divided into uncertainty in the linear trend and uncertainty in the residuals around the trend. The intercept and the slope of the trend are considered variables with normal probability distributions. Using the method of least squares, the mean values of the slope and the intercept are computed to be 15.73 kPa/m and 2.79 kPa, respectively. The standard deviations are estimated to be 2.49 kPa/m and 3.62 kPa (Equations 3-21 and 3-22). The correlation coefficient between the slope and the intercept is found to be –0.92 (Equation 3-23). The uncertainty of the residuals is represented by the experimental probability distribution function in Figure 9–3.

The uncertainty of the undrained shear strength of the underlying silty clays is modeled in the same way. The mean values of the slope and intercept of the trend are estimated to be –1.77 kPa/m and 7.21 kPa, respectively. The standard deviations are computed to be 0.07 kPa/m and 0.63 kPa. The correlation coefficient between the two variables is 0.86. The uncertainty of the residuals is represented by the experimental CDF in Figure 9–4. Table 9-2 summarizes the statistical parameters and probability distributions of all input variables.

3.2.1.2 Bjerrum's Vane Correction Factor

The field vane test is probably the most widely used test for assessing the undrained shear strength of soft clays. Based on back analyses of a number of embankment and excavation slope failures, Bjerrum (1972) reported discrepancies between the measured and the back-calculated undrained shear strength. He attributed them to strain rate effects and anisotropy. Bjerrum (1972, 1973) then proposed an empirical factor (as a function of the plasticity index) to correct the measured vane strength, Figure 9–5. Aas et al. (1986) compiled data from other investigators, in addition to Bjerrum's data, as shown in Figure 9–5. The scatter of the data around Bjerrum's recommended curve is substantial indicating high uncertainty. It is, therefore, important to address the uncertainty surrounding Bjerrum's vane correction factor in any probabilistic analysis.

Table 9-2 Statistical parameters and CDFs of the input variables – Muar Trial Embankment

Input Variable			**Soil Variability**			**Systematic Uncertainty**		
			E[--]	**σ[--]**	**CDF**	**E[--]**	**σ[--]**	**CDF**
Embankment Strength; $S_{u\text{-}Fill}$ (kPa)			60.0	12.0	N.	--	--	--
Strength of Weathered clay crust; $S_{u\text{-}cr}$ (kPa)	Trend	Slope	--	--	--	15.73	2.49	N.
		Intercept	--	--	--	2.79	3.62	N.
	Residuals; $\varepsilon_{Su\text{-}cr}$		0.00	4.55	Exper.	--	--	--
	Bjerrum factor; μ_{cr}		--	--	--	0.75	0.15	N.
Strength of silty clay layers; $S_{u\text{-}C}$ (kPa)	Trend	Slope	--	--	--	-1.77	0.07	N.
		Intercept	--	--	--	7.21	0.63	N.
	Residuals; $\varepsilon_{Su\text{-}C}$		0.00	2.45	Exper.	--	--	--
	Bjerrum factor; μ_C		--	--	--	0.80	0.15	N.

N. - Normal distribution; Exper. - Experimental (or observed) distribution

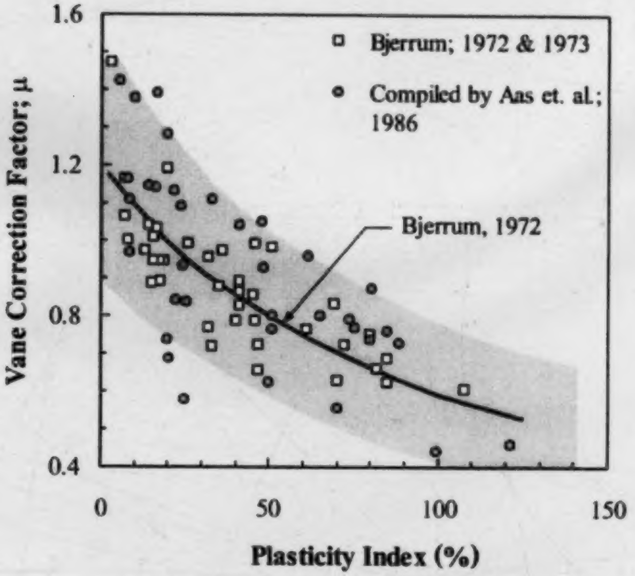

Figure 9–5 Bjerrum's vane correction factor

The scatter of the data around Bjerrum's curve is nearly constant irrespective of the value of the plasticity index, Figure 9–5. Thus, the uncertainty around Bjerrum's curve can be represented by a constant standard deviation. In the stability analyses in the following sections, Bjerrum's vane correction factor is modeled as a normally distributed random variable with a mean given by Bjerrum's recommended curve and a constant standard deviation estimated from the scatter of the data around the curve. The standard deviation of Bjerrum's factor is calculated to be 0.15. Because of the high plasticity of the clay crust and the underling soft clays (Table 9-1), Bjerrum's vane correction factors are applied to the vane strength of both layers. The two factors are regarded as variables. Based on Atterberg limits, the mean values of Bjerrum's factors are estimated to be 0.75, 0.80, respectively. Table 9-2 summarizes the statistical parameters of the two variables representing the vane correction factor.

3.2.2 Critical Slip Surface

In locating the probabilistic critical slip surface, two candidate surfaces were considered; the deterministic critical slip surface obtained in Section 3.1 and the surface based on the Hassan and Wolff (1999) algorithm. Hassan and Wolff's surface is obtained by performing a deterministic analysis with the undrained shear strength of the silty clay layers reduced to the mean minus one standard deviation. The reduction includes the trend, the residuals and Bjerrum vane correction factor. Figure 9–1 shows the two candidate surfaces. Using 30,000 iterations, the two surfaces are analyzed probabilistically taking into account the spatial variability of soil properties as outlined in the following sections. The probabilities of unsatisfactory performance are estimated to be 20.42% and 23.79% for Hassan and Wolff surface and the deterministic critical slip surface, respectively. The latter surface is, thus, considered the probabilistic critical surface and is used in the subsequent stability analyses.

3.2.3 Spatial Variability

Marine deposits (such the Malaysian soft clays) tend to be largely homogenous with a continuous, rather than erratic, pattern of variability. The little scatter of the field vane data of the silty clay layers around the trend, Figure 9–2, is in support of this argument. It is, thus, more likely that the horizontal and vertical autocorrelation distances of the marine deposits at the valley of the Muar river are at the upper ends of the typical ranges reported in Chapter 5. A range of 30-40m is postulated as a possible range for the horizontal autocorrelation distance and 1-3m as a possible range for the vertical autocorrelation distance. The geometry of the critical slip surface, Section 3.2.2, suggests that the analysis is not dominated by the spatial structure along a specific direction. Hence, the variability of soil strength is roughly approximated by an isotropic spatial structure with an equivalent autocorrelation distance that is function of both the vertical and the horizontal autocorrelation distances. Based on Equation 5-6, the equivalent autocorrelation distance is in the range of 5-15m. The probabilistic stability analyses in the following sections are based on an intermediate value of 10m. The sensitivity of the probability of unsatisfactory performance to other values of the autocorrelation distance is investigated in Section 3.2.7.

The spatial variability of soil parameters along the failure surface is accounted for by dividing the slip surface into segments and modeling the average parameters over the length of these segments as correlated variables (Chapter 5). The failure surface cuts through the weathered crust at two locations separated by a distance longer than the scale of fluctuation $\delta \cong 20$m, Figure 9–1. The length of the two segments of the failure surface within the crust are also less than δ. Thus, the spatial variability of the undrained shear strength of the crust is modeled by two uncorrelated variables, each representing the average strength over a segment of the failure surface. Each variable is represented by the observed probability distribution of the residuals, Figure 9–3. Following the same approach, the failure surface within the silty clay layers is divided into two segments (based on δ=20m). Two variables, having the observed CDF of the residuals, Figure 9–4, are used to model the variability of the undrained shear strength of the silty clays. For the embankment geometry before failure, the correlation coefficient between the two variables is estimated to be 0.08 (Equation 5-5).

3.2.4 Stability Analysis – Geometry Before Failure (H=4.7m)

A spreadsheet model mimicking the embankment geometry, soil stratigraphy and critical slip surface is prepared. The settlement of the embankment is accounted for by assuming that the underlying very soft clay is displaced laterally. Thus, the thickness of that layer under the embankment is reduced by the observed settlement (S=0.7m). The Bishop method of slices is used in the spreadsheet model. The model includes 5 uncertain parameters; the undrained shear strength of the fill material, the weathered crust and the silty clay layers and Bjerrum vane correction factors for the crust and the silty clays. The uncertainties in these parameters (bias, statistical uncertainty and spatial variability) are taken into account through 11 input variables, some of which are correlated, as outlined in Sections 3.2.1 and 3.2.3.

Based on a few trial simulations, the optimum number of iterations is assessed to be 10,000. Using a seed number of 31069, the mean factor of safety is calculated to be 1.11 with a standard deviation of 0.15. The probability of unsatisfactory performance is estimated to be 23.79%. Figure 9–6 shows the histogram and CDF of the factor of safety. The simulation process is repeated 25 times using different seed values to assess the reliability of the estimated probability of unsatisfactory performance. The results are summarized in a histogram form in Figure 9–7. The mean probability of unsatisfactory performance is 24.05% with the 95% confidence interval ranging between 23.95-24.15%.

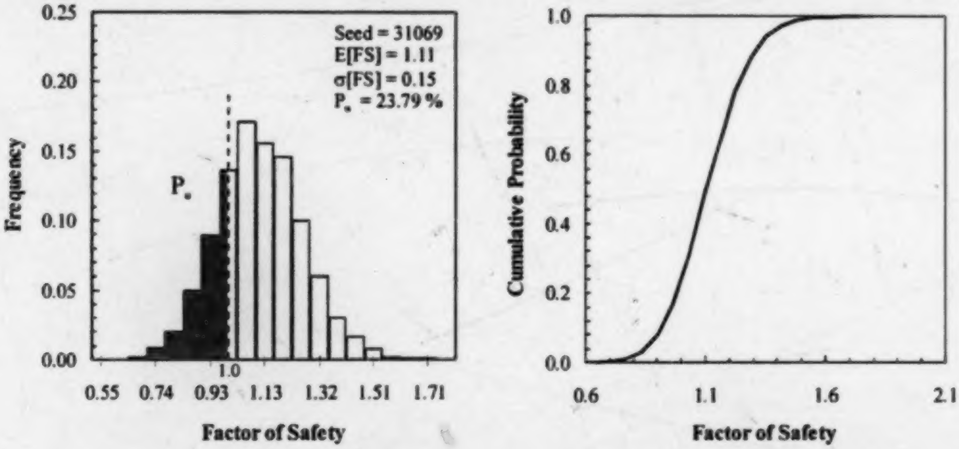

Figure 9–6 Histogram and CDF of the factor of safety, Muar Embankment (H=4.7m) – Proposed Methodology

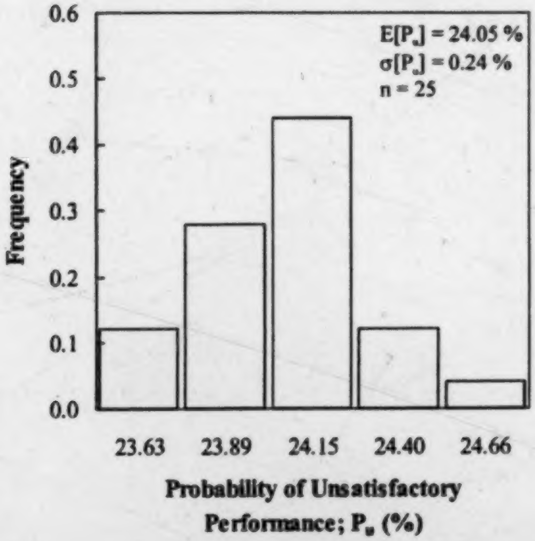

Figure 9–7 Histogram of the probability of unsatisfactory performance, Muar Embankment (H=4.7m) – Proposed Methodology

3.2.5 Stability Analyses – Embankment Geometry Modified

Aiming at assessing the probability of unsatisfactory performance associated with an acceptable design based on conventional practice, the stability of the embankment is analyzed at different stages during construction, i.e., different embankment heights. Four cases are considered including heights of 2.5, 3.3, 3.5 and 4.0m above ground surface. The analyses are conducted following the same approach described in Section 3.2.4. Each case involved locating the probabilistic critical slip surface, assessing the optimum number of iterations and accounting for spatial variability and systematic uncertainty. Figure 9–8 shows the variation of the probability of unsatisfactory performance and the factor of safety with the embankment height. The estimate of the probability of unsatisfactory performance for each case is the average of the results of 10 simulations. The plot indicates little increase in the probability of unsatisfactory up to a height of about 3.3m followed by a sharp increase in the probability value as the embankment height exceeds 3.5m.

3.2.6 Stability Analysis – Acceptable Embankment Design (H=3.3m)

Based on experience and judgement, conventional slope practice targets a design factor of safety in the order of 1.3-1.4 for the short-term stability of slopes in soft soils. For the Muar embankment, the computed factor of safety at failure (H=4.7m) is 1.11. Taking this into account, it is judged that an embankment height of 3.3m (FS=1.42, Figure 9–8) is an acceptable design from the conventional practice point of view. The stability of that embankment is studied in more detail. Figure 9–9 shows the histogram and the CDF of the factor of safety obtained by Monte Carlo simulation using 30,000 iterations. The mean factor of safety is 1.42 with a standard deviation of 0.20. The probability of unsatisfactory performance is estimated to be 1.29%. Figure 9–10 shows the histogram of the probability of unsatisfactory performance based on the results of 25 simulations. The mean probability of unsatisfactory performance is 1.38% with the 95% confidence interval ranging between 1.36-1.40%

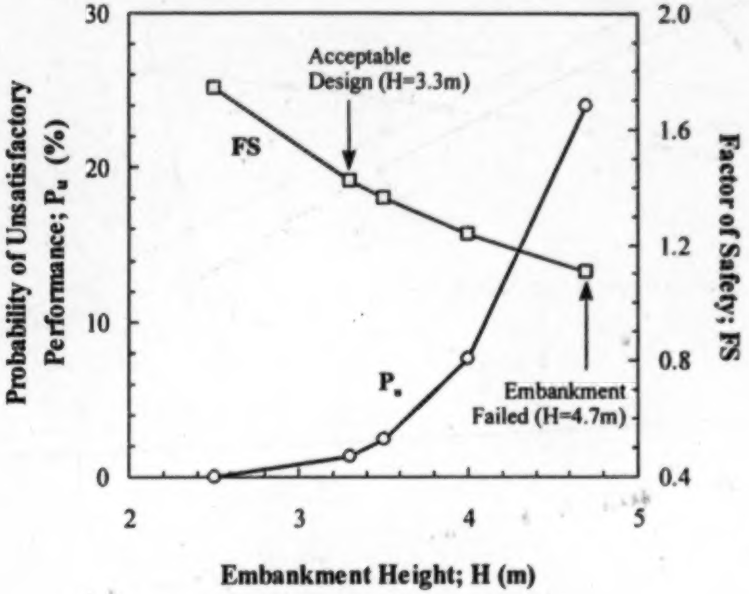

Figure 9–8 Variation of the probability of unsatisfactory performance and the factor of safety with embankment height, Muar Embankment – Proposed Methodology

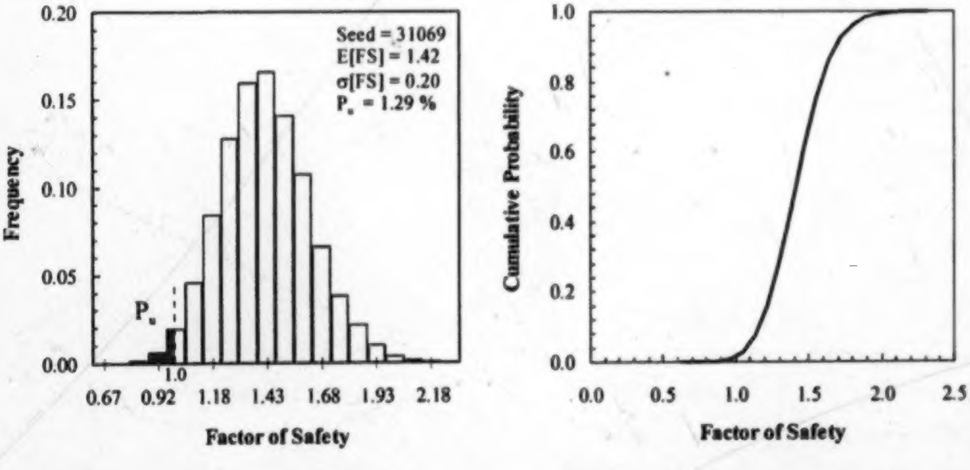

Figure 9–9 Histogram and CDF of the factor of safety, Muar Embankment (H=3.3m) – Proposed Methodology

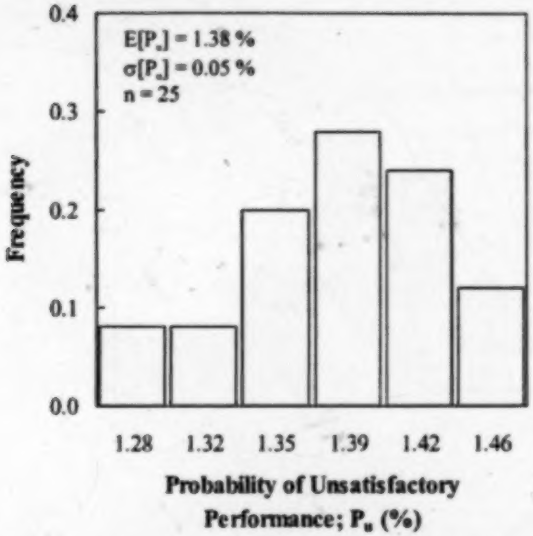

Figure 9–10 Histogram of the probability of unsatisfactory performance, Muar Embankment (H=3.3m) – Proposed Methodology

A sensitivity analysis is performed to assess the relative contributions of the input variables to the uncertainty of the factor of safety. Figure 9–11 shows Spearman rank correlation coefficients for all 11 input variables. Interestingly enough, the plot indicates that the impact of the uncertainty in Bjerrum's vane correction factor on the reliability of the analysis is comparable (if not larger) to that of the spatial variability of the undrained shear strength. The plot also reflects the significance of the longstanding issue still facing practitioners in designing embankments on soft soils, and that is the contribution of fill strength to the stability of the embankment. These two variables, Bjerrum's factor and fill strength, are among the main contributors to the uncertainty of the stability analysis, Figure 9–11. The decisions on the value of the vane correction factor and on how much of the measured fill strength to take into account in the design are subjective and largely depend on the designer's experience and judgement. This explains the significant scatter of the predictions of the fill thickness of the Muar embankment at failure (2.75 – 9.75m) made by the 30 professionals who participated in the study organized by the Malaysian Highway Authority (refer to Chapter 4, Figure 4-1). As expected, the uncertainty of the strength of the weathered clay crust has a small impact on the reliability of the analysis. The uncertainties of the mean trends of the strength of the crust and the soft clay layers also have minimal impacts on the analysis.

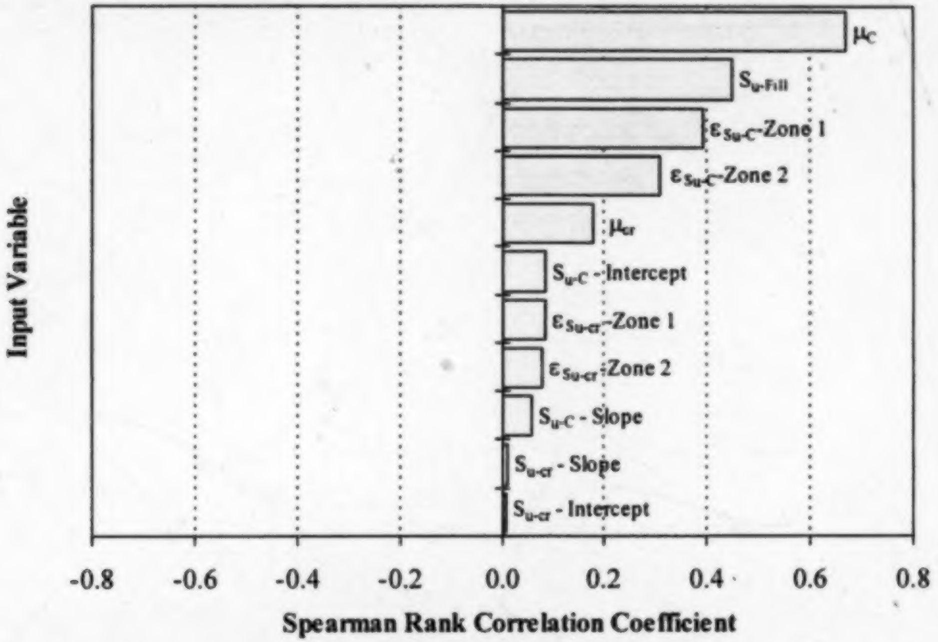

Figure 9–11 Sensitivity analysis results, Muar Embankment (H=3.3m) – Proposed Methodology

The stability analysis of the 3.3m embankment is repeated using the alternative approach based on the probability distributions of the *spatially averaged* soil parameters. The probability distribution of the average undrained shear strength of the silty clay layers over the length of the failure surface is estimated by simulation in a separate spreadsheet following the approach outlined in Chapter 7. Using a seed number of 31069 and 30,000 iteration, the probabilistic stability analysis yielded almost the same results as the analysis modeling the variability of soil strength along the failure surface. The mean factor of safety and the probability of unsatisfactory performance are estimated to be 1.42 and 1.34%, respectively, compared to 1.42 and 1.29% for the analysis modeling variability along failure surface. Figure 9–12 compares the CDFs of the factor of safety from both analyses.

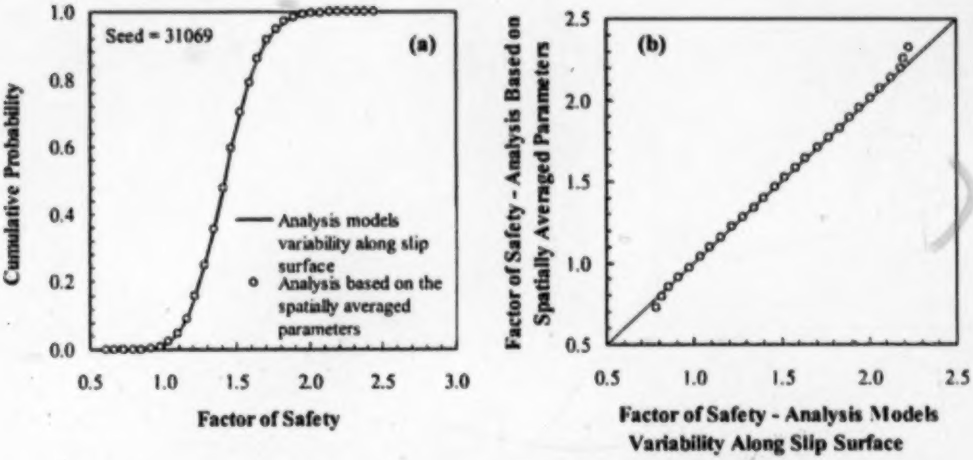

Figure 9–12 Comparison of the factor of safety from the analysis modeling soil variability along slip surface and that based on the spatially averaged parameters, Muar Embankment; a) Probability distribution functions, b) Q-Q plot

3.2.7 Sensitivity of the Analysis to the Autocorrelation Distance

As indicated in Section 3.2.3, the range 5-15m is presumed as the likely range of the autocorrelation distance of the marine clays at the site of the Muar embankment. Since all probabilistic analyses in the previous sections are based on an autocorrelation distance of 10m, it is essential to examine the sensitivity of the analysis to other values. The probability of unsatisfactory performance is computed for different assumptions of the autocorrelation distance as shown in Figure 9–13. The more continuous the soil variability is (i.e., the larger autocorrelation distance), the smaller the impact of spatial averaging on the analysis and the higher the uncertainty of the factor of safety. As the autocorrelation distance increased from 5m to 15m, the probability of unsatisfactory performance increased from 1.06% to 1.67%. While acknowledging that the probability of unsatisfactory performance does vary with the assumption of the autocorrelation distance, the difference is not significant from a practical point of view. Stating that the probability of unsatisfactory performance of the embankment is somewhere in between 1.1-1.7% is not unreasonable.

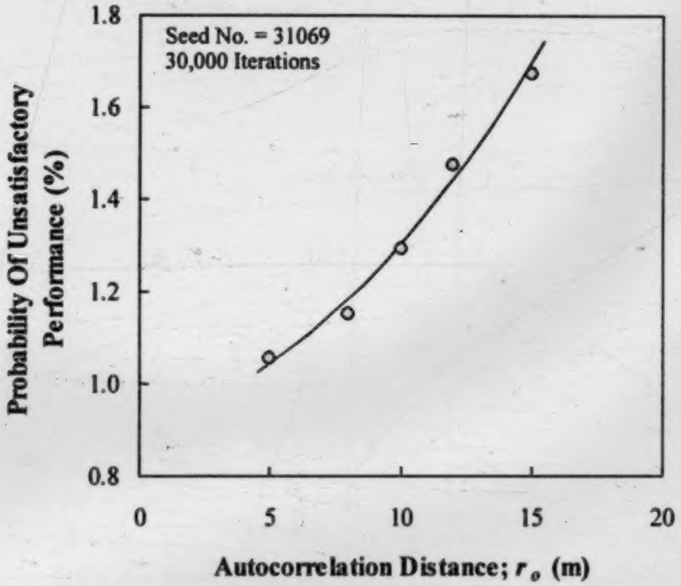

Figure 9–13 Variation of the probability of unsatisfactory performance with the autocorrelation distance, Muar Embankment (H=3.3m)

3.3 Naïve Analysis

The stability of the acceptable embankment design (3.3m high) is also analyzed following the naïve approach. The uncertainties in the undrained shear strength of the crust and the silty clay layers are assessed according to the observed variability reflected by the vane measurements. The estimated trends, Figure 9–2, are treated deterministically and the variability around the trends are modeled by the CDF of the residuals, Figure 9–3 and Figure 9–4. The uncertainty surrounding Bjerrum's vane correction factor and the shear strength of the fill are accounted for as outlined in Sections 2.3 and 3.2.1.2. Table 9-3 summarizes the statistical parameters and probability distributions of the input variables.

Table 9-3 Statistical parameters of the input variables – Naïve Analysis

Input Variable		Mean	Standard Deviation	Probability Distribution
Undrained shear strength of fill material; $S_{u\text{-}Fill}$ (kPa)		60.0	12.0	Normal
Weathered clay crust	Residuals of undrained shear strength; $\varepsilon_{Su\text{-}cr}$ (kPa)	0.00	4.55	Experimental CDF
	Bjerrum vane correction factor; μ_{cr}	0.75	0.15	Normal
Very soft and soft silty clay layers	Residuals of undrained shear strength; $\varepsilon_{Su\text{-}C}$ (kPa)	0.00	2.45	Experimental CDF
	Bjerrum vane correction factor; μ_C	0.80	0.15	Normal

A spreadsheet model using Bishop's method of slices and the deterministic critical slip surface is prepared. A Monte Carlo simulation using 30,000 iterations and a seed number of 31069 is perform[illegible]he mean factor of safety is found to be 1.42 with a standard deviation of 0.22. The probability of unsatisfactory performance is estimated to be 1.75%. The simulation is repeated 25 times and the estimated probabilities are summarized in histogram form in Figure 9–14. The mean probability of unsatisfactory performance is 1.80% with the 95% confidence interval ranging between 1.77-1.83%. Unlike most of the case studies analyzed in the previous chapters, the probability of unsatisfactory performance based on the naïve analysis is very close to that of the analysis accounting for spatial variability. This is attributed to the smaller size of the failure surface compared to the autocorrelation distance. As a result, the difference between the variance of point measurements of shear strength and the variance of the average shear strength along the slip surface is small bringing the two analyses closer.

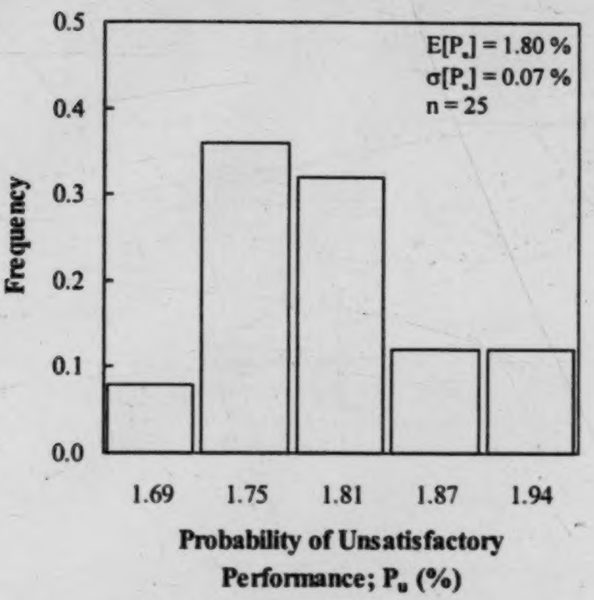

Figure 9–14 Histogram of the probability of unsatisfactory performance, Muar Embankment (H=3.3m) – Naïve Analysis

A sensitivity analysis is also performed to assess the relative contributions of the various sources of uncertainty to the uncertainty of the factor of safety. Figure 9–15 shows Spearman rank correlation coefficients for all input variables. Similar conclusions to those of the analysis accounting for spatial variability can be drawn. Firstly, the uncertainty surrounding Bjerrum's factor has a larger impact on the reliability of the design than does the observed variability of the undrained shear strength. Secondly, the reliability of Bjerrum's factor and the contribution of fill strength are still major sources of uncertainty in designing embankments on soft soils.

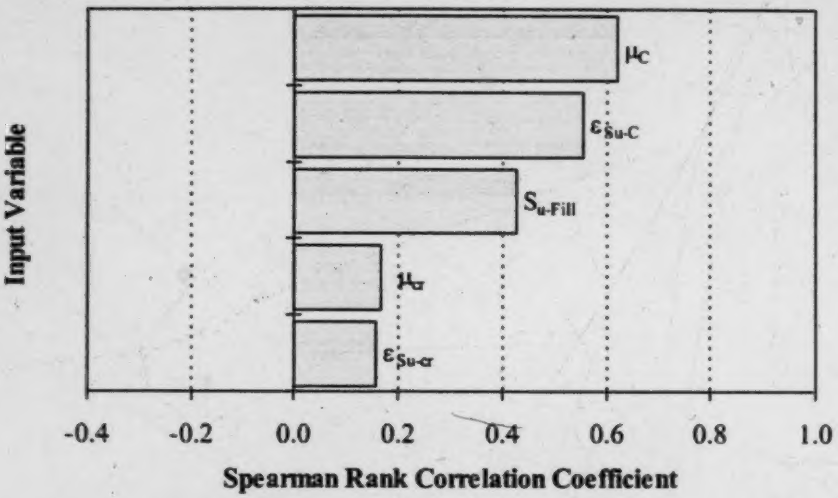

Figure 9–15 Sensitivity analysis results, Muar Embankment (H=3.3m) – Naïve Analysis

4. SUMMARY

The proposed probabilistic methodology is applied to the Muar trial embankment in Malaysia. The probability of unsatisfactory performance associated with the embankment geometry before failure is estimated to 24.05% indicating that failure was expected. An embankment 3.3m high above ground surface is assessed to be an acceptable design from conventional practice point of view. The probability of unsatisfactory performance associated with that height is estimated to be 1.38%. This estimate is in the same range as the probability of unsatisfactory performance of the 6m high dyke of the James Bay case (1-3% range) while both are much larger than the probabilities associated with the acceptable designs of the other cases analyzed so far (P_u<0.5%). The two cases, however, have many features in common. Both are small embankments constructed on soft clays whose strength is measured using field vane. The uncertainty surrounding the operational shear strength of embankment material is deemed significant in the two cases. More importantly, the problem domain (in terms of slope geometry and the extent of the slip surface) in either case is small and comparable in size to the autocorrelation distance. Hence, the variance reduction due to spatial averaging is insignificant and the uncertainties of the average properties are not much less than the point variances leading to the high probabilities of unsatisfactory performance.

The latter observation suggests that the frequency of small-scale failures is higher than large-scale failures, which is consistent with what is observed in real life. The issue of the scale of failure and its relation to the failure frequency cannot be addressed in a conventional deterministic slope analysis. It is discussed in more detail in Chapter 11.

The results of the sensitivity analysis reveal some very interesting observations. First, the uncertainty of Bjerrum's vane correction factor is substantial and could have a larger impact on the reliability of the analysis than does the uncertainty of the undrained shear strength itself. Second, the vane correction factor and the contribution of fill strength to stability are still major sources of uncertainty in designing embankments on soft soils.

CHAPTER 10

CONGRESS STREET OPEN CUT

The proposed probabilistic methodology is applied to the Congress Street Open Cut in Chicago that failed in 1952. The geometry before failure is first analyzed, then the slope angle of the cut is reduced to various values and the analysis is repeated. The slope geometry that is deemed acceptable from a conventional practice point of view is analyzed in more detail. The following sections present a brief description of the failure, the local geology and the soil conditions and detail the deterministic and probabilistic analyses undertaken.

1. INTRODUCTION

A portion of the subway system of the downtown area of Chicago City was constructed by open excavation. In the summer of 1952, a section of the open cut at Congress Street just east of Halsted Street failed. The excavation had side slopes of 1.35h:1v and failure occurred when the depth of excavation reached 14.25m. Figure 10–1 shows the geometry of the slope before failure. The length of the failed section was approximately 61 metres. As a result of the failure, a near vertical escarpment was formed at ground surface and a crack was developed near the centreline at the bottom of the excavation. Ireland (1954) described the failure and the stability analysis undertaken to assess the factor of safety at failure.

2. GEOLOGY OF THE CHICAGO AREA

Almost all of the subsoil in the Chicago area was deposited during the Pleistocene. The most recent glaciation, the Wisconsin, is the only glaciation that has a major impact on the local geology. The glacier advanced towards the area through the Lake Michigan basin. During movement, significant quantities of Devonian shale were excavated from the basin and mixed with the materials brought by the glacier from formations at localities farther north. Most of the soil formations in the Chicago area are deposited by the Wisconsin glacier. As a result, they are primarily clays and silts derived from the Devonian shale. There is also evidence to suggest that these deposits were laid down in six till sheets, some of which were totally eroded. Each of these sheets has its own terminal moraine and represents an advance and retreat of the ice sheet. The clayey deposits are overlain in many localities by sand deposited in the glacial lakes formed by the impounded meltwater from the glacier. The clayey deposits are underlain by the Niagaran Limestone which belongs to the Paleozoic era. The surface of the limestone is highly irregular. Peck and Reed (1954) provided a summary of the geology of the Chicago area.

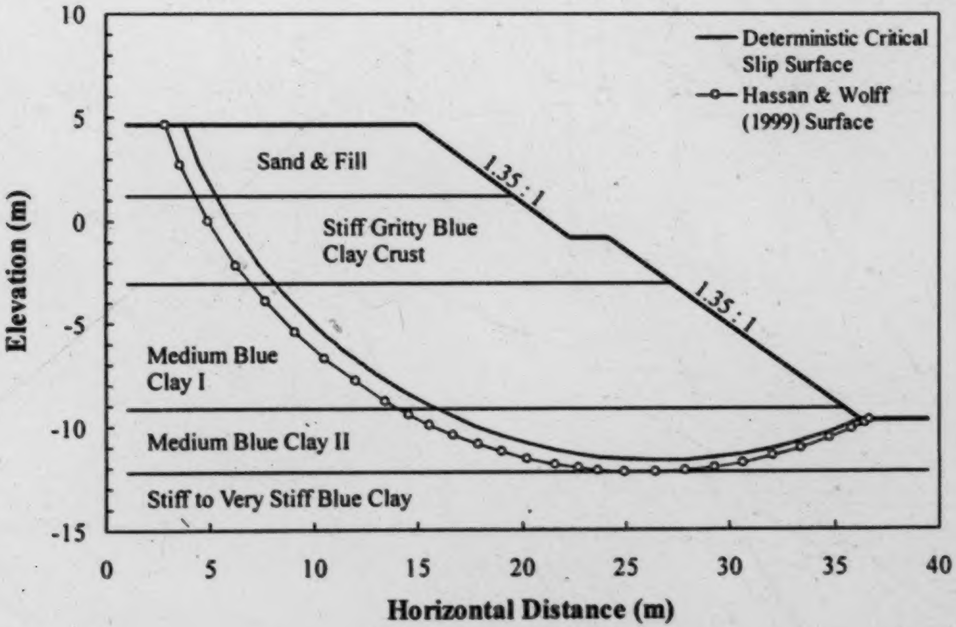

Figure 10–1 Geometry and soil stratigraphy of the Congress Street open cut

3. SOIL CONDITIONS

The subsurface conditions at the Chicago area were extensively investigated by hundreds of boreholes during the construction of the subway system. Peck and Reed (1954) prepared a summary report detailing the soil conditions of the area. Ireland (1954) provided information on the local soil conditions at the failure site based on 8 nearby borings. The assessment in the following sections is based on both sources.

3.1 Stratigraphy

The stratigraphy at the site of the failure comprises a top layer of sand and miscellaneous fill of about 3.4 m thick. Based on SPT data, Peck and Reed (1954) reported that the relative density of the sand in this area is erratic and is generally low. The sand is underlain by a gritty blue clay that extends to bedrock. The clay, however, varies in consistency and can be divided into a number of sub-layers that belong to different till sheets as outlined in Section 2. Immediately below the sand, a crust of stiff gritty blue clay, 4.3 m thick, is encountered. It is believed to have gained its strength by desiccation as a result of extreme low water levels of Lake Chicago. Ireland (1954) reported that the crust has a structure of joints and fissures. The crust is underlain by a layer of medium stiff, gritty blue clay of about 6.1m thickness which in turn is underlain by another layer, 3.1 m thick, of medium stiff blue clay. The two layers have the same composition but they differ in strength. Hereafter, they are referred to as Blue Clay I and Blue Clay II, respectively. Peck and Reed (1954) reported that these layers contain numerous limestone and shale pebbles, sand and silt pockets, large boulders and occasionally thin stratified deposits. Blue Clay II is underlain by a stiff to very stiff gritty blue clay layer that extends to the end of borings. The stiff clay is also of the same composition as the overlying medium clays, however, it is sandier with much more pebbles, silt pockets and sand lenses. Figure 10–1 shows the soil stratigraphy at the site of the failure.

3.2 Soil Properties

The relative density of the top sand layer is assessed on the basis of SPT results. Unfortunately, no data were available at the exact location of the failure. Peck and Reed (1954), however, reported that the relative density of the sand at the area surrounding the failure site is generally low ranging between very loose to medium dense. Based on this information, the sand is judgmentally assigned a friction angle of 30 degrees. Ireland (1954) used the same value when assessing the stability of the cut.

As indicated in Section 2, the various clay layers are of the same origin. As such, the differences in Atterberg limits are very small. On average, the plastic limit for all clay layers is about 17% and the liquid limit is about 32%. The moisture contents of the layers, however, vary reflecting the variation of strength. The desiccated crust has a moisture content of about 21% while those of the Blue Clay I and the Blue Clay II are 24% and 26%, respectively.

The strength of the different clay layers is assessed based on an extensive number of unconfined compressive strength tests. The tests were conducted on specimens prepared from 2" diameter shelby tube samples. Peck and Reed (1954) and Ireland (1954) reported that the variability of the compressive strength of the glacial blue clays is significant and erratic. Unfortunately, the actual data of the borings surrounding the failure site were not available. Ireland (1954), however, provided the mean, standard deviation and the number of tests for each layer, Table 10-1. The coefficients of variation of the stiff gritty clay crust, the Blue Clay I and the Blue Clay II are 0.50, 0.26 and 0.32, respectively. The three values indicate high uncertainty in the strength of the clay layers. The exceptionally high uncertainty in the strength of the stiff clay crust reflects the presence of a structure of joints and fissures (Section 3.1) which often leads to a significant variability in strength from one specimen to another.

Table 10-1 Statistical parameters of the unconfined compressive strength of the clay layers

Soil Layer	Unconfined Compressive Strength (kPa)		
	No. of Tests	Mean	Standard Deviation
Stiff gritty blue clay crust	38	112.6	55.8
Blue Clay I	55	65.8	17.4
Blue Clay II	33	84.2	26.9

In connection with the soil testing program of the Chicago subway, Peck (1940) compared the unconfined compressive strength of specimens carefully prepared from block samples with the compressive strength of specimens obtained from the immediate vicinity using the standard 2" diameter shelby tube sampler. Based on the results of 13 tests, he reported that the strength of the block, and presumably less disturbed, samples is about 35% higher than that of the shelby tube samples. Peck (1940) attributed that loss of strength to mechanical disturbance during sampling. In analyzing the failure of the Congress street cut, Ireland (1954) applied a correction factor of 1.35 to the measured unconfined compressive strength of all clay layers. Based on Peck's (1940) data, Tang et al. (1976) estimated the coefficient of variation of the correction factor to be 0.025.

4. SLOPE STABILITY ANALYSES

4.1 Deterministic Analysis

The stability of the Congress street open cut before failure is analyzed deterministically using Slope/W software and the Bishop method of slices assuming a circular failure surface. The mean values of the measured shear strength of the various layers, Section 3.2, are used in the analysis. The correction factor proposed by Peck (1940) to account for the effect of sampling disturbance is applied to the undrained shear strength of the Blue Clay I and the Blue Clay II. The samples based on which Peck (1940) estimated the correction factor were all at the level of the subway tunnel below the stiff fissured clay crust. In addition, the operational strength of the stiff desiccated crust largely depends on the extent and structure of fissures rather than on the measured unconfined compressive strength. As such, it was decided not to apply the correction factor to the undrained shear strength of the stiff crust.

The stability analysis yielded a factor of safety of 1.13. Figure 10–1 shows the critical slip surface. The fact that the factor of safety at failure is above one suggests that some of the strength parameters are overestimated. This is likely to be the undrained shear strength of the stiff clay crust. The mean strength used in the analysis may not be a proper representation of the operational undrained shear strength particularly since the measurements exhibit significant scatter.

4.2 Probabilistic Analysis – Proposed Methodology

4.2.1 Input Variables

Based on the discussions in Section 3, the undrained shear strength of the stiff blue clay crust, the Blue Clay I and the Blue Clay II are considered random variables. The mean and variance of each variable are obtained based on the results of unconfined compressive strength tests as reported by Ireland (1954). The testing data were not available to assess the actual probability distributions of the variables. As such, the three variables are assigned parametric probability distributions. Wu and Kraft (1967) reported that the unconfined compressive strength of three clay till deposits from different sites fit the lognormal distribution "reasonably well". Fredlund and Dahlman (1972) also reported that the probability distribution of the unconfined compressive strength of Lake Edmonton sediments approaches a lognormal distribution. Based on that, the probability distributions of the undrained shear strength of the three layers are assumed lognormal. Since the reported standard deviations of the strength of the layers are very high, the lognormal distribution also has the advantage of eliminating the potential of sampling negative values during simulation.

The uncertainty surrounding the correction factor proposed by Peck (1940) to account for the effect of sampling disturbance is also taken into account. The correction factor is regarded as a bias factor (refer to Equation 5-7) with a mean equal to 1.35 and a standard deviation equal to 0.034. The mean is the value of the correction factor proposed by Peck and the standard deviation is based on Tang et al (1976) assessment of the scatter in Peck's data. The probability density function of the bias factor is assumed normal.

The statistical uncertainty of the mean values of the undrained shear strength of the three clay layers are represented by 3 random variables with zero means and standard deviations estimated using Equation 3-20. The variables are assumed normally distributed and are combined with the variables representing soil variability in an additive form as indicated in Chapter 5. Table 10-2 summarizes the statistical parameters and probability distributions of all input variables.

Table 10-2 Statistical parameters and CDFs of the input variables – Congress Street Open Cut

Soil Unit	Input Variable	Soil Variability			Systematic Uncertainty		
		E[--]	σ[--]	CDF	E[--]	σ[--]	CDF
Stiff clay crust	Undrained shear strength; $S_{u\text{-}cr}$ (kPa)	56.3	27.9	LogN.	0.0	4.53	N.
Blue Clay I	Undrained shear strength; $S_{u\text{-}BC\,I}$ (kPa)	32.9	8.7	LogN.	0.0	1.17	N.
Blue Clay II	Undrained shear strength; $S_{u\text{-}BC\,II}$ (kPa)	42.1	13.5	LogN.	0.0	2.34	N.
Blue Clay I & II	Bias factor; B	--	--	--	1.35	0.034	N.

N. - Normal distribution; LogN. - LogNormal distribution

4.2.2 Critical Slip Surface

In locating the probabilistic critical slip surface, two candidate surfaces are examined; the deterministic critical surface and the surface based on the Hassan and

Wolff (1999) algorithm. The latter is obtained by performing a series of deterministic stability analyses with the strength of each clay layer reduced in turn by one standard deviation. The surface corresponding to the reduced strength of the Blue Clay II yielded the lowest factor of safety and is thus considered the most critical based on the Hassan and Wolff criterion.

Probabilistic stability analyses (as outlined in the following sections) of the slope geometry before failure indicated that the probability of unsatisfactory performance associated with the deterministic critical slip surface is 29.11% and that of the Hassan and Wolff surface is 28.31%. The former is, thus, considered the probabilistic critical slip surface and is used in the subsequent analyses. As the slope geometry is modified (Section 4.2.5), the deterministic critical slip surface is not always the most critical in probabilistic terms. For each case, the deterministic surface and the Hassan and Wolff surface are examined to determine the surface that yields higher probability of unsatisfactory performance.

4.2.3 Spatial Variability

As indicated in Sections 2 and 3.1, the subsoil in the Chicago area comprises a random mixture of clays, silts and other materials. As such, its variability is expected to be high and erratic, both laterally and with depth. This is confirmed by the observations of Peck and Reed (1954) and Ireland (1954). The autocorrelation distance(s) of such formations is likely to be small, towards the lower ends of the typical ranges reported in Chapter 5. A range of 20-30 m is postulated as a possible range of the autocorrelation distance in the horizontal direction and 1-3 m as a possible range for the vertical autocorrelation distance. The geometry of the slip surface, Figure 10–1, implies that the analysis is not dominated by the spatial structure along a specific direction. Hence, the variability of the undrained shear strength of the clay layers is approximated by an isotropic spatial structure with an equivalent autocorrelation distance. Using Equation 5-6, the range of the equivalent autocorrelation distance is estimated to be 4-10 m. The analyses in the following sections are based on an intermediate value of 7 m. The sensitivity of the probability of unsatisfactory performance to other values of the autocorrelation distance is investigated in Section 4.2.6.

The spatial variability of the undrained shear strength of the clay layers is accounted for as outlined in Chapter 5. The portion of the slip surface within each layer is divided into segments of length δ. The average strength over the length of each segment is considered a variable and is represented by the point CDF of the corresponding soil layer (Table 10-2). The correlation coefficients between the averages are estimated using Equation 5-5. For an autocorrelation distance equal to 7m, the lengths of the segments of the slip surface within the stiff crust and the Blue Clay I are less than $\delta \cong 14$ m. Thus, the strength of either layer is represented by one variable only.

4.2.4 Stability Analysis – Geometry Before Failure (1.35h:1v)

A spreadsheet model mimicking the slope geometry, the soil stratigraphy and the deterministic critical slip surface (refer to Section 4.2.2) is prepared. The Bishop method of slices is used in the model. The spreadsheet includes 4 uncertain parameters (the undrained shear strength of the stiff clay crust, the Blue Clay I and the Blue Clay II and the bias factor) represented by five random variable, two of which are correlated.

Based on a few trial simulations, the optimum number of iterations is estimated to be 15,000. Using a seed number of 31069, the mean factor of safety is calculated to be 1.13 with a standard deviation of 0.22. The probability of unsatisfactory performance is estimated to be 29.11%. Figure 10–2 shows the histogram and the CDF of the factor of safety. The simulation is repeated 25 times using different seed numbers to assess the reliability of the estimated probability. The results are summarized in a histogram form in Figure 10–3. The mean probability of unsatisfactory performance is 29.11% with the 95% confidence interval ranging between 29.02-29.20 %.

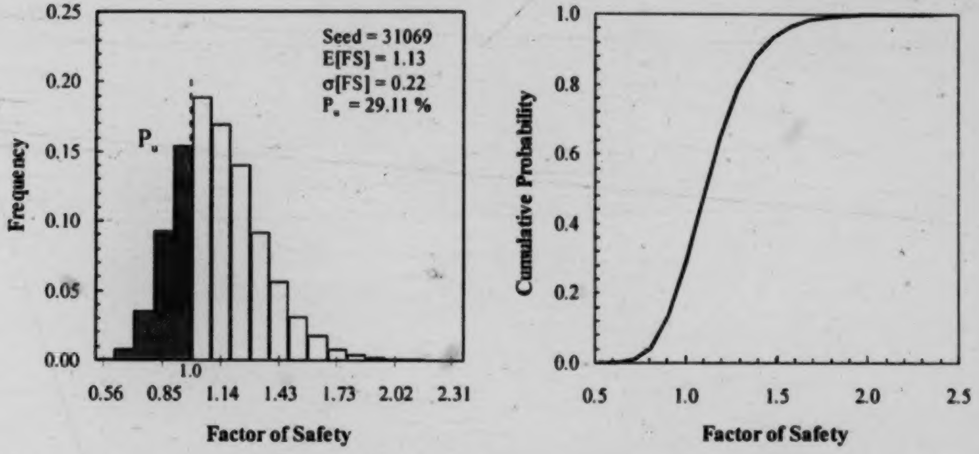

Figure 10–2 Histogram and CDF of the factor of safety, Congress Street Cut (1.35:1) – Proposed Methodology

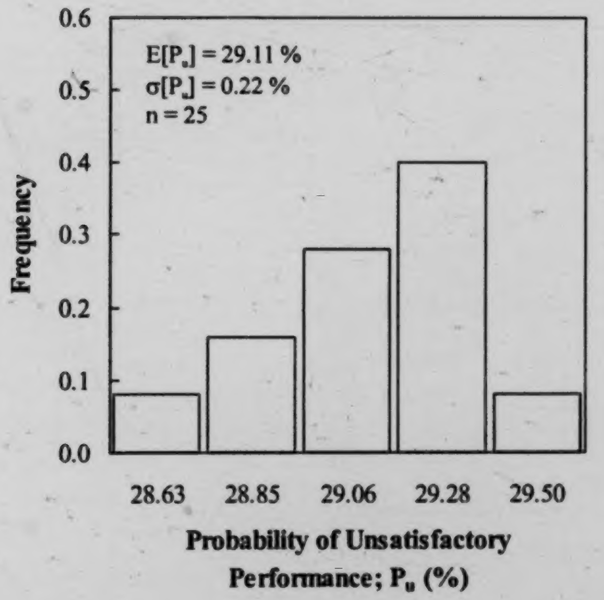

Figure 10–3 Histogram of the probability of unsatisfactory performance, Congress Street Cut (1.35:1) – Proposed methodology

4.2.5 Stability Analyses – Slope Geometry Modified

In order to assess the probability of unsatisfactory performance associated with an acceptable design based on conventional practice, the inclination of the cut slope is reduced to various values and the stability of the modified slopes is analyzed probabilistically. Five different slopes (h:v) are considered; 1.75:1, 2.0:1, 2.5:1 and 3.0:1. The same approach adopted for the analysis of the geometry before failure (Section 4.2.4) is applied in analyzing the stability of the modified slopes. That included locating the probabilistic critical slip surface, preparing a spreadsheet model and accounting for spatial variability and systematic uncertainty. For each case, Monte Carlo simulation is repeated 10 times using different seed numbers. The outcome of the analysis is taken as the average of the outputs of the 10 simulations. Figure 10–4 shows the variation of the probability of unsatisfactory performance and the factor of safety with the slope angle. The plot indicates limited increase in the probability of unsatisfactory performance as the slope angle increased from 18.4 degrees to 21.8 degrees followed by a sharp increase in the probability up to failure. The rate of decay of the probability of unsatisfactory performance as the slope angle is reduced (i.e., higher factor of safety) is much slower than the Lodalen and the Muar cases. This is attributed to the high and erratic variability of the undrained shear strength of the clay layers.

4.2.6 Stability Analysis – Acceptable Cut Design (2.5h:1v)

As indicated in Chapter 9, it is a common practice to design the short-term stability of earth slopes to factors of safety in the range of 1.3-1.4. For the Congress Street Cut, the factor of safety at failure is estimated to be 1.13. In addition, the uncertainty in the undrained shear strength of the clay layers is significant. Taking that into account, it is judged that a slope of 2.5h:1v (FS=1.44) is an acceptable design from the conventional practice point of view. The stability of that slope is assessed in some detail in the following paragraphs.

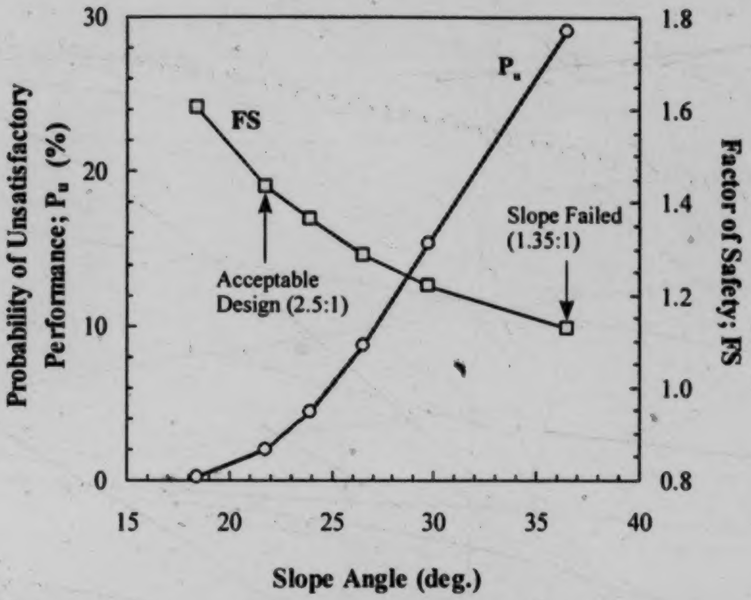

Figure 10–4 Variation of the probability of unsatisfactory performance and the factor of safety with the slope angle, Congress Street Cut – Proposed Methodology

Using a seed number of 31069 and 30,000 iterations, the mean factor of safety is estimated to 1.44 with a standard deviation of 0.24. The probability of unsatisfactory performance is estimated to be 1.97%. Figure 10–5 shows the histogram and the probability distribution function of the factor of safety. The simulation is repeated 25 times using different seed numbers and the computed probabilities of unsatisfactory performance are summarized in a histogram form in Figure 10–6. The mean probability of unsatisfactory performance is estimated to be 2.02% with the 95% confidence interval ranging between 1.99-2.05%.

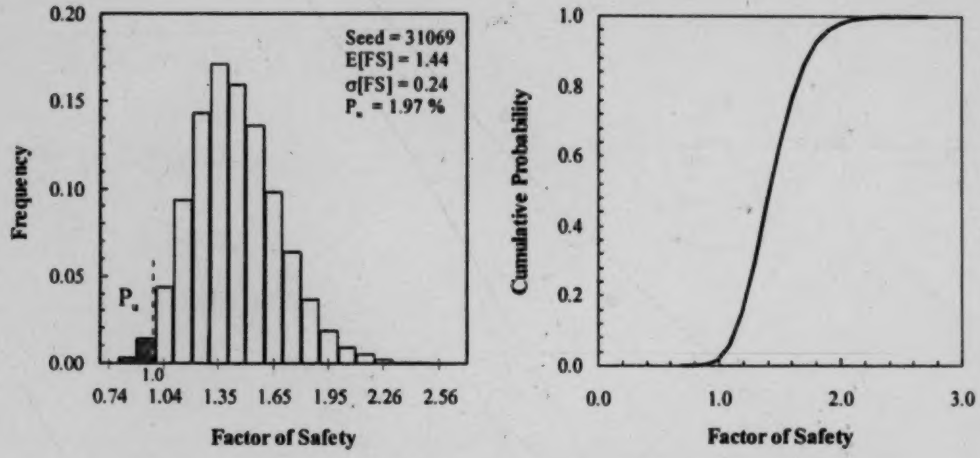

Figure 10–5 Histogram and CDF of the factor of safety, Congress Street Cut (2.5:1) – Proposed Methodology

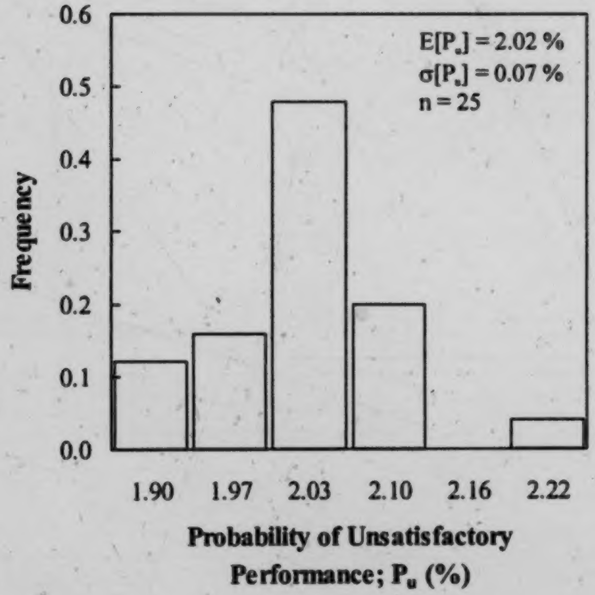

Figure 10–6 Histogram of the probability of unsatisfactory performance, Congress Street Cut (2.5:1) – Proposed Methodology

A sensitivity analysis is performed to assess the relative contributions of the different sources of uncertainty to the reliability of the design. Figure 10–7 shows Spearman rank correlation coefficients for all input variables. The plot indicates that the uncertainty surrounding the strength of the Blue Clay II is by far the most influential source of uncertainty. Even though the physical contribution of the stiff clay crust to the stability of the cut is small (because of its small thickness), it is ranked as the second major source of uncertainty. This reflects the high uncertainty surrounding the operational strength of the crust due to the presence of fissures and joints. The graph also shows that the impact of the uncertainty due to soil variability on the analysis is much larger than that of the systematic uncertainty (i.e., bias factor and statistical errors). This observation is important because it implies that the analysis could be sensitive to the value of the autocorrelation distance.

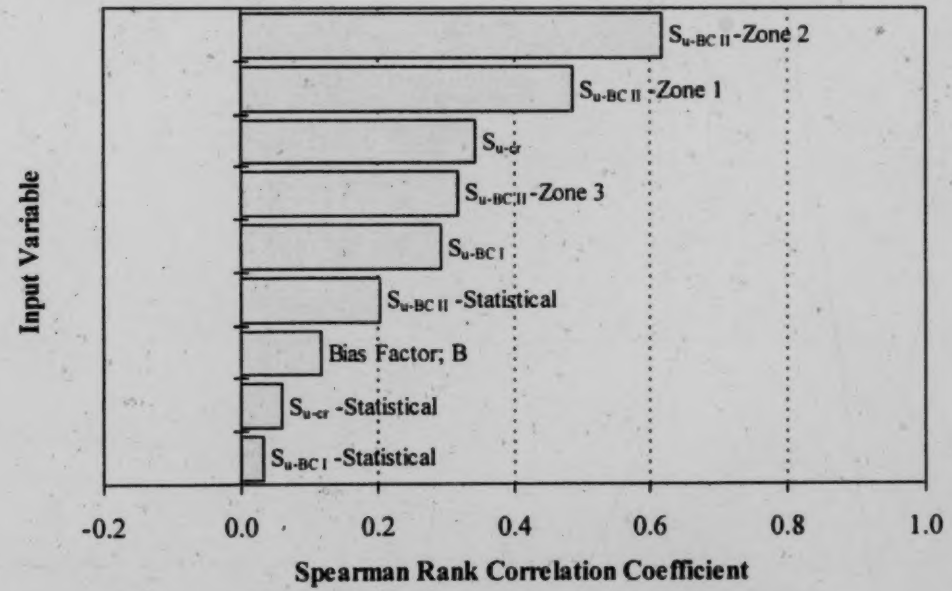

Figure 10–7 Sensitivity analysis results, Congress Street Cut (2.5:1) – Proposed Methodology

The preceding analyses are based on an autocorrelation distance of 7 m. The sensitivity of the estimated probability of unsatisfactory performance to the value of the autocorrelation distance is investigated. The stability of the 2.5:1 slope is reassessed using different values of the autocorrelation distance. Figure 10–8 shows the variation of the probability of unsatisfactory performance as the autocorrelation distance is varied within the range estimated in Section 4.2.3. The plot indicates that the probability of unsatisfactory performance is somewhat sensitive to the value of the autocorrelation distance. As the autocorrelation distance is increased from 4 to 10 m, the probability of unsatisfactory performance increased from 0.69% to 3.59%. This sensitivity stems from two factors. First, the analysis is dominated by the uncertainty due to the spatial variability of the strength (rather than systematic uncertainty) which magnifies the impact of variance reduction due to spatial averaging. Second, the erratic nature of the clay till formations causes the reduction in the variance of the *average strength* along the slip surface to be sensitive to the value of the autocorrelation distance.

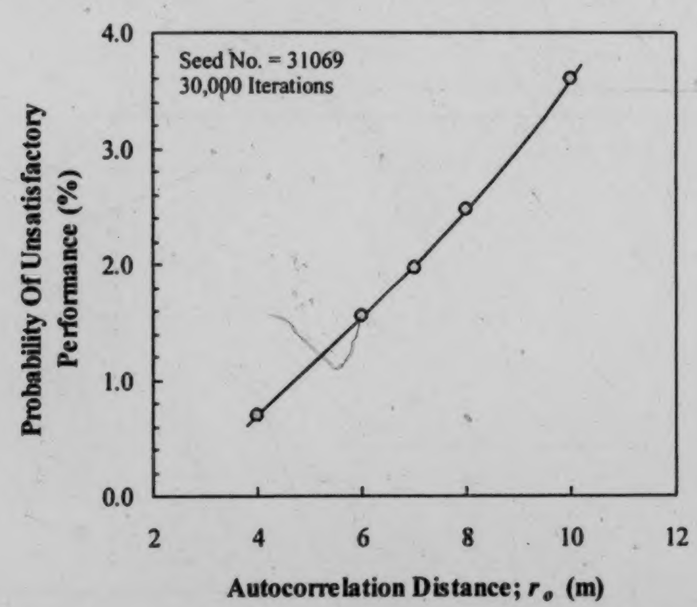

Figure 10–8 Variation of the probability of unsatisfactory performance with the autocorrelation distance, Congress Street Cut (2.5:1)

4.3 Naïve Analysis

The acceptable slope geometry (2.5h:1v) is also analyzed following the naïve approach. The analysis accounts for the uncertainty of the of the undrained shear strength of the clay layers as reflected by the scatter of the results of the unconfined compressive strength tests only. The mean strength parameters are regarded as deterministic values. The uncertainty of the bias factor proposed by Peck (1940) is taken into account. Table 10-3 summarizes the statistical parameters and probability distributions of the input variables.

Table 10-3 Statistical parameters and CDFs of the input variables – Naïve Analysis

Soil Unit	Input Variable	Mean	Standard Deviation	Probability Distribution
Stiff clay crust	Undrained shear strength; $S_{u\text{-}cr}$ (kPa)	56.3	27.9	LogN.
Blue Clay I	Undrained shear strength; $S_{u\text{-}BC\,I}$ (kPa)	32.9	8.7	LogN.
Blue Clay II	Undrained shear strength; $S_{u\text{-}BC\,II}$ (kPa)	42.1	13.5	LogN.
Blue Clay I & II	Bias factor; B	1.35	0.034	N.

N. - Normal distribution; LogN. - LogNormal distribution

A spreadsheet model is prepared using Bishop's method of slices and the Hassan and Wolff surface which is found more critical than the deterministic critical slip surface. Using a seed number of 31069 and 30,000 iterations, the simulation yielded a mean factor of safety of 1.44 with a standard deviation of 0.33. The probability of unsatisfactory performance is estimated to be 5.98%. Based on 25 simulations, the mean probability of unsatisfactory performance is estimated to be 6.05% with the 95% confidence interval ranging between 6.02-6.09%. Figure 10–9 shows the histogram of the probability of unsatisfactory performance. Similar to the Muar case, the naïve probability is not significantly higher than the probability estimated using the more rigorous approach in

Section 4.2.6. This is attributed to the fact that the length of the failure surface within each layer is comparable to the scale of fluctuation ($\delta \cong 14$ m). As a result, the uncertainty of the strength estimated directly from the point measurements (naïve approach) is not significantly higher than the uncertainty of the *average* strength along the failure surface (proposed methodology).

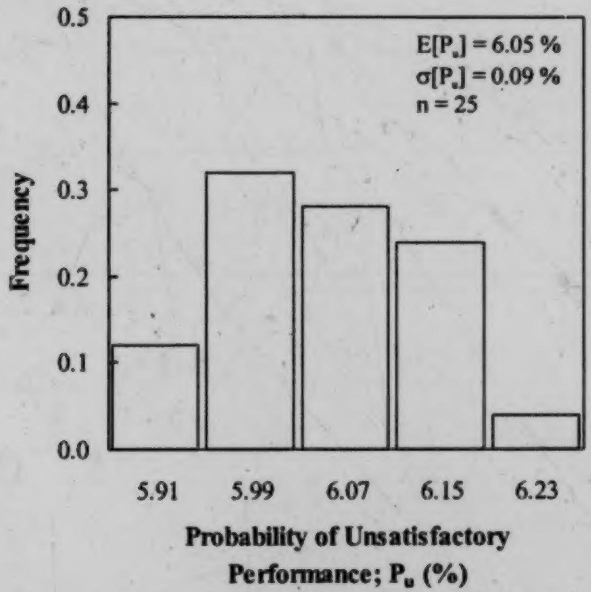

Figure 10–9 Histogram of the probability of unsatisfactory performance, Congress Street Cut (2.5:1) – Naïve Analysis

A sensitivity analysis is also performed to assess the relative contributions of the different sources of uncertainty. Figure 10–10 shows Spearman rank correlation coefficients for all input variables. The plot indicates that the uncertainty of the strength of the Blue Clay II is by far the most significant source of uncertainty. It also shows that the uncertainty of the bias factor has a negligible impact on the analysis.

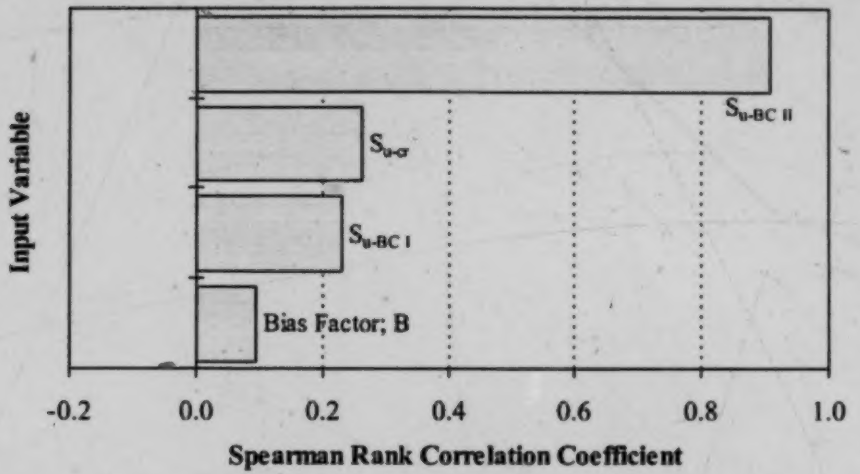

Figure 10–10 Sensitivity analysis results, Congress Street Cut (2.5:1) – Naïve analysis

5. SUMMARY

The proposed probabilistic methodology is applied to the Congress Street Open Cut in Chicago. The probability of unsatisfactory performance associated with the geometry before failure (slope 1.35h:1v) is estimated to be 29.11% indicating that failure was expected. Based on conventional slope design practice, a cut slope of 2.5h:1v is considered an acceptable design. The probability of unsatisfactory performance associated with that slope is estimated to be 2.02%. This estimate is shown, however, to be somewhat sensitive to the value of the autocorrelation distance. The sensitivity is attributed to the very high spatial variability of the strength and the erratic nature of the clay till formations. This suggests that for soil deposits exhibiting high and erratic variability, the results of a probabilistic analysis could be sensitive to the assumption of the autocorrelation distance. If such sensitivity is large enough to impede the decision-making process, obtaining a site-specific estimate of the autocorrelation distance may be worth the effort.

CHAPTER 11

STABILITY OF GRANITIC SOIL SLOPES IN HONG KONG

The significant variability of the shear strength of Hong Kong granitic soil is assessed based on a large database of triaxial test results. Generalized (or regional) probability distributions characterizing the variability of strength parameters are estimated. Four case studies of slope failures in Hong Kong are back analyzed probabilistically to quantify the uncertainty of pore water pressure at failure. The four cases are then re-designed to an acceptable geometry according to the current slope design practice. The probabilities of unsatisfactory performance associated with the four slopes are estimated. The following sections describe the deterministic and probabilistic analyses undertaken

1. INTRODUCTION

With a population exceeding six million and land area of about 1000 sq. km, Hong Kong is considered one of the most densely populated urban areas in the world. Much of the territory comprises natural and man-made slopes resulting in an intense urbanization at and around steep slopes. Hong Kong also experiences heavy seasonal rainfall (nearly 2000mm of rain during the wet season from May to October) which, in many cases, triggers landslides. Slope failures in Hong Kong are often sudden with no prior warning and involve rapid debris movement. Many of these slides result in fatalities and injuries. The recorded history of landslide fatalities in Hong Kong dates back to as early as 1917 when 73 people died due to the collapse of a building in Po Hing Fong caused by a landslide. In 1978, the government of Hong Kong established the Geotechnical Control Office (currently known as the Geotechnical Engineering Office) to oversee the safety of earth slopes. Since then, significant efforts have been made to identify and mitigate the slopes that pose a danger to the public. The slope problem in

Hong Kong has been the subject of many studies; the most important of which are Lumb (1975) and Brand (1985).

Assessing the safety of an earth slope in Hong Kong is, however, a challenging task. This is attributed to the extreme uncertainties in the shape and depth of the potential slip surface, the soil or rock strength parameters and the pore water pressure at failure. The slip surface is often non-circular and frequently governed by the structure of joints within the soil or rock. The shear strength parameters vary significantly because of the high variability of Hong Kong residual soils and the presence of relict and clay in-filled joints. Out of the three parameters, pore water pressure is the one most difficult to evaluate. The magnitude of the pore pressure depends on the intensity and frequency of rainfall and the structure of joints and fissures within the slope. Both are extremely difficult to predict. In the light of these substantial uncertainties, Kay (1998) questioned the applicability of the conventional slope design practice to slopes in Hong Kong. Probabilistic and risk analyses are better alternatives for such cases of extreme uncertainty.

2. GRANITIC SOILS OF HONG KONG

2.1 Origin and Formation

A substantial part of Hong Kong is underlain by Mesozoic igneous rocks; mainly granites and volcanics. Hong Kong soils are mainly "Residual Soils" formed by in-situ decomposition of these rocks. As a result of differences in mineralogical composition and texture (volcanics having much finer grains), soils produced from both rocks have different characteristics. While both soils exhibit significant variability, the volcanics are extremely heterogeneous and closely jointed (joint spacing ≈ 0.25m). The density and stochastic nature of the joints associated with the volcanic soils are major sources of model uncertainty. Quantifying mass strength and pore pressures at failure are extremely difficult. As a result, the rate of slope failures in volcanic soils is higher than in granitic soils. Because of our limited capabilities in dealing with these sources of uncertainties, volcanic soils are not considered in this work. This study is focused mainly on slopes in granitic soils, particularly cut slopes. Cut slope failures are by far the most common form of landslides in Hong Kong (Brand, 1985)

Granitic rocks underlie large areas in Hong Kong; including the main urban areas of Victoria Harbor, north coast of Hong Kong Island, Kowloon Peninsula and Kun Tong and Tsun Wan districts. Fresh granite is typically composed of feldspar (up to 70%), quartz (30-40%) and small proportions of biotite and other minerals. Chemical action of water combined with physical and thermal processes alters the feldspar and biotite fractions into kaolinite clay mineral leading to the decomposition of the granite. The rate of decomposition is controlled by granite grain size and joint spacing. Depending on the degree of weathering, the decomposed granite may range from coarse sand to silty clayey sand. Boulders may also be present.

The Geotechnical Engineering Office of Hong Kong (GCO 1988) adopted a six-grade system to classify the weathered rock material. Grade I is fresh rock and Grade VI is residual soil that bears no features of the parent rock. Grade IV (highly decomposed granite) and grade V (completely decomposed granite) are considered soils that still retain some features of the original rock (texture, fabric, jointing). They are referred to as *Saprolite*.

2.2 Engineering Properties

For engineering purposes, materials grades IV to VI are treated as soils while grades I to III are treated as rocks. The majority of cut slope failures in Hong Kong are in soils of weathering grades IV to VI (Brand, 1985). Grade VI soil is often encountered at surface, thus contributing very little to the stability of slopes. This assessment of properties is concerned only with decomposed granites grades IV and V (highly and completely decomposed granites). Due to variations in the mineralogical composition and grain size of the parent rock and in the weathering processes (e.g., alteration, leaching etc.), these soils are largely heterogeneous, even for the same material grade. Such heterogeneity is a major problem in characterizing soil properties for engineering applications. Estimating representative shear strength parameters for slope stability analyses is a pronounced example.

The general characteristics of the fresh rock and the physics of the decomposition processes are, however, not significantly different across the territory. As a result, the nature and degree of heterogeneity are not site dependent. Lumb (1962, 1965) reported that no trends were found between samples of the same soil type from different locations. He also noted that the variability (in terms of standard deviation) within one site is not much less than the variability over the entire study area which covered a large part of Hong Kong. Lumb's observations imply that the properties of the decomposed granite could be statistically homogeneous across the territory. Based on that, it was decided to assess the physical and mechanical properties on a regional, rather than site specific, basis. The testing results used in the assessment were collected from Lumb (1962, 1965), Hencher (1983a, 1983b), Siu and Premchitt (1988), Shelton and Cooper (1984) and Pun and Ho (1996).

2.2.1 Physical Properties

The gradation and void ratio of these types of soils can vary considerably over relatively short distances. Based on the available data (refer to above references), the fines content varies between 12-26% for the highly decomposed granite (HDG) and between 4-51% for the completely decomposed granite (CDG). The clay fraction is mainly kaolinite and varies (as a percentage) considerably depending on the composition of the parent rock, the intensity of hydrothermal alteration and the amount of leaching. The percent of fines is one of the main factors controlling the strength of the decomposed granite (Siu and Premchitt, 1988; Pun and Ho, 1996). The void ratio ranges between 0.56-1.05 for the CDG and 0.58-0.84 for the HDG (very few data were available for the HDG). Lumb (1962) noted that the void ratio, while highly variable, tends to increase as the distance from the fresh rock face increases. The dry unit weight ranges between 14.2-16.5 kN/m^3 and 13.4-16.2 kN/m^3 for the HDG and the CDG, respectively. The permeability of residual soils in general is high. Hong Kong granitic soils are no exception. Brand (1985) noted that the permeability of Hong Kong soils ranges between 10^{-4}-10^{-6} m/sec. Such relatively high permeability allows rainwater to infiltrate easily into most soils in Hong Kong influencing the degree of saturation and perched water levels.

Due to the seasonal variations in rainfall and the high infiltration rates, the degree of saturation of Hong Kong soils varies throughout the year. Often the variations extend for considerable depths. Lumb (1962) observed that the degree of saturation of decomposed granite could be as low as 50% and as high as 90%. The strength of residual soils is largely influenced by the degree of saturation. When fully saturated, the cohesion drops to very low values, or even zero, and the soil behaves like a frictional material. As a result, the variation of the degree of saturation has a serious impact on the stability of natural and cut slopes.

2.2.2 Shear Strength

The shear strength parameters of the HDG and CDG are assessed based on the results of consolidated undrained triaxial tests with pore pressure measurements as well as consolidated drained tests. The results of a large number of tests were gathered from the references cited previously.

Slope failures in Hong Kong are generally shallow leading to relatively low effective stresses acting on the slip surface; typically 30-200 kPa (Brand, 1985). For testing convenience triaxial tests are usually conducted at much higher confining stresses. Brand (1985) noted that the strength envelopes of Hong Kong residual soils are curved at low confining stresses. He commented that strength inferences based on a linear projection of the results of triaxial tests performed at high stress levels underestimate the available shear strength for Hong Kong slopes. Based on Brand's argument, a mean effective stress threshold of $p' = 400$ kPa is set (judgmentally) and all tests conducted under higher stresses are discarded. Some of the consolidated undrained tests are multi-stage tests, where the same specimen is consolidated and sheared a number of times under increasing confining stresses. Fearing that this may lead to a reduction in strength due to the destruction of the inherent soil structure, only the results of the first stages of these tests are considered (assuming zero effective cohesion). As this assessment is concerned mainly with the strength of the soil matrix, the results of specimens failing on clearly defined joints are also discarded.

Following this screening process, 62 consolidated undrained tests and 39 consolidated drained tests remain; each test comprises 2-4 specimens. Comparative studies on granitic soils (Lumb, 1965; Massey, 1983; Shen 1985) showed no significant difference between the effective shear strength parameters obtained from consolidated drained tests and consolidated undrained tests with pore pressure measurements. Hence, in assessing the statistical characteristics of shear strength parameters, the results of the two test types are combined.

Out of the 101 test results, the principal stresses at failure (σ_1' and σ_3') of only 59 specimens from three localities were available; 37 of which are CDG and 22 are HDG. Figure 11–1 shows the p'-q plots of the specimens grouped by location and weathering grade. The plot indicates some useful observations. Firstly, the strength does not seem to vary much from one location to another (Figure 11–1a). This is in harmony with the observations of Lumb (1965) and Pun and Ho (1996). Secondly, the strength of the HDG is only slightly higher than the strength of the CDG (Figure 11–1b). Furthermore, within any single site there are samples classified as HDG and others as CDG. This is expected since the degree of weathering could vary over short distances. It is attributed to variations in feldspar content, grain size of the rock, joint spacing and weathering microenvironments. In addition, weathering is a continuous process and a distinct boundary between the two grades is only hypothetical. Despite that the degree of rock decomposition, usually, decreases with depth, available data did not indicate higher strength at deeper elevations.

The above observations provide a reasonable ground for assessing the variability of shear strength on a regional basis and dealing with the HDG and CDG as one class of material. The variability of the weathering degree (highly decomposed to completely decomposed) could be regarded as one of the random processes contributing to the variability of the strength. As such, the triaxial test results of the HDG and the CDG from all locations are combined together to estimate the statistical characteristics of the shear strength parameters (C′, ϕ′).

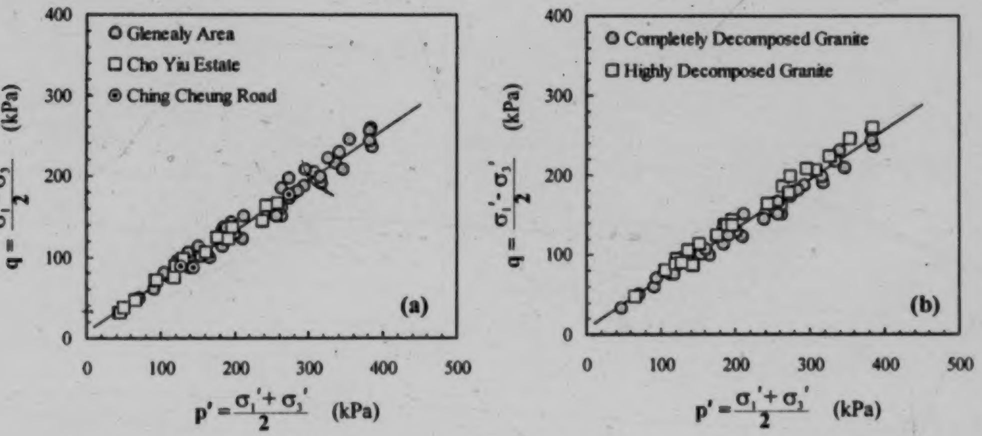

Figure 11–1 p′-q plots of triaxial tests on granitic soils; a) Based on location, b) Based on weathering grade

Based on the available data, the effective friction angle of the granitic soils varies between a minimum of 28 degrees and a maximum of 49 degrees. The mean and standard deviation are estimated to be 37.8 and 4.5 degrees, respectively. Figure 11–2 shows the probability histogram and the cumulative distribution function of the friction angle. The shape of the histogram approaches a lognormal density function. A lognormal parametric distribution with the experimental mean and standard deviation is plotted on the same graph. The match between the CDFs of the experimental and parametric distributions is very close as shown in Figure 11–2 (right plot). This is also confirmed by the Q-Q plot in Figure 11–3, which is almost a 45-degree line.

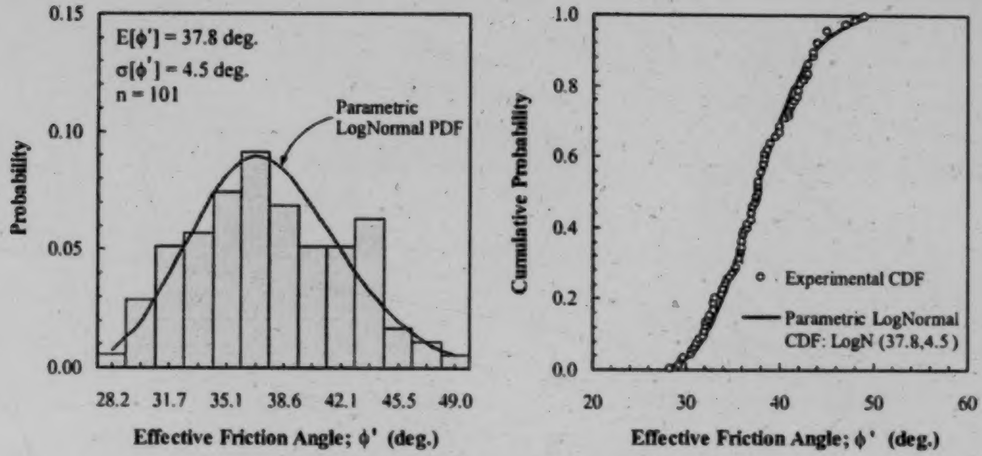

Figure 11–2 Probability histogram and CDF of the effective friction angle of the granitic soils (HDG and CDG) of Hong Kong

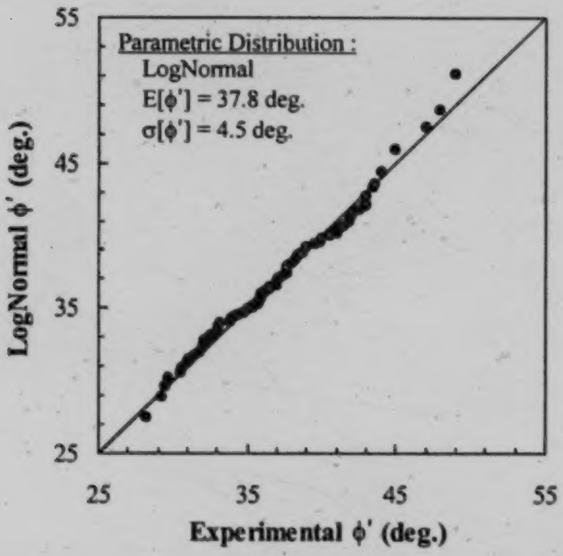

Figure 11–3 Q-Q plot of the effective friction angle of the granitic soils of Hong Kong (HDG and CDG)

As would be expected for such a type of soil, the effective cohesion varies significantly. It ranges between zero and 25 kPa. The mean is estimated to be 5.6 kPa with a standard deviation of 5.6 kPa; that is a coefficient of variation of 1. Figure 11–4 shows the histogram and the CDF of the data. The presence of a correlation between the tangent of the friction angle and the cohesion is also investigated. Figure 11–5 is a scatter plot of the two parameters. The graph indicates almost no correlation (possibly a negative, but very poor correlation).

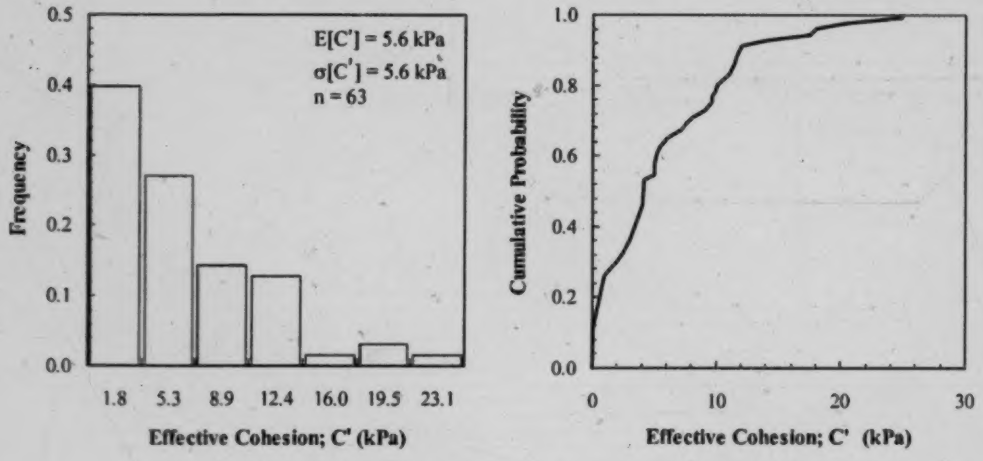

Figure 11–4 Histogram and CDF of the effective cohesion of the granitic soils of Hong Kong (HDG and CDG)

In the following sections, the estimated probability distributions of the friction angle and effective cohesion (Figure 11–2 and Figure 11–4) are referred to as *regional* distributions. These generalized distributions are based on a reasonable database from different locations and are believed to be a reliable representation of the variability of the strength parameters of the matrix of granitic soils in Hong Kong. However, they may not necessarily be valid at all locations. Site-specific shear strength measurements are essential to confirm or update these generalized distributions. The Bayesian approach (Ang and Tang, 1975) could be very useful in updating the distributions based on additional site-specific data.

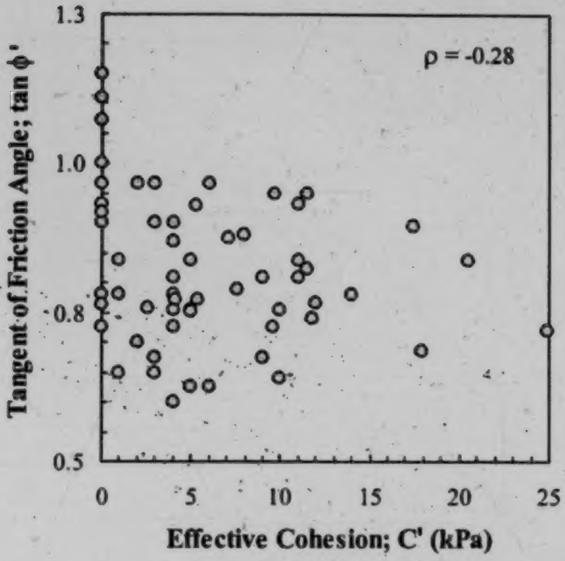

Figure 11–5 Scatter plot of tangent of friction angle and effective cohesion, Hong Kong granitic soils (HDG and CDG)

3. SLOPE STABILITY ANALYSES

Slope failures in Hong Kong are attributed mainly to the variability of shear strength and pore water pressure. The uncertainties associated with predicting the operational shear strength parameters and pore pressures at failure are of paramount significance. Probabilistic slope stability analyses are of great value in such cases.

Unless failure occurs along weak undetected joint planes, quantifying the uncertainty of soil matrix shear strength is possible with a reasonable level of reliability (Section 2.2.2). Unfortunately, almost all failures are triggered by the increase in pore water pressure during rainfalls of high intensity. Pore water pressure at failure is the most critical factor in slope stability analyses in Hong Kong and is by far the most difficult to predict. For example, Brand (1985) reported that the piezometric head in a Hong Kong slope increased by 5m in only 18 hours during a rainstorm in June of 1982. The water table dropped quickly when the rain stopped. Also, Sweeney and Robertson (1979) reported a 12m increase in groundwater level in one piezometer during an intense rainstorm while another piezometer at a nearby location showed only 3m increase. Pore pressures are controlled by factors such as rainfall intensity, duration and frequency, infiltration rate, soil macro-permeability and joint structure and infilling. Quantifying the uncertainty of the water pressure requires stochastic analyses of the uncertainties associated with these factors and a competent model to integrate them; a formidable task.

A probabilistic slope stability analysis invariably requires an estimate of the probability distribution of pore water pressure. An effort to quantify the probability distribution of the pore water pressure associated with slope failures in Hong Kong is undertaken. Recognizing the difficulties associated with an analytical solution (as outlined above), a phenomenological approach is adopted. The pore pressure ratio, r_u, is used to model the pore pressure along the slip surface. Slope failures provide valuable information that can be used effectively in quantifying pore pressure uncertainty. Firstly, the factor of safety at failure is equal to one. Secondly, the uncertainty of the location and shape of the slip surface is, often, largely reduced by post-failure field observations (e.g., scarp of the slide, toe bulging, zones of disturbance in retrieved soil samples, ...). Case histories of slope failures in Hong Kong were collected and analyzed probabilistically with the factor of safety as a deterministic input (FS=1) and the pore pressure ratio as the output. Thus, the output of the analysis is the probability distribution of the pore pressure ratio. The estimated pore pressures are the resultant pressures that triggered the failure of the investigated slopes, regardless of the preceding events or processes (e.g., rainfall, rate of infiltration, ...). It should be noted that the pore pressure ratio, as used here, is not intended to characterize the distribution of the pore pressure along the slip surface; this would be a severe simplification for a complex problem. Rather, it is an index that induces an impact equivalent to that of the complex and unknown pore water pressure.

The investigated case studies are then re-designed to an acceptable geometry based on the back-calculated pore pressure ratio. The proposed probabilistic methodology is applied to assess the stability of the modified slopes using the inferred probability distributions of pore pressure ratio and the regional distributions of the friction angle and cohesion.

In searching for case studies, cases where failure was controlled by the strength and structure of a joint system (a form of model uncertainty) were avoided. Four case studies were obtained; Cho Yiu Estate (Siu and Premchitt, 1988), Tsing Yi: 1 (Hencher, 1983a), Ching Cheung Road (Hencher, 1983b) and Shek Kip Mei landslide (FMSW, 2000). The 4 case studies involved sliding failure modes and are classified, in terms of the volume of the failure mass, as massive (volume > 500m^3; GEO, 1999). Failures of that size are not very common in Hong Kong. However, they are, usually, the most devastating failures. The conclusions inferred in this chapter are relevant, mainly, to massive deep-seated sliding failures. Other failure modes (e.g., debris flows, rock falls) are not considered in this study. The following sections describe the slides and the deterministic and probabilistic analyses undertaken.

3.1 Cho Yiu Estate Landslide

3.1.1 Background

On July 30 1987, during an intense rainstorm, a major slope failure occurred at Lim Cho street just below block 4 of Cho Yiu Estate, Tsuen Wan. That section of the slope is about 225 m long and 17.0 m high. It is mainly a rock cut slope except for the part that failed, 30 m long, that is a soil slope. The height of the soil part of the slope is about 13m with 40 degrees inclination (1.2h:1v). Field inspection shortly after failure indicated that failure was largely translational with a rupture surface comprising a set of planes. Displaced material was granitic soil and rock fragments (0.1-1.0m in size) and had a volume of about 1200 m^3. It completely blocked Lim Cho Street. The slope was investigated in 1979 and inspected shortly before failure and was found satisfactory. Figure 11–6 shows a cross-section of the slope before failure. Immediately after failure the Geotechnical Engineering Office of Hong Kong undertook a detailed investigation to study the cause of failure (Siu and Premchitt, 1988). The investigation comprised field inspection, aerial photo analysis, topographic survey, geological mapping and field and laboratory testing. The main findings of the investigation are highlighted within Sections 3.1.2 to 3.1.5.

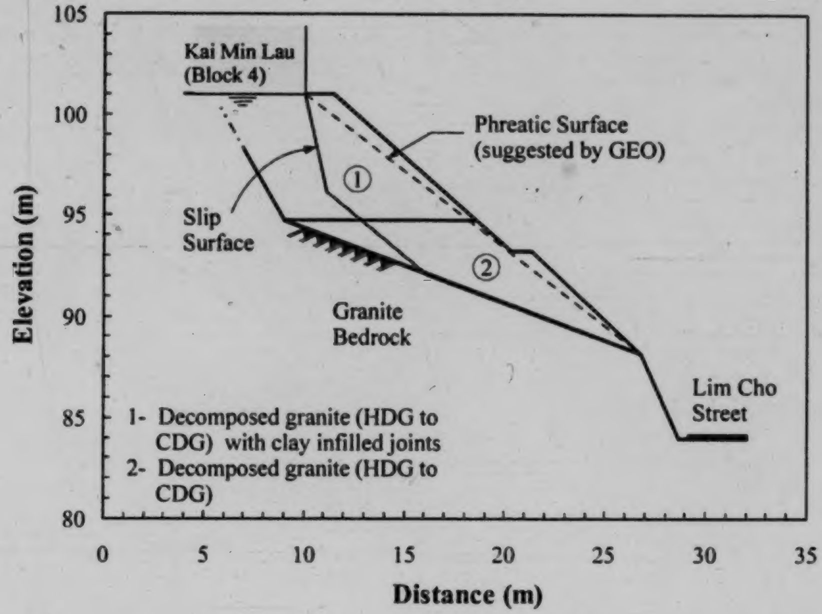
Kai Min Lau
(Block 4)
Phreatic Surface
(suggested by GEO)
①
Slip
Surface
②
Granite
Bedrock
Lim Cho
Street
1- Decomposed granite (HDG to CDG) with clay infilled joints
2- Decomposed granite (HDG to CDG)
Elevation (m)
105
100
95
90
85
80
0
5
10
15
20
25
30
35
Distance (m)

Figure 11–6 Geometry, stratigraphy and slip surface of the Cho Yiu landslide

3.1.2 Local Geology

The geology of the area is granite weathered to different degrees (HDG to CDG) overlying fresh granite bedrock as shown in Figure 11–6. The bedrock surface has a U-shaped valley with much deeper elevations at the central part of the slope compared to the northern and southern sections. Two main sets of discontinuities were observed in the bedrock. The first set strikes parallel to the slope with dip angles ranging between 20–50 degrees and daylights in the rock portion of the slope face. The other set also strikes parallel to the slope face with near vertical dip angle. It is likely that the pattern of joints in the bedrock is also present in the overlying granitic soil. The granite in the area is mainly coarse grained with irregular intrusions of fine grained granite in the upper parts of the slope. Varying weathering degrees and abundant clay infilled joints were noted on the upper failure scar at the contacts between the coarse and fine granites.

3.1.3 Rainfall and Groundwater

Failure occurred during an intense rainstorm when 42mm, 210mm and 557mm of rain were recorded during periods of one hour, 11 hours and 9 days before failure, respectively. Field inspection immediately after failure did not indicate any seepage from the exposed surfaces, however large quantities of water were flowing onto the slope from a broken drainage pipe. No piezometers were available at the time of failure and those installed after failure did not record any groundwater table. During remedial works, seepage from the rock face in the lower part of the slope was noticed.

GEO (Siu and Premchitt, 1988) concluded that the permanent groundwater is at great depth below bedrock surface and reported that seepage is due to surface water flowing through joints and preferential flow paths within the soil mass. The seeping water may have come from infiltration of rain water, overflow from blocked slope drainage channels, leakage from the broken drainage pipe of the residential block at the top of the slope or a combination of all these. The clay infills reported in the joints in the upper part of the slope may have blocked water flow in some locations leading to high water pressures. For stability analysis purposes, the GEO postulated a linear piezometric surface with atmospheric pressure at the toe (where some seepage was observed) and the water table at ground surface at the top of the slope as shown in Figure 11–6. No field data of the water pressure at failure were available to verify this hypothetical surface.

3.1.4 Rupture Surface

The rupture surface was apparently planar with a dip angle to the horizontal of 30 - 40 degrees in the middle and lower parts, increasing to 50 - 60 degrees in the upper part. At the crest, the scarp was nearly vertical. In most parts, the rupture surface was located just above and parallel to the bedrock surface. Clay infilled relict joints were noticed in the upper parts of the rupture surface while a joint plane (no reports of clay infill) dipping at an angle of 40 – 50 degrees was reported to correspond with the middle and lower parts. Siu and Premchitt (1988) suggested that failure was largely along pre-existing discontinuities within the soil mass. Figure 11–6 shows the inferred geometry of the slip surface. Notice that failure exposed part of the foundations of the residential building located at the slope crest (Block 4, Figure 11–6).

3.1.5 Shear Strength

The investigation into the cause of the failure included 4 consolidated undrained triaxial tests and 1 consolidated drained test performed on specimens prepared from undisturbed block samples. The results of these tests are included in the database used in strength assessment in Section 2.2.2. Figure 11–7 shows the p′-q plot of the consolidated undrained (single stage) and consolidated drained triaxial tests. The samples were described as containing extremely narrow to tight, closely-spaced microfractures. One specimen, however, contained a clay infilled joint. When tested in a multi-stage consolidated undrained test, the specimen yielded a lower strength as shown in Figure 11–7.

In their assessment of the strength, Siu and Premchitt (1988) divided the data into two categories (in addition to the specimen with clay infilled joint); samples failing by bulging and samples failing along rupture planes and joints. Each material has different shear strength parameters as shown in Figure 11–7. Because of the relict joints observed in the field, Siu and Premchitt (1988) rejected the upper failure envelope (samples failing by bulging). They considered the envelope corresponding to specimens failing on rupture planes to be an adequate representation of the shear strength along the slip surface (except for the upper portion). The strength parameters defining that envelope are very close to the mean values of the regional distributions (C′= 5.6 kPa, ϕ′= 37.8 deg.). For the upper part of the slip surface, where abundant clay infilled joints were observed, they adopted the lower envelope with C′= 0 kPa and ϕ′=31.5 degrees.

The probabilistic analyses in the following section are based on the regional probability distributions of strength parameters (Figure 11–2, Figure 11–4). Referring to the field observation by Siu and Premchitt, the application of these distributions were limited to the middle and lower parts of the slip surface. Along the upper portion, where abundant clay infilled joints were noted, the strength parameters proposed by the GEO (C'= 0 kPa and ϕ'=31.5 deg.) are used. These values were estimated based on the results of one triaxial test and one large drained shear box test only. Figure 11–6 shows the zones (proposed by GEO) over which the two strength categories are applied.

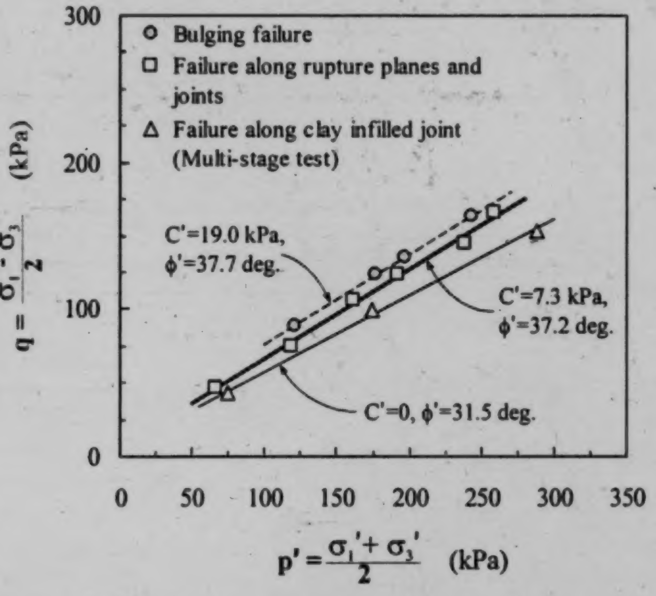

Figure 11–7 p'-q plot of the consolidated undrained (single stage) and consolidated drained triaxial tests, Cho Yiu slide

3.1.6 Deterministic Stability Analyses

The stability of the slope before failure is evaluated deterministically using Slope/W software and the Spencer method of slices. The slip surface and the phreatic surface postulated by GEO, Figure 11–6, are adopted in the analysis. Using the regional strength parameters (C'=5.6, ϕ'= 37.8 deg.) for the middle and lower parts of the slip surface and the joint parameters (C'=0, ϕ'= 31.5 deg.) for the upper portion, the factor of safety is estimated to be 0.75. Using GEO estimates (C'=7.3 kPa, ϕ'= 37.2 deg.), the factor of safety is calculated to be 0.78. To achieve a factor of safety of one, either the in-situ shear strength is higher than the values used in the analysis or the pore water pressure is lower or a combination of both. Since there were no observations at all to support the postulated phreatic surface, it is seems more likely that the pore water pressure is overestimated. A back analysis using the regional parameters indicated that the pore pressure ratio at failure is about 0.25.

Using the back calculated pore pressure, the slope is re-designed to what would be an acceptable geometry according to current slope design practice. Because of the existing residential complex at slope crest and the highway at the foot of the slope (Figure 11–6), a design factor of safety of 1.5 is targeted. This is a relatively conservative value with respect to the normal practice in Hong Kong. However, it is judged that the consequences of failure are substantial and warrant a more cautious design. The modified design has a slope angle of about 30 degrees (1.78h:1v) compared to 40 degrees for the failed configuration. The probability of unsatisfactory performance of the revised design is estimated in Section 3.1.9.

3.1.7 Quantifying Pore Pressure Uncertainty

The probability distribution of the pore pressure ratio at failure is estimated using a probabilistic back analysis. A spreadsheet model mimicking the slope geometry before failure, the soil stratigraphy and the slip surface is prepared. The factor of safety is taken as a deterministic input value of one and the pore pressure ratio is modeled as the output. The Spencer method of slices is used in the model. The effective shear strength parameters of the decomposed granite at the middle and lower parts of the slip surface (Figure 11–6) are regarded as random input variables. The regional probability distributions (Figure 11–2 and Figure 11–4) are adopted in the model. The shear strength along the upper portion of the slip surface is modeled deterministically using the parameters recommended by the GEO (Section 3.1.5). The point CDFs of the shear strength parameters are used directly in the analysis, without variance reduction, to obtain the point CDF of the pore pressure ratio.

Using a seed value of 31069 and 10,000 iterations, the mean pore pressure ratio is estimated to be 0.25 with a standard deviation of 0.11 (i.e., a coefficient of variation of 0.44) indicating substantial uncertainty. The pore pressure ratio ranges between a minimum of –0.12 (i.e., suction) and a maximum of 0.67. Figure 11–8 shows the histogram and the probability distribution of the pore pressure ratio. In slope design, it is a common practice to ignore suction. A threshold of zero pore pressure ratio is added to the spreadsheet and used in all subsequent simulations. Based on the results of 25 simulations, an average probability distribution of the pore pressure ratio at failure is estimated, as shown in Figure 11–9.

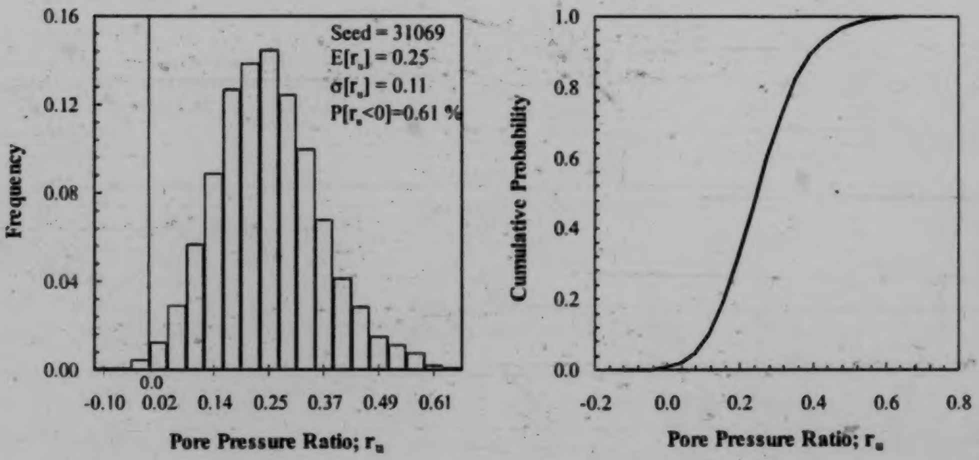

Figure 11–8 Histogram and CDF of the pore pressure ratio at failure – Cho Yiu landslide

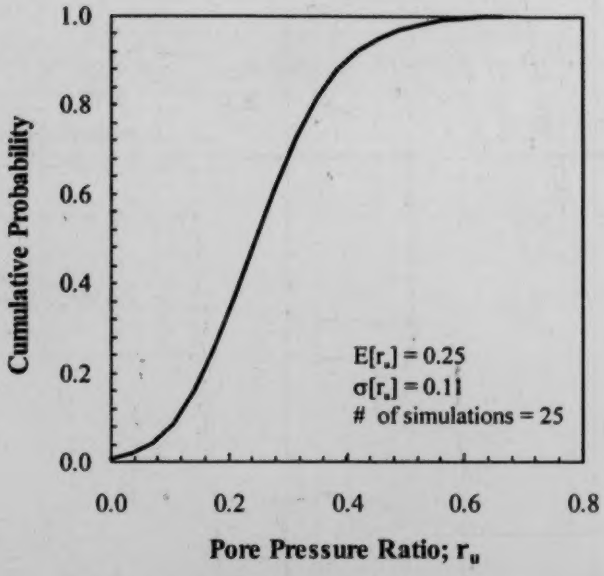

Figure 11–9 Probability distribution of pore pressure ratio at failure – Cho Yiu landslide

3.1.8 Spatial Variability of Residual Soil Properties

The spatial variability of residual soils differs from normal soils in a number of ways. The variability of residual soils is not attributed to their depositional environment, but rather to the weathering processes which are random, highly variable and independent of orientation. So, the properties of residual soils and their pattern of variability are likely to be random and independent of direction; that is soil variability is isotropic although erratic. Quantifying the spatial structure of such material is a difficult task requiring significant amounts of data. The author is aware of no studies addressing the pattern of spatial variability of residual soils.

Some assumptions have to be made to account for the spatial variability of Hong Kong granitic soils in the probabilistic stability analyses. First, the spatial structure is assumed isotropic (i.e., isotropic autocorrelation distance). Second, a small value of the autocorrelation distance is selected to reflect the erratic nature of this material. A value in the order of the vertical autocorrelation distances reported in the literature (Chapter 5), r_o = 5m, is assumed. While there is no hard data to backup these assumptions, they are (to the author's judgement) deemed reasonable. Lumb (1983) suggested (no data were available) that the horizontal and vertical scales of fluctuation, $\delta \approx 2r_o$, are on the same order and "perhaps" in the range of 1-5m.

3.1.9 Probabilistic Stability Analyses

The stability of the modified slope geometry (slope angle ≈ 30 degrees) is assessed probabilistically using the methodology proposed in Chapter 5. Based on the discussions in the previous sections, three input parameters are treated as variables; the friction angle and cohesion of the decomposed granite at the middle and lower parts of the slip surface and the pore pressure ratio. Figure 11–5 shows no correlation between the effective cohesion and the friction angle; thus they are modeled as independent variables. The observed failure mode of the failed geometry is judged to also govern the modified design. A planar slip surface comprising 3 planes coinciding with the those observed in the field is postulated as the potential failure mode.

The spatial variability of the strength parameters and pore pressure ratio are accounted for as outlined in Chapter 5. The slip surface is divided into segments of length equal to δ=10m and a residual portion. The uncertainty of the average parameters over the length of each segments is represented by the point probability distributions (Figure 11–2, Figure 11–4 and Figure 11–8). The correlation coefficients between these local averages are estimated using Equation 5-5 and taken into account in Monte Carlo simulation. The strength parameters and pore pressure ratio are modeled separately as the former are applied along the middle and lower portions of the slip surface while the latter is acting along the entire length of the slip surface. In total, the variability of the three parameters are represented by 9 variables, some of them are correlated.

The optimum number of iterations is estimated to be 25,000. Using a seed number of 31069, the mean factor of safety is calculated to be 1.54 with a standard deviation of

0.26. The probability of unsatisfactory performance is estimated to be 1.15%. Figure 11–10 shows the histogram and CDF of the factor of safety. A sensitivity analysis is also performed to assess the relative contributions of the input variables to the uncertainty in the factor of safety. Figure 11–11 shows Spearman rank correlation coefficients for all input variables. The uncertainty of the pore pressure ratio has the largest impact on the reliability of the slope performance. The uncertainties in cohesion and friction angle contribute almost equally to the overall uncertainty of the factor of safety.

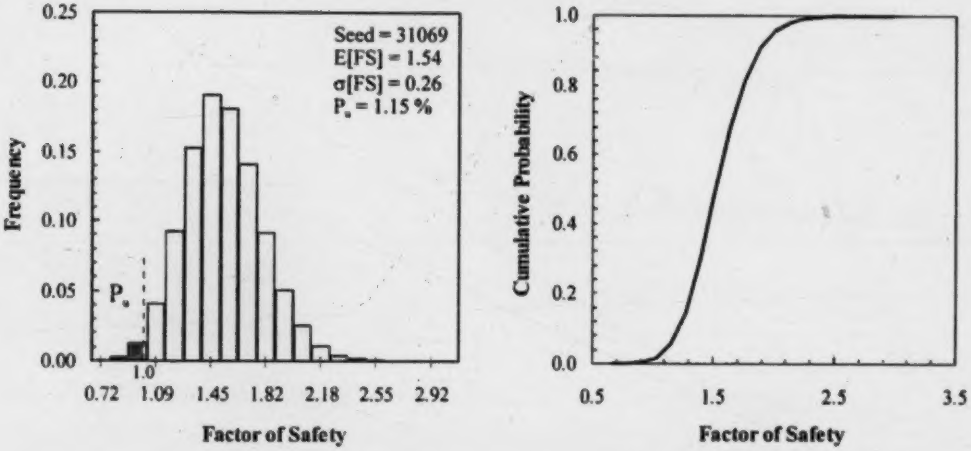

Figure 11–10 Histogram and CDF of the factor of safety, Cho Yiu slope (acceptable design) – Proposed Methodology

The analyses described in the above sections are based on an autocorrelation distance of 5m. The sensitivity of the estimated probability of unsatisfactory performance to variations in the autocorrelation distance is investigated by repeating the simulation using different r_o values, while maintaining the same seed value and number of iterations. Figure 11–12 shows the variation of the probability of unsatisfactory performance with the autocorrelation distance. Similar to the Congress Street Cut (Chapter 10), the probability of unsatisfactory performance is relatively sensitive to the assumption of the autocorrelation distance. The computed probabilities varied between 0.19% and 4.95% as the autocorrelation distance increased from 3m to 10m.

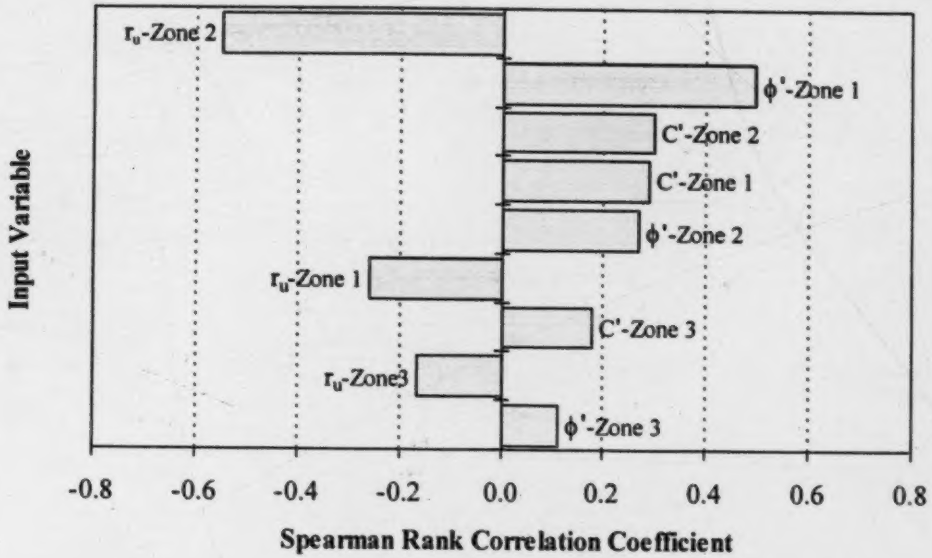

Figure 11–11 Sensitivity analysis results, Cho Yiu slope (acceptable design)

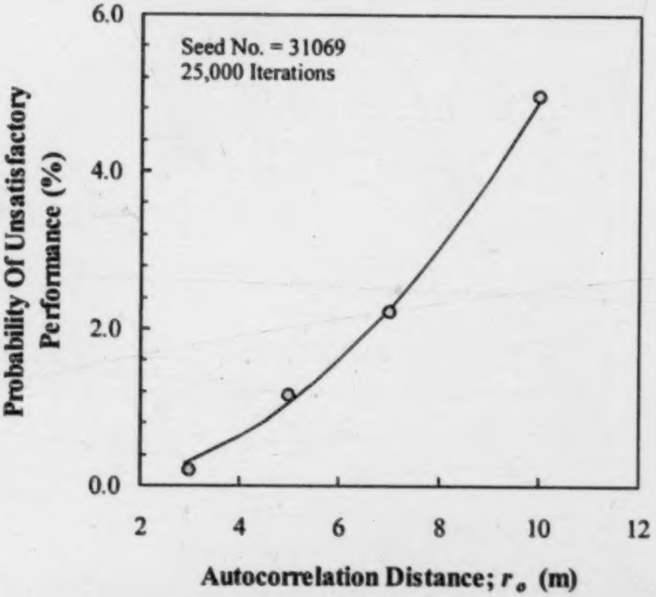

Figure 11–12 Variation of the probability of unsatisfactory performance with the autocorrelation distance, Cho Yiu slope (acceptable design)

Using an autocorrelation distance of 5m, 25 simulations (25,000 iterations each) are performed using different seed numbers. The mean probability of unsatisfactory performance is estimated to be 1.10% with the 95% confidence interval ranging between 1.07-1.13%. Figure 11–13 shows the histogram of the probability of unsatisfactory performance.

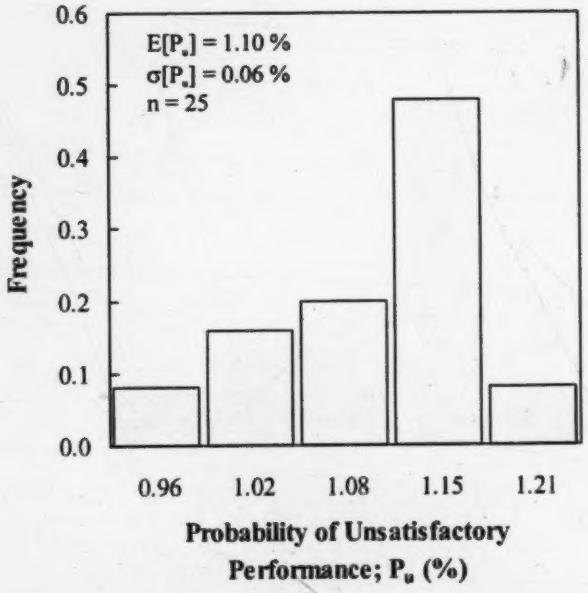

Figure 11–13 Histogram of the probability of unsatisfactory performance, Cho Yiu slope (acceptable design) – Proposed Methodology

The re-designed (i.e., acceptable) slope is also analyzed using the naïve approach. The spreadsheet model included three input variables; the friction angle and cohesion along the middle and lower sections of the slip surface and the pore pressure ratio. The probability distributions obtained in Sections 2.2.2 and 3.1.7 are used to model the three variables. Based on 25 simulations, using 25,000 iterations, the mean probability of unsatisfactory performance is estimated to be 6.54% with the 95% confidence interval ranging between 6.49-6.58%. Figure 11–14 shows the histogram of the probability of unsatisfactory performance.

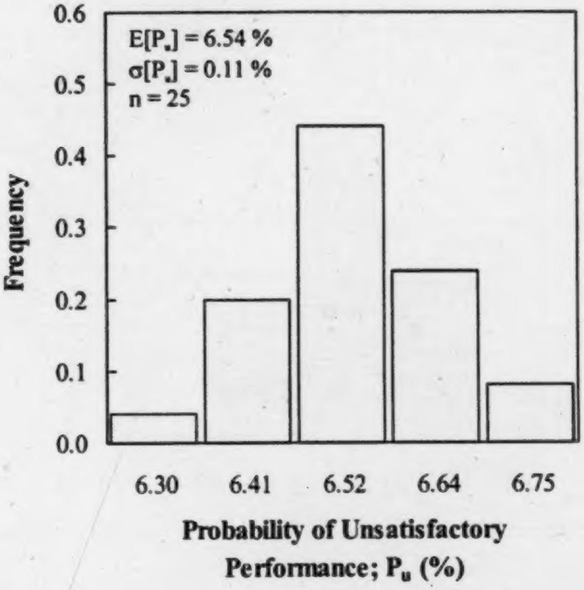

Figure 11–14 Histogram of the probability of unsatisfactory performance, Cho Yiu slope (acceptable design) – Naïve Analysis

3.2 Tsing Yi (1) Landslide

3.2.1 Background

On June 30 1982, a major cut slope above Tsing Yi: 1 trunk road at the south west corner of Tsing Yi island was reported to show signs of incipient failure. A downward movement of nearly 1m was observed. The displaced material was about 70m wide with an estimated mass of 20,000 tonnes. As a result of the movement, surface drainage channels were distorted and tension cracks were formed behind the scarp of the slide. Further movements were observed in response to heavy rainfall during the month of August and a minor slide occurred at the southern end of the failure on August 16. Prior to failure, the height of the slope was about 45m with an overall slope angle of 35 degrees (1.4h:1v). Figure 11–15 shows a cross-section of the slope before failure. The failure of such a gentle slope and the slow rate of movement are uncommon features to slope failures in Hong Kong.

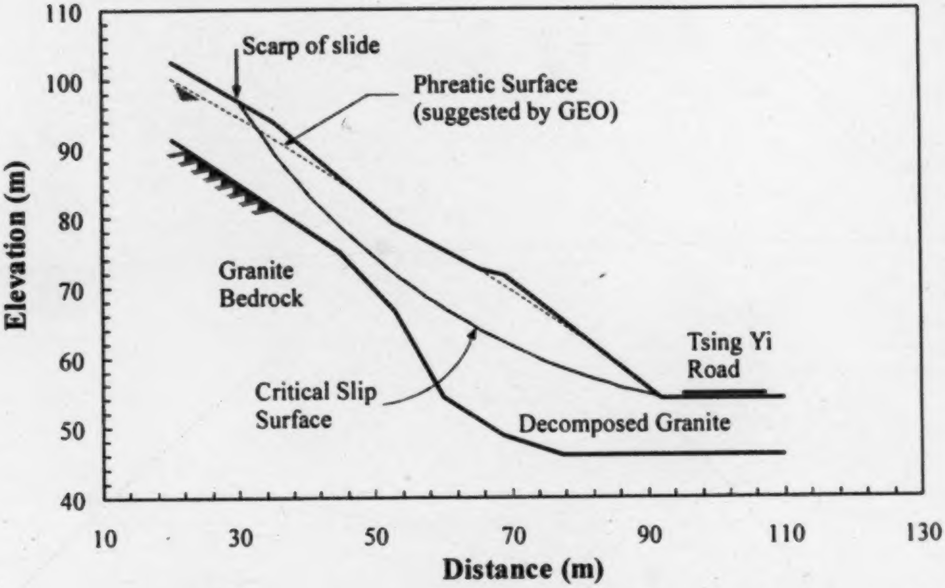

Figure 11–15 Cross-section and stratigraphy of Tsing Yi: 1 slide

The slope was cut to its final geometry in 1979. The original design was based on a comprehensive site investigation program and was thought, at the time, to be conservative. The investigation indicated very high pore pressures within the slope. As a result, two rows of horizontal drains were installed to control the water table. Following the failure, the GCO launched a detailed investigation to identify the cause of the failure and to assess the appropriate remedy measures. The program included field inspection, aerial photo analysis, soil investigation and pore water pressure and slope movement monitoring. Hencher (1983a) provided a detailed description of the slide and the investigation into its cause.

3.2.2 Local Geology

Based on the limited geological information available, the slope profile comprises a coarse grained granite intruded by dykes of feldspar porphyry and fine grained granite. The granite is decomposed to various degrees throughout the slope with large boulders (up to 10m in size) occurring at the cut face in some locations. The site investigation at the design stage indicated that the fresh bedrock was located at a shallow depth. The investigation after failure indicated that the depth of the bedrock is highly variable across the site. It is shallow only at the top of the slope and increases to nearly 20m at the toe. Figure 11–15 shows the inferred stratigraphy at the site of the slope. Hencher (1983a) pointed that the erroneous interpretation of the bedrock elevation in the initial investigation eliminated the possibility of a deep-seated failure leading to the overestimation of the stability of the slope.

3.2.3 Rainfall and Groundwater

The daily rainfall records in the area over the period from May to August indicated 2 major rainstorms (end of May and mid August) with peak rainfall of about 300mm in either case. Because of the remote location of the slope, the exact time and date of the failure are not known. Hencher (1983a), however, suspected that failure was triggered by the heavy rainfall at the end of May.

During the mid August storm, a piezometer installed close to the crest of the slope indicated a 1.5-2.0 m rise in groundwater table above its stable elevation. Seepage near the toe of the slope was also reported. No flow from the drainage pipes was observed even during heavy rainstorms implying that they were not effective. Based on these observations, Hencher (1983a) suggested that the slope was largely saturated due to a temporary rise in the perched groundwater table. He then postulated that the groundwater table at the time of failure was almost at ground surface as shown in Figure 11–15. The post-failure investigation also indicated the presence of lower permanent groundwater table within the bedrock.

3.2.4 Rupture Surface

The surface features at the site revealed little about the depth and geometry of the rupture surface. It is known, however, that the slip surface goes through the backscarp of the slide and daylights at the toe of the slope. Hencher (1983a) suggested that failure was rotational through the soil matrix of the slope. He based his conclusion on the observed vertical bulging at the toe and the lack of any damage to the road at the foot of the slope. Examination of the samples retrieved during the post-failure investigation did not provide any indication of the depth of failure.

3.2.5 Shear Strength

The site investigation prior to the construction of the slope included 28 saturated triaxial compression tests. Unfortunately, the testing results were not available to the author. Hencher (1983a), however, reported that the measured shear strength parameters varied considerably. The initial design was based on an effective cohesion of 10 kPa and an effective friction angle of 35 degrees. These parameters are close to the regional values (C'=5.6 kPa, ϕ'=37.8 deg.). The post failure investigation included triaxial and direct shear box tests. The results were consistent with those of the initial investigation.

3.2.6 Deterministic Stability Analyses

The stability of the slope before failure (Figure 11–15) is analyzed deterministically using Slope/W software and the Spencer method of slices. The phreatic surface proposed by the Hencher (1983a) is adopted in the analysis. The slip surface is assumed circular through the observed scarp at the top of the slope. The stability of the slope is analyzed using the regional strength parameters, then using the initial design parameters reported by Hencher (Section 3.2.5). The calculated factors of safety are 0.58 and 0.62, respectively. Such low factors of safety imply that either the shear strength is underestimated or the assumed phreatic surface largely overestimates the pore pressure conditions. Assuming the phreatic surface is true, a factor of safety of unity could be achieved using various combinations of strength parameters. One such combinations is C'=20 kPa and ϕ'=46 degrees. That strength range is high for Hong Kong granitic soils. It, thus, more likely that the assumption of full saturation of the slope is a conservative one. Using a factor of safety of unity and the regional shear strength parameters, the pore pressure ratio at failure is estimated to be 0.21.

Using the back-calculated pore pressure ratio, the slope is re-designed to an acceptable geometry. The relatively remote location of the slope and the slow movement rate of the slide mass may warrant a less conservative design. Targeting a factor of safety of 1.3, the modified design has a slope angle of 27 degrees (2h:1v), compared to 35 degrees for the failed geometry. The stability of the revised design is assessed probabilistically in Sections 3.2.8.

3.2.7 Quantifying Pore Pressure Uncertainty

A probabilistic back analysis is performed to estimate the probability distribution of the pore pressure ratio at failure. A spreadsheet model mimicking the slope geometry before failure, the soil stratigraphy and the critical slip surface is prepared. The factor of safety is considered a deterministic input equal to one and the Spencer method of slices is used in the model. The shear strength parameters of the decomposed granite are modeled as input variables having the regional probability distributions (Figure 11–2 and Figure 11–4). Using a seed value of 31069 and 10,000 iterations, the histogram and probability distribution of the pore pressure ratio are estimated as shown in Figure 11–16. The distribution has a mean value of 0.21 with a standard deviation of 0.11; a coefficient of variation of 0.52. Similar to the Cho Yiu case, the pore pressure ratio is highly uncertain. It ranges between -0.23 (i.e., suction) and 0.59. In subsequent simulations, a zero threshold is added to the spreadsheet model to eliminate the negative pore pressure ratio for slope design purposes. Based on the results of 25 simulations, an average probability distribution of the pore pressure ratio is estimated and shown in Figure 11–17.

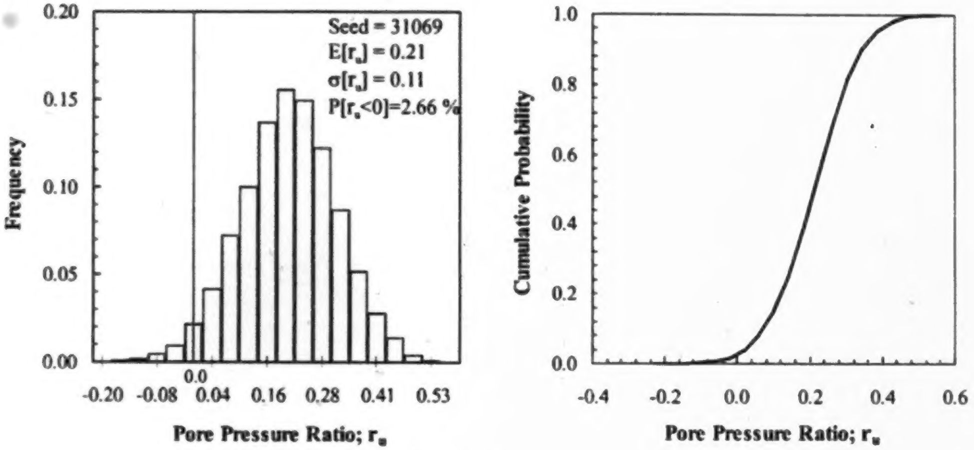

Figure 11–16 Histogram and CDF of the pore pressure ratio at failure – Tsing Yi: 1 landslide

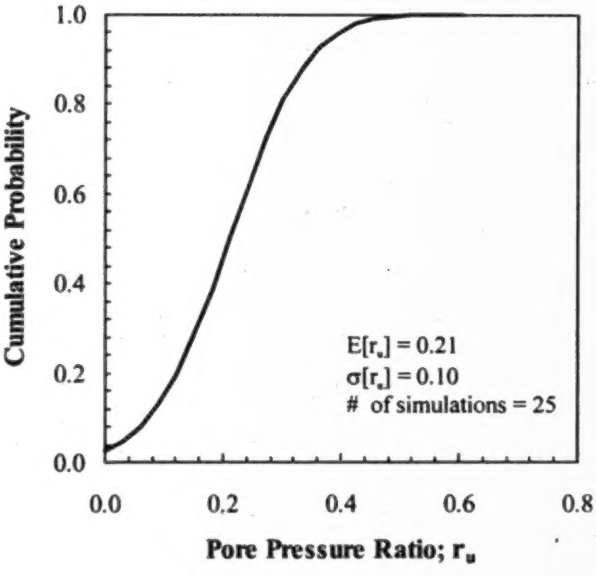

Figure 11–17 Probability distribution of pore pressure ratio at failure – Tsing Yi: 1 landslide

3.2.8 Probabilistic Stability Analyses

The stability of the modified design, 27 degrees slope, is analyzed probabilistically using the proposed methodology (Chapter 5). The effective strength parameters and the pore pressure ratio are considered input variables with the probability distributions shown in Figure 11–2, Figure 11–4 and Figure 11–17. The cohesion and friction angle are considered independent. The critical slip surface is assumed circular. The probabilistic critical slip surface is obtained through a set of deterministic analyses that examined the deterministic critical surface as well as the surfaces based on the Hassan and Wolff (1999) algorithm.

A spreadsheet model mimicking the geometry, stratigraphy and the probabilistic critical slip surface is prepared. The spatial variability of the strength parameters and the pore pressure ratio is accounted for by dividing the slip surface into segments of length δ=10m as outlined in Chapter 5. In total, 36 input variables, some of which are correlated, are defined to account for the variability of strength and pore pressure along the slip surface. Using a seed number of 31069 and 30,000 iterations, the mean factor of safety is estimated to be 1.34 with a standard deviation of 0.10. Figure 11–18 shows the histogram and the CDF of the factor of safety. The probability of unsatisfactory performance is estimated to be 0.02%. A sensitivity analysis is also performed and Figure 11–19 shows Spearman rank correlation coefficients for all input variables. The plot indicates that the uncertainties of the pore pressure ratio and friction angle have comparable contributions to the uncertainty of the factor of safety. The uncertainty of the cohesion has the least impact on the design. The simulation is repeated using different values of the autocorrelation distance to assess its impact on the estimated probability of unsatisfactory performance. The results are summarized in Figure 11–20. The probability of unsatisfactory performance increased from a near zero value for an autocorrelation distance of 4m to 0.39% for a distance of 10m.

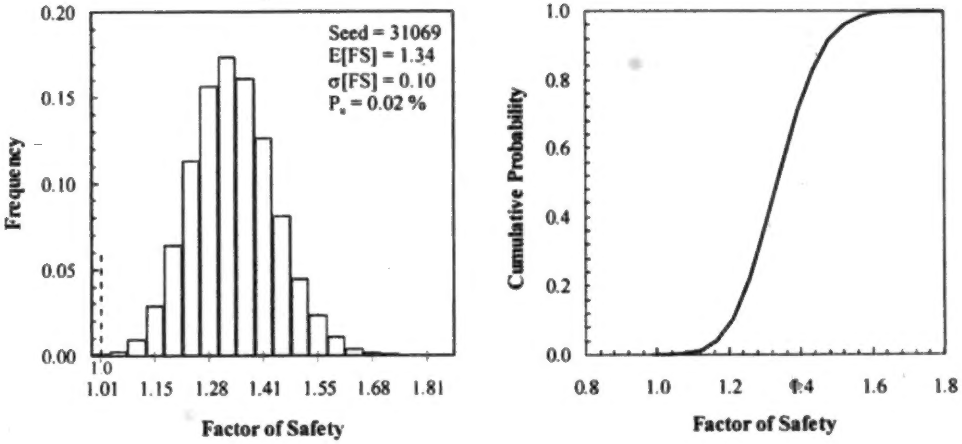

Figure 11–18 Histogram and CDF of the factor of safety, Tsing Yi: 1 slope (acceptable design) – Proposed Methodology

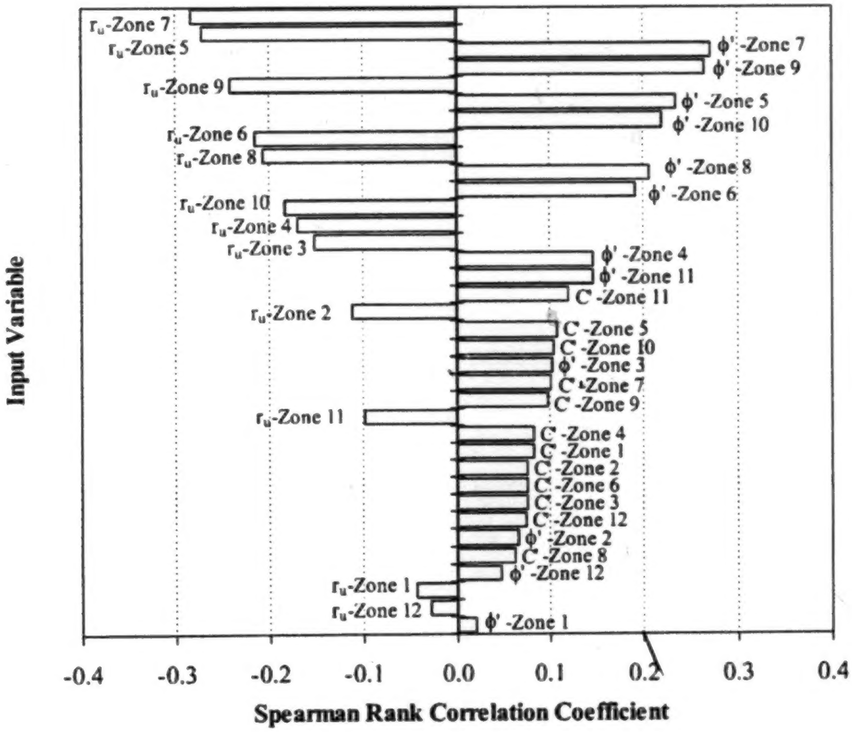

Figure 11–19 Sensitivity analysis results, Tsing Yi: 1 slope (acceptable design) – Proposed Methodology

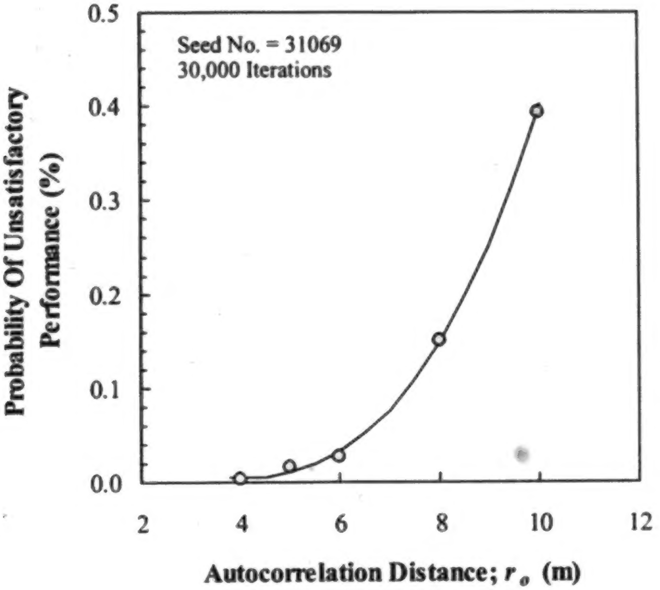

Figure 11–20 Variation of the probability of unsatisfactory performance with the autocorrelation distance, Tsing Yi: 1 slope (acceptable design)

Twenty five simulations are performed using different seed numbers and an autocorrelation distance of 5m. The computed probabilities of unsatisfactory performance are summarized in histogram form in Figure 11–21. The mean probability of unsatisfactory performance is estimated to be 0.01%. This very low value is attributed to the large size of the slip surface, 116m long, compared to the autocorrelation distance. The variances (or uncertainty) of the *mean* strength and pore pressure ratio along the slip surface are largely reduced by spatial averaging . This, in turn, reduced the variance of the factor of safety leading to the small probability of unsatisfactory performance.

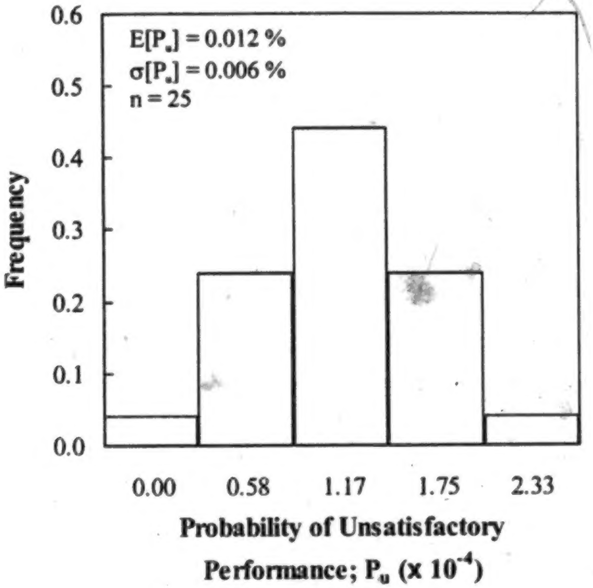

Figure 11–21 Histogram of the probability of unsatisfactory performance, Tsing Yi: 1 slope (acceptable design) – Proposed Methodology

The modified slope geometry is also analyzed using the naïve approach. The spreadsheet model includes 3 input variables representing the shear strength parameters of the decomposed granite and the pore pressure ratio. The regional probability distributions of the cohesion and friction angle (Section 2.2.2) and the back-calculated distribution of pore pressure ratio (Section 3.2.7) are used in the model. Twenty five Monte Carlo simulations were run using different seed numbers and 30,000 iterations for each simulation. The histogram of the computed probabilities of unsatisfactory performance is shown in Figure 11–22. The mean probability of unsatisfactory performance is estimated to be 13.22% with the 95% confidence interval ranging between 13.15-13.30%.

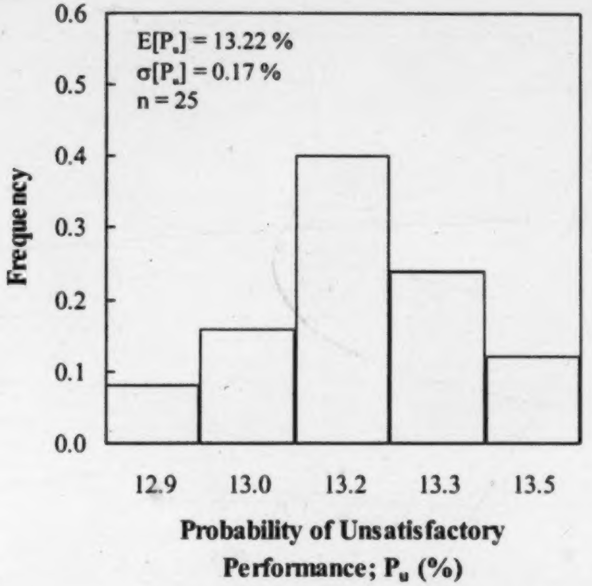

Figure 11–22 Histogram of the probability of unsatisfactory performance, Tsing Yi: 1 slope (acceptable design) – Naïve Analysis

3.3 Ching Cheung Road Landslide

3.3.1 Background

In the early morning of August 24, 1982; a section of the cut slope of Ching Cheung Road, Hong Kong, failed. The road was totally blocked by the failure debris and was closed for traffic for about 2 months. The cut was 30 m high and had an inclination of about 50 degrees (0.84h:1v). Failure occurred on a dry day and the debris moved, apparently, in a dry manner which is unusual to slope failures in Hong Kong. Two previous slides occurred in the same manner at nearby locations on the same road in 1972. Figure 11–23 shows a cross-section of the slope before failure. A study of the causes of the failure was undertaken by the Geotechnical Control Office of Hong Kong (Hencher, 1983b). The main findings of the study are highlighted in the following sections.

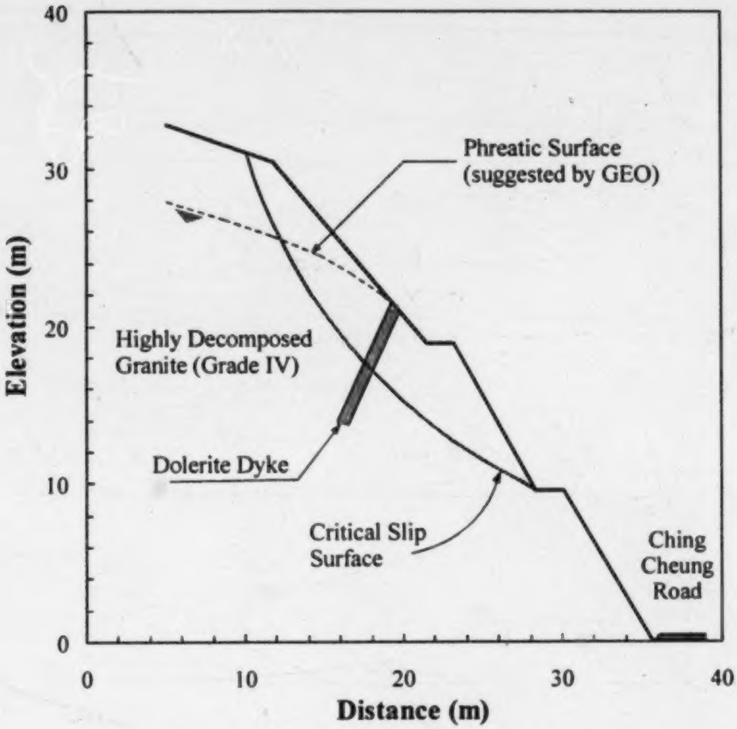
40
30
20
10
0
0
10
20
30
40
Elevation (m)
Distance (m)
Phreatic Surface
(suggested by GEO)
Highly Decomposed
Granite (Grade IV)
Dolerite Dyke
Critical Slip
Surface
Ching
Cheung
Road

Figure 11–23 Cross-section and stratigraphy of Ching Cheung Road landslide

3.3.2 Local Geology

The site geology is mainly coarse grained, highly decomposed granite (Grade IV). Few cobbles and boulders were observed particularly at the lower portion of the failure scar. Schmidt hammer measurements implied increasing strength and density with depth. Extensive random microfractures and joints caused the granite to be very friable. A number of decomposed dolerite dykes cut through the granite at various locations. Some of these dykes were continuous for distances of several metres.

3.3.3 Rainfall and Groundwater

As mentioned above, failure occurred on a dry day. Rainfall records, however, showed that the month of August of 1982 was the wettest August ever since the beginning of rainfall records. Two major rainstorms occurred prior to failure. The storm preceding failure, August 15-19, involved an intense rainfall amounting to 522.8mm. No seepage was reported immediately after failure, however one day latter water ponds were observed at slope toe. Seepage from a point high up within the failure scar above a thick dolerite dyke was also noted few days latter. For stability analyses, Hencher (1983b) postulated a high phreatic surface that intersects with slope face at the observed seepage point, Figure 11–23. He assumed that the portion of the slope below the dolerite dyke was dry due to the impedance of water flow by the relatively impermeable dykes. There was no field evidence to support that hypothesis.

3.3.4 Shear Strength

The shear strength of the subsurface material was assessed based on the results of a few direct shear tests and consolidated undrained triaxial tests with pore pressure measurements. The tests were conducted on specimens prepared from block samples obtained at 2 different locations in the failure scar. Three multistage triaxial tests were conducted on decomposed granite specimens and another 3 tests on dolerite specimens. Based on the results of the first stages of these tests, the strength parameters are estimated as follows;

	γ_d (kN/m^3)	C' (kPa)	ϕ' (deg.)
Decomposed granite	14.5	12	37.5
Decomposed dolerite	--	26	24.0

The measured friction angle of the decomposed granite is very similar to the mean value of the regional distribution whereas the measured cohesion is higher than the regional value. The shear strength of the dolerite is lower than the granite strength. Apparently, the extent of these dykes was limited such that GCO (Hencher, 1983b) described its contribution to the overall strength as "not important". They indicated, however, that the measured permeability of the dolerite (1.7x10^{-7} m/s) is one order of magnitude less than that of the granite, which may affect groundwater flow.

3.3.5 Failure Mechanism

Hencher (1983b) postulated that failure occurred because of the damming effect of the dolerite dykes, owing to their lower permeability. Water accumulated behind the dykes during heavy rain. Because of delayed water migration, water levels continued to rise behind the dykes even after the rain stopped. High water pressure built up along the rupture surface till the factor of safety was reduced to unity and the slope failed. Hencher, however, pointed that it is highly coincidental that 3 slides (1972 and 1982) within the same slope occur in the same manner. He provided no details about the geometry of the rupture surface, but he did not indicate that failure was joint controlled. In the subsequent stability analyses, a circular slip surface is assumed.

3.3.6 Deterministic Stability Analyses

The stability of the cut before failure is analyzed deterministically using Slope/W software and the Spencer method of slices assuming a circular slip surface. The pore water pressure conditions postulated by Hencher (1983b) is adopted. Using the measured strength parameters ($C'= 12$ kPa, $\phi'= 37.5$ deg.), the factor of safety is calculated to be 0.90. Using the mean values of the regional distributions ($C'= 5.6$ kPa, $\phi'= 37.8$ deg.), a factor of safety of 0.75 is obtained. In either case, the pore pressure hypothesis of Hencher clearly overestimates the true conditions. A back-analysis is performed using the regional strength parameters and a factor of safety of unity. The pore pressure ratio at failure is estimated to be –0.04. Figure 11–23 shows the critical slip surface. The small negative value of the pore pressure ratio implies that suction was existent within the slope and that failure occurred when it was almost eliminated by the infiltration of rainwater.

The slope is re-designed to an acceptable geometry based on the conventional slope design practice. The negative pore pressure is discarded in the design and the slope is assumed dry (i.e., $r_u=0$). Targeting a design factor of safety of 1.3, the modified geometry has an overall inclination of about 35 degrees (1.4h:1v), compared to 50 degrees (0.85h:1v) for the original geometry. The reliability of the modified geometry is assessed probabilistically in Section 3.3.8.

3.3.7 Quantifying Pore Pressure Uncertainty

The geometry of the slope before failure is back-analyzed probabilistically to quantify the uncertainty associated with the pore pressure ratio. A spreadsheet model mimicking the slope geometry, stratigraphy and critical slip surface is prepared. The factor of safety is modeled as a deterministic input equal to one and the regional probability distributions of strength parameters are used to represent the strength of the decomposed granite. Using a seed value of 31069 and 12,000 iterations, the mean pore pressure ratio at failure is estimated to be –0.05 with a standard deviation of 0.12 and a minimum-maximum range of -0.53 to 0.38. These figures reflect a substantial uncertainty in the pore pressure conditions. Figure 11–24 shows the histogram and the CDF of the pore pressure ratio at failure. The probability of having a negative pore pressure at failure is high, almost 66%, suggesting that suction had an important role in maintaining the stability of the cut in the past. As mentioned earlier, slope design practice do not rely on suction to provide stability. In order to estimate the probability distribution of the pore pressure for re-designing the cut, a zero threshold is imposed on the pore pressure ratio. The simulation is repeated 25 times and the results are averaged to obtain a representative probability distribution of the pore pressure ratio at failure, Figure 11–25. The distribution has a near zero mean, $E[r_u]=0.03$, and a standard deviation of 0.06. The minimum-maximum range of the distribution is 0.0 - 0.38.

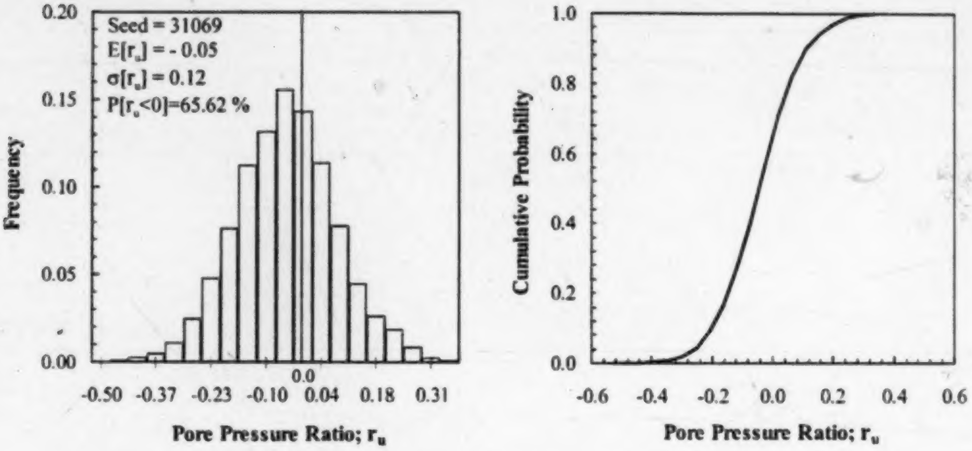

Figure 11–24 Histogram and CDF of pore pressure ratio at failure – Ching Cheung Road landslide

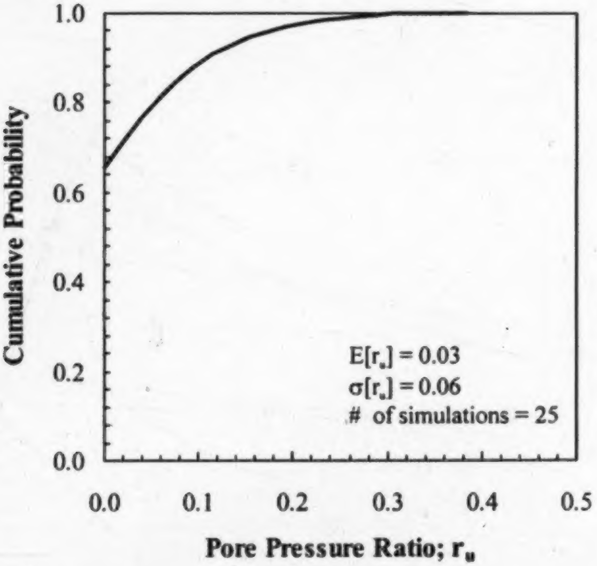

Figure 11–25 Probability distribution of pore pressure ratio at failure – Ching Cheung Road landslide

3.3.8 Probabilistic Stability Analyses

The stability of the modified (i.e., acceptable) slope geometry, 35 degrees slope, is analyzed probabilistically using the proposed methodology. A spreadsheet model mimicking the slope geometry and stratigraphy is prepared. The regional probability distributions of strength parameters, Figure 11–2 and Figure 11–4, and the back-calculated distribution of the pore pressure ratio, Figure 11–25, are used in the model. The deterministic critical slip surface is found more critical, in terms of the probability of unsatisfactory performance, than the Hassan and Wolff surface and is adopted in the spreadsheet. To account for the spatial variability of the input parameters, the slip surface is divided into segments, as outlined in Chapter 5, based on an autocorrelation distance of 5m. The local averages of strength parameters and pore pressure ratio over the length of each segment are considered random variables having the point CDFs. In total, 18 variables are defined to model the spatial variability of the strength and the pore pressure. The correlation coefficients between these variables are estimated using Equation 5-5.

The optimum number of iterations is estimated to be 32,000. Using a seed number of 31069, the mean factor of safety is computed to be 1.31 with a standard deviation of 0.12. The probability of unsatisfactory performance is 0.13%. Figure 11–26 shows the histogram and the CDF of the factor of safety. A sensitivity analysis is performed and Spearman rank correlation coefficients for all input variables are shown in Figure 11–27. The uncertainty of the friction angle has the largest impact on the analysis followed by that of the cohesion. The uncertainty of the pore pressure ratio has the smallest impact on the reliability of the design. This is attributed mainly to the zero truncation limit imposed on the probability distribution of the back-calculated pore pressure ratio to discard suction at the design stage. As a result, the variance of the pore pressure ratio and consequently its impact on the uncertainty of the factor of safety is largely reduced.

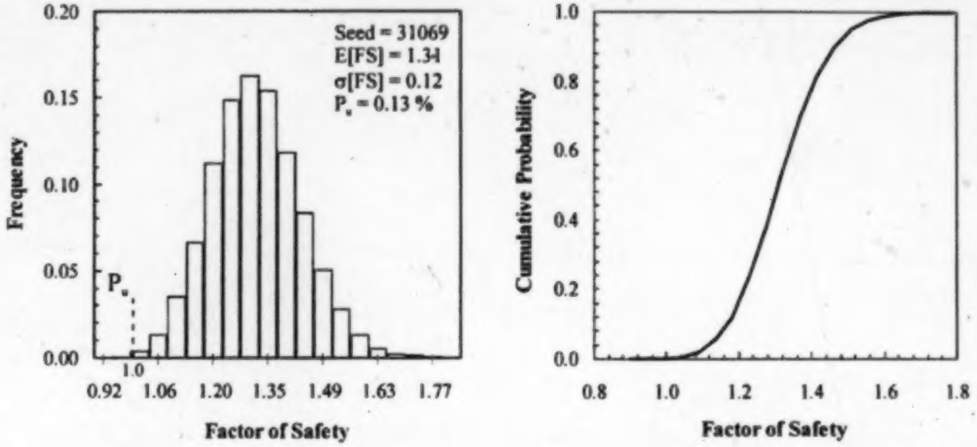

Figure 11–26 Histogram and CDF of the factor of safety, Ching Cheung Road (acceptable slope) – Proposed Methodology

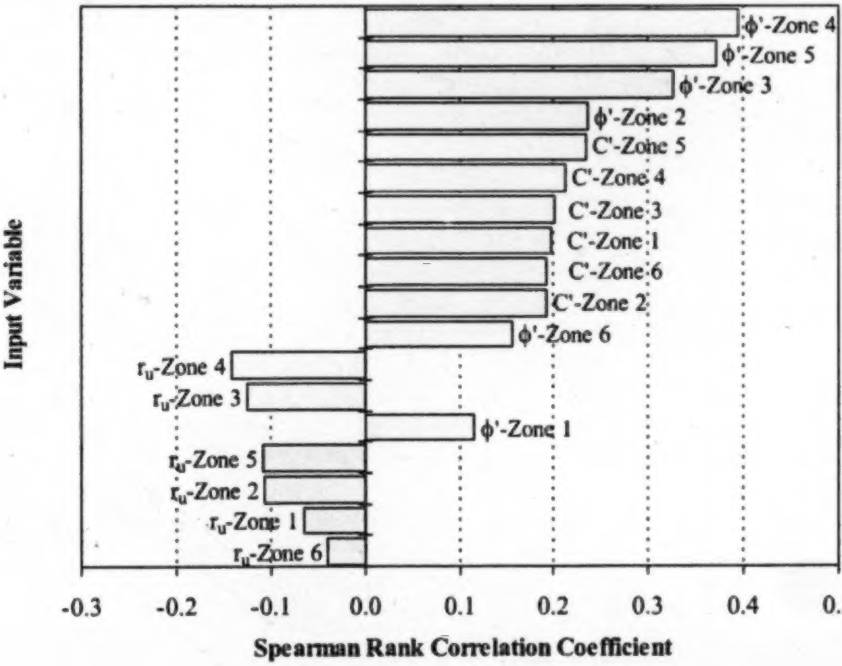

Figure 11–27 Sensitivity analysis results, Ching Cheung Road (acceptable slope) – Proposed Methodology

Figure 11–28 shows the results of a parametric study to assess the effect of the autocorrelation distance on the computed probability of unsatisfactory performance. Four simulations are performed using different autocorrelation distances; 3, 5, 7 and 10m. The probability of unsatisfactory performance increased from 0.01% for an autocorrelation distance of 3m to 1.62% for an autocorrelation distance of 10m. The results suggest that the autocorrelation distance could have an important effect on the estimated probabilities of unsatisfactory performance. Adopting an autocorrelation distance of 5m, 25 simulations are performed using different seed numbers. Figure 11–29 shows the histogram of the computed probabilities of unsatisfactory performance. The mean value is estimated to be 0.13% with the 95% confidence interval ranging between 0.13-0.14%.

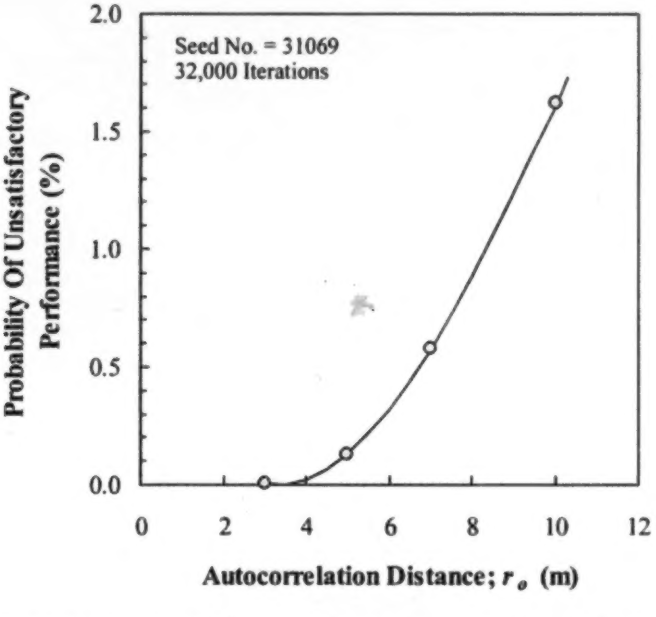

Figure 11–28 Variation of the probability of unsatisfactory performance with the autocorrelation distance, Ching Cheung Road (acceptable design)

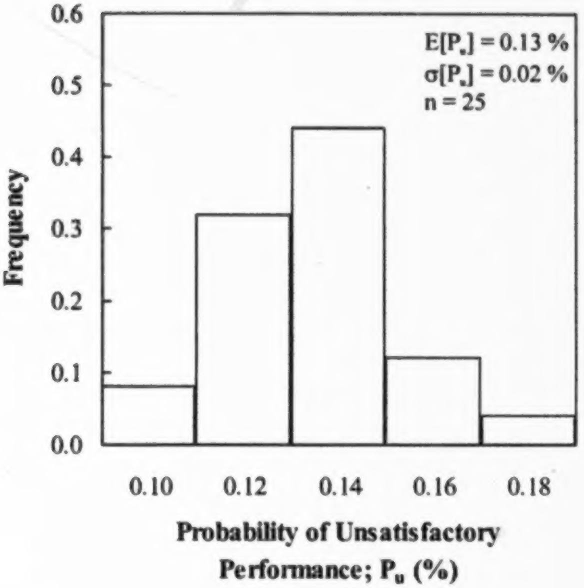

Figure 11–29 Histogram of the probability of unsatisfactory performance, Ching Cheung Road (acceptable slope) – Proposed Methodology

The re-designed slope is also analyzed based on the naïve approach. Three variables, shear strength parameters and pore pressure ratio, are considered in the spreadsheet model. Twenty five Monte Carlo simulation, 32,000 iterations each, are performed. The histogram of the computed probabilities of unsatisfactory performance is shown in Figure 11–30. The mean probability of unsatisfactory performance is 10.27% with the 95% confidence interval ranging between 10.23-10.31%.

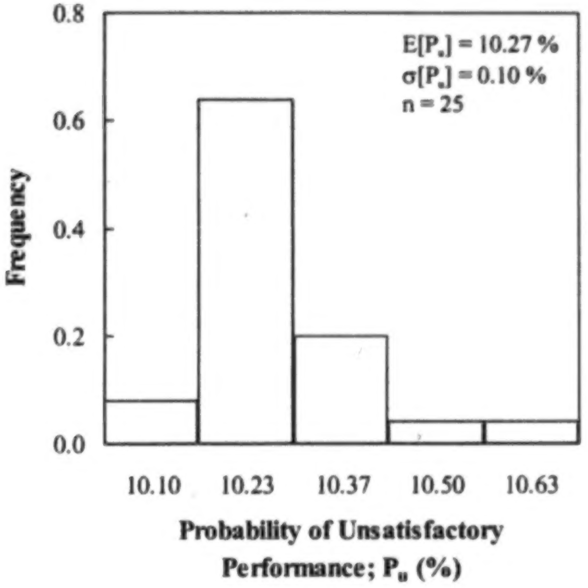

Figure 11–30 Histogram of the probability of unsatisfactory performance, Ching Cheung Road (acceptable slope) – Naïve Analysis

3.4 Shek Kip Mei Landslide

3.4.1 Background

On August 25, 1999 the cut slope behind housing Blocks Nos. 36 and 38 of Shek Kip Mei Estate was noted to suffer from signs of distress. Heaving of a concrete pavement at the foot of the slope, outward movement (up to 1m) at the toe, cracking of the chunam cover protecting the slope surface, detachment of debris from localized areas, failure of a high steel fence along the toe and the development of tension cracks were reported. Over the following days, additional slope movements and cracking were noted and seepage along the toe was observed.

A comprehensive investigation into the failure was sponsored by the Geotechnical Engineering Office of Hong Kong. It included geological mapping, drilling and sampling, pumping tests, double-ring infiltration tests, percolation tests, installation and monitoring of tensiometers, geophysical survey and laboratory testing. A final report summarizing the findings of the investigation was produced by Fugro Maunsell Scott Wilson joint venture (FMSW, 2000) and forms the basis of the account given here.

The displaced portion of the slope had an average height of about 21m. The slope consists of two sections of different geometry; a northern part and a southern part. The geometry of the northern part comprises 5 batters each dipping at an angle of 55 degrees to the horizontal (0.7h:1v) with 1-2m wide berms in between (Figure 11–31). The profile at the southern part is relatively irregular with average slope angles of 30 and 50 degrees at the upper and lower portions, respectively. The modes of instability were also different. In the northern part, failure was largely translational and characterized by a well-developed main scarp and significant outward movement. In the southern part, it was structurally controlled, immobile, and characterized by extensive surface cracking and bulging. The complex subsurface conditions and mode of failure at the southern part are major sources of model uncertainty. Our ability to reliably quantify such sources of uncertainty is, to date, very limited. Hence, this study is focused entirely on the stability of the northern part of the slope.

The displaced mass of the northern slope was approximately 37m wide and 31m long. It moved downwards at the main scar by about 1.2m and outwards, horizontally, at the toe by up to 1m. A tension crack up to 0.3m wide, 1.5m deep and 18.0m long developed between the main scarp and the displaced mass. The displaced material remained largely intact and had an estimated volume of about 2500 m^3.

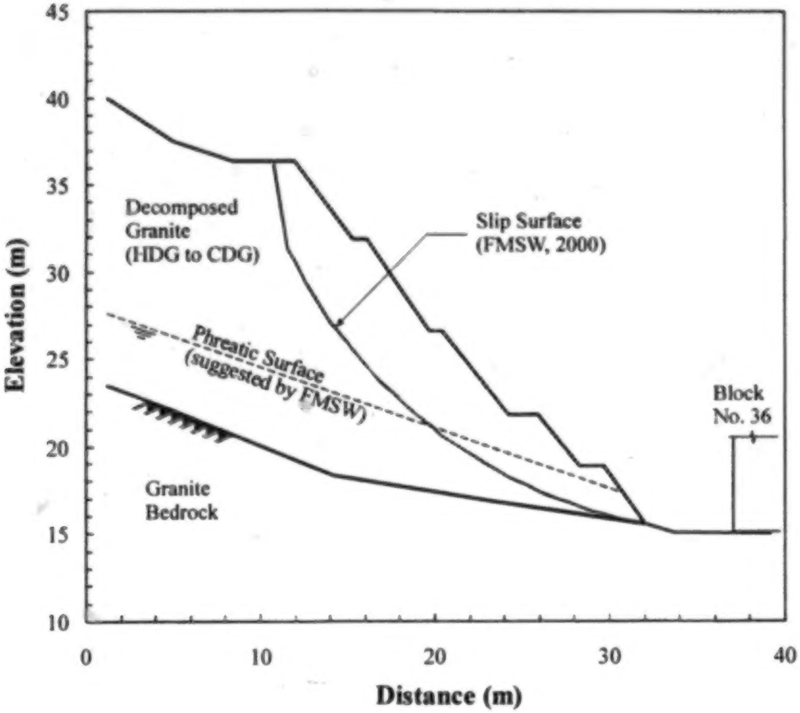
45
40
35
30
25
20
15
10
Elevation (m)
0
10
20
30
40
Distance (m)
Decomposed Granite (HDG to CDG)
Slip Surface (FMSW, 2000)
Phreatic Surface (suggested by FMSW)
Block No. 36
Granite Bedrock

Figure 11–31 Geometry and stratigraphy of Shek Kip Mei Estate landslide, Northern Slope

3.4.2 Local Geology

The site of the slide is underlain by medium-grained granite of Jurassic to Cretaceous age. The slope profile comprises highly to completely decomposed granite with corestones of moderately to slightly decomposed granite. A set of closely to extremely closely spaced discontinuities dip at 55-85 degrees to the west and northwest into the slope. Infilling of the joints with kaolinite and manganese deposits was reported. Other joint sets dipping to the east and southeast at angles of 52-88 degrees were also reported. These joints formed release planes along the flanks of the failure scar. Some sub-horizontal discontinuities were also noted. The depth of the interface between the weathered material and the fresh bedrock varied across the site ranging between 15m below the crest of the slope to about 5m at the toe area. Figure 11–31 shows the stratigraphy at the site.

3.4.3 Rainfall and Groundwater

Failure occurred on the last day of a 4-day intense rainstorm. The data from an automatic raingauge located 1 km from the site of the slide indicated 115.5mm and 133.5mm of rainfall over periods of 12 and 24 hours before failure, respectively. The total rainfall during the storm was about 690mm. It was considered one of the most intense rainfall events experienced in that area. Shortly after failure and up to 2 months thereafter, seepage was observed along the toe of the slope. Field observations and assessment of slope hydrology indicated a permanent base groundwater table within or close to the surface of the bedrock. The presence of an upper preferential groundwater regime within the decomposed granite was also a possibility. Data from tensiometers installed in the decomposed granite indicated suction ranging between 25-80 kPa within the top 5.5m. FMSW (2000) suggested that failure occurred due to a combination of suction reduction by the infiltration of rainwater and a rise in the base groundwater table. In spite of the detailed investigation undertaken, the prevailing groundwater conditions at the time of failure are uncertain.

3.4.4 Rupture Surface

Detailed logging of borehole full-length core samples and the walls of test pits and trial trenches allowed important inferences about the geometry and nature of the rupture surface. At some locations along the toe, the slip surface was planar within a soft clay layer dipping at a shallow angle, 6-20 degrees, to the horizontal. At the crest, the rupture surface was partially along a shallow soil-infilled tension crack. The majority of the surface, between the crest and toe, was located within a remolded, completely decomposed granite. The maximum depth of the slip surface below ground was around 8m. Based on the previous observations, the FMSW (2000) report postulated the semi-circular slip surface shown in Figure 11–31.

3.4.5 Shear Strength

Samples retrieved during the post-failure investigation were tested in the laboratory to assess the physical and mechanical properties of the decomposed granite.

Classification tests indicated that the soil is silty gravelly sand with fines content ranging between 10-20%. The shear strength parameters were obtained from unconsolidated undrained triaxial tests with pore pressure measurements. The testing results indicated that the effective cohesion is about 8 kPa and the friction angle is 38 degrees. These parameters are very close to the mean values of the regional probability distributions (C'=5.6 kPa and ϕ'=37.8 deg.).

3.4.6 Deterministic Stability Analyses

The stability of the slope geometry before failure is analyzed using Slope/W software and the Spencer method of slices. In their diagnosis of the failure, FMSW (2000) pointed to the combination of suction reduction due to infiltration and rise in the base groundwater table as the likely cause of failure. Assuming zero suction, they estimated that a 1.8m rise in the base groundwater table (refer to Figure 11–31) was adequate to trigger failure. Because of the intense rainfall before failure, the extensive tension cracks and the damage to the chunam protective cover, the assumption of a zero suction is reasonable. The slip surface used in this assessment is the same surface inferred by FMSW based on field observations, Figure 11–31. Using the strength parameters of the FMSW report (Section 3.4.5) and adopting their scenario of pore pressure development, the factor of safety is computed to be 1.10. Using the regional strength parameters, the factor of safety is estimated to be 1.04. Based on a back analysis (FS=1), the pore pressure ratio analogous to the prevailing pore pressure conditions at failure is estimated to be 0.11. The value is used for re-designing the slope to an acceptable geometry based on conventional slope practice. Because of the residential buildings at the toe of the slope, a design factor of safety of 1.4 is adopted. The same configuration of the failed slope, 5 batters separated by berms, is maintained. The modified design has an overall slope angle of 31.2 degrees (1.65h:1v), compared to 44 degrees of the failed geometry. The stability of the revised design is analyzed probabilistically in Section 3.4.8.

3.4.7 Quantifying Pore Pressure Uncertainty

The slope geometry before failure is back-analyzed to estimate the probability distribution of the pore pressure ratio at failure. A spreadsheet model mimicking the geometry and stratigraphy is prepared. Spencer's method of slices and the slip surface inferred by FMSW, Figure 11–31, are used in the model. The factor of safety is taken as a deterministic input of one and the regional probability distributions of the friction angle and cohesion are adopted. A Monte Carlo simulation using a seed number of 31069 and 15,000 iterations is performed. The mean pore pressure ratio is estimated to be 0.09 with a standard deviation of 0.12. It ranges between a minimum of –0.39 to a maximum of 0.55. Figure 11–32 shows the histogram and the CDF of the pore pressure ratio. A zero pore pressure ratio threshold is added to the spreadsheet model and the simulation is repeated 25 times using different seed numbers. Figure 11–33 shows the probability distribution of the pore pressure ratio based on averaging the results of all 25 simulations. The mean pore pressure ratio is 0.10 with a standard deviation of 0.10. The plot suggests that there is a 23% probability that failure occurred under a condition of negative or zero pore pressure ratio.

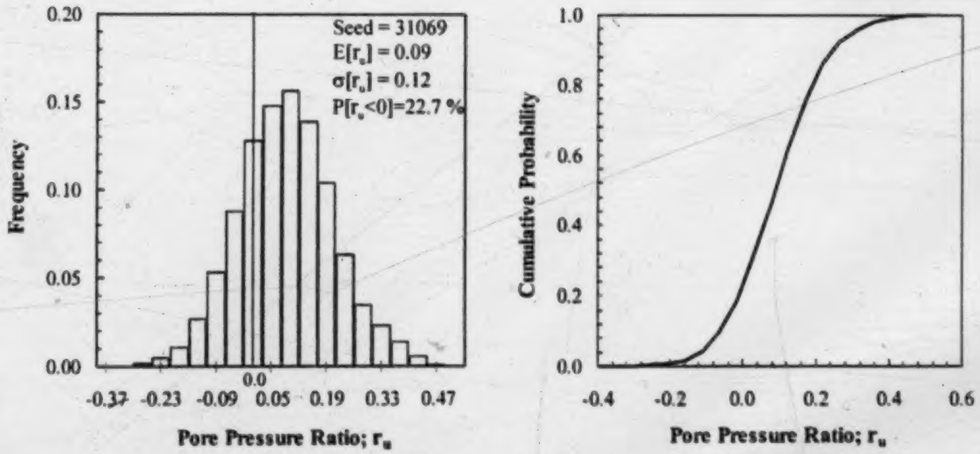

Figure 11–32 Histogram and CDF of the pore pressure ratio at failure – Shek Kip Mei landslide

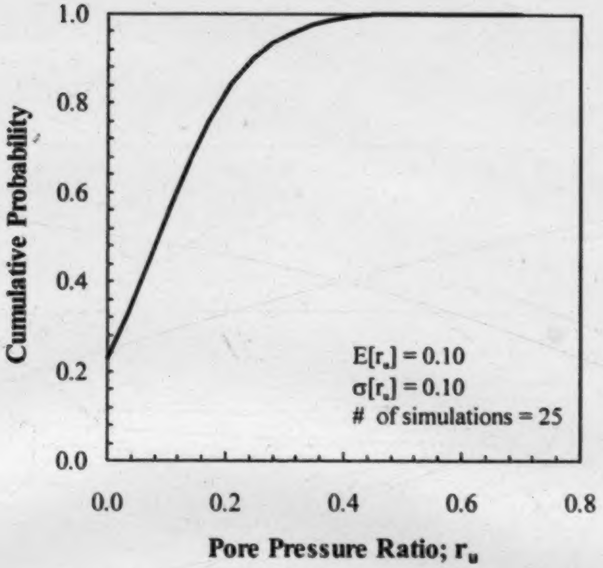

Figure 11–33 Probability distribution of pore pressure ratio at failure – Shek Kip Mei landslide

3.4.8 Probabilistic Stability Analyses

The stability of the revised slope geometry (31.2 degrees inclination) is analyzed probabilistically using the methodology of Chapter 5. A spreadsheet model mimicking the geometry and stratigraphy is prepared. The Spencer method of slices is used in the model. The friction angle and cohesion of the decomposed granite and the pore pressure ratio are considered variables with the probability distributions shown in Figure 11–2, Figure 11–4, and Figure 11–33. The slip surface is assumed circular. The surface corresponding to the Hassan and Wolff (1999) criterion is adopted in the spreadsheet. The trace of the slip surface is divided into segments 10m long, assuming an autocorrelation distance of 5m. The local average properties and parameters over the length of each segment are represented by the relevant point CDFs. In total, 15 variables are needed to model the spatial variability of the strength parameters and the pore pressure ratio. The correlations between adjacent local averages are evaluated and taken into account in Monte Carlo simulation, as outlined in Chapter 5.

The optimum number of iterations is assessed to be 32,000. Using a seed number of 31069, the mean factor of safety is calculated to be 1.45 with a standard deviation of 0.17. The probability of unsatisfactory performance is 0.23%. Figure 11–34 shows the histogram and the CDF of the factor of safety. A sensitivity analysis is also performed and Figure 11–35 shows Spearman rank correlation coefficients for all input variables. The plot does not indicate the dominance of any variable; the uncertainties of the friction angle, the cohesion and the pore pressure ratio have comparable contributions to the uncertainty of the factor of safety.

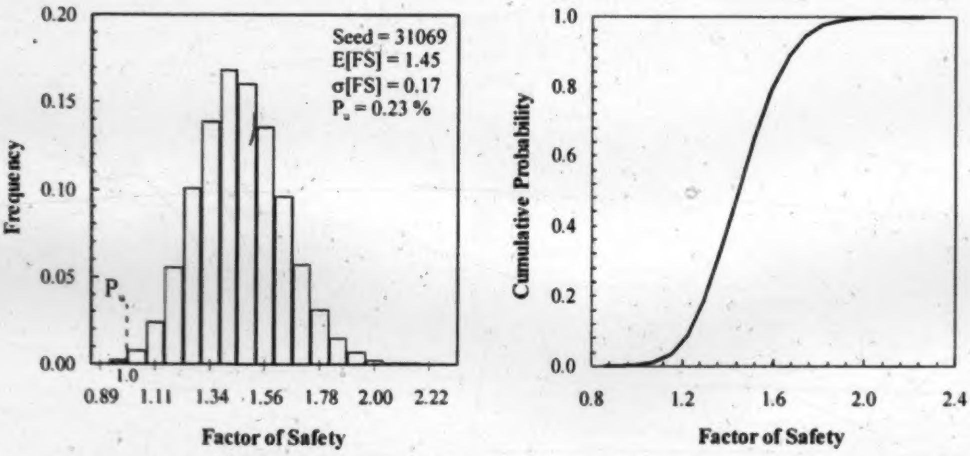

Figure 11–34 Histogram and CDF of the factor of safety, Shek Kip Mei slope (acceptable design) – Proposed Methodology

Four Monte Carlo simulations are performed using different autocorrelation distances. Figure 11–36 is a plot of the computed probabilities of unsatisfactory performance versus the autocorrelation distances. As the autocorrelation distance increased from 3m to 10m, the probability of unsatisfactory performance increased from 0.01% to 2.05%. Adopting an autocorrelation distance of 5m, 25 simulations are performed using different seed numbers. Figure 11–37 shows the histogram of the probability of unsatisfactory performance based on the results of all simulations. The mean probability of unsatisfactory performance is 0.21% with the 95% confidence interval ranging between 0.20-0.22%.

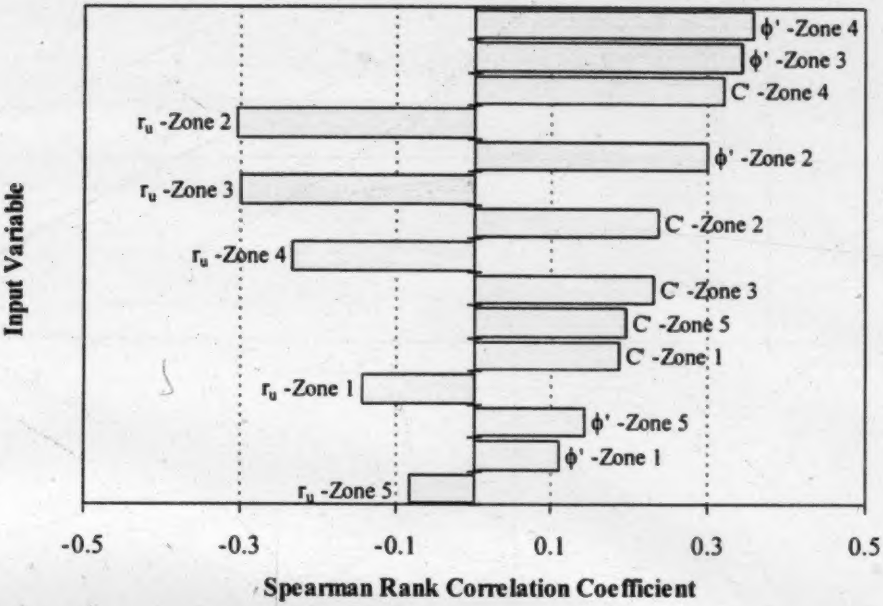

Figure 11–35 Sensitivity analysis results, Shek Kip Mei slope (acceptable design) – Proposed Methodology

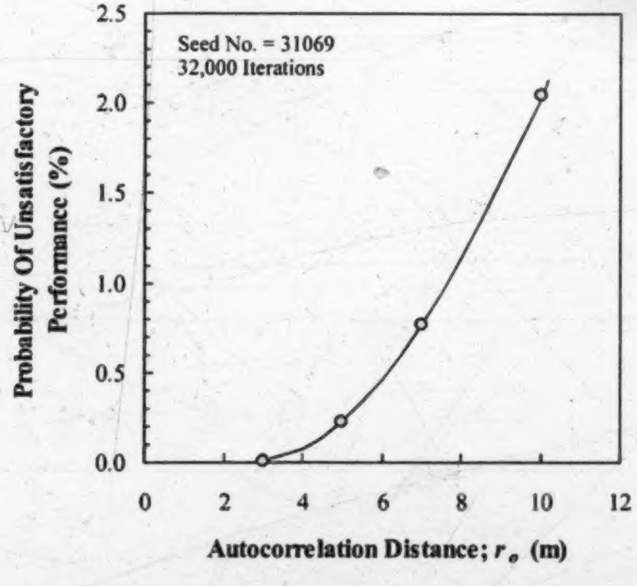

Figure 11–36 Variation of the probability of unsatisfactory performance with the autocorrelation distance, Shek Kip Mei slope (acceptable design)

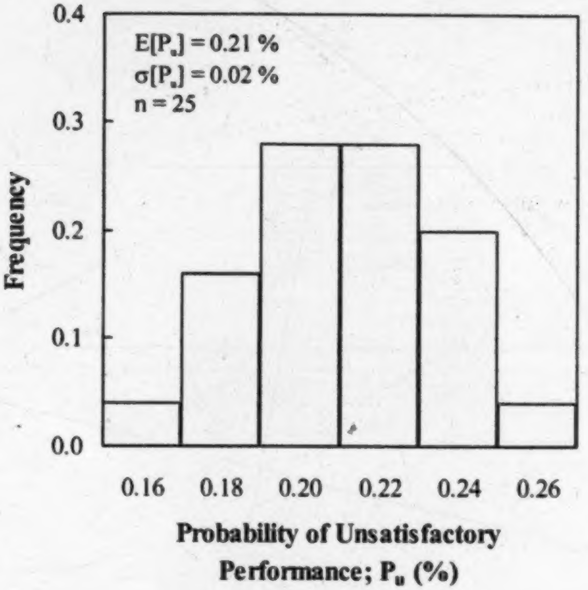

Figure 11–37 Histogram of the probability of unsatisfactory performance, Shek Kip Mei slope (acceptable design) – Proposed Methodology

The modified design is also analyzed using the naïve approach. The spreadsheet model includes 3 variables representing the strength parameters and the pore pressure ratio. Twenty five simulations are performed using 32,000 iteration for each simulation. The computed probabilities of unsatisfactory performance are presented in histogram form in Figure 11–38. The mean probability of the unsatisfactory performance is 8.03% with the 95% confidence interval 7.99-8.07%.

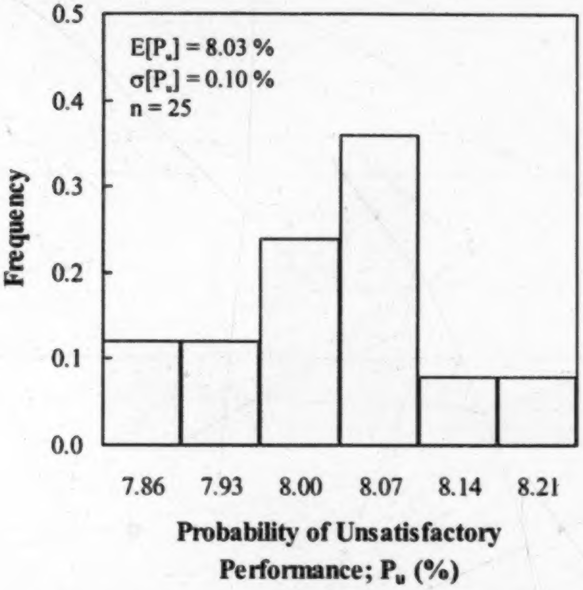

Figure 11–38 Histogram of the probability of unsatisfactory performance, Shek Kip Mei slope (acceptable design) – Naïve Analysis

4. SCALE OF FAILURE

So far, the stability analyses presented in this chapter are focused on deep-seated failures, in excess of hundreds of cubic metres in volume, involving the entire or most of the height of the slope. This type of failure is, often, the most devastating with the potential of inducing severe damage and many fatalities or injuries. Small scale failures (less than 100 cubic metres in volume) are, however, common in Hong Kong and cannot be ignored. This section examines the probability of unsatisfactory performance associated with small failures.

The stability of the acceptable (i.e., re-designed) slopes of the case studies in Section 3 is analyzed deterministically assuming smaller slip surfaces. For each case, failure is restricted to a portion of the slope, e.g. upper 1/3 of slope height, and the critical slip surface is located using the regional strength parameters and the back-calculated pore pressure ratio. Two critical slip surfaces are determined for each slope to represent a small-scale failure and a medium-scale failure. The small geometry of the Cho Yiu Estate slope did not allow such division and only the three other cases (Tsing Yi: 1, Ching Cheung Road and Shek Kip Mei) are considered in this assessment.

For each case study, the probability of unsatisfactory performance associated with the small and the medium slip surfaces are estimated by simulation and following the same procedures described in Sections 3.2.8, 3.3.8 and 3.4.8 above. For each case study and slip surface, the simulation is repeated 10 times using different seed numbers and the results are averaged. Figure 11–39, Figure 11–40 and Figure 11–41 summarize the results of the analyses of the Tsing Yi: 1 slope, the Ching Cheung Road and the Shek Kip Mei slope, respectively. Each figure shows the slip surfaces and the associated probabilities of unsatisfactory performance and factors of safety. Surface number 1 in each figure represents the failure of the entire slope and refers to the slip surface analyzed in Section 3.2.8, 3.3.8 or 3.4.8. Surface number 2 refers to the failure of the upper 2/3 of the slope whereas surface number 3 represents the failure of the top 1/4 to1/3 of the slope height.

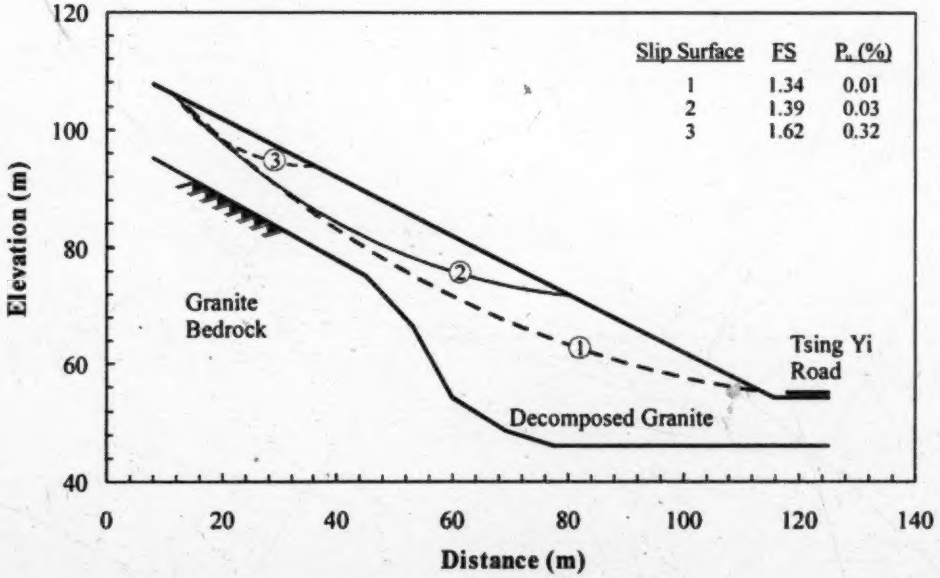

Slip Surface	FS	P_u (%)
1	1.34	0.01
2	1.39	0.03
3	1.62	0.32

Figure 11–39 Effect of scale of failure on probability of unsatisfactory performance and factor of safety - Tsing Yi: 1 slope (acceptable design)

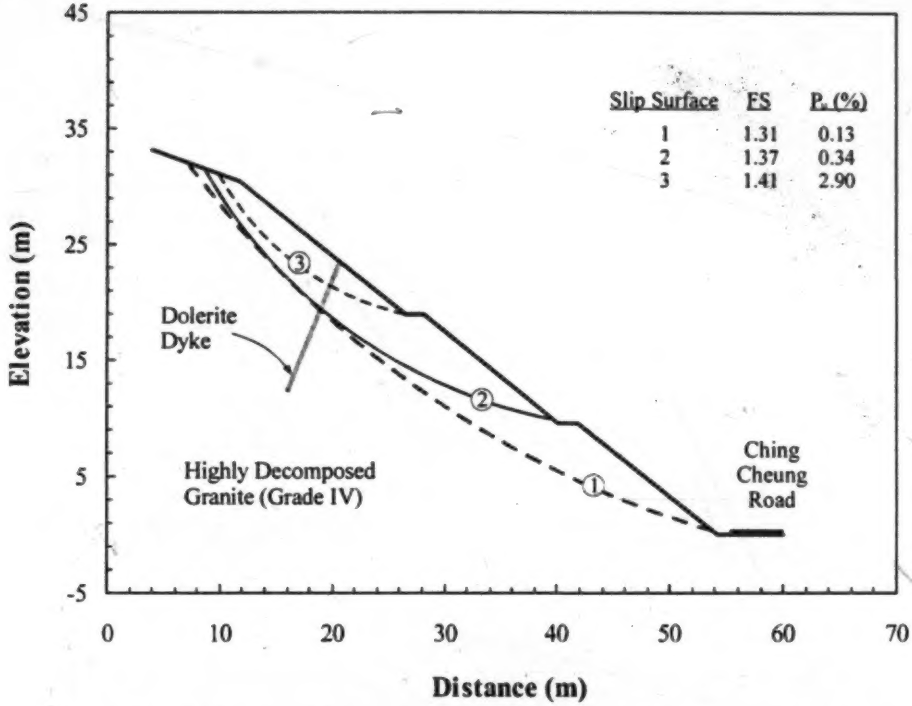

Figure 11–40 Effect of scale of failure on probability of unsatisfactory performance and factor of safety – Ching Cheung Road (acceptable design)

For the Tsing Yi slope, the factors of safety for slip surfaces 1, 2 and 3 are 1.34, 1.39 and 1.62, respectively, whereas the probabilities of unsatisfactory performance are 0.01%, 0.03 and 0.32%. For the Ching Cheung Road, the factors of safety are 1.31, 1.37 and 1.41, and the probabilities of unsatisfactory performance are 0.13%, 0.34% and 2.9%. For the Shek Kip Mei slope, the factors of safety are 1.45, 1.56 and 1.83 and the associated probabilities of unsatisfactory performance are 0.21%, 0.84% and 6.06%.

The results of the three case studies are consistent and illustrate a very interesting observation. Smaller slip surfaces have higher probabilities of unsatisfactory performance than larger surfaces despite their higher factors of safety. This might seem unusual, however it is logical within the context of spatial variability. The concept of spatial variability emphasizes that soil properties and pore pressures vary from one location to another. As such, a weak zone of completely decomposed granite might be followed by a stronger less weathered zone which in turn is followed by another weak zone, and so forth. The extent or dimensions of the weak/strong zones are proportional to the autocorrelation distance. As indicated in Section 3.1.8, Hong Kong residual soils are erratic and characterized by small autocorrelation distances. A slip surface which is very long compared to the autocorrelation distance passes through many weak and strong zones. The low and high strength at different locations along the slip surface tend to balance each other, reducing the uncertainty of the average strength. The same concept applies for the pore pressure. As a result, the uncertainty of the factor of safety, and consequently, the probability of unsatisfactory performance are reduced. On the other hand, a very small slip surface may fall entirely within a weak zone or within a strong zone. Thus, the uncertainty of the mean strength along the slip surface is higher which is reflected in a higher probability of unsatisfactory performance. The conventional deterministic approach based on the factor of safety clearly fails to address this issue of scale of failure.

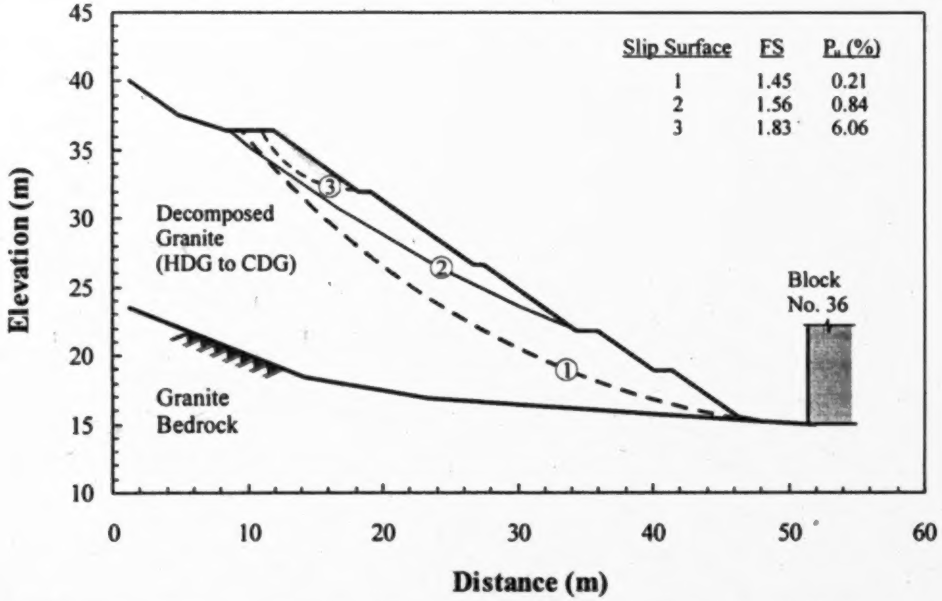

Slip Surface	FS	P_u (%)
1	1.45	0.21
2	1.56	0.84
3	1.83	6.06

Figure 11–41 Effect of scale of failure on probability of unsatisfactory performance and factor of safety – Shek Kip Mei slope (acceptable design)

It is not surprising, therefore, to observe that the frequency of small failures is much higher than large failures. The Geotechnical Engineering Office of Hong Kong (GEO, 1999) classifies slope failures based on the scale of failure into minor (failure volume<$50m^3$), major (failure volume of $50m^3$ to $500m^3$) and massive (failure volume>$500m^3$). In 1999, GEO published a review (GEO, 1999) of all landslide incidents in the years 1997 and 1998. The report included the number of incidents of minor, major and massive failures, Table 11-1. Similarly, ERM (1997) reported the number of landslide incidents along the BRIL roads over the period 1982 to 1996 grouped by the volume of the failed mass, Table 11-1. The number of minor failures is clearly much higher than the number of massive failures.

Table 11-1 Observed and theoretical ratios of the frequencies of occurrence of the different scales of failure

Case Study	Ratio of the Frequencies of Occurrence		
	Minor Failure ($<50m^3$)	**Major Failure** (50-$500m^3$)	**Massive Failure** ($>500m^3$)
Landslide incidents in 1997 and 1998 (GEO, 1999)	27.0 (703)	2.2 (58)	1 (26)
Landslide incidents along BRIL roads for the period 1982-1996 (ERM, 1997)	31.8 (286)	3 (27)	1 (9)
Tsing Yi 1 slope	32.0	3.0	1
Ching Cheung Road	22.3	2.6	1
Shek Kip Mei slope	29.9	4.0	1

(703) Number of minor failure incidents in 1997 and 1998

The probability of unsatisfactory performance may be interpreted as the probability (or frequency) of failure of a volume of soil equal to that encompassed by the critical slip surface. A crude analogy between massive failure and slip surface 1, major failure and slip surface 2, and minor failure and slip surface 3 could be made. Thus, the ratios of the probabilities of unsatisfactory performance of slip surfaces 1 to 3 can be compared with the ratios of the observed frequencies of the 3 scales of failure as shown in Table 11-1. The close numerical agreement between the observed and computed ratios is, probably, fortuitous. However, the conceptual agreement, minor failures are much more frequent than massive failures, is evident.

Despite the higher probabilities of unsatisfactory performance of minor failures, they do not control the overall design of large slopes for feasibility considerations. For example, flattening the entire Shek Kip Mei slope (20.8m high) to deal with the high probability of unsatisfactory performance of a minor failure at slope crest is not practical because of space limitations and economics. Instead, minor failures are dealt with more efficiently by local stabilization techniques. In Hong Kong, soil nailing has proved to be very successful and is widely used to deal with local unstable sections.

5. SUMMARY AND DISCUSSION

The variability of the shear strength parameters of Hong Kong granitic soils is quantified statistically based on a relatively large database of triaxial test results. There is reasonable evidence to support the adequacy of a regional assessment of the shear strength parameters. Generalized probability distributions of the effective cohesion and friction angle are established. The uncertainty in the friction angle is relatively low, whereas the uncertainty in the effective cohesion is significant. These distributions can be used in the probabilistic assessment of the stability of granitic soil slopes in Hong Kong. Site-specific shear strength measurements are, however, essential to confirm or update these distributions. The Bayesian approach could be useful in updating the regional distributions based on additional site-specific data.

Four cases of slope failures in Hong Kong granitic soil are studied; Cho Yiu slide, Tsing Yi: 1 slide, Ching Cheung Road slide and Shek Kip Mei slide. Given the uncertainty of the shear strength parameters, the slopes are back-analyzed to quantify the uncertainty of the pore water pressure. The probability distribution of the pore pressure ratio at failure is established for each slope. In all cases, the uncertainty of the pore pressure ratio is shown to be substantial.

Because of the small cohesion of Hong Kong granitic soils, the back-calculated pore pressure ratio is not very sensitive to slope height. Instead, it is largely controlled by the slope angle. Figure 11–42 shows the probability distributions of the pore pressure ratio of the four investigated cases. As the slope angle decreases, the mean pore pressure ratio at failure increases and the distribution shifts to the right. These CDFs define the magnitudes and probabilities of pore pressures at which failure of a slope of a specific inclination is likely to occur given the variability of soil strength. In a probabilistic slope assessment, these distributions may be used as design criteria. A sensible slope design should have an adequate safety, in terms of the probability of unsatisfactory performance, when subjected to such pore pressures. Clearly, estimating the probability distribution of the pore pressure ratio for the design of any slope based on its angle only, without consideration of slope hydrology, is a very crude approximation. However, it still may be of value as an initial estimate.

The four case studies are re-designed to acceptable geometry based on conventional slope design practice. The probability of unsatisfactory performance is estimated for all cases. The estimated probabilities are relatively sensitive to the autocorrelation distance. A similar observation is noted with the Congress Street cut in Chapter 10. Two features are common between the Congress Street cut and Hong Kong cases. First, both analyses are dominated by the uncertainty due to the spatial variability of the input parameters, rather than systematic sources of uncertainty. Second, Hong Kong granitic soil and the glacial clay till of the Congress Street cut are both erratic and characterized by short autocorrelation distances. This affirms the conclusion of Chapter 10 that soil deposits exhibiting erratic variability require careful attention, and probably site-specific studies, in assessing the autocorrelation distance.

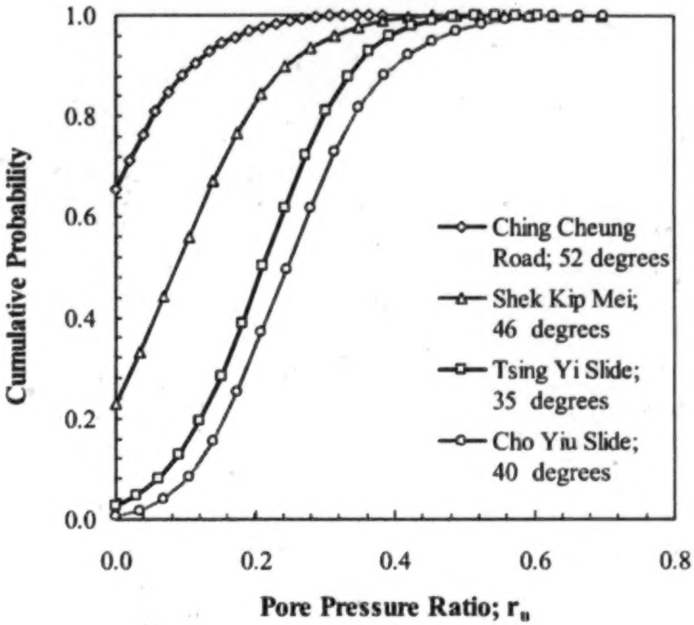

Figure 11–42 Comparison between probability distributions of the pore pressure ratios at failure for all the analyzed case studies

The probabilities of unsatisfactory performance associated with different failure scales were estimated for the Tsing Yi: 1 slope, the Ching Cheung slope and the Shek Kip Mei slope. Minor failures are shown to have much higher probabilities of unsatisfactory performance than massive failures, even though they have higher factors of safety. This results from the consideration of the spatial variability of the input parameters, which the conventional deterministic approach fails to address. The ratios between the probabilities of unsatisfactory performance of minor, major and massive failures compare very well with the ratios of their occurrence in reality.

CHAPTER 12

PROBABILISTIC SLOPE STABILITY ANALYSIS
SUMMARY AND DISCUSSION

The objectives of this work are stated in Chapter 1. The results of the conducted deterministic and probabilistic analyses are presented in Chapters 5 through 11. The following sections summarize the outcome of the study in the light of the objectives set and the obtained results. The discussion follows, more or less, the same order in which the objectives are listed.

1. PROBABILISTIC SLOPE ANALYSIS – WHY?

Slope engineering is among the geotechnical issues most dominated by uncertainty. The inherent spatial variability of input parameters (e.g., soil properties, pore water pressure), the scarcity of data, the common use of highly uncertain empirical factors and the limitations of analytical models are all important factors contributing to the overall uncertainty of a slope design. Conventional slope analysis and design methods, based on the factor of safety, do not consider uncertainty in any direct way and rely entirely on experience and judgement for the subjective account of its impact on design. Engineering judgement is an essential ingredient in any geotechnical design. Unfortunately, it is difficult to transfer this judgement from the experienced to the inexperienced (Lumb, 1980).

Probabilistic slope stability analysis is a rational means to quantify and account for the impact of uncertainty on slope performance. In addition to the mean value of the factor of safety, which is similar to the output from a conventional slope design, a probabilistic analysis provides additional valuable information. The variance of the factor of safety, the probability of unsatisfactory performance and the reliability index are all measures of the reliability of the analysis. By estimating the likelihood or probability of a certain state (e.g., failure) occurring, probabilistic analysis, in a way, quantifies aspects of judgement and experience. It, thus, provides greater insight into design reliability and enhances the decision-making process. A probabilistic analysis is also the first step towards the more comprehensive approach of risk management applied to slope instability hazards.

2. PROBABILISTIC SLOPE ANALYSIS METHODOLOGY

The successful integration of probabilistic slope stability analysis into professional practice relies largely on the practicality of the analytical techniques. The analyses in Chapters 6-11 demonstrate the flexibility and practicality of the proposed probabilistic slope analysis methodology (Chapter 5) in dealing with a wide variety of real life slope problems. The methodology utilizes readily available software such as @Risk, for Monte Carlo simulation, and the familiar spreadsheet program Excel. The underlying procedures and concepts are simple and transparent, requiring only fundamental knowledge of statistics and probability theory.

The methodology accounts for the spatial variability of soil parameters along the slip surface using Vanmarcke's approximate model for a one-dimensional random field (Vanmarcke; 1977a, 1983). It also accounts for bias in the empirical factors/correlations used in the analysis and the statistical uncertainty due to limited amounts of data. Observed non-parametric probability distributions of soil parameters and distributions based on expert judgment can be readily incorporated into the analysis. Upon obtaining new information, the analysis is updated by simply changing a few cells in the spreadsheet and running a new Monte Carlo simulation. The output of the analysis is presented in the form of the probability distribution of the factor of safety, based on which the probability of unsatisfactory performance and the reliability index are evaluated.

3. SPATIAL VARIABILITY AND NAÏVE ANALYSIS

Soil compositions and properties vary from one location to another, even within homogenous layers. That variability, or scatter, is one of the main sources of parameter uncertainty. It is, therefore, intuitive to take spatial variability into account in any probabilistic analysis. The proposed probabilistic methodology accounts for spatial variability by modeling the spatial structures of the input parameters in a semi-empirical form. The spatial structure is characterized by an autocorrelation distance which describes the pattern of soil variability. A large autocorrelation distance reflects smooth continuous variability whereas a short distance reflects erratic variability. The naïve analysis, on the other hand, ignores spatial variability. It assumes the autocorrelation distance to be infinitely large which implies that the values of an input variable are the same at all locations.

Table 12-1 and Table 12-2 summarize the results of the probabilistic analyses based on the proposed probabilistic methodology for the safe and failed slopes, respectively, whereas Table 12-3 summarizes the results based on the naïve approach (all tables are included at the end of the chapter). The computed probabilities of unsatisfactory performance of the naïve approach (safe slopes) are much higher than those based on the proposed methodology. The reliability indices of the latter are, consequently, much lower. Figure 12–1 compares the results of the two analyses in terms of the ratio of the probability of unsatisfactory performance from the naïve analysis to that from the proposed methodology; hereafter referred to as the *probability ratio*. The plot shows that the naïve analysis overestimates the probability of unsatisfactory performance, by up to 3 orders of magnitude in one case (Tsing Yi: 1 slope).

The difference between the two analyses arises from the reduction in the variances of the input variables in the proposed methodology due to spatial averaging. Slope performance, in normal conditions, is controlled by the average soil properties and pore pressure ratio along the slip surface and not by the high or low values at some locations. The variance of the average of a spatially varying quantity is less than the point variance.

The amount of reduction is a function of the ratio of the autocorrelation distance, r_o, to the length of the slip surface; known as the variance reduction factor, *f* (refer to Chapter 3). A factor of 1 (i.e., $r_o \approx$ ½ the length of the slip surface within the layer whose uncertainty dominates the analysis) indicates no variance reduction, which is the case of a naïve analysis. Figure 12–2 is a plot of the variance reduction factor versus the probability ratio. As the variance reduction factor decreases, the gap between the outputs of the naïve analysis and the proposed methodology widens.

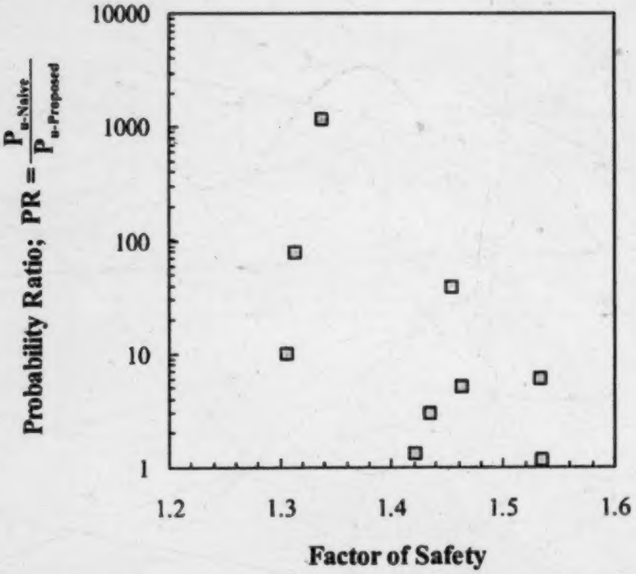

Figure 12–1 Probability ratio versus factor of safety for safe slopes

A literature review indicated that the range within which the autocorrelation distances of geotechnical properties vary is not large. For practical purposes, the autocorrelation distance can, thus, be evaluated judgmentally based on the typical ranges in the literature, as described in Chapter 5. Consideration of the geological processes controlling the formation/deposition of soil layers is of great value in guiding the selection of an empirical estimate. It is, however, important to assess the impact of different assumptions of the autocorrelation distance on the probability of unsatisfactory performance. Each of the case studies considered in this work (except for the James Bay dykes) is re-analyzed using different autocorrelation distances. Figure 12–3 shows the variation of the probability of unsatisfactory performance with the autocorrelation distance for the cases whose soil formations were characterized by continuous spatial variability (i.e., large r_o). These include the marine clay-shale of the Syncrude Cell 23, the homogenous marine clay of the Lodalen slope and the soft marine clay of the Muar embankment. The solid symbols represent the analyses based on the most likely autocorrelation distance for each case. The points denoted by the letter N represent the results of the naïve analyses (i.e., r_o is large enough to have no impact on the analysis). Beyond each of these points the probability of unsatisfactory remains constant irrespective of the autocorrelation distance. A threshold of 2×10^{-2} probability (upper limit of the probability of unsatisfactory performance associated with acceptable slopes; Section 5.1 below) is also plotted on the figure. Figure 12–4 shows the results of the cases characterized by erratic spatial variability (i.e., small r_o). These include the clay till of the Congress Street cut and the residual granitic soil of Hong Kong.

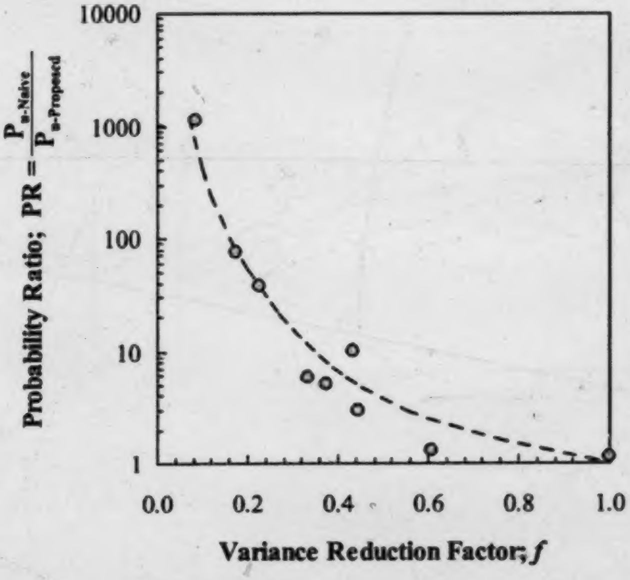

Figure 12–2 Probability ratio versus variance reduction factor

Figure 12–3 indicates that, within practical limits, the probability of unsatisfactory performance is not sensitive to the autocorrelation distance for soil formations exhibiting continuous spatial variability. For soils characterized by erratic variability, Figure 12–4, the probability of unsatisfactory performance increases with the increase in the autocorrelation distance. The rate of increase, however, diminishes rapidly as the autocorrelation distance increases beyond 10m which is consistent with the trend of Figure 12–3. This suggests that for soil deposits exhibiting erratic variability, the results of a probabilistic analysis could be sensitive to the assumption of the autocorrelation distance. Accounting for the spatial variability of such formations may, thus, require some extra effort in assessing a site/formation specific autocorrelation distance. A special exploration program could be designed (in terms of the number and spacing of tests) and conducted to estimate the site and soil specific autocorrelation distances. This, however, could be an expensive solution for the typical site investigation budget of many projects.

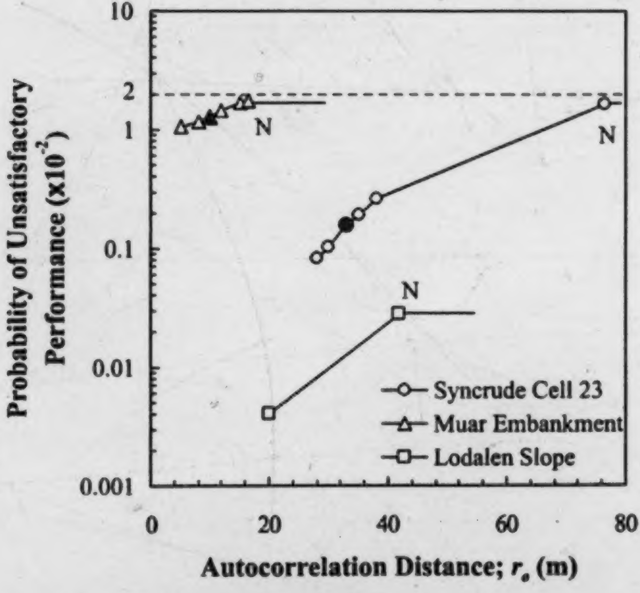

Figure 12–3 Effect of autocorrelation distance on probability of unsatisfactory performance, Safe Slopes - Soil formations exhibiting continuous spatial variability (solid symbols refer to the analyses based on the most likely r_o values, letter N refers to naïve analysis)

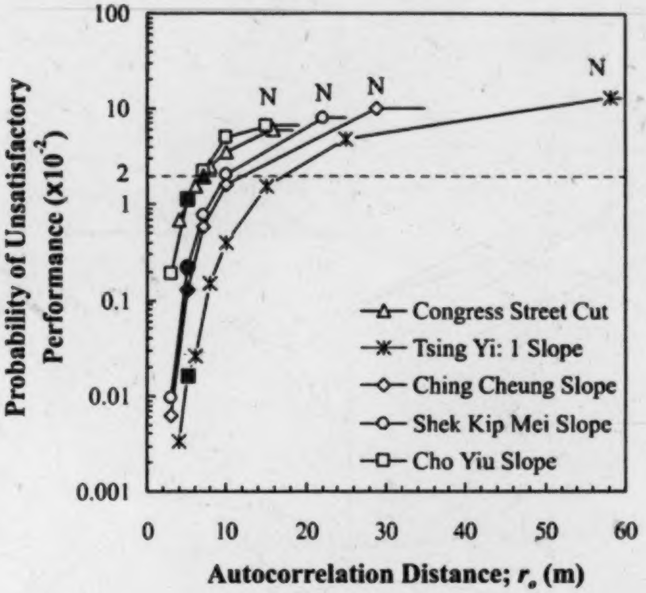

Figure 12–4 Effect of autocorrelation distance on probability of unsatisfactory performance, Safe Slopes - Soil formations exhibiting erratic spatial variability (solid symbols refer to the analyses based on the most likely r_o values, letter N refers to naïve analysis)

4. CALIBRATION OF PROBABILISTIC SLOPE ANALYSIS

Providing a link between current slope design practice and probabilistic slope stability analysis (i.e., a calibration process) is an important step for the integration of probabilistic techniques into geotechnical engineering practice. That link will help practitioners understand and reflect on the meanings of the computed probabilities of unsatisfactory performance. Ten case studies are analyzed probabilistically and deterministically for the calibration process. The studies (Chapters 6-11) compare the factor of safety and the probability of the unsatisfactory performance and highlights the role of uncertainty and its impact on the reliability of the analysis. They also serve as illustrations to the implementation of probabilistic techniques in practice.

The following notes are important for a proper interpretation of the computed probability of unsatisfactory performance. The probabilistic methodology of Chapter 5 accounts for the spatial variability of soil properties along the slip surface through Vanmarcke's empirical models for a one-dimensional random field. The models lead to a smaller variance reduction (due to spatial averaging) compared to more rigorous models. As a result, the computed probability of unsatisfactory performance could be higher than the absolute unknown probability.

Despite, the effort by the designer to address all sources of uncertainty, there is always the possibility of undetected uncertainties that are not taken into account (e.g., human mistakes). Hence, the estimated probability of unsatisfactory performance should be regarded as a lower bound to the actual probability. A computed zero probability of unsatisfactory performance (e.g., Lodalen slope) is viewed as an insignificant probability rather than a no failure condition. For such reasons, comparing the probabilities of unsatisfactory performance of alternative designs for the same problem is thought to be of greater value than the absolute probabilities of the designs.

The computed probability also does not reflect the effect of time. In other words, it assumes that the uncertainties considered in the analysis are invariant with time. If, for example, pore water pressure varies with time, the probabilistic analysis should be repeated using revised input probability distributions. It is also important to note that the probability of unsatisfactory performance as used in this study, reflects the probability or potential of the slope collapsing. It does not address serviceability issues such as slope movement and cracking, surface erosion and excessive seepage.

Finally, an estimate of the annual hazard probability is required in quantitative risk analyses (Chapter 13). The computed probabilities of unsatisfactory performance in Chapters 6-11 represent the probability of occurrence of a hazardous event over the lifetime of the conditions considered in the analysis (e.g., type of loading, environmental conditions), which vary from one case to another. Assessing the annual hazard probability is, thus, a case-specific exercise. For example, the pore water pressures in the Hong Kong cases are a result of the intense rainstorms experienced in that area. The annual hazard probability should, therefore, be referenced to the return period of rainstorm. In contrast, the pore water pressure in the Lodalen case was in a steady state condition and there are no reasons to believe that soil properties would vary with time. The annual hazard probability should, legitimately, be referenced to the lifetime of the slope, say a 100 years or so. In the Muar embankment case, the probability of unsatisfactory performance is evaluated for an undrained loading condition. The short duration of that type of loading (say, 6 months to 1 year) is a justified basis for evaluating the annual hazard probability.

5. PROBABILISTIC SLOPE DESIGN CRITERIA

5.1 Probability of Unsatisfactory Performance

The probability of unsatisfactory performance is the main safety index used in this study to describe the state of a slope. It is, thus, essential to understand the meaning of the computed probabilities and to estimate probabilistic design criteria to judge the adequacy of a design or compare alternative designs. Also, a high risk situation may arise from either a high probability of unsatisfactory performance or high failure consequences or both. Understanding the meaning and acceptability of the computed probability greatly assist in the decision-making. For example, a small-probability, high-consequences situation is dealt with more efficiently by reducing the consequences rather than lowering an already small probability of unsatisfactory performance.

In order to provide guidelines on the probability limit associated with satisfactory slope performance, conventional design practice is calibrated in probabilistic terms. Two classes of slopes are considered: failed slopes and safe slopes. Table 12-1 summarizes the output of the probabilistic analyses of the slopes that are deemed safe, whereas Table 12-2 summarizes the probabilistic outputs of the failed slopes. Figure 12–5 is a plot of the factor of safety versus the probability of unsatisfactory performance for all the analyzed cases (Figure 12–9 in page 319 shows the data for a factor of safety greater than 1.3 plotted on a larger scale). The distinction between failed and safe slopes is very clear. The probability of unsatisfactory performance of most of the safe slopes is less than $2x10^{-2}$, or 2%. As the factor of safety drops below a value of about 1.3, the probability of unsatisfactory performance increases sharply.

Based on Figure 12–5, it seems that a probability of unsatisfactory performance of $2x10^{-2}$ marks the limit of what is deemed acceptable slope design practice. A probability of unsatisfactory performance of 2% could, thus, be regarded as an upper design threshold. It should be noted, however, that this is only one of several criteria involved in the design process. For example, high failure consequences and/or inadequate serviceability (e.g., excessive deformations and cracking) may necessitate adopting more stringent design criteria. It is also emphasized that the use of the probability of unsatisfactory performance is not intended to replace the factor of safety. Instead, the two indices, used together, will provide a greater insight into the acceptability of the design. For example, a very small probability of unsatisfactory performance (i.e., high reliability) justifies adopting lower design factors of safety than normal provided that the serviceability of the slope is not compromised. If the computed probability of unsatisfactory performance is deemed high, it could be reduced through targeting a higher design factor of safety or through improving design reliability by reducing the uncertainty of the input parameters.

A noteworthy observation is that the estimated threshold of $2x10^{-2}$ probability is more relaxed than the typical values in the literature. For example, Lumb (1983) regarded a failure probability of $1x10^{-2}$ as high and requiring design changes. Similarly, the US Corps of Engineers (1995) recommended a target probability of unsatisfactory performance of $3x10^{-5}$ for a “Good” performance level. This suggests that what is deemed as an acceptable design practice is, in fact, less reliable than commonly thought.

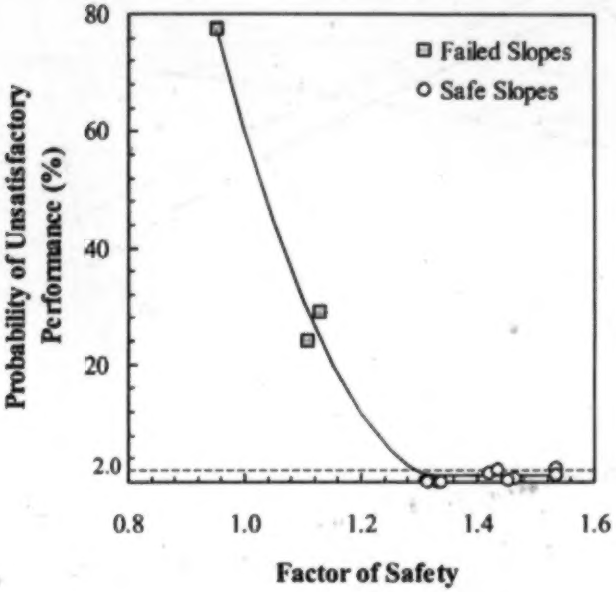

Figure 12–5 Probability of Unsatisfactory performance versus factor of safety for the safe and failed slopes – Proposed Methodology

5.2 Reliability Index

The reliability index is another common probabilistic safety measure. It is defined as the distance between the mean factor of safety and the limiting state, FS=1, expressed in units of the standard deviation of the factor of safety (refer to Chapter 4). Figure 12–6 shows a plot of the factor of safety versus the reliability index for all the analyzed cases. Failed slopes have reliability indices less than 0.8 whereas the safe slopes have a minimum reliability index of 1.8 with most of the cases having indices higher than 2.0. A minimum reliability index of 2.0 could, thus, serve as another probabilistic slope design criterion. It corresponds to a probability of unsatisfactory performance on the order of $2x10^{-2}$.

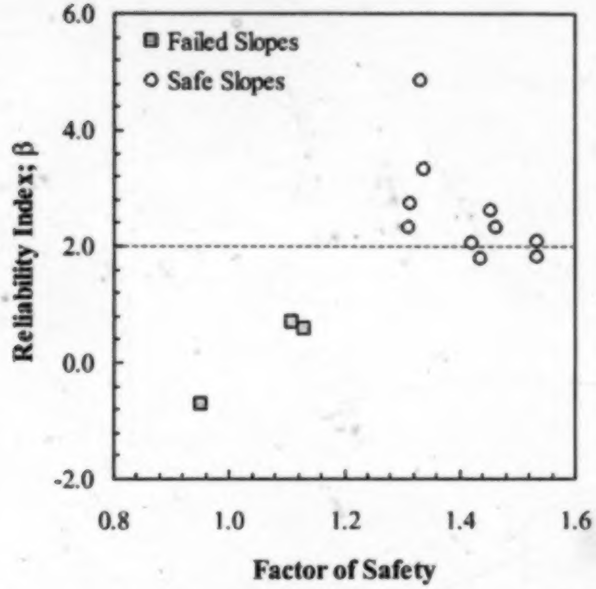

Figure 12–6 Reliability Index versus factor of safety – Proposed Methodology

Figure 12–7 is a plot of the probability of unsatisfactory performance versus reliability index; the higher the reliability index, the lower the probability of unsatisfactory performance. The plot, however, shows that the reliability index is less sensitive to changes in design than the probability of unsatisfactory performance. An increase in the reliability index from 1.8 to 3.3, corresponds to more than two orders of magnitude difference in the probabilities of unsatisfactory performance. The reliability index is, however, more stable than the probability of unsatisfactory performance, particularly when estimating very small probabilities (less than, say, $1\text{x}10^{-3}$). In such cases, the level of noise in the computations may affect the precision of the calculated probability. For example, a probability of unsatisfactory performance of $1\text{x}10^{-4}$, implies that a simulation with 30,000 iterations will have only 3 iterations with factors of safety less than one. Because of the randomness of the simulation process, other simulations may yield, for example, zero, 6 or even larger number of iterations with factors of safety less than one. The level of noise (0 to $2\text{x}10^{-4}$) is comparable or higher than the probability being estimated ($1\text{x}10^{-4}$) which, inevitably, reduces the precision of the analysis. The precision of the computed probability could be improved by substantially increasing the number of iterations (probably to a minimum of 250,000 iterations). This, however, translates into a need for higher computing capabilities beyond those of spreadsheet-based simulation software, and a much longer computer time. It is, thus, recommended to use the two indices (probability of unsatisfactory performance and reliability index) together in judging the adequacy of a slope design.

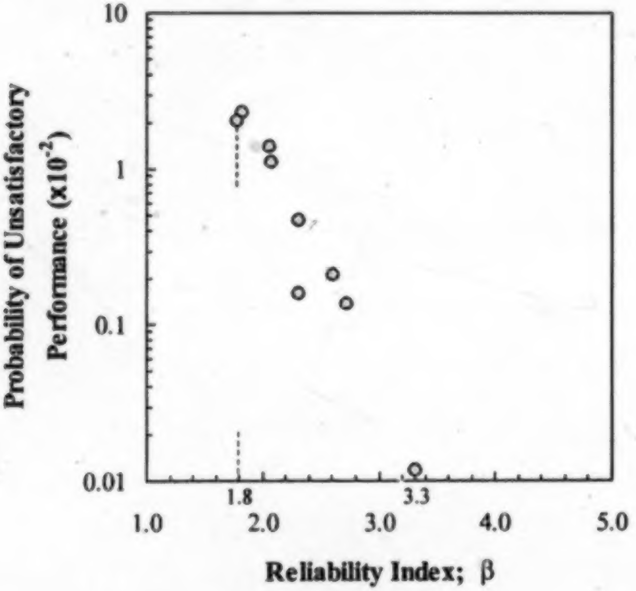

Figure 12–7 Probability of unsatisfactory performance versus reliability index; Safe Slope – Proposed Methodology

If the probability distribution of the factor of safety is normally distributed, the probability of unsatisfactory performance is analytically related to the reliability index as follows;

$$P_u = \Phi(-\beta) \qquad (12\text{-}1)$$

where Φ( ) is the cumulative probability distribution of a standard normal density function. Figure 12–8 is a plot of reliability index versus probability of unsatisfactory performance for all the undertaken analyses. The theoretical relation given by Equation 12-1 above is plotted on the same graph. The figure indicates that the probability of unsatisfactory performance is uniquely related to the reliability index regardless of the assumptions involved in the analysis. The relation is close to Equation 12-1 only when the probability of unsatisfactory performance is high. As the probability decreases (i.e., reliability index increases), the gap between the two relations widens. In the absence of any information about the shape of the probability density function of the factor of safety (e.g., FOSM analysis), the probability of unsatisfactory performance is estimated based on an assumed shape; commonly a normal distribution. Figure 12–8 suggests that the normality assumption overestimates the probability of unsatisfactory performance, particularly if it is small, i.e., safe slopes.

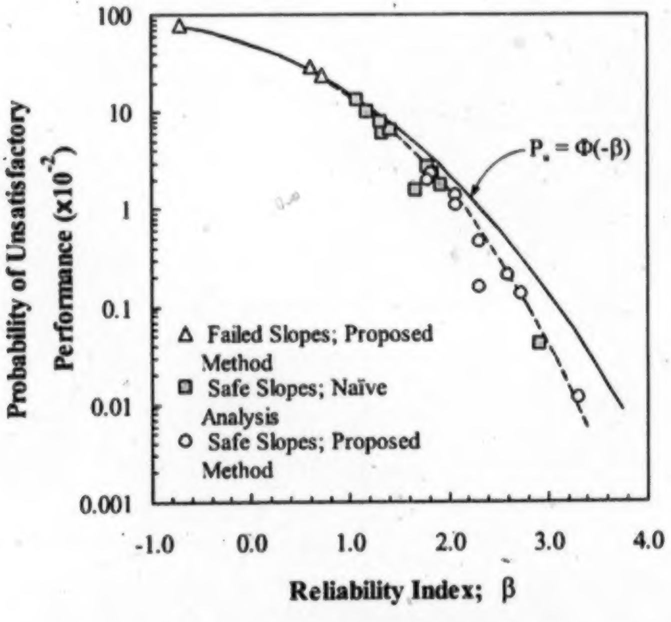

Figure 12–8 Relationship between probability of unsatisfactory performance and reliability index

6. INSIGHTS OF PRACTICAL VALUE

6.1 Probabilistic Versus Deterministic Slope Analyses

Figure 12–9a is a plot of the probability of unsatisfactory performance versus the factor of safety for the safe slopes only. The plot clearly illustrates the limitation of conventional slope practice. For example, the Lodalen slope designed for a factor of safety of 1.33 has a near zero probability of unsatisfactory performance whereas the Congress Street Cut designed for a factor of safety of 1.44 has a probability of unsatisfactory performance of $2\text{x}10^{-2}$. In other words, the slope designed for a lower factor of safety is safer than that designed for a higher factor of safety. Such inconsistency is a direct result of ignoring uncertainty; the input parameters of the Lodalen slope are highly reliable whereas those of the Congress Street Cut are highly unreliable. The traditional assumption of higher safety levels with the increase in the factor of safety (ignoring uncertainty) is, thus, not always valid.

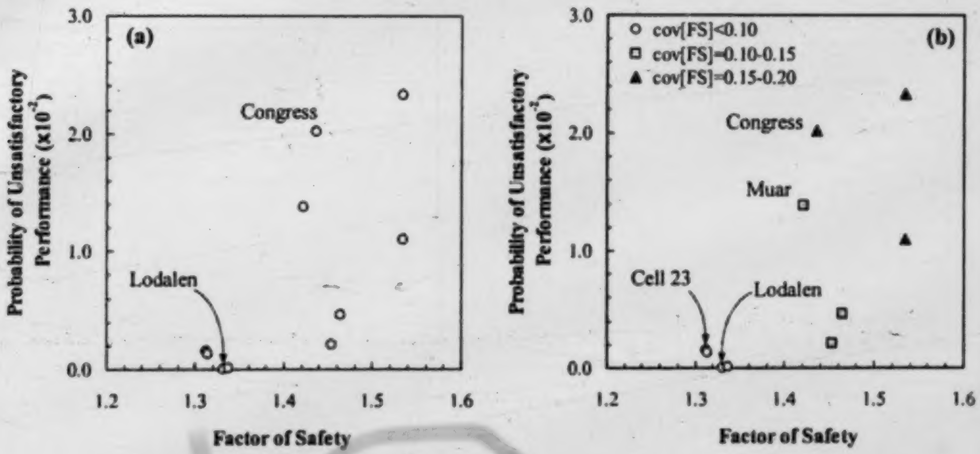

Figure 12–9 Probability of unsatisfactory performance versus factor of safety; Safe Slopes – Proposed Methodology (data are grouped by the coefficient of variation of the factor of safety in the right plot)

Lacasse and Nadim (1996) reached a similar conclusion analyzing a pile foundation. The heavily loaded pile, installed in 1976, was re-analyzed in 1989 after a new site investigation and an assessment of the environmental and gravity loads were completed. The original design had a factor of safety of 1.79 and a failure probability of 5×10^{-3}, whereas those of the 1989 analysis (based on the new data) were 1.4, and 1×10^{-4}, respectively. Although the pile had a factor of safety less than what was perceived at the time of design, it is, in fact, safer. The added information led to a lower factor of safety, but also reduced the uncertainty in the load and resistance and improved the reliability of the analysis.

Figure 12–9b sheds some light on the handling of uncertainty in the current deterministic design practice. The plot is the same as Figure 12–9a, except that the data are grouped by the coefficient of variation of the factor of safety. The coefficient of variation is the ratio of the standard deviation to the mean value and is a measure of the uncertainty of the mean; the higher the coefficient of variation the less reliable the mean is. It is, thus, an expression of the level of overall uncertainty involved in the analysis. As the confidence in the input parameters and site conditions decreases (i.e., higher uncertainty), conventional slope practice resorts, judgmentally, to a higher factor of safety and a presumably more conservative design. A critical question, however, arises. How conservative is conservative enough? Without formally accounting for uncertainty, that question cannot be answered and the impact of a subjective conservatism can never be known. Figure 12–9b shows that all the slopes involving high uncertainty (e.g., Congress Street cut, Muar trial embankment) are in fact less reliable than those involving small uncertainty (e.g., Lodalen slope, Syncrude tailings dyke) even though they are designed for higher factors of safety. The factor of safety alone can give a misleading sense of safety and is not a sufficient safety indicator.

6.2 Sensitivity Analysis

The results of sensitivity analyses, in terms of Spearman rank correlation coefficients, are of significant practical value. The analysis quantifies the contributions of the uncertainty of the input variables to the overall design uncertainty. As a result, resources, whether intellectual or physical, can be rationally allocated towards reducing the uncertainty of the variables with the largest impact on design. The relative impacts of systematic uncertainty and uncertainty due to inherent spatial variability can also be inferred from the sensitivity analysis results. This information is of interest. Systematic uncertainty has a consistent effect at all locations within the domain of the problem (i.e., no spatial averaging). It, thus, could have a major impact on design. Unlike the uncertainty due to inherent spatial variability, systematic uncertainty can be reduced (e.g., by increasing the number of data, avoiding highly uncertain empirical correlations and factors, etc.). If the analysis is dominated by systematic uncertainty, that implies a high potential for improving design reliability with relative ease. Furthermore, a dominant role of systematic uncertainty indicates a smaller effect of spatial variability and, consequently, a lesser impact of the assumption of the autocorrelation distance on the probability of unsatisfactory performance.

The sensitivity analyses undertaken throughout this study indicate that the uncertainty of the Bjerrum vane correction factor is substantial and may even exceed the uncertainty due to the spatial variability of the undrained shear strength. The results of these analyses, actually, quantify the concerns raised by researchers (Milligan, 1972; Schmertmann and Morgenstern, 1977) about the reliability of Bjerrum's vane correction factor. They also warn about the use of various empirical factors and correlations (e.g., empirical correlations between strength parameters and SPT blow counts or CPT tip resistance) without proper understanding of their limitations and, more importantly, their reliability.

7. PROBABILISTIC SLOPE DESIGN GUIDELINES

Assessing and quantifying uncertainty is the first and most crucial step in any probabilistic analysis. The designer should seek all possible means to reduce uncertainty to as low as reasonably achievable. This includes gearing the site investigation towards a better characterization of highly variable parameters with large impact on design, examining the validity and limitations of any empirical factors/correlations used in the analysis and seeking expert opinions in assigning subjective uncertainty values. It also includes minimizing human uncertainty by applying adequate quality control measures to ensure that sound engineering is being practiced.

The discussions in the preceding sections reveal some valuable design guidance. First, the safety condition of a slope as portrayed by the factor of safety alone is incomplete and an apparently conservative design is not always safer. Second, by quantifying design reliability, a probabilistic stability analysis provides an enhanced picture of the state of the slope and allows a more consistent design criterion. Slopes designed to the same probability of unsatisfactory performance have comparable safety levels; which is not necessarily the case with slopes designed to the same factor of safety. Third, a probability of unsatisfactory performance of 2×10^{-2} marks the upper limit of what is deemed acceptable practice. It is analogous to a minimum reliability index of about 2.0. The use of the two indices together to judge the adequacy of a design in a probabilistic assessment is recommended.

Slope design is based on two criteria; failure prevention and serviceability. The probabilistic analyses in this study are based on limit equilibrium models and are, therefore, concerned with failure only. Adopting a probabilistic design criterion of 2×10^{-2}, the Lodalen slope can be designed to a factor of safety as low as 1.15 (3.25h:1v). That geometry is unlikely to collapse, however, experience suggests that the serviceability of the slope could be largely compromised as a result of excessive deformations. There is, therefore, a need to empirically set a minimum design factor of safety as a means of controlling deformations. A more rational approach, however, is to develop alternative analyses, deterministic and probabilistic, to better understand and control slope movements. Future research may, for example, investigate the value and practicality of a probabilistic assessment of the pattern and magnitude of deformations. Stochastic finite element analysis is a powerful promising tool that has been widely applied to estimate the probability of settlement of shallow foundations (Baecher and Ingra, 1981; Zeitoun and Baker, 1992; Paice et al., 1994). In slope engineering, Kraft and Mukhopadhyay (1977) made an isolated attempt to account for deformations by formulating the performance function of the slope in terms of crest movement. They defined the probability of failure as the probability of crest movement exceeding a prescribed allowable percentage of slope height. The details of their work, however, are not clear.

Other serviceability considerations (e.g., surface erosion, extensive seepage) should also be considered. Judging the adequacy of a slope design is, thus, governed by a failure criterion, a serviceability criterion and failure consequences.

Table 12-1 Summary of the results of probabilistic slope stability analyses; Safe Slopes – Proposed Methodology

Case Study	Slope Geometry		Factor of Safety				Probability of Unsatisfactory Performance (10^{-2})		Reliability Index; β	Variance Reduction Factor; f④	Type of Analysis
	Angle① (deg.)	Height (m)	E[FS]	σ[FS]	c.o.v.②	Skewness③	$E[P_u]$	$\sigma[P_u]$			
James Bay; Design 1	7.4	12.0	1.46	0.20	0.14	0.30	0.47	0.04	2.32	0.37	Total Stress
James Bay; Design 2	18.4	6.0	1.54	0.29	0.19	0.36	2.33	0.06	1.82	1.0	Total Stress
Syncrude Dyke; Cell 23	8.4	44.3	1.31	0.14	0.10	0.59	0.16	0.02	2.31	0.43	Effective Stress
Lodalen Slope	14.0	17.0	1.33	0.07	0.05	0.01	0.00	0.00	4.85	0.24	Effective Stress
Muar Trial Embankment	26.6	3.3	1.42	0.20	0.14	0.23	1.38	0.05	2.07	0.61	Total Stress
Congress Street Open Cut	20.8	14.3	1.44	0.24	0.17	0.52	2.02	0.07	1.78	0.44	Total Stress
Cho Yiu Estate	29.4	12.8	1.54	0.26	0.17	0.35	1.10	0.07	2.08	0.33	Effective Stress

① Overall slope angle (including berms, change in slope, ….)

② Coefficient of variation

③ Coefficient of Skewness

④ Computed for the variable with the largest contribution to the uncertainty of the factor of safety

Table 12-1 Summary of the results of probabilistic slope stability analyses; Safe Slopes – Proposed Methodology (cont'd)

Case Study	Slope Geometry		Factor of Safety				Probability of Unsatisfactory Performance (10^{-2})		Reliability Index; β	Variance Reduction Factor; f④	Type of Analysis
	Angle① (deg.)	Height (m)	E[FS]	σ[FS]	c.o.v.②	Skewness③	$E[P_u]$	$\sigma[P_u]$			
Ching Cheung Road	35.6	30.4	1.31	0.12	0.09	0.25	0.13	0.02	2.73	0.17	Effective Stress
Tsing Yi (1) Slope	26.6	51.7	1.34	0.10	0.08	0.21	0.01	0.01	3.32	0.09	Effective Stress
Shek Kip Meí Slope	31.2	20.8	1.45	0.17	0.12	0.24	0.21	0.02	2.61	0.23	Effective Stress

① Overall slope angle (including berms, change in slope, ...)

② Coefficient of variation

③ Coefficient of Skewness

④ Computed for the variable with the largest contribution to the uncertainty of the factor of safety

Table 12-2 Summary of the results of probabilistic slope stability analyses; Failed Slopes – Proposed Methodology

Case Study	Slope Geometry		Factor of Safety				Probability of Unsatisfactory Performance (10^{-2})		Reliability Index; β	Variance Reduction Factor; *f* ④	Type of Analysis
	Angle① (deg.)	Height (m)	E[FS]	σ[FS]	c.o.v.②	Skewness③	$E[P_u]$	$\sigma[P_u]$			
Lodalen Slide	26.6	17.0	0.95	0.06	0.07	0.02	77.38	0.24	-0.72	0.39	Effective Stress
Muar Trial Embankment	26.6	4.7	1.11	0.15	0.14	0.16	24.05	0.24	0.72	0.54	Total Stress
Congress Street Open Cut	34.0	14.3	1.13	0.22	0.19	0.63	29.11	0.22	0.60	0.67	Total Stress

① Overall slope angle (including berms, change in slope, ...)

② Coefficient of variation

③ Coefficient of Skewness

④ Computed for the variable with the largest contribution to the uncertainty of the factor of safety

Table 12-3 Summary of the results of probabilistic slope stability analyses; Safe Slopes – Naïve Analysis

Case Study	Slope Geometry		Factor of Safety				Probability of Unsatisfactory Performance (10^{-2})		Reliability Index; β	Type of Analysis
	Angle① (deg.)	Height (m)	E[FS]	σ[FS]	c.o.v.②	Skewness③	$E[P_u]$	$\sigma[P_u]$		
James Bay; Design 1	7.4	12.0	1.46	0.25	0.17	0.32	2.37	0.09	1.84	Total Stress
James Bay; Design 2	18.4	6.0	1.54	0.30	0.20	0.34	2.70	0.06	1.78	Total Stress
Syncrude Dyke; Cell 23	8.4	44.3	1.31	0.19	0.14	0.86	1.60	0.07	1.66	Effective Stress
Lodalen Slope	14.0	17.0	1.33	0.11	0.09	-0.01	0.04	0.01	2.93	Effective Stress
Muar Trial Embankment	26.6	3.3	1.42	0.22	0.16	0.33	1.80	0.07	1.92	Total Stress
Congress Street Open Cut	20.8	14.3	1.44	0.33	0.23	0.84	6.05	0.09	1.33	Total Stress
Cho Yiu Estate	29.4	12.8	1.53	0.38	0.25	0.42	6.53	0.09	1.42	Effective Stress

① Overall slope angle (including berms, change in slope, ….)

② Coefficient of variation

③ Coefficient of Skewness

Table 12-3 Summary of the results of probabilistic slope stability analyses; Safe Slopes – Naïve Analysis (cont'd)

Case Study	Slope Geometry		Factor of Safety				Probability of Unsatisfactory Performance (10^{-2})		Reliability Index; β	Type of Analysis
	Angle① (deg.)	Height (m)	E[FS]	σ[FS]	c.o.v.②	Skewness③	$E[P_u]$	$\sigma[P_u]$		
Ching Cheung Road	35.6	30.4	1.31	0.27	0.20	0.55	10.27	0.10	1.18	Effective Stress
Tsing Yi (1) Slope	26.6	51.7	1.34	0.32	0.24	0.57	13.22	0.17	1.07	Effective Stress
Shek Kip Mei Slope	31.2	20.8	1.46	0.35	0.24	0.47	8.04	0.10	1.31	Effective Stress

① Overall slope angle (including berms, change in slope, ...)

② Coefficient of variation

③ Coefficient of Skewness

CHAPTER 13

TOWARDS A QUANTITATIVE RISK ANALYSIS FOR SHEK KIP MEI SLOPE

Estimating the probability of unsatisfactory performance of a given slope is by itself a major step ahead of the traditional deterministic factor of safety. However, it still falls short of addressing the totality of the landslide problem. Without addressing failure consequences, the risk assessment would remain incomplete. The failure consequences of a large slope in a densely populated area are clearly different from those of a small slope in a remote location, although they could have similar probabilities of unsatisfactory performance. By combining hazard frequency and failure consequence, quantitative risk analysis (QRA) provides a rational basis for judging the acceptability of a slope. In this chapter, a site-specific QRA is undertaken to assess the landslide risk of the re-designed (i.e., acceptable) Shek Kip Mei slope (Section 3.4.8 and Figure 11-41, Chapter 11). In line with the objectives listed in Chapter 1, the analyses presented here illustrates the use and value of the probability of unsatisfactory performance as an input to site-specific QRA studies. The assessment is focused entirely on estimating the risk of loss of life for the residents of Block 36 at the foot of the slope. The risks of injury, property loss or environmental damage are not considered. The following sections describe the analyses undertaken and the logic behind the judgements made.

1. OBSERVATIONS RELEVANT TO THE ANALYSIS

The failure of the Shek Kip Mei slope is described in detail in the report prepared by Fugro Maunsell Scott Wilson Joint Venture (FMSW, 2000). A summary focusing on the technical factors contributing to the failure is presented in Chapter 11. The observations and surroundings relevant to the risk analysis are extracted from FMSW

(2000) report and summarized below. They are deemed applicable to the assessment of the risk associated with the modified (i.e., acceptable) slope geometry.

- The slope is located to the rear of a residential building (Block 36). The building is about 54m x 10m, with the longitudinal direction parallel to the slope. The building is 6 floors high and is situated only 5m from the toe of the slope. No information was available on the number of residents in the building.
- The width of the landslide was about 37m; nearly 1.75 times the height of the slide (i.e., height difference between the highest point on the scarp and the slide toe point).
- The timing of the slide (morning of August 25, 1999) and the absence of any water-carrying services suggested that it was triggered by the rainstorm of August 21-25. The return period of the storm was estimated to be 31 years. It should be noted that estimating the return period of a storm in relation to a landslide incident is a difficult task because of the possible role of antecedent rainfall in triggering the slide.
- The mobility of the displaced mass was limited and most of the material remained on the slope. Nonetheless, the detachment and collapse of localized areas on the slope resulted in relatively mobile material.
- Numerous signs of slope distress were observed which prompted the Geotechnical Engineering Office of Hong Kong to order the evacuation of Block 36.
- The interaction between the northern and southern parts of the slope is, apparently, small. The failure modes of the two parts were markedly different and no evidence of a subsequent failure triggered by initial instability was observed. The different local geological and hydrological conditions in the two sections are probably the main factors behind that lack of interaction.

2. RISK ANALYSIS

A brief overview of QRA methods and types is presented in Chapter 2. Because of its ability to account for a high level of detail, event tree analysis is considered the most suitable technique for site-specific QRA studies. Care should be taken, however, that the level of detail corresponds to the amount of data available. The precision of a highly detailed analysis based on limited data could be misleading. Exercising engineering judgment and subjective assessment of some of the inputs to the risk analysis (particularly consequence assessment) is almost inevitable. By breaking down the risk analysis into a number of simpler scenarios, event trees greatly facilitate the exercising of transparent and consistent judgment. Wong et al. (1997) pointed out that subjective estimates are naturally open to debate. The division of the problem into a number of elementary components also reduces the scope of debate, as all the assumptions made may not be in dispute, and facilitates more effective communication and discussion of the assessors' judgments.

An event tree analysis is undertaken to demonstrate the implementation of a site-specific QRA study for the Shek Kip Mei slope. Only the risk of loss of life is considered in the assessment. Three different hazards are identified as described in Section 2.1. For each hazard, an event tree comprising a number of possible scenarios relevant to the failure of the Shek Kip Mei slope is prepared and the frequency of each scenario is estimated. The analysis addresses the temporal variability of the elements at risk, the development of signs of slope distress, the efficiency of warning and emergency response measures, the travel distance of the debris and the amount of protection offered by the building. The structure of the event tree is described in Section 2.2 and illustrated in Figure 13–4, Figure 13–5 and Figure 13–6 at the end of the chapter. The likely consequence of each event tree scenario is obtained based on estimates of the number and vulnerability of the people at risk, as described in Section 2.3.

It should be noted that not all the information needed for the analysis was available and some assumptions had to be made (e.g., number of residents in Block 36, type of structure of the building). An effort is made to ensure that these assumptions are reasonable and not entirely arbitrary.

2.1 Hazard Assessment

Hazard assessment includes hazard identification and frequency estimation. As outlined in Chapter 11, only slides are considered in this study. Other failure modes (e.g., liquefaction, washout) are not taken into account. As such, the estimated risk (Section 2.4) should be regarded as a lower bound to the total risk of slope failure.

Three hazards are addressed in this assessment. All are sliding shear failures but of different scales. Each hazard refers to one of the slip surfaces shown in Figure 11-41 of Chapter 11. Table 13-1 summarizes the hazards considered in the analysis. The volume of the slide is estimated on the assumption that the width is 1-2 times the height. In estimating the probabilities of unsatisfactory performance of these hazards (Chapter 11), time was not a factor. In other words, the pore pressure conditions considered in the analysis are assumed to prevail at all times. In reality, those pore pressures are a result of the rainstorm of August 21-25, 1999, which has an estimated return period of 31 years. The annual probability of each hazard (Table 13-1) is, thus, the product of the probability of unsatisfactory performance and the annual frequency of the triggering rainstorm (3.2×10^{-3}).

Table 13-1 Hazards addressed in risk analysis - Shek Kip Mei slope

Hazard No.	Description	Failure Height (m)	Estimated Slide Volume (m^3)	Slip ① Surface No.	Hazard Probability (per year)
1	Deep-seated failure involving total height of slope	20.8	2500-5000	1	0.67×10^{-4}
2	Shallow failure involving 70% of slope height	14.6	300-600	2	2.72×10^{-4}
3	Shallow localized failure at the top of the slope	4.5	25-50	3	1.96×10^{-3}

① Refer to Figure 11-41, Chapter 11

2.2 Event Tree Development

2.2.1 Time Of The Day

The time of the landslide as used in the analysis refers to the day or night, rather than the absolute time. The probabilities of the slide occurring during the day or night are intuitively similar and equal to 0.5. The consequences of failure could, however, be markedly different. Given that signs of slope distress occur, the effectiveness of warning measures and the efficiency of emergency response (e.g., evacuation of the building) are largely reduced during the night compared to the daytime. More importantly, the number of building occupants (i.e., elements at risk) varies significantly between the day and night.

2.2.2 Signs of Slope Distress/Warning and Response Measures

The failure of the original geometry of Shek Kip Mei slope did not occur suddenly and numerous signs of slope distress were noted (Section 1). Block 36 was evacuated in response to these signs. It is judged that the same scenario is likely to happen, should the modified geometry also fail. The development of signs of slope distress is judgmentally assigned a probability of occurrence of 0.85. The probability of effective warning and evacuation measures is 0.80 during the daytime. The darkness of the night is, however, likely to hinder these efforts. The probability of an efficient warning and emergency response is reduced to 0.50 during the night. In the absence of signs of slope distress prior to failure, i.e. sudden collapse of the slope, the probability of an effective warning and emergency response is considered zero.

2.2.3 Travel of Displaced Material

The travel distance of landslide debris defines the extent of the area affected by the slide and is, thus, one of the most important factors in assessing the failure consequences. The travel of the debris is governed by factors such as slope height and gradient, type of soil forming the slope, failure mode, scale of failure, degree of disintegration of the failed mass during movement, amount of water in the debris and the gradient of the downslope area. Given the complexities in quantifying these factors, predicting the debris travel distance is an extremely difficult task.

Based on the large and detailed database of slope failure incidents in Hong Kong, Wong and Ho (1996) and Wong et al. (1997) established empirical correlations between the landslide volume and the apparent angle of friction for different failure modes. The apparent angle of friction is the inclination of the line joining the tip of the displaced material and the crown of the slide. For practicality, Wong et al. (1997) used the inclination of the line joining the slope crest and the tip of the debris (travel angle) to describe the travel distance. They commented that most slope failures in Hong Kong are shallow and the travel angle tends to be very close to the apparent angle of friction. The database of rain-induced sliding failures gathered by Wong et al.(1997) is used in this study to assess the likely ranges of the debris travel angle for the hazards identified in Section 2.1.

Based on the estimated failure scale, three travel angles are assigned for each hazard to account for the uncertainty of travel distance predictions. The probability of each travel angle is evaluated judgmentally based on the database of Wong et al. (1997) and the field observations of debris mobility at Shek Kip Mei slide (Section 1). For Hazard No. 1, a travel angle in the range of 25-30 degrees is considered reasonable. The corresponding outward movements at the toe of the slope are in the range of 10m to 2m, respectively, which are consistent with the observed low mobility of the failed mass (Section 1). Because of the large volume of failure, there is a small chance that the mobility of the debris may increase by the break up of the failed material during movement. A travel angle of 20 degrees is also considered. Three travel angles, 20, 25 and 30 degrees, are taken into account in the event tree with respective probabilities of 0.05, 0.55 and 0.40. Figure 13–1 shows the limit of debris run-out for each scenario.

For Hazard No. 2 (landslide volume of 300-600m^3), the database of Wong et al. (1997) suggests a travel angle in the range of 30-40 degrees. Since the overall slope angle is only 33 degrees, the upper values in that range are not applicable (travel angle cannot be steeper than the slope angle). Three travel angles are considered in the analysis; 25, 30 and 32.5 degrees. The latter 2 values represent the most likely angles and are assigned probabilities of 0.60 and 0.35, respectively. The 25 degrees angle is considered unlikely and assigned a low probability of 0.05.

The travel angles adopted for Hazard No. 3 (localized failure) are 30, 32.5 and 35 degrees. The 35 degrees angle implies that the debris is immobile. Based on the field observations of Section 1 (debris from localized failures was relatively mobile), it is considered unlikely and assigned a low probability of 0.10. The 30 and 32.5 degrees angles are thought to be the most probable values and assigned probabilities of 0.35 and 0.55, respectively. The selected travel angles and the corresponding probabilities are shown on the event tree branches in Figure 13–4, Figure 13–5 and Figure 13–6 for Hazards 1, 2 and 3, respectively.

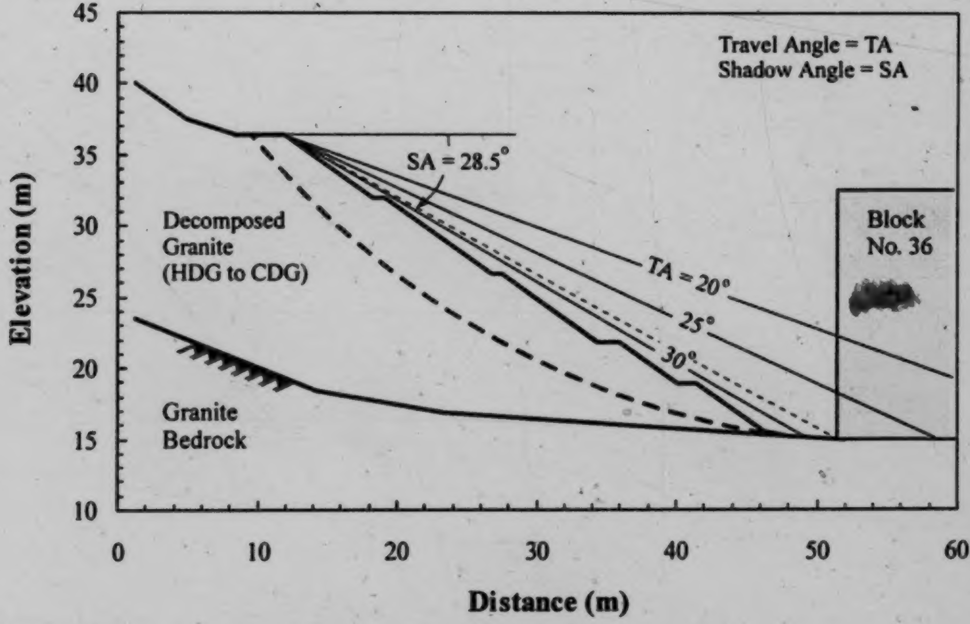

Figure 13–1 Limits of landslide debris run-outs for Hazard No. 1 relative to the location of Block 36

2.2.4 Effect of Failure on Block 36

Should failure occur, the probability of death and the number of people at risk depend largely on the effect of the slide on the nearby residential building, Block 36. In other words, the interaction between the debris and the structure at risk. Three scenarios are considered; the building collapses under the impact of the debris, the building does not collapse but the debris enters into the ground floor and the building withstands the impact and suffers no damage. The likelihood of each scenario is a function of the scale of failure, debris travel angle, impact energy and building structure. The proximity of a facility to the slide could be expressed in terms of the "shadow angle" (Wong et al., 1997). It is defined as the inclination of the line joining the crest of the slope and the toe of the facility. For Block 36, the shadow angle is about 28.5 degrees. Comparing the shadow angle with the debris travel angles, Figure 13–1, suggests that damage to Block 36 can only be attained as a results of an impact by debris with a travel angle less than 30 degrees. No information is available about the structure of Block 36. However, it is judged that the building is likely to collapse under the impact of a large volume (massive failure) of highly mobile debris (travel angle of 20 degrees). Slides with debris travel angles higher than 30 degrees are assumed to have no effect on the building. The probabilities of the three postulated scenarios are evaluated judgmentally based on the debris travel angle, the shadow angle and the size of the slide. The proposed values are indicated on the branches of the event trees in Figure 13–4, Figure 13–5 and Figure 13–6.

2.3 Consequence Assessment

2.3.1 Number of People at Risk

The first step in assessing failure consequences is to evaluate the number of people endangered by the slide (i.e., elements at risk), should it occur. That number largely depends on the time of failure (i.e., day or night) as well as the portion of the building affected by the debris. For example, if the building collapses, all the residents present at the time of failure are at risk. On the other hand, if the building did not collapse but the debris enters the building, only those residents in the ground floor are at risk. For

Hazards No. 2 and 3 (major and minor failures), the amounts of debris are limited and only portions of the ground floor (e.g., equal to the width of the slide) would be affected by the slide.

In the absence of any information regarding the number of residents in Block 36, the assessment is based on an assumed population density of 0.05 person/m^2 per floor. The same figure was used by ERM (1996) in assessing the risks from boulder falls in 4 study areas in Hong Kong. As mentioned in Section 1, the building comprises 6 floors. Only 25% of the residents are assumed to be present during the daytime. The number of people at risk for each event tree scenario is estimated and shown next to the tree branch in Figure 13–4, Figure 13–5 and Figure 13–6.

2.3.2 Probability of Death

Having estimated the number of people at risk, the next step is to estimate their vulnerability, or the probability of death. It refers to the likelihood of an occupant of Block 36 being killed as a result of the landslide debris striking the building. The probability value is governed primarily by the extent of damage to the building (e.g., building collapse, debris entering ground floor without the building collapsing) and the volume of landslide debris (i.e., failure scale). There are no technical means, yet, to estimate the probability of death and it is solely based on judgment. ERM (1999), however, indicated that past incidents of total building collapse in Hong Kong involved a high mortality rate of possibly 90% or higher of building occupants. DNV (1996) exercised their judgement in estimating the probability of death for a number of event tree scenarios resembling the impact of landslide debris on a wide range of facilities (road, footpath, squatter, building, …) situated at the toe of the slope. Likewise, the probabilities of death in this assessment are estimated judgmentally. Reference is made, however, to the DNV (1996) study. The adopted probabilities of death are summarized in Table 13-2.

Table 13-2 Probability of death of occupants of Block 36 – Shek Kip Mei slope

Hazard No.	Failure Scale (m^3)	Effect on Building	Probability of Death
1	2500-5000	• Building Collapses • Debris enters building • No impact on Building	1.0 0.6 0.0
2	300-600	• Building Collapses • Debris enters building • No impact on Building	0.7 0.4 0.0
3	25-50	• Debris enters building • No impact on Building	0.1 0.0

2.4 Risk Estimation

The risk of loss of life from a sliding failure of the Shek Kip Mei slope is evaluated in terms of the societal risk to the residents of Block 36 (i.e., population at risk). Figure 13–4, Figure 13–5 and Figure 13–6 show the event tree analysis and the consequence assessment for hazards 1 to 3, respectively. The outcome of the analysis is an estimate of the frequency of occurrence of each event tree scenario, f, and the corresponding expected number of fatalities, N. For example, Scenario No. 15 in Figure 13–4 (collapse of Block 36 following an impact by a moderately mobile debris resulting from a sudden massive slope failure during the daytime) has a frequency of occurrence of 6.94×10^{-7} per year and an expected number of fatalities of 40.5 persons. The number of fatalities is obtained by multiplying the number of people at risk by the probability of death. The frequency of occurrence of each of the estimated fatality figures is the product of the probabilities of all the relevant tree branches. The analysis is performed using an Excel spreadsheet. The computations are, thus, fully automated. This greatly facilitates updating the analysis upon obtaining additional information or examining its sensitivity to any input parameter.

The computed societal risk is presented in two forms; the potential loss of life (PLL) and the F-N curve. The potential loss of life is the average annual fatality rate associated with the failure of Shek Kip Mei slope. It is equal to the summation of the products of the frequency of occurrence and the number of fatalities for all scenarios for all hazards. For the Shek Kip Mei slope, the PLL is estimated to be 8.08×10^{-4} per year. A break down of this figure is illustrated in Table 13-3. The risk of loss of life as a result of a massive slope failure (Hazard No. 1) represents 95% of the total risk whereas the risk associated with a minor failure (Hazard No. 3) is almost zero. Also, the risks associated with the scenarios involving the collapse of Block 36 during the night is about 5.71×10^{-4} per year; nearly 71% of the total PLL.

Table 13-3 Annual potential loss of life (PLL) as a result of a sliding failure of the Shek Kip Mei Slope

Hazard		**Potential Loss of Life for All Event Tree Scenarios**		**Potential Loss of Life Due to Building Collapse during night (per year)**
No.	**Description**	**PLL (per year)**	**% of Total**	
1	Massive Failure (2500-5000 m^3)	7.67×10^{-4}	94.9	5.49×10^{-4}
2	Major Failure (300-600 m^3)	4.08×10^{-5}	5.1	2.21×10^{-5}
3	Minor Failure (25-50 m^3)	0.00	0.0	0.00
Total =		8.08×10^{-4}		5.71×10^{-4}

The F-N curve is a plot of the frequency of occurrence of N or more fatalities (i.e., cumulative frequency), F, versus the number of fatalities, N. It is computed by summing all the frequencies corresponding to event tree scenarios (Figure 13–4 to Figure 13–6) with a number of fatalities equal to or more than N. Figure 13–2 shows the F-N curves of Hazards 1 and 2 (Hazard No. 3 has zero fatalities). There is more than an order magnitude difference between the two curves. Figure 13–3 shows the F-N curve of the total risk due to Hazards 1, 2 and 3. The calculated risk figures and F-N plots are discussed in more detail in Section 3.

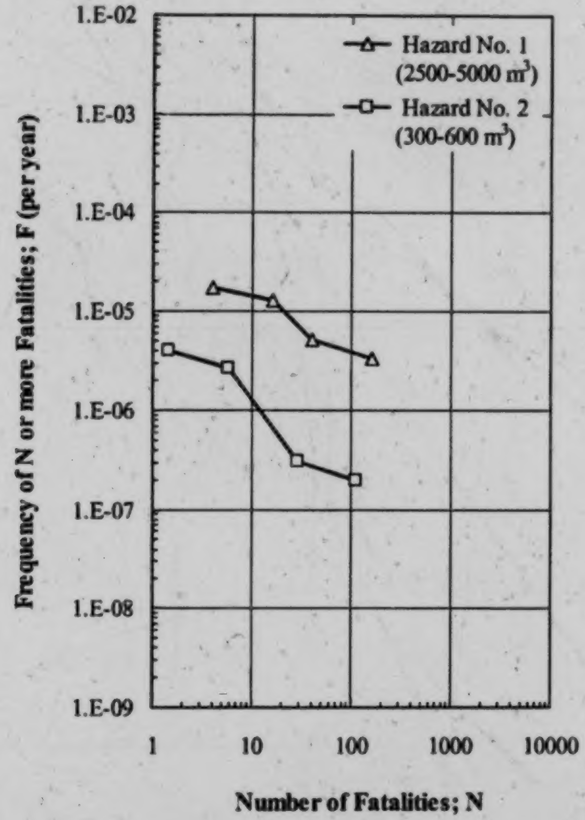

Figure 13–2 Calculated F-N curves for Hazards Nos. 1 and 2 - Shek Kip Mei slope

3. SUMMARY AND DISCUSSION

The risk of loss of life as a result of the failure of the Shek Kip Mei slope is assessed. The analysis accounts for one failure mode only; sliding failure triggered by rainfall. As such, the estimated risk figures should be regarded as a lower bound to the total risk. Three hazards are considered in the analysis based on the failure scale; massive failure (2500-5000 m^3), major failure (300-600 m^3) and minor failure(25-50 m^3). The assessment takes into account the annual frequency of each hazard, the temporal and spatial distribution of the population at risk, the development of signs of slope distress prior to failure and the efficiency of emergency response system. It also addresses the travel distance of the debris, the degree of protection offered by the building structure and the number of people at risk. The total potential loss of life is estimated to be 8.08x10^{-4} per year and the total F-N curve for the 3 hazards addressed is shown in Figure 13–3.

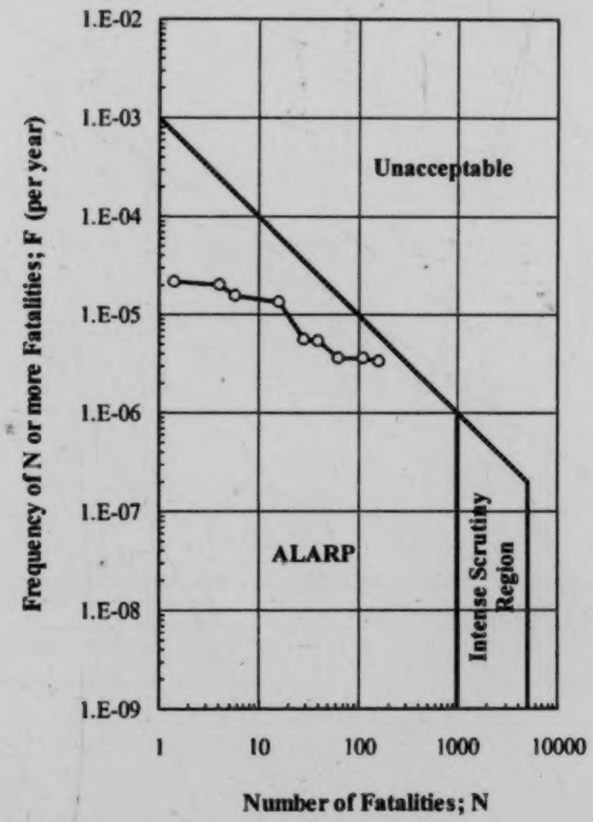

Figure 13–3 Calculated F-N curve for sliding failure of Shek Kip Mei slope and the ERM (1999) risk acceptance criteria

The F-N curves for Hazard No. 1 (Figure 13–2) and the total risk (Figure 13–3) are very similar, in fact they could not be plotted on the same graph because they almost coincide with each other. This indicates that the majority of the total risk is attributed to Hazard No. 1. This is also evident from examining the estimated values of the potential loss of life. The PLL of Hazard No. 1 constitutes 95% of the total value whereas the contributions of Hazards 2 and 3 are 5% and 0%, respectively. This supports the argument made in Chapter 11 that the high probability of unsatisfactory performance of the minor failure should not be the governing criterion for designing the slope as a whole. Instead, local stabilization techniques could be used if the risks associated with a minor failure are deemed high. The consequence assessment is dominated by one scenario; the collapse of Block 36 during the night, which contributes almost 71% of the total PLL. Despite its small frequency of occurrence (3.58×10^{-6} per year; a return period of 279,000 years), the expected high level of fatalities has largely magnified the contribution of such a rare scenario to the total risk.

A rigorous assessment of the acceptability of the estimated risk is beyond the scope of the study. However, some general comments ought to be made. The interim risk criteria for landslides and boulder falls from natural terrain proposed by ERM (1999) and Reeves et al. (1999) is compared to the F-N curve of the total risk as shown in Figure 13–3. The F-N curve falls within the ALARP (as low as reasonably practicable) region. This means that the risk level is tolerable; however, practical risk mitigation measures need to be considered and evaluated in a cost-benefit analysis. If such measures are proved to be cost effective, they should be implemented.

As discussed above, 95% of the risk is attributed to a massive slope failure whose probability of unsatisfactory performance is estimated in Chapter 11 to be 2.1×10^{-3}. This probability value is low compared to the acceptance threshold of 2×10^{-2} established in Chapter 12; i.e., the slope is reasonably safe from a technical point of view. On the other hand, the consequences of such a massive failure are significant (refer to the event tree in Figure 13–4). As such, the risk mitigation alternatives will be more efficient if they aim at reducing the failure consequences (particularly at the higher end of the number of fatalities) rather than lowering the already small probability of unsatisfactory performance. Unfortunately, with the size of failure and the proximity of Block 36 to the slope, there may not be many practical options available.

There are additional items to be noted. First, the risk criteria of ERM (1999) and Reeves et al. (1999) are for total risk from all credible hazards whereas the calculated total F-N curve (Figure 13–3) refers to sliding failure only. Second, these criteria are untried, yet, and the authors emphasized that they should be regarded as guidelines only. Third, the criteria are developed for landslides from natural terrain and not for man-made slopes. An acceptance criterion for man-made slopes, such as the subject cut at Shek Kip Mei, would be more stringent. ERM (1999) noted, however, that because of the high incidence of landslides in Hong Kong, the public may not perceive much difference between a landslide from natural terrain and the failure of a man-made slope.

Based on the above considerations, the risk evaluation undertaken in this section does not reflect a complete picture of the risk level of the Shek Kip Mei slope. Rather, it is intended to be an illustration of the concepts and the insights gained through a QRA study.

SHEK KIP MEI SLOPE - RISK ANALYSIS

Hazard No. 1 : Deep-Seated Failure Involving Total Height of Slope

Failure Height = 20.8m, Estimated Volume = 2500-5000 m^3

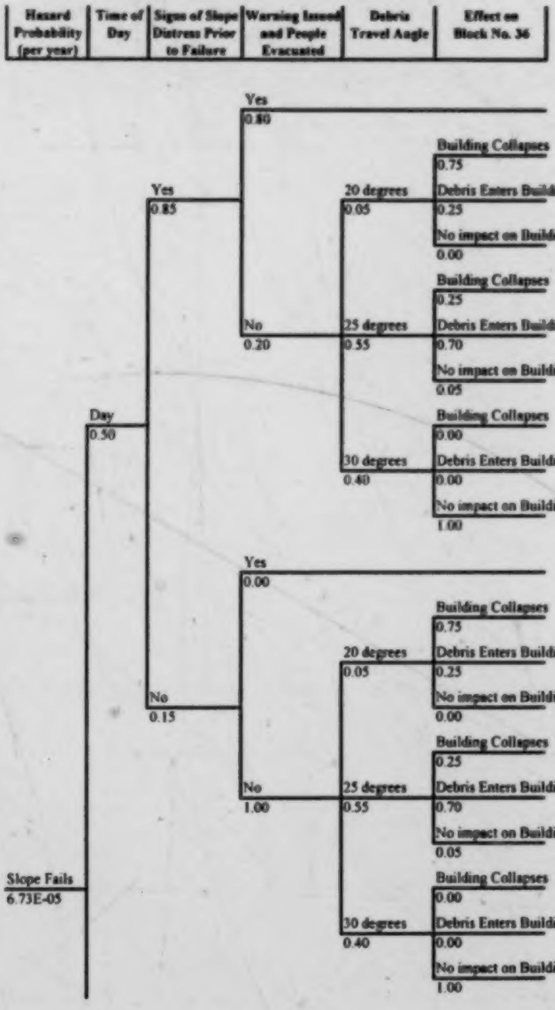
Hazard Probability (per year)
Time of Day
Signs of Slope Distress Prior to Failure
Warning Issued and People Evacuated
Debris Travel Angle
Effect on Block No. 36
Yes
0.80
Building Collapses
0.75
Yes
0.85
20 degrees
0.05
Debris Enters Building
0.25
No impact on Building
0.00
Building Collapses
0.25
No
0.20
25 degrees
0.55
Debris Enters Building
0.70
No impact on Building
0.05
Day
0.50
Building Collapses
0.00
30 degrees
0.40
Debris Enters Building
0.00
No impact on Building
1.00
Yes
0.00
Building Collapses
0.75
20 degrees
0.05
Debris Enters Building
0.25
No
0.15
No impact on Building
0.00
Building Collapses
0.25
No
1.00
25 degrees
0.55
Debris Enters Building
0.70
No impact on Building
0.05
Slope Fails
6.73E-05
Building Collapses
0.00
30 degrees
0.40
Debris Enters Building
0.00
No impact on Building
1.00

Scenario No.	Scenario Frequency (per year)	Number of people at Risk	Probability of Death	Number of Fatalities (N)	Potential Loss of Life (per year)
1	2.29E-05	0.0	0.0	0.00	0.00E+00
2	2.15E-07	40.5	1.0	40.50	8.69E-06
3	7.15E-08	6.8	0.6	4.05	2.90E-07
4	0.00E+00	0.0	0.0	0.00	0.00E+00
5	7.87E-07	40.5	1.0	40.50	3.19E-05
6	2.20E-06	6.8	0.6	4.05	8.92E-06
7	1.57E-07	0.0	0.0	0.00	0.00E+00
8	0.00E+00	40.5	1.0	40.50	0.00E+00
9	0.00E+00	6.8	0.6	4.05	0.00E+00
10	2.29E-06	0.0	0.0	0.00	0.00E+00
11	0.00E+00	0.0	0.0	0.00	0.00E+00
12	1.89E-07	40.5	1.0	40.50	7.67E-06
13	6.31E-08	6.8	0.6	4.05	2.56E-07
14	0.00E+00	0.0	0.0	0.00	0.00E+00
15	6.94E-07	40.5	1.0	40.50	2.81E-05
16	1.94E-06	6.8	0.6	4.05	7.87E-06
17	1.39E-07	0.0	0.0	0.00	0.00E+00
18	0.00E+00	40.5	1.0	40.50	0.00E+00
19	0.00E+00	6.8	0.6	4.05	0.00E+00
20	2.02E-06	0.0	0.0	0.00	0.00E+00

Figure 13–4 Event tree analysis and consequence assessment for Hazard No. 1 – Shek Kip Mei Slope

SHEK KIP MEI SLOPE - RISK ANALYSIS

Hazard No. 1 : Deep-Seated Failure Involving Total Height of Slope

Failure Height = 20.8m, Estimated Volume = 2500-5000 m^3

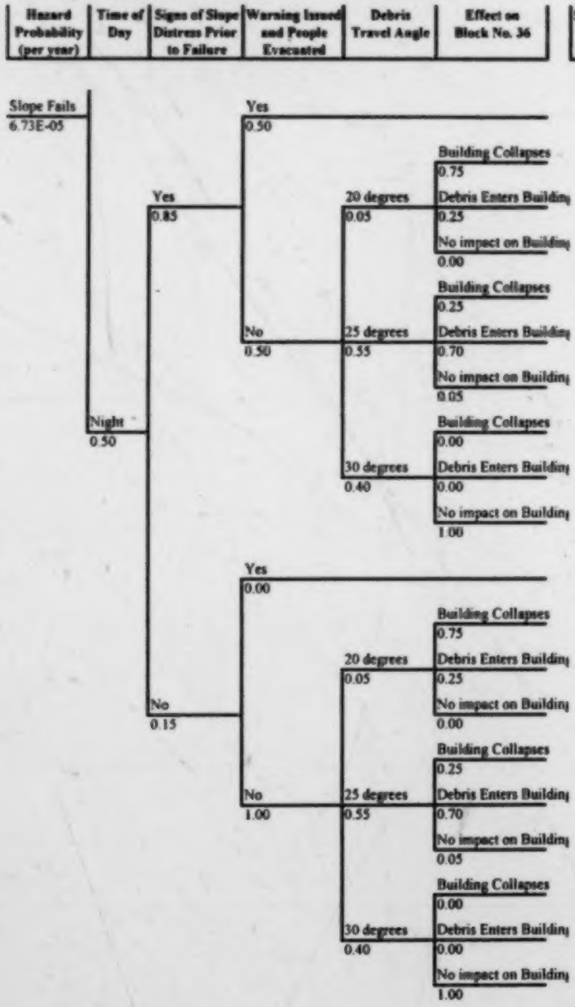
Hazard Probability (per year)
Time of Day
Signs of Slope Distress Prior to Failure
Warning Issued and People Evacuated
Debris Travel Angle
Effect on Block No. 36
Slope Fails
6.73E-05
Night
0.50
Yes
0.85
No
0.15
Yes
0.50
No
0.50
Yes
0.00
No
1.00
20 degrees
0.05
25 degrees
0.55
30 degrees
0.40
Building Collapses
Debris Enters Building
No impact on Building
0.75
0.25
0.00
0.25
0.70
0.05
0.00
0.00
1.00

Scenario No.	Scenario Frequency (per year)	Number of people at Risk	Probability of Death	Number of Fatalities (N)	Potential Loss of Life (per year)
21	1.43E-05	0.0	0.0	0.00	0.00E+00
22	5.36E-07	162.0	1.0	162.00	8.69E-05
23	1.79E-07	27.0	0.6	16.20	2.90E-06
24	0.00E+00	0.0	0.0	0.00	0.00E+00
25	1.97E-06	162.0	1.0	162.00	3.19E-04
26	5.51E-06	27.0	0.6	16.20	8.92E-05
27	3.93E-07	0.0	0.0	0.00	0.00E+00
28	0.00E+00	162.0	1.0	162.00	0.00E+00
29	0.00E+00	27.0	0.6	16.20	0.00E+00
30	5.72E-06	0.0	0.0	0.00	0.00E+00
31	0.00E+00	0.0	0.0	0.00	0.00E+00
32	1.89E-07	162.0	1.0	162.00	3.07E-05
33	6.31E-08	27.0	0.6	16.20	1.02E-06
34	0.00E+00	0.0	0.0	0.00	0.00E+00
35	6.94E-07	162.0	1.0	162.00	1.12E-04
36	1.94E-06	27.0	0.6	16.20	3.15E-05
37	1.39E-07	0.0	0.0	0.00	0.00E+00
38	0.00E+00	162.0	1.0	162.00	0.00E+00
39	0.00E+00	27.0	0.6	16.20	0.00E+00
40	2.02E-06	0.0	0.0	0.00	0.00E+00
			PLL =	Σ	7.67E-04

Figure 13-4 Event tree analysis and consequence assessment for Hazard No. 1 – Shek Kip Mei Slope (cont'd)

SHEK KIP MEI SLOPE - RISK ANALYSIS

Hazard No. 2 : Shallow Failure Involving 70% of Slope Height

Failure Height = 14.6m, Estimated Volume = 300-600 m^3

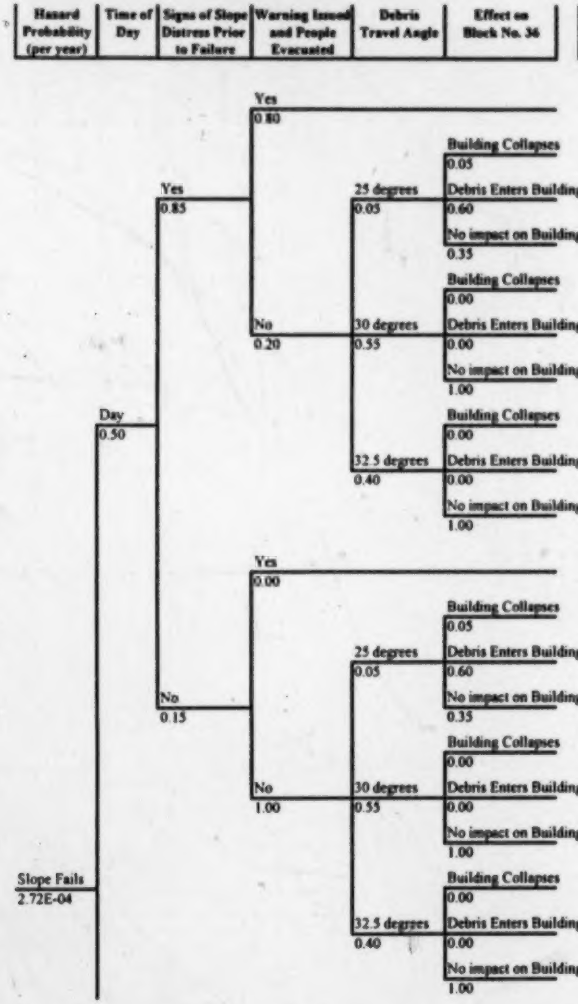
Hazard Probability (per year)
Time of Day
Signs of Slope Distress Prior to Failure
Warning Issued and People Evacuated
Debris Travel Angle
Effect on Block No. 36
Slope Fails
2.72E-04
Day
0.50
Yes
0.85
No
0.15
Yes
0.80
No
0.20
Yes
0.00
No
1.00
25 degrees
0.05
30 degrees
0.55
32.5 degrees
0.40
Building Collapses
0.05
Debris Enters Building
0.60
No impact on Building
0.35
Building Collapses
0.00
Debris Enters Building
0.00
No impact on Building
1.00

Scenario No.	Scenario Frequency (per year)	Number of people at Risk	Probability of Death	Number of Fatalities (N)	Potential Loss of Life (per year)
1	9.23E-05	0.0	0.0	0.00	0.00E+00
2	5.77E-08	40.5	0.7	28.35	1.64E-06
3	6.93E-07	3.7	0.4	1.46	1.01E-06
4	4.04E-07	0.0	0.0	0.00	0.00E+00
5	0.00E+00	40.5	0.7	28.35	0.00E+00
6	0.00E+00	3.7	0.4	1.46	0.00E+00
7	1.27E-05	0.0	0.0	0.00	0.00E+00
8	0.00E+00	40.5	0.7	28.35	0.00E+00
9	0.00E+00	3.7	0.4	1.46	0.00E+00
10	9.23E-06	0.0	0.0	0.00	0.00E+00
11	0.00E+00	0.0	0.0	0.00	0.00E+00
12	5.09E-08	40.5	0.7	28.35	1.44E-06
13	6.11E-07	3.7	0.4	1.46	8.92E-07
14	3.56E-07	0.0	0.0	0.00	0.00E+00
15	0.00E+00	40.5	0.7	28.35	0.00E+00
16	0.00E+00	3.7	0.4	1.46	0.00E+00
17	1.12E-05	0.0	0.0	0.00	0.00E+00
18	0.00E+00	40.5	0.7	28.35	0.00E+00
19	0.00E+00	3.7	0.4	1.46	0.00E+00
20	8.15E-06	0.0	0.0	0.00	0.00E+00

Figure 13–5 Event tree analysis and consequence assessment for Hazard No. 2 – Shek Kip Mei Slope

SHEK KIP MEI SLOPE - RISK ANALYSIS

Hazard No. 2 : Shallow Failure Involving 70% of Slope Height

Failure Height = 14.6m, Estimated Volume = 300-600 m^3

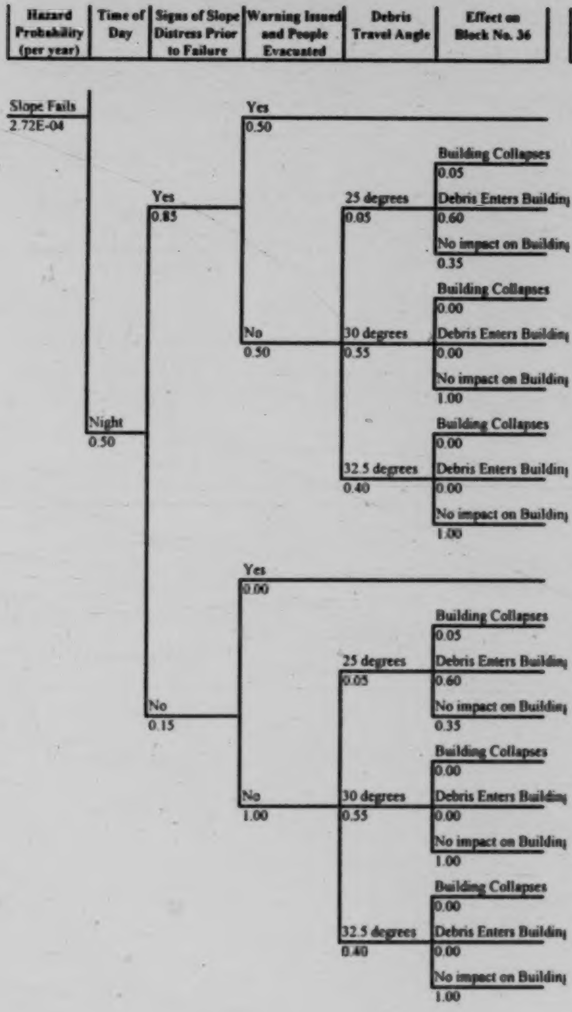
Hazard Probability (per year)
Time of Day
Signs of Slope Distress Prior to Failure
Warning Issued and People Evacuated
Debris Travel Angle
Effect on Block No. 36
Slope Fails
2.72E-04
Night
0.50
Yes
0.85
No
0.15
Yes
0.50
No
0.50
Yes
0.00
No
1.00
25 degrees
0.05
30 degrees
0.55
32.5 degrees
0.40
Building Collapses
0.05
Debris Enters Buildin
0.60
No impact on Buildin
0.35
Building Collapses
0.00
Debris Enters Buildin
0.00
No impact on Buildin
1.00

Scenario No.	Scenario Frequency (per year)	Number of people at Risk	Probability of Death	Number of Fatalities (N)	Potential Loss of Life (per year)
21	5.77E-05	0.0	0.0	0.00	0.00E+00
22	1.44E-07	162.0	0.7	113.40	1.64E-05
23	1.73E-06	14.6	0.4	5.84	1.01E-05
24	1.01E-06	0.0	0.0	0.00	0.00E+00
25	0.00E+00	162.0	0.7	113.40	0.00E+00
26	0.00E+00	14.6	0.4	5.84	0.00E+00
27	3.17E-05	0.0	0.0	0.00	0.00E+00
28	0.00E+00	162.0	0.7	113.40	0.00E+00
29	0.00E+00	14.6	0.4	5.84	0.00E+00
30	2.31E-05	0.0	0.0	0.00	0.00E+00
31	0.00E+00	0.0	0.0	0.00	0.00E+00
32	5.09E-08	162.0	0.7	113.40	5.77E-06
33	6.11E-07	14.6	0.4	5.84	3.57E-06
34	3.56E-07	0.0	0.0	0.00	0.00E+00
35	0.00E+00	162.0	0.7	113.40	0.00E+00
36	0.00E+00	14.6	0.4	5.84	0.00E+00
37	1.12E-05	0.0	0.0	0.00	0.00E+00
38	0.00E+00	162.0	0.7	113.40	0.00E+00
39	0.00E+00	14.6	0.4	5.84	0.00E+00
40	8.15E-06	0.0	0.0	0.00	0.00E+00
			PLL =	Σ	4.08E-05

Figure 13-5 Event tree analysis and consequence assessment for Hazard No. 2 – Shek Kip Mei Slope (cont'd)

SHEK KIP MEI SLOPE - RISK ANALYSIS

Hazard No. 3 : Shallow Localized Failure at Top of Slope Involving 20% of Its Height

Failure Height = 4.5m, Estimated Volume = 25-50 m^3

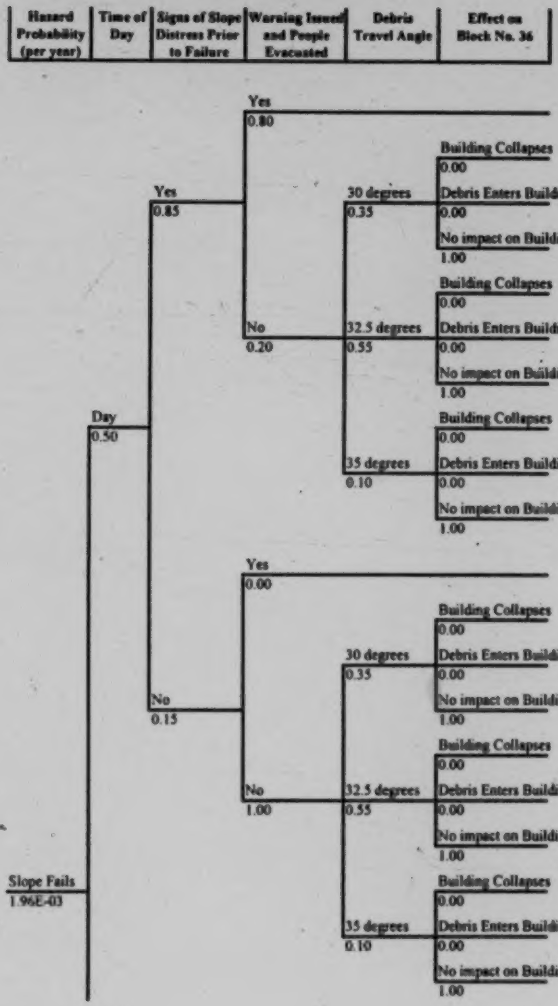
Hazard Probability (per year)
Time of Day
Signs of Slope Distress Prior to Failure
Warning Issued and People Evacuated
Debris Travel Angle
Effect on Block No. 36
Slope Fails
1.96E-03
Day
0.50
Yes
0.85
No
0.15
Yes
0.80
No
0.20
Yes
0.00
No
1.00
30 degrees
0.35
32.5 degrees
0.55
35 degrees
0.10
Building Collapses
0.00
Debris Enters Building
0.00
No impact on Building
1.00

Scenario No.	Scenario Frequency (per year)	Number of people at Risk	Probability of Death	Number of Fatalities (N)	Potential Loss of Life (per year)
1	6.65E-04	0.0	0.0	0.00	0.00E+00
2	0.00E+00	40.5	0.4	16.20	0.00E+00
3	0.00E+00	1.3	0.1	0.13	0.00E+00
4	5.82E-05	0.0	0.0	0.00	0.00E+00
5	0.00E+00	40.5	0.4	16.20	0.00E+00
6	0.00E+00	1.3	0.1	0.13	0.00E+00
7	9.14E-05	0.0	0.0	0.00	0.00E+00
8	0.00E+00	40.5	0.4	16.20	0.00E+00
9	0.00E+00	1.3	0.1	0.13	0.00E+00
10	1.66E-05	0.0	0.0	0.00	0.00E+00
11	0.00E+00	0.0	0.0	0.00	0.00E+00
12	0.00E+00	40.5	0.4	16.20	0.00E+00
13	0.00E+00	1.3	0.1	0.13	0.00E+00
14	5.13E-05	0.0	0.0	0.00	0.00E+00
15	0.00E+00	40.5	0.4	16.20	0.00E+00
16	0.00E+00	1.3	0.1	0.13	0.00E+00
17	8.06E-05	0.0	0.0	0.00	0.00E+00
18	0.00E+00	40.5	0.4	16.20	0.00E+00
19	0.00E+00	1.3	0.1	0.13	0.00E+00
20	1.47E-05	0.0	0.0	0.00	0.00E+00

Figure 13–6 Event tree analysis and consequence assessment for Hazard No. 3 – Shek Kip Mei Slope

SHEK KIP MEI SLOPE - RISK ANALYSIS

Hazard No. 3 : Shallow Localized Failure at Top of Slope Involving 20% of Its Height

Failure Height = 4.5m, Estimated Volume = 25-50 m^3

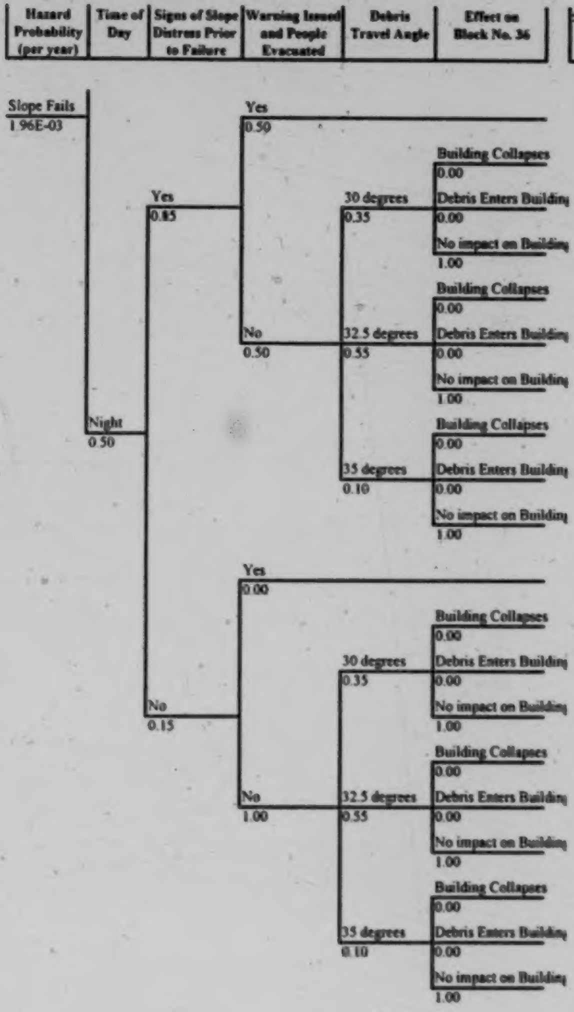
Hazard Probability (per year)
Time of Day
Signs of Slope Distress Prior to Failure
Warning Issued and People Evacuated
Debris Travel Angle
Effect on Block No. 36
Slope Fails
1.96E-03
Night
0.50
Yes
0.85
No
0.15
Yes
0.50
No
0.50
Yes
0.00
No
1.00
30 degrees
0.35
32.5 degrees
0.55
35 degrees
0.10
Building Collapses
0.00
Debris Enters Building
0.00
No impact on Building
1.00

Scenario No.	Scenario Frequency (per year)	Number of people at Risk	Probability of Death	Number of Fatalities (N)	Potential Loss of Life (per year)
21	4.15E-04	0.0	0.0	0.00	0.00E+00
22	0.00E+00	162.0	0.4	64.80	0.00E+00
23	0.00E+00	5.0	0.1	0.50	0.00E+00
24	1.45E-04	0.0	0.0	0.00	0.00E+00
25	0.00E+00	162.0	0.4	64.80	0.00E+00
26	0.00E+00	5.0	0.1	0.50	0.00E+00
27	2.28E-04	0.0	0.0	0.00	0.00E+00
28	0.00E+00	162.0	0.4	64.80	0.00E+00
29	0.00E+00	5.0	0.1	0.50	0.00E+00
30	4.15E-05	0.0	0.0	0.00	0.00E+00
31	0.00E+00	0.0	0.0	0.00	0.00E+00
32	0.00E+00	162.0	0.4	64.80	0.00E+00
33	0.00E+00	5.0	0.1	0.50	0.00E+00
34	5.13E-05	0.0	0.0	0.00	0.00E+00
35	0.00E+00	162.0	0.4	64.80	0.00E+00
36	0.00E+00	5.0	0.1	0.50	0.00E+00
37	8.06E-05	0.0	0.0	0.00	0.00E+00
38	0.00E+00	162.0	0.4	64.80	0.00E+00
39	0.00E+00	5.0	0.1	0.50	0.00E+00
40	1.47E-05	0.0	0.0	0.00	0.00E+00
			PLL =	Σ	0.00E+00

Figure 13-6 Event tree analysis and consequence assessment for Hazard No. 3 – Shek Kip Mei Slope (cont'd)

CHAPTER 14

CONCLUSIONS

Probabilistic slope stability analysis is a rational means to incorporate uncertainty into the design process. It is also the most suitable approach for estimating hazard frequency for site-specific QRA studies. One of the main conclusions of this study is that probabilistic analyses can be implemented in practice with relative ease. The stated obstacles impeding the adoption of such techniques into geotechnical practice are more apparent than real.

A spreadsheet approach for probabilistic slope stability analysis is developed in Chapter 5. The methodology is based on Monte Carlo simulation using the commercial software @Risk and Excel. The underlying procedures and concepts are simple and transparent, requiring only fundamental knowledge of statistics and probability theory. At the same time, the analysis accounts for the spatial variability of the input variables, the statistical uncertainty due to limited data and the bias in the empirical factors and correlations used.

The outputs of the probabilistic analyses of the James Bay dykes, based on this approach, are compared with those based on the FOSM method in Chapter 6. The results of the two analyses are in good agreement. The methodology is further tested through the analysis of 10 case studies (Chapters 6-11). The cases involved effective and total stress analyses, complex stratigraphy and geometry and circular and non-circular slip surfaces. Two different slope analysis methods are used; the Bishop method and the Spencer method. The proposed spreadsheet approach proved practical and flexible in handling such a wide variety of slope problems.

The results of the probabilistic analyses highlight the limitation of the factor of safety. Some slopes designed for high factors of safety are found to be less reliable than slopes designed for lower factors of safety. Such inconsistency is a direct result of ignoring uncertainty in conventional slope design practice. The factor of safety alone can give a misleading sense of safety and is not a sufficient safety indicator. The probability of unsatisfactory performance and the reliability index are more consistent safety measures.

The study also calibrates acceptable slope design practice in probabilistic terms (Chapter 12). A probability of unsatisfactory performance of 2×10^{-2} is regarded as an upper design threshold in relation to slope failures. It is equivalent to a reliability index of 2.0. It is emphasized, however, that other considerations, such as failure consequences and serviceability, may necessitate the adoption of more stringent design criteria. The study affirms that combining, rather than replacing, conventional deterministic slope analysis and probabilistic analysis provides greater insight into design reliability and enhance the decision-making process.

Another important conclusion (Chapter 12) is that slopes deemed acceptable based on current slope design practice are in fact less reliable than commonly thought. An influential engineering organization such as the US Corps of Engineers (1995), for example, suggested that a "Good" performance level is equivalent to a probability of unsatisfactory performance in the range of 3×10^{-5} or a reliability index of 4.0. The analyses presented in this study show that acceptable, or safe, slopes have much higher probabilities of unsatisfactory performance and much lower reliability indices. The heavily instrumented and monitored Syncrude Cell 23 dyke, for example, is considered an adequate design while it has a probability of unsatisfactory performance of 1.6×10^{-3} and a reliability index of 2.3.

The inherent spatial variability of soil properties and pore pressure is one of the main sources of parameter uncertainty. Probabilistic analyses ignoring spatial variability and assuming perfect correlations (i.e. naïve analyses) are inadequate. The study shows that the naïve analysis significantly overestimates the probability of unsatisfactory performance (Chapter 12). Furthermore, the results of the analysis in some cases seem unrealistic. For example, the inclination of the Tsing Yi: 1 slope (Chapter 11) is flattened from 35 degrees at failure to 26.6 degrees for what is deemed an acceptable design. Yet, the probability of unsatisfactory performance based on the naïve approach remains very high, 1.3×10^{-1}, and the reliability index is very low, 1.07.

The practical value of quantifying the relative contributions of the various sources of uncertainty to the overall uncertainty of the factor of safety through sensitivity analyses, using Spearman rank correlation coefficient, cannot be underestimated. Such information allows the available resources, whether intellectual or physical, to be rationally allocated towards reducing the uncertainty of the variable(s) with the largest impact on design. Furthermore, quantifying the relative impacts of systematic uncertainty and uncertainty due to spatial variability is also of practical value. For example, problems dominated by systematic uncertainty are less influenced by the spatial variability of the input parameters and, consequently, less sensitive to the assumption of the autocorrelation distance. In addition, the potential for improving design reliability of such problems is high, as systematic uncertainty can be reduced which is not the case with the uncertainty due to inherent spatial variability.

In addition to the above main conclusions, several detailed conclusions are reached. The probability of unsatisfactory performance and the reliability index are noted to be uniquely related regardless of the assumptions involved in the analyses. The two indices are analytically related if the probability distribution of the factor of safety is assumed to be normal. That latter relationship is commonly used in estimating the probability of unsatisfactory performance when approximate probabilistic methods, e.g. FOSM, are used. The results of this study show, however, that the assumption of normality overestimates the probability of unsatisfactory performance for small probability ranges (Chapter 12).

The probability of unsatisfactory performance is found to be more sensitive and to better reflect design changes than the reliability index (Chapter 12). On the other hand, the lower sensitivity of the reliability index makes it more stable and less affected by noise in the analysis. It is, thus, recommended to consider both indices in assessing the adequacy of a slope design. It is also important to note that the computed probability of unsatisfactory performance is a lower bound to the actual unknown probability because of the possibility of undetected uncertainties that are not taken into account. Comparing the probabilities of unsatisfactory performance of alternative designs is, thus, more reliable than the absolute probabilities of the designs.

Given the limited amounts and the wide spacing of data in a typical site investigation program, the uncertainty surrounding the analytical estimation of the autocorrelation distance is significant, as discussed in Chapter 5. A literature review indicated that the range within which the autocorrelation distances of geotechnical properties vary is not large. Thus, empirical estimates based on the typical ranges reported in the literature and making due consideration of the geological processes controlling the formation/deposition of the subject material could be made. The continued compilation of the results of spatial variability assessments (particularly the autocorrelation distance) of various soils and properties to expand the available database would improve the reliability of the empirical estimates.

Within practical limits, the probability of unsatisfactory performance is found insensitive to the autocorrelation distance for soil formations exhibiting continuous spatial variability with equivalent isotropic autocorrelation distances in excess of 10m. This is, however, not the case for soils characterized by erratic variability. If the sensitivity of the probability of unsatisfactory performance to the assumption of the autocorrelation distance is large enough to impede the decision-making process, an exploration program designed to evaluate the site/formation specific autocorrelation distance(s) could be required.

The sensitivity analyses undertaken in this study showed that the uncertainty of Bjerrum's vane correction factor is substantial and could have a larger impact on the reliability of the design than does the uncertainty of the undrained shear strength itself. This warns that the reliability of a design could be undermined by the use of empirical factors and correlations without the designer even realizing this. Understanding the limitations and, more importantly, the reliability of such factors/correlations prior to using them is essential.

The probabilistic stability analyses of Hong Kong case studies (taking spatial variability into account) highlight the effect of the volume, or scale, of failure on the probability of unsatisfactory performance. Small failures have higher probabilities of unsatisfactory performance than larger failures although they could have higher factors of safety. This, in fact, is consistent with the observed frequencies of occurrence of small and large failures. The conventional deterministic approach, based on the factor of safety, does not address this issue of failure scale.

In many areas of geotechnical engineering, particularly slope engineering, there is an ongoing shift towards quantitative risk analysis. Risk analysis comprises hazard assessment and consequence assessment. The case of probabilistic slope stability analysis or hazard frequency estimation is, to a large extent, concluded. The value of such analyses is evident, the tools and techniques, including the proposed methodology, are well founded and guidelines for probabilistic slope design are proposed is this study. Some refinements are, however, still needed. These include developing practical means to evaluate and incorporate the spatial variability of pore water pressure into the analysis and expanding the available database of autocorrelation distances to improve the reliability of the empirical estimates. On the other hand, the case for consequence assessment is far from complete. As illustrated in Chapter 13, the assessment is largely subjective based on the assessor's judgement. There is an ample room for further research to improve and advance consequence assessment.

Probabilistic slope stability analysis is based on limit equilibrium and is, thus, concerned mainly with slope failure. The issue of slope serviceability is usually addressed judgmentally. An assessment of slope movement taking into account the uncertainty of soil deformation characteristics is seldom performed. In fact, there are hardly any studies of probabilistic evaluation of slope deformation. This is another area where further research is needed to develop practical methods, deterministic as well as probabilistic, to estimate and assess slope movements and their effects on serviceability.

REFERENCES

Aas, G., Lacasse, S., Lunne, T., and Hoeg, K. 1986. Use of in situ tests for foundation design on clay. In *Use of in Situ Tests in Geotechnical Engineering*, Proceedings of In Situ'86. Geotechnical Special Publication No. 6, ASCE, Blacksburg, USA, June 23-25, pp 1-30.

Abbott, B., Bruce, I., Savigny, W., Keegan, T., and Oboni, F. 1998. A methodology for the assessment of rockfall hazard and risk along transportation corridors. Proceedings of the 8th International Association of Engineering Geology Congress, pp 1195-1200.

AIT, 1989. Laboratory test data on soil samples from the Muar flats test embankment. Asian Institute of Technology. Research Report – Phase II

Alencar, J., Morgenstern, N.R., and Chan, D.H. 1994. Analysis of foundation deformations beneath the Syncrude tailings dyke. Canadian Geotechnical Journal, 31: 868-884.

Alonso, E.E. 1976. Risk analysis of slopes and its application to slopes in Canadian sensitive clays. Geotechnique, 26, (3):453-472.

Anderson, L.R., Sharp, K.D., Bowles, D.S., and Canfield, R.V. 1984. Application of methods of probabilistic characterization of soil properties. Proceedings of ASCE Symposium on Probabilistic Characterization of Soil Properties - Bridge Between Theory and Practice. Atlanta, USA, May 17, pp 90-105.

Anderson, L.R., Bowles, D.S., Pack, R.T., and Keaton, J.R. 1996. A risk-based method for landslide mitigation. Proceedings of the 7th International Symposium on Landslides, Trondheim, Norway, June 17-21, pp 135-140.

Ang, A.H-S, and Tang, W.H. 1975. *Probability concepts in engineering planning and design, Volume I Basic principles.* John Wiley & Sons, New York.

Ang, A.H-S, and Tang, W.H. 1984. *Probability concepts in engineering planning and design, Volume II Decision, risk and reliability.* John Wiley & Sons, New York.

API 1993. Recommended practice for planning designing and constructing fixed offshore platforms – load and resistance factor design. American Petroleum Institute, Report RP2A-LRFD. Texas, USA.

Asaoka, A., and A-Grivas, D. 1981. Short term reliability of slopes under static and seismic conditions. National Academy of Science. Transportation Research Record No. 809, pp 64-70.

Asaoka, A., and A-Grivas, D. 1982. Spatial variability of the undrained strength of clays. Journal of the Geotechnical Engineering Division, ASCE, 108, (5): 743-756.

Azzouz, A.S., Baligh, M.M., and Ladd, C.C. 1983. Corrected field vane strength for embankment design. Journal of the Geotechnical Engineering Division, ASCE, 109, (5): 730-734.

Baecher, G.B. 1984. On estimating autocovariance of soil properties. Proceedings of 4th ASCE Specialty Conference on Probabilistic Mechanics and Structural Reliability, Berkeley, USA, January, pp 214-218.

Baecher, G.B. 1984. Just a few more tests and we'll be sure. Proceedings of ASCE Symposium on Probabilistic Characterization of Soil Properties - Bridge Between Theory and Practice, Atlanta, USA, May 17, pp1-18.

Baecher, G.B. 1986. Geotechnical error analysis. Transportation Research Record, 1105, pp 23-31.

Baecher, G.B 1987. Statistical Analysis of Geotechnical Data. Final Report No. GL-87-1, USACE Waterways Experiment Station, Wicksburg, MI.

Baecher, G.B, Einstein, H.H., Vanmarcke, E.H., and Veneziano, D. 1984. Discussion of "Conventonal and probabilistic embankment design". Journal of the Geotechnical Engineering Division, ASCE, 110, (7): 989-991.

Baecher, G.B, and Ingra, T.S. 1981. Stochastic FEM in settlement predictions. Journal of the Geotechnical Engineering Division, ASCE, 107, (4): 449-463

Baecher, G.B, Marr, W.A., Lin, J.S., and Consla, J. 1983. Critical parameters for mine tailing embankments. Bureau of Mines, U.S. Department of Interior.

Basra, G., and Kirwan, B. 1998. Collection of offshore human error probability data. Reliability Engineering and System Safety, 61: 77-93.

Benson, C.H. 1991. Predicting excursions beyond regulatory threshholds of hydraulic conductivity from quality control measurements. Proceedings of the 1st Canadaian Conference on Environmental Geotechnics, Montreal, Canada, May 14-15, pp 447-454.

Bergado, D.T., and Anderson, L.R. 1985. Stochastic analysis of pore-pressure uncertainty for the probabilistic assessment of the safety of earth slopes. Soils and Foundations, 25, (2): 87-105.

Bergado, D.T., Patron, B.C., Youyongwatana, W., Chai, J.C., and Yudhbir 1994. Reliability-based analysis of embankment on soft Bangkok clay. Structural Safety, 13: 247-266.

Bishop, A.W. 1955. The use of the slip circle in the stability analysis of slopes. Geotechnique, 5, (1): 7-17.

Bishop, A.W., and Bjerrum, L. 1960. The relevance of the triaxial test to the solution of stability problems. Research Conference on Shear Strength of Cohesive Soils, Colorado, USA. ASCE, Soil Mechanics and Foundation Division. pp 437-501.

Bjerg, P.L., Hinsby, K., Christensen, T.H., and Gravesen, P. 1992. Spatial variability of hydraulic conductivity of an unconfined sandy aquifer determined by mini slug test. Journal of Hydrology, 136: 107-122.

Bjerrum, L. 1966. Mechanism of progressive failure in slopes of overconsolidated plastic clays and clay shales. The 3rd Terzaghi Lecture, ASCE Structural Engineering Conference, Miami, USA.

Bjerrum, L. 1972. Embankments on soft ground. Proceedings of ASCE Specialty Conference on Performance of Earth and Earth-Supported Structures. Purdue University, Lafayette, USA, June 11-14. Volume 2. pp 1-54.

Bjerrum, L. 1973. Problems of soil mechanics and construction on soft clays. Proceedings of 8th International Conference on Soil Mechanics and Foundation Engineering. Moscow. Volume 3. pp 111-159.

Brand, E.W. 1982. Analysis and design in residual soils. Proceedings of the ASCE Specialty Conference on Engineering and Construction in Tropical and Residual Soils, Honolulu, January 11-15, pp 89-143.

Brand, E.W. 1985. Predicting the performance of residual soil slopes. Proceedings of the 11th International Conference on Soil Mechanics and Foundation Engineering, San Francisco, August 12-16. Volume 5, pp 2541-2578.

Brand, E.W. 1988. Special lecture: Landslide risk assessment in Hong Kong. Proceedings of the 5th International Symposium on Landslides, Lausanne, Switzerland, July 10-15. Volume 2, pp 1059-1074.

Brand, E.W., and Premchitt, J. 1989. Comparison of the predicted and observed performance of the Muar test embankment. Proceedings of the Symposium on Trial Embankments on Malaysian Marine Clays. Kuala Lumpur, Malaysia, November. Volume 3.

Bunce, C.M., Cruden, D.M., and Morgenstern, N.R. 1995. Hazard assessment for rock fall on a B.C. highway. Proceedings of the 48th Canadian Geotechnical Conference, Vancouver, September 26-29, pp 499-508.

CSA 1991. Risk analysis requirements and guidelines. Publication of the Canadian Standard Association, CAN/CSA-Q634-91.

Casagrande, A. 1965. The role of calculated risk in earthwork and foundation engineering. Journal of the Soil Mechanics Division, ASCE, 91, (4): 1-40.

Chiasson, P., Lafleur, J., Soulie, M., and Law, K.T. 1995. Characterizing spatial variability of a clay by geostatistics. Canadian Geotechnical Journal, 32: 1-10.

Chowdhury, R.N. 1984. Recent developments in landslide studies: Probabilistic methods, State-of-the-Art-Report - session VII (a). Proceedings of the 4th International Symposium on Landslides, Toronto, Canada, September 16-21. Volume 1, pp 209-228.

Chowdhury, R.N. 1996. Aspects of risk assessment for landslides. Proceedings of the 7th International Symposium on Landslides, Trondheim, Norway, June 17-21, pp 183-188.

Chowdhury, R.N., and Tang, W.H. 1987. Comparison of risk models for slopes. Reliability and Risk Analysis in Civil Engineering 2: Proceedings of 5th International Conference on Applications of Statistics and Probability in Soil and Structural Engineering, Vancouver, Canada, May 25-29. Volume 2. pp 863-869.

Christian, J.T. 1984. Discussion of "Conventional and probabilistic embankment design". Journal of the Geotechnical Engineering Division, ASCE, 110, (7): 991-993.

Christian, J.T. 1996. Reliability methods for stability of existing slopes. In *Uncertainty in the Geologic Environment: From theory to Practice*, Proceedings of Uncertainty'96. Geotechnical Special Publication No. 58, ASCE, NY, USA, August 31-July 3. Volume 2. pp 409-419.

Christian, J.T., and Baecher, G.B. 1999. Point estimate method as numerical quadrature. Journal of Geotechnical and Geoenvironmental Engineering, ASCE, 125, (9): 779-786.

Christian, J.T., Ladd, C.C., and Baecher, G.B. 1994. Reliability and Probability in Stability Analysis. Journal of Geotechnical Engineering Division, ASCE, 120, (2): 1071-1111.

Claes, A. 1996. Application of a probabilistic approach in slope stability analyses. Proceedings of the 7th International Symposium on Landslides, Trondheim, Norway, June 17-21, pp 1137-1142.

Cornell, C.A. 1969. A probability based structural code. American Concrete Institute Journal, 66: 974-985.

Cornell, C.A. 1972. First order uncertainty analysis of soils deformation and stability. Proceedings of 1st International Conference on Applications of Statistics and Probability to Soil and Structural Engineering, Hong Kong, September 13-16, 1971, pp 129-144.

Cruden, D., and Fell, R. (eds.) 1997. Landslide risk assessment. Proceedings of the International Workshop on Landslide Risk Assessment, Honolulu, USA, February 19-21. A.A. Balkema.

Crystal Ball 1996. Monte Carlo simulation software for spreadsheet risk analysis. Decisioneering Inc., Colorado, USA.

Decisioneering, 1996. Crystal Ball: Monte Carlo simulation software for spreadsheet risk analysis. Decisioneering Inc., Colorado, USA.

DeGroot, D.J. 1996. Analyzing spatial variability of in situ soil properties. In *Uncertainty in the Geologic Environment: From theory to Practice*, Proceedings of Uncertainty'96. Geotechnical Special Publication No. 58, ASCE, NY, USA, August 31-July 3. Volume 1. pp 210-238.

DeGroot, D.J., and Baecher, G.B. 1993. Estimating autocovariance of in-situ soil properties. Journal of the Geotechnical Engineering Division, ASCE, 119, (1): 147-166.

DeGroot, D.J., and Baecher, G.B. 1994. Closure to "Estimating autocovarianve of in-situ soil properties". Journal of the Geotechnical Engineering Division, ASCE, 120, (8): 1455-1457.

D'Elia, B., Distefano, D., Esu, F., and Federico, G. 1988. Deformations and stability of high cuts in a structurally complex formation. Proceedings of 5th International Symposium on Landslides. Lausanne, Switzerland. Volume 1. pp 599-604.

deMello, V.F.B. 1977. Reflections on design decisions of practical significance to embankment dams. 17th Rankine Lecture, Geotechnique, 27, (3): 279-355.

Deutsch, C.V., 1996. Constrained modeling of histograms and cross plots with simulated annealing. Technometrics, 38, (3): 266-274.

Deutsch, C.V., 2000. Personal communication.

Deutsch, C.V., and Journel, A.G. 1998. *GSLIB: Geostatistical software library and user's guide*. Second edition. Oxford University Press, New York.

Dhillon, B.S. 1986. *Human reliability with human factors*. Pergamon, Oxford.

DNV Technica (1996). Quantitative landslip risk assessment of pre-GCO man-made slopes and retaining walls. A Report for the Geotechnical Engineering Office, Civil Engineering Department, Government of Hong Kong. Agreement No. GEO 6/95.

Dougherty, E.M. and Fragola, J.R. 1988. *Human reliability analysis : a systems engineering approach with nuclear power plant applications.* John Wiley & Sons, New York.

Duncan, J.M. 2000. Factors of safety and reliability in geotechnical engineering. Journal of the Geotechnical and Geoenvironmental Engineering, ASCE, 126, (4): 307-316.

EBA Engineering Consultants Ltd., 1986a. Triaxial compression testing: Pgs, Pgc, Kcw and Kca units; volume 1; text and index test results. Report prepared for Syncrude Canada Ltd. Ref . No.: 0104-6795.

EBA Engineering Consultants Ltd., 1986b. Direct shear testing: Pgs, Pgc, Kcw and Kca units; volume 1; text and index test results. Report prepared for Syncrude Canada Ltd. Ref . No.: 0104-6796.

Einstein, H.H., 1988. Special Lecture: Landslide risk assessment procedure. Proceedings of the 5th International Symposium on Landslides, Lausanne, Switzerland, July 10-15, Volume 2, pp 1075-1090.

Einstein, H.H., and Baecher, G.B. 1982. Probabilistic and statistical methods in engineering geology. I. Problem statement and introduction to solution. Rock Mechanics, Supp., 12: 47-61.

ERM-Hong Kong Limited 1996. QRA of boulder fall hazards in Hong Kong: Phase 2 study. Report No. C1453, prepared for the Civil Engineering department of the Government of Hong Kong.

ERM-Hong Kong Limited 1997. Slope failures along BRIL roads: quantitative risk assessment & ranking. Report No. C1644, prepared for the Geotechnical Engineering Office, Civil Engineering department of the Government of Hong Kong.

ERM-Hong Kong Limited 1999. Landslides and boulder falls from natural terrain: interim risk guidelines. Report No. 75, prepared for the Geotechnical Engineering Office, Civil Engineering department of the Government of Hong Kong.

Fair, A.E. and Handford, G.T. 1986. Overview of tailings dyke instrumentation program at Syncrude Canada Ltd. Proceedings of the International Symposium on

Geotechnical Stability in Surface Mining, Calgary, Canada, November 6-7, pp 245-253.

Fell, R. 1994. Landslide risk assessment and acceptable risk. Canadian Geotechnical Journal, 31: 261-272.

Fell, R., Finlay, P., and Mostyn, G. 1996. Framework for assessing the probability of sliding of cut slopes. Proceedings of the 7th International Symposium on Landslides, Trondheim, Norway, June 17-21, pp 201-208.

Fell, R., and Hartford, D. 1997. Landslide risk management. In *Landslide Risk Assessment*, Cruden & Fell (eds.). Proceedings of The International Workshop on Landslide Risk Assessment, Honolulu, USA, February 19-21, pp 51-109.

Fenton, G.A., and Vanmarcke, E.H. 1991. Spatial variation in liquefaction risk assessment. Geotechnical Engineering Congress 1991. Geotechnical Special Publication No. 27, ASCE, Boulder, Colorado, June 10-12. Volume 1. pp 594-607.

Ferkh, Z., and Fell, R. 1994. Design of embankments on soft clay. Proceedings of 13th International Conference on Soil Mechanics and Foundation Engineering, New Delhi, India, January 5-10. Volume 2. pp 733-738.

Finlay, P.J. 1996. The risk assessment of slopes. Ph.D. Thesis, School of Civil Engineering, University of New South Wales.

Finlay, P.J., and Fell, R. 1997. Landslides: risk perception and acceptance. Canadian Geotechnical Journal, 34: 169-188.

Fredlund, D.G., and Dahlman, A.E. 1972. Statistical geotechnical properties of glacial Lake Edmonton sediments. Proceedings of 1st International Conference on Applications of Statistics and Probability to Soil and Structural Engineering, Hong Kong, September 13-16, pp 203-228.

FMSW 2000. Report on the Shek Kip Mei landslide of 25 August 1999. Prepared by Fugro Maunsell Scott Wilson Joint Venture for the Geotechnical Engineering Office, Government of Hong Kong.

GCO 1988. Guide to rock and soil descriptions (Geoguide 3). Geotechnical Control Office, 195 p.

GEO 1999. Review of 1997 and 1998 landslides. Landslide Study Report No. LSR 15/99. Geotechnical Engineering Office, Civil Engineering Department, The Government of Hong Kong.

Gilbert, R.B., Wright, S.G., and Liedtke, E. 1998. Uncertainty in back analysis of slopes: Kettleman Hills case history. Journal of Geotechnical and Geoenvironmental Engineering, ASCE, 124, (12): 1167-1176.

Glynn, E.F., Veneziano, D., and Einstein, H.H. 1978. The probabilistic model for shearing resistance of jointed rock. Proceedings of the 19th US Symposium on Rock Mechanics, Nevada, USA, pp 66-76.

Goovaerts, P. 1997. *Geostatistics for natural resources evaluation.* Oxford University Press, New York.

Griffiths, D.V., and Fenton, G.A. 1993. Seepage beneath water retaining structures founded on spatially random soil. Geotechnique, 43, (4): 577-587.

Griffiths, D.V., and Fenton, G.A. 2000. Influence of soil strength spatial variability on the stability of an undrained clay slope by finite element. In *Slope Stability 2000*, Proceedings of Sessions of GEO-DENVER 2000. Geotechnical Special Publication No. 101, ASCE, Colorado, USA, August 5-8. pp 184-193.

Hachich, W., and Vanmarcke, E.H. 1983. Probabilistic updating of pore pressure fields. Journal of Geotechnical Engineering Division, ASCE, 109, (3): 373-387.

Hahn, G.J, and Shapiro, S.S. 1967. *Statistical Models in Engineering*. John Wiley & Sons, Inc.

Hardingham, A.D., Ho, K.K.S., and Smallwood, A.R.H. 1998. Quantitative risk assessment of landslides – a case history from Hong Kong. In *Slope Engineering in Hong Kong*. Li, Kay and Ho (eds.), Balkema, pp145-151.

Harr, M.E. 1977. *Mechanics of particulate media – a probabilistic approach.* McGraw-Hill.

Harr, M.E. 1987. *Reliability-based design in civil engineering.* McGraw-Hill Inc, USA.

Harr, M.E. 1989. Probabilistic estimates for multivariate analyses. Applied Mathematical Modelling, 13, (5): 313-318.

Hassan, A., and Wolff, T. 1999. Search algorithm for minimum reliability index of earth slopes. Journal of Geotechnical and Geoenvironmental Engineering, ASCE, 125, (4): 301-308.

Hassan, A., and Wolff, T. 2000. Effect of deterministic and probabilistic models on slope reliability index. In *Slope Stability 2000*, Proceedings of Sessions of GEO-DENVER 2000. Geotechnical Special Publication No. 101, ASCE, Colorado, USA, August 5-8. pp 194-208.

Hencher, S.R. 1983a. Landslide studies 1982: Case study No. 8 , Tsing Yi (1). Geotechnical Control Office, Hong Kong, Special Project Report SPR 9/83.

Hencher, S.R. 1983b. Landslide studies 1982: Case study No. 10, Ching Cheung Road. Geotechnical Control Office, Hong Kong, Special Project Report SPR 11/83.

Hencher, S.R., Massey, J.B., and Brand, E.W. 1984. Application of back analysis to Hong Kong landslides. Proceedings of the IVth International Symposium on Landslides, Toronto, September 6-21. Volume 1. pp 631-638.

Hoeg, K., and Murarka, R.P. 1974. Probabilistic analysis and design of a retaining wall. Journal of Geotechnical Engineering Division, ASCE, 100, (3): 349-366.

Honjo, Y., and Kuroda, K. 1991. A new look at fluctuating geotechnical data for reliability design. Soils and Foundations, 31, (1):110-120.

Holtz, R.D., and Krizek, R.J. 1972. Statistical evaluation of soil test data. Proceedings of 1st International Conference on Applications of Statistics and Probability to Soil and Structural Engineering, Hong Kong, September 13-16, 1971. pp 229-266.

Insley, A.E. 1965. A study of a large compacted clay embankment-fill failure. Canadian Geotechnical Journal, 2: 274-286.

Ireland, H.O. 1954. Stability analysis of the Congress street open cut in Chicago. Geotechnique, 4, (4): 163-168.

Isaaks, E.H., and Srivastava, R.N. 1989. An introduction to applied geostatistics. Oxford University Press, New York.

IUGS Working Group on Landslides, Committee on Risk Assessment 1997. Quantitative risk assessment for slopes and landslides – The state of the art. In *Landslide Risk*

Assessment, Cruden & Fell (eds.). Proceedings of the International Workshop on Landslide Risk Assessment, Honolulu, USA, February 19-21, pp 3-12.

Jaksa, M.B., Brooker, P.I., and Kaggwa, W.S. 1997. Inaccuracies associated with estimating random measurement errors. Journal of Geotechnical and Geoenvironmental Engineering, ASCE, 123, (5): 393-401.

Janbu, N. 1973. Slope stability computations. In *Embankment Dam Engineering*, Casagrande Volume. Editors Hirschfield and Poulos. John Wiley & Sons, New York, pp 47-86.

Janbu, N., Kjekstad, O., and Senneset, K., 1977. Slide in overconsolidated clay below embankment. Proceedings of 9th International Conference on Soil Mechanics and Foundation Engineering, Tokyo, Japan. Volume 2. pp 95-102.

Janbu, N. 1996. Slope stability evaluations in engineering practice. Proceedings of the 7th International Symposium on Landslides, Trondheim, Norway, June 17-21, pp 17-34.

Journel, A.G. 1986. Geostatistics: Models and tools for the earth sciences. Mathematical Geology, 18, (1): 119-140.

Journel, A.G. 1994. Modeling uncertainty: some conceptual thoughts. In *Geostatistics for the next century*, R. Dimitrakopoulos, editor. Kluwer, Dordrecht. pp 30-43.

Journel, A.G., and Huijbregts, CH.J. 1978. *Mining Geostatistics*. Academic Press Inc., London.

Kaufman, R.I., and Weaver, F.J. 1967. Stability of Atchafalaya levees. Journal of Soil Mechanics and Foundation Division, ASCE, 93, 157-176.

Kay, J.N. 1993. Probabilistic design of foundations and earth structures. In *Probabilistic Methods in Geotechnical Engineering*, Li & Lo (eds.). Balkema, Rotterdam. pp 49-62.

Kay, J.N. 1995. Uncertainties in geotechnical design. Australian Civil Engineering Transactions, 37, (1): 51-60.

Kay, J.N. 1998. Assessment of slope safety for the residual soil slopes in Hong Kong. Soils and Foundations, 38, (4): 95-103.

Keaveny, J.M., Nadim, F., and Lacasse, S. 1989. Autocorrelation functions for offshore geotechnical data. Proceedings of the 5th International Conference on Structural Safety and Reliability, San Francisco, USA, August 7-11, pp 263-270.

Kim, H-S., Major, G., and Ross-Brown, D.M. 1978. Applications of Monte Carlo techniques to slope stability analyses. Proceedings of the 19th US Symposium on Rock Mechanics, Nevada, USA, pp 28-39.

Kraft, L.M., and Mukhopadhyay, J. 1977. Probabilistic analysis of excavated earth slopes. Proceedings of the Ninth International Conference on Soil Mechanics and Foundation Engineering, Tokyo, Japan. Volume 2, pp 109-116.

Kulatilake, P.H.S.W., and Ghosh, A. 1988. An investigation into accuracy of spatial variation estimation using static cone penetrometer data. Proceedings of the 1st International Conference on Penetration testing, Orlando, USA, pp 815-821.

Kulatilake, P.H.S.W., and Miller, K.M. 1987. A scheme for estimating the spatial variation of soil properties in three dimensions. Proceedings of 5th International Conference on Structural Safety and Reliability, Vancouver, Canada. Volume 2, pp 669-677.

Kulhawy, F.H. 1996. From Casagrande's "calculated risk" to reliability-based design in foundation engineering. Civil Engineering Practice, Journal of the Boston Society of Civil Engineers, 11, (2): 43-56.

Kulhawy, F.H., and Mayne, P.W. 1990. Manual on estimating soil properties for foundation design. A Report prepared for Electric Power Research Institute. El-6800, Research Project 1493-6. Cornell University, NY.

Kulhawy, F.H., and Phoon, K.K. 1996. Engineering judgment in the evolution from deterministic to reliability-based foundation design. In *Uncertainty in the Geologic Environment: From theory to Practice*, Proceedings of Uncertainty'96. Geotechnical Special Publication No. 58, ASCE, NY, USA, August 31-July 3. Volume 1. pp 29-48.

Kulhawy, F.H., Roth, M.S., and Grigoriu, M.D. 1991. Some statistical evaluation of geotechnical properties. Proceedings of 6th International Conference on Applications of Statistics and Probability in Civil Engineering, Mexico city. Volume 2, pp 705-712.

Kuwahara, H., and Yamamoto, M. 1987. Safety evaluation and reliability-based design of braced excavations. Reliability and Risk Analysis in Civil Engineering 2: Proceedings of 5th International Conference on Applications of Statistics and Probability in Soil and Structural Engineering, Vancouver, Canada, May 25-29. Volume 2. pp 703-709.

Lacasse, S. 1999. The importance of dealing with uncertainties in foundation analysis. In *Geotechnical Engineering for Transportation Infrastructure*. Barends et. al. (eds.). Balkema, Rotterdam. pp 385-392.

Lacasse, S., and Goulois, A. 1989. Uncertainty in API parameters for predictions of axial capacity of driven pile in sand. 21st OTC Houston, Texas, USA. Paper 6001, pp 353-358.

Lacasse, S., and de Lamballerie, J.Y. 1995. Statistical treatment of CPT data. Proceedings of CPT'95, Linkoping, Sweden.

Lacasse, S., and Nadim, F. 1996. Uncertainties in characterizing soil properties. In *Uncertainty in the Geologic Environment: From theory to Practice*, Proceedings of Uncertainty'96. Geotechnical Special Publication No. 58, ASCE, NY, USA, August 31-July 3. Volume 1. pp 49-75.

Ladd, C.C. 1983. Geotechnical exploration in clay deposits with emphasis on recent advances in laboratory and in-situ testing and analysis of data scatter. Journal of Civil and Hydraulic Engineering, Taiwan, 10, (3): 3-35.

Ladd, C.C., Dascal, O., Law, K.T., Lefebrve, G., Lessard, G., Mersi, G., and Tavenas, F. 1983. Report of the subcommittee on embankment stability-annex II. Committee of Specialists on Sensitive Clays on the NBR Complex. Societe d'Energie de la Baie James, Montreal, Quebec, Canada.

Lambe, P.C. 1996. Residual soils. In *Landslides: Investigation and Mitigation*. Special Report No. 247, pp 507-524. Transportation Research Board, Washington, D.C.

Law, A.M., and MaComas, M.G. 1986. Pitfalls in the simulation of manufacturing systems. Proceedings of the Winter Simulation Conference, Washington D.C., pp 539-542.

Lee, E.M., Brunsden, D., and Sellwood, M. 2000. Quantitative risk assessment of coastal landslide problems, Lyme Regis, UK. Proceedings of the 8th International Symposium on Landslides, Cardiff, UK, June 26-30. Volume 2, pp 899-904.

Lee, M.E., Clark, A.R., and Guest, S. 1998. An assessment of coastal landslide risk, Scarborough, UK. Proceedings of the 8th International Association of Engineering Geology (IAEG) Congress, pp 1787-1794.

Lefebvre, G., Pare, J.J., and Dascal, O. 1987. Undrained shear strength in the surficial weathered crust. Canadian Geotechnical Journal, 24: 23-24.

Leiba, M.M., and Baynes, F. 2000. Quantitative landslide risk assessment of Cairns, Australia. Proceedings of the 8th International Symposium on Landslides, Cardiff, UK, June 26-30. Volume 2, pp 1059-1064.

Li, K.S. 1991. Discussion on: Probabilistic potentiometric surface mapping. Journal of Geotechnical Engineering Division, ASCE, 117, (9): 1457-1458.

Li, K.S. 1992a. A point estimate method for calculating the reliability index of slopes. Proceedings of the 6th Australia-New Zealand Conference on Geomechanics, Christchurch, pp 448-451.

Li, K.S. 1992b. A unified solution scheme for slope stability analysis. Proceedings of the 6th International Symposium on Landslides, Christchurch, New Zealand, February 10-14, pp 481-486.

Li, K.S. 1994. Discussion of "Estimating autocovariance of in-situ soil properties". Journal of the Geotechnical Engineering Division, ASCE, 120, (8): 1454-1455.

Li, K.S., and Lee, I.K. 1991. The assessment of geotechnical safety. In *Selected Topics in Geotechnical Engineering – Lumb Volume*. Li, K.S. (ed.). University of New South Wales, Australia. pp195-229.

Li, K.S., and Lumb, P. 1987. Probabilistic design of slopes. Canadian Geotechnical Journal, 24: 520-535.

Li, K.S., and White, W. 1987. Reliability index of slopes. Reliability and Risk Analysis in Civil Engineering 2: Proceedings of 5th International Conference on Applications of Statistics and Probability in Soil and Structural Engineering, Vancouver, Canada, May 25-29. Volume 2, pp 755-762.

Low, B.K., and Tang, W.H. 1997. Probabilistic slope analysis using Janbu's generalized procedure of slices. Computers and Geotechnics, 21, (2): 121-142.

Low, B.K., and Tang, W.H. 1997. Reliability analysis of reinforced embankments on soft ground. Canadian Geotechnical Journal, 34: 672-685.

Lumb, P. 1962. The properties of decomposed granite. Geotechnique, 12: 226-243.

Lumb, P. 1965. The residual soils of Hong Kong. Geotechnique, 15: 180-194.

Lumb, P. 1966. The variability of natural soils. Canadian Geotechnical Journal, 3, (2): 74-97.

Lumb, P. 1970. Probability of failure in earth works. Proceedings of 2nd Southeast Asian Conference on Soil Engineering, Singapore. pp 139-147.

Lumb, P. 1975. Slope failure in Hong Kong. Quarterly Journal of Engineering Geology, 8: 31-65.

Lumb, P. 1980. Thirty years of soil engineering in Hong Kong. In *Selected Topics in Geotechnical Engineering – Lumb Volume*. Li, K.S. (ed.). University of New South Wales, Australia. pp 18-38.

Lumb, P. 1983. Statistical soil mechanics. Proceedings of the 7th Asian Regional Conference on Soil Mechanics and Foundation Engineering, Haifa. Volume 2, pp 67-81.

Mace, A.E. 1964. Sample-size determination. Reinhold Publishing Corporation, New York.

Major, G., Ross-Brown, D.M., and kim, H-S. 1978. A general probabilistic analysis for three-dimensional wedge failures. Proceedings of the 19th US Symposium on Rock Mechanics, Nevada, USA, pp 45-56.

Mardia, K.V., and Marshall, R.J. 1984. Maximum likelihood estimation of models for residual covariance in spatial regression. Biometrika, 71, (1): 135-146.

Marek, J.M., and Savely, J.P. 1978. Probabilistic analysis of the plane shear failure mode. Proceedings of the 19th US Symposium on Rock Mechanics, Nevada, USA, pp 40-44.

Massey, J.B. 1983. Shear strength of Hong Kong residual soil: a review of work carried out by the Geotechnical Control Office. Geotechnical Control Office, Hong Kong, Report 25/83.

Matsuo, M., and Kuroda, K. 1974. Probabilistic approach to design of embankments. Soils and Foundations, 14, (2):1-17.

McGuffey, V., Grivas, D., Iori, J., and Kyfor, Z. 1982. Conventional and probabilistic embankment design. Journal of the Geotechnical Engineering Division, ASCE, 108, (10): 1246-1254.

McKay, M.D., Beckman, R.J., and Conover, W.J. 1979. A comparison of three methods for selecting values of input variables in the analysis of output from a computer code. Technometrics, 21, (2): 239-245.

McMahon, B.K. 1975. Probability of failure and expected volume of failure in high rock slopes. Proceedings of the 2nd Australia-New Zealand Conference on Geomechanics, Brisbane, pp 308-313.

Melchers, R.E. 1993. On the treatment of uncertainty information in PRA. In *Probabilistic Risk and hazard Assessment*, Melchers and Stewart (eds.). Proceedings of the Conference on Probabilistic Risk and Hazard Assessment, Newcastle, Australia, September 22-23, pp 13-26.

Melchers, R.E., and Stewart, M.G. (eds.) 1993. Probabilistic risk hazard assessment. Proceedings of the Conference on Probabilistic Risk and Hazard Assessment, Newcastle, Australia, September 22-23, 1993. A.A. Balkema.

Meyerhof, G.G. 1970. Safety factors in soil mechanics. Canadian Geotechnical Journal, 7: 349-355.

Milligan, V. 1972. Panel Discussion, Session I: Embankments on Soft Ground. Proceedings of the ASCE Specialty Conference on Performance of Earth and Earth-Supported Structures, Purdue University, Lafayette, USA. Volume 3, pp 41-48.

Moon, A.T., Olds, R.J., Wilson, R.A., and Burman, B.C. 1992. Debris flow risk zoning at Montrose, Victoria. Proceedings of the 6th International Symposium on Landslides, Christchurch, New Zealand, February 10-14, pp 1015-1022.

Morgan, G.C., Rawlings, G.E., and Sobkowicz J.C. 1992. Evaluating total risk to communities from large debris flows. In *Geotechnique and Natural Hazards*. Proceedings of the 1st Canadian Symposium on Geotechnique and Natural Hazards, Vancouver, Canada, May 6-9, pp 225-236.

Morgenstern, N.R. 1995. Managing risk in geotechnical engineering. Proceeding of the 10th Pan American Conference on Soil Mechanics and Foundation Engineering. Volume 4, in press.

Morgenstern, N.R. 1997. Toward landslide risk assessment in practice. In *Landslide Risk Assessment*, Cruden & Fell (eds.). Proceedings of The International Workshop on Landslide Risk Assessment, Honolulu, USA, February 19-21, pp 15-23.

Morgenstern, N.R. 1998. Geotechnics and mine waste management – an update. Proceedings of Workshop on Risk Assessment and Contingency Planning in Tailings Management Systems. Buenos Aires, International Council on Metals in the Environmental, pp 171-175.

Morgenstern, N.R. 2000. Performance in geotechnical predictions. The First Lumb Lecture, Hong Kong, May 10.

Morgenstern, N.R., and Price, V.E. 1965. The analysis of the stability of general slip surfaces. Geotechnique, 15, (1): 79-93.

Mostyn, G.R., and Li, K.S. 1993. Probabilistic slope stability analysis - State-of-play. In *Probabilistic Methods in Geotechnical Engineering*, Li & Lo (eds.). pp 89-109.

Neowhouse, M.M. 1993. The use of software based qualitative risk assessment methodologies. In *Probabilistic Risk and hazard Assessment*, Melchers and Stewart (eds.). Proceedings of the Conference on Probabilistic Risk and Hazard Assessment, Newcastle, Australia, September 22-23, pp 147-155.

Neter, J., Wasserman, W., and Kutner, M.H. 1990. *Applied linear statistical models*. Third edition, Richard D. Irwin Inc., USA.

Nguyen, V.U., and Chowdhury, R.N. 1984. Probabilistic study of spoil pile stability in strip coal mines - two techniques compared. International Journal of Rock Mechanics, Mining Science and Geomechanics, 21, (6): 303-312.

Nguyen, V.U., and Chowdhury, R.N. 1985. Simulation for risk analysis with correlated variables. Geotechnique, 35, (1): 47-58.

Nicol, D. 1994. The Syncrude Mildred lake tailings dyke redesign. Transactions of the Eighteenth International Congress on Large Dams, Durban, South Africa, November 7-11. Volume 3, pp 145-184.

Paice, G.M., Griffiths, D.V., and Fenton, G.A. 1994. Influence of spatially random soil stiffness on foundation settlement. Proceedings of the Conference on Vertical and Horizontal Deformation of Foundations and Embankments. College Station, Texas, USA. Part 1, pp. 628-639.

Palisade Corporation, 1996. @Risk: risk analysis and simulation add-in for Microsoft Excel or Lotus 1-2-3. Palisade Corporation, Newfield, NY, USA.

Peck, R.B. 1940. Sampling methods and laboratory tests for Chicago subway soils. Proceedings of the Purdue Conference on Soil Mechanics and Its Applications. Purdue University, Lafayette, USA, September 2-6, pp 140-150

Peck, R.B. 1967. Stability of natural slopes. Journal of the Soil Mechanics and Foundation Division, ASCE, 93, (4): 403-417.

Peck, R.B. 1973. Influence of non-technical factors on the quality of embankment dams. In *Embankment Dam Engineering,* Casagrande Volume. Editors Hirschfield and Poulos. John Wiley & Sons, New York, pp 201-208.

Peck, R.B., and Reed, W.C. 1954. Engineering properties of Chicago subsoils. University of Illinois Engineering Experimental Station, Bulletin No. 423.

Pentz, D.L. 1982. Slope stability analysis techniques incorporating uncertainty in critical parameters. In *Stability in Surface Mining*. Brawner, C.O. (ed.). Volume 3, pp 197-228.

Phoon, K.K., and Kulhawy, F.H. 1996. On quantifying inherent soil variability. In *Uncertainty in the Geologic Environment: From theory to Practice*, Proceedings of

Uncertainty'96. Geotechnical Special Publication No. 58, ASCE, NY, USA, August 31-July 3. Volume 1. pp 326-340.

Phoon, K.K., and Kulhawy, F.H. 1999. Characterization of geotechnical variability. Canadian Geotechnical Journal, 36: 612-624.

Phoon, K.K., Kulhawy, F.H., and Grigoriu, M.D. 1995. Reliability-based design of foundations for transmission structures. Report No. TR-105000, Electric Power Research Institute, Palo Alto.

Pierson, L.A. 1992. Rockfall hazard rating system. Transportation Research Board, No. 1343, pp 6-13, Washington, D.C.

Polous, H.G., Lee, Y.C., and Small, J.C. 1990. Predicted and observed behaviour of a test embankment on Malaysian soft clays. Research Report No. R620, University of Sydney.

Premchitt, J., Brand, E.W., and Phillipson, H.B. 1986. Landslides caused by rapid groundwater changes. Groundwater in Engineering Geology, Proceedings of the 21th Annual Conference of the Engineering Group of the Geological Society, London, September 15-19, 1985. pp 87-94.

Priest, D.S., and Brown, E.T. 1983. Probabilistic stability analysis of variable rock slopes. Transactions of the Institute of Mining and Metallurgy (*Section A: Mining Industry*), 92: A1-A12.

Pun, W.K., and Ho, K.K.S. 1996. Analysis of triaxial tests on granitic saprolite performed at Public Works Central Laboratory. Geotechnical Engineering Office, Hong Kong, Discussion Note DN 4/96, 72p.

Rogowski, A.S. 1990. Relationship of laboratory and field-determined hydraulic conductivity in compacted clay layer. Report to United States Environmental Protection Agency, EPA/600/2-90/025.

Reeves, A., Chan, H.C., and Lam, K.C. 1998. Preliminary quantitative risk assessment of boulder falls in Hong Kong. In *Slope Engineering in Hong Kong*. Li, Kay and Ho (eds.), Balkema, pp185-191.

Reeves, A., Ho, K.K.S., and Lo, D.O.K. 1999. Interim risk criteria for landslides and boulder falls from natural terrain. In *Geotechnical Risk Management*, Proceedings of the 18th Annual Seminar. The geotechnical Division of the Hong Kong Institution of Engineers. May 14, pp 129-136.

Ronold, K.O. 1990. Random field modeling of foundation failure modes. Journal of Geotechnical Engineering Division, ASCE, 116, (4): 554-570.

Rosenblueth, E. 1975. Point estimates for probability moments. Proceedings of National Academy of Sciences, USA, 72, (10): 3812-3814.

Rosenblueth, E. 1981. Two-point estimates in probabilities. Applied Mathematical Modeling, 5: 329-335.

Russo, D., and Jury, W.A. 1988. Effect of sampling network on estimates of the covariance function of stationary fields. Journal of the Soil Science Society of America, 52: 1228-1234.

Samdal, U.N, Kortner, H., and Grammeltvedt, J.A. 1992. A user's view on quantification of human reliability. International Conference on Hazard Identification and Risk Analysis, Human Factors and Human Reliability in Process safety. Orlando, USA, January 15-17, pp 281-292.

Salmon, G.M., and Hartford, D.N.D. 1995. Risk analysis for dam safety. International Water Power & Dam Construction. March issue, pp 42-47.

Salmon, G.M., and Hartford, D.N.D. 1995. Risk analysis for dam safety - Part II. International Water Power & Dam Construction. March issue, pp 38-39.

Schmertmann, J.S., and Morgenstern, N.R. 1977. Discussion to Session I : Stress-Deformation and Strength Characteristic. Proceedings of the Ninth International Conference on Soil Mechanics and Foundation Engineering, Tokyo, Japan. Volume 3, pp 356-359.

Schuster, R.L. 1999. Concepts of risk-based decision making with emphasis on geotechnical engineering and slope hazards. In *Geotechnical Risk Management*, Proceedings of the 18th Annual Seminar. The geotechnical Division of the Hong Kong Institution of Engineers. May 14, pp 1-21.

Seed, R.B., Mitchell, J.K., and Seed, H.B. 1990. Kettleman Hills waste landfill slope failure. II Stability analyses. Journal of Geotechnical Engineering Division, ASCE, 116, (4): 669-690.

Sevaldson, R.A. 1956. The slide in Lodalen, October 6, 1954. Geotechnique, 6, (4): 167-82.

Shelton, J.C., and Cooper, A.J. 1984. The shear strength of decomposed granite from Glenealy area. Geotechnical Engineering Office, Hong Kong, Technical Note TN 1/84, 41p.

Shen, J.M. 1985. GCO research into unsaturated shear strength 1978-1982. Geotechnical Control Office, Hong Kong, Research Report PR 1/85.

Singh, A. 1972. How reliable is safety factor in foundation engineering?. Proceedings of 1st International Conference on Applications of Statistics and Probability to Soil and Structural Engineering, Hong Kong, September 13-16, 1971. pp 389-424.

Siu, K.L., and Premchitt, J. 1988. Landslides studies 1987: Cho Yiu Estate. Geotechnical Engineering Office, Hong Kong, Special Project Report SPR 3/88, 61p.

Skempton, A.W. 1964. Long-term stability of clay slopes. Fourth Rankine Lecture, Geotechnique, 14: 77-102.

Skempton, A.W. 1977. Long trem stability of cuttings in brown London clay. Special lecture, Proceedings of 9th International Conference on Soil Mechanics and Foundation Engineering, Tokyo, Japan.

Skempton, A.W. 1985. Geotechnical aspects of the Carsington dam failure. Proceedings of the 11th International Conference on Soil Mechanics and Foundation Engineering, San Francisco, USA, Volume 5. pp 2581-2591.

Soulie, M., Montes, P., and Silvestri, V. 1990. Modeling spatial variability of soil parameters. Canadian Geotechnical Journal, 27: 617-630.

Sowers, G.F., 1991. The human factor in failures. Civil Engineering, ASCE, March, pp72-73.

Spencer, E. 1967. A method of analysis of the stability of embankments assuming inter-slice forces. Geotechnique, 17: 11-26.

Strange, P.G. 1990. The classification of granitic rocks in Hong Kong and their sequence of emplacement in Sha Tin, Kowloon and Hong Kong Island. Geotechincal Society of Hong Kong Newsletter, 8, part 1, 18-27.

Sweeney, D.J., and Robertson, P.K. 1979. A fundamental approach to slope stability problems in Hong Kong. Hong Kong Engineer, October issue: 35-44.

Swain, A.D., and Guttman, H.E. 1983. Human reliability analysis with emphasis on nuclear power plant applications. NUREG/CR – 1278, USNRC, Washington, DC 20555.

Syncrude Canada, 1988. N.W. corridor (1988/89/90) overburden slope design project: Laboratory test report, Volume 1. Operations Laboratory.

Syncrude Canada, 1991. Summary of geotechnical testing for the 1990 S4 dump project for in-situ overburden units and dump fill.

Syncrude Canada, 1992. Report on the performance of the Mildred lake tailings dyke and south west sand storage facility during 1991 and the proposed construction for 1992. Report submitted to: Alberta Environment Dam Safety Branch; and Energy Resources Conservation Board.

Syncrude Canada, 1997. Report on the performance of Mildred lake settling basin during 1996 and the construction proposal for 1997. Report submitted to: Alberta Environment Protection Dam Safety Branch; and Alberta Energy and Utilities Board.

Tang, W.H. 1979. Probabilistic evaluation of penetration resistances. Journal of the Geotechnical Engineering Division, ASCE, 105, (10): 1173-1191.

Tang, W.H. 1984. Principles of probabilistic characterization of soil properties. Proceedings of ASCE Symposium on Probabilistic Characterization of Soil Properties - Bridge Between Theory and Practice. Atlanta, USA, May 17, pp 74-98.

Tang, W.H., Li, V.K.S., and Cheung, R.W.M. 1999. Some uses and misuses of reliability methods in geotechnical engineering. In *Geotechnical Risk Management*, Proceedings of the 18th Annual Seminar. The geotechnical Division of the Hong Kong Institution of Engineers. May 14, pp 89-96.

Tang, W.H., Yucemen, M.S., and Ang, A.H.S. 1976. Probability-based short term design of slopes. Canadian Geotechnical Journal, 13: 201-215.

Tavenas, F., Leroueil, S., and Roy, M. 1980. A new approach to the stability analysis of embankments on sensitive clays. The behaviour of embankments on clay foundations. Canadian Geotechnical Journal, 17: 236-260.

Tejchman, A., Gwizdala, K., and Brzozowski, T. 1996. Quasi-probabilistic method of slope stability analysis. Proceedings of the 7th International Symposium on Landslides, Trondheim, Norway, June 17-21, pp 1381-1385.

Thompson, K.D., Stedinger, J.R., and Heath, D.C. 1997. Evaluation and presentation of dam failure and flood risks. Journal of Water Resources Planning and Management, ASCE, 123, (4): 216-227.

Thurber Consultants, 1984. Syncrude tailings dyke deformation and stability analyses. Report to Syncrude Canada. Ref. No.: 17/539-25-1019H.

Thurber Consultants, 1989. Tailings dyke stability analysis: cells 8-18 and 23. Report to Syncrude Canada. Ref. No.: 05/17/539-67C.

Tobutt, D.C. 1982. Monte carlo simulation methods for slope stability. Computers and Geosciences, 8, (2): 199-208.

Tobutt, D.C., and Richards, E.A. 1979. The reliability of earth slopes. International Journal for Numerical and Analytical Methods in Geomechanics, (3): 323-354.

US Army Corps of Engineers 1992. Reliability Assessment of Navigation Structures. Engineering Technical Letter No. 1110-2-532, Washington DC.

US Army Corps of Engineers 1995. Introduction to Probability and Reliability Methods for Use in Geotechnical Engineering. Engineering Technical Letter No. 1110-2-547, Washington DC.

Vanmarcke, E.H. 1977a. Probabilistic modeling of soil profiles. Journal of the Geotechnical Engineering Division, ASCE, 103, (11): 1227-1246.

Vanmarcke, E.H. 1977b. Reliability of earth slopes. Journal of the Geotechnical Engineering Division, ASCE, 103, (11): 1247-1265.

Vanmarcke, E.H. 1980. Probabilistic stability analysis of earth slopes. Engineering Geology, 16: 29-50.

Vanmarcke, E.H. 1983. Random fields: analysis and synthesis. The MIT Press, Cambridge, Massachusetts, England.

Vaughan, P.R., and Walbancke, H.J. 1975. The stability of cut and fill slopes in boulder clay. Proceedings of the Symposium on Engineering Behavior of Glacial Materials. Birmingham, England, pp 209-219.

Viberg, L. 1984. Landslide risk mapping in soft clays in Scandinavia and Canada. Proceedings of the 4th International Symposium on Landslides, Toronto, Canada, September 16-21. Volume 1, pp 325-348.

Walpole, R.E., and Myers, R.H. 1978. Probability and statistics for engineers and scientists. 2nd edition. Macmillan Publishing Co., Inc., New York, USA.

Whitman, V.W. 1984. Evaluating calculated risk in geotechnical engineering. Journal of Geotechnical Engineering Division, ASCE, 110, (2): 145-188.

Whitman, V.W. 1996. Organizing and evaluating uncertainty in geotechnical engineering. In *Uncertainty in the Geologic Environment: From theory to Practice*, Proceedings of Uncertainty'96. Geotechnical Special Publication No. 58, ASCE, NY, USA, August 31-July 3. Volume 1. pp 1-28.

Wolff, T.F. 1985. Analysis and design of embankment dam slopes: a probabilistic approach. Thesis submitted in partial fulfillment of the requirements for the degree of Doctor of Philosophy, Purdue University, IN.

Wolff, T.F. 1991. Application Brief - Embankment reliability versus factor of safety: before and after slide repair. International Journal for Numerical and Analytical Methods in Geomechanics, 15: 41-50.

Wolff, T.F. 1996. Probabilistic slope stability in theory and practice. In *Uncertainty in the Geologic Environment: From theory to Practice*, Proceedings of Uncertainty'96. Geotechnical Special Publication No. 58, ASCE, NY, USA, August 31-July 3. Volume 2. pp 419-433.

Wolff, T.F., and Harr, M.E. 1987. Slope design for earth dams. Reliability and Risk Analysis in Civil Engineering 2: Proceedings of 5th International Conference on Applications of Statistics and Probability in Soil and Structural Engineering, Vancouver, Canada, May 25-29. Volume 2. pp 725-732.

Wong, H.N., and Ho, K.K.S. 1996. Travel distance of landslide debris. Proceedings of the 7th International Symposium on Landslides, Trondheim, Norway, June 17-21, pp 417-422.

Wong, H.N., and Ho, K.K.S. 1998. Overview of risk of old man-made slopes and retaining walls in Hong Kong. Quantitative risk assessment of landslides – a case history from Hong Kong. In *Slope Engineering in Hong Kong*. Li, Kay and Ho (eds.), Balkema, pp193-200.

Wong, H.N., Ho, K.S.S., and Chan, Y.C. 1997. Assessment of Consequence of landslides. In *Landslide Risk Assessment*, Cruden & Fell (eds.). Proceedings of the International Workshop on Landslide Risk Assessment, Honolulu, USA, February 19-21, pp 111-149.

Wu, T.H. 1974. Uncertainty, Safety, and decision in soil engineering. Journal of Geotechnical Engineering Division, ASCE, 100, (3): 329-348.

Wu, T.H. 1992. Prediction and mapping of landslide hazards. Proceeding of the 2nd US-Asia Conference on Engineering for Mitigating Natural Hazards Damage, Yogyakarta, Indonesia, pp G10-1 to G10-08.

Wu, T.H., and Kraft, L.M. 1967. The probability of foundation safety. Journal of the Soil Mechanics and Foundation Division, ASCE, 93, (5): 213-231.

Wu, T.H., Lee, I.M., Potter, J.C., and Kjekstad, O. 1987. Uncertainties in evaluation of strength of marine sand. Journal of the Geotechnical Engineering Division, ASCE, 113, (7): 719-738.

Wu, T.H., Tang, W.H., and Einstein, H.H. 1996. Landslide hazard and risk assessment. In *Landslides: Investigation and Mitigation*. Special Report No. 247, pp 106-118. Transportation Research Board, Washington, D.C.

Wu, T.H., Tang, W.H., Sangrey, D.A., and Baecher, G.B. 1989. Reliability of offshore foundations-State of the art. Journal of the Geotechnical Engineering Division, ASCE, 115, (2): 157-178.

Wu, T.H., Thayer, W.B., and Lin, S.S. 1975. Stability of embankment on clay. Journal of Geotechnical Engineering Division, ASCE, 101, (9): 913-932.

Yucemen, M.S., and Tang, W.H. 1975. Long term stability of slopes, a reliability approach. Proceedings of 2nd International Conference on Applications of Statistics and Probability in Soil and Structural Engineering, Aachen, Germany, September 15-18, pp 215-230.

Yucemen, M.S., and Al-Homoud, A.S. 1990. Probabilistic three-dimensional stability analysis of slopes. Structural Safety, 9: 1-20.

Zeitoun, D.G., and Baker, R. 1992. A stochastic approach for settlement predictions of shallow foundations. Geotechnique, 42, (4): 617-629.

APPENDIX I

EXAMPLE OF SPREADSHEET MODEL
JAMES BAY CASE STUDY
DESIGN 1

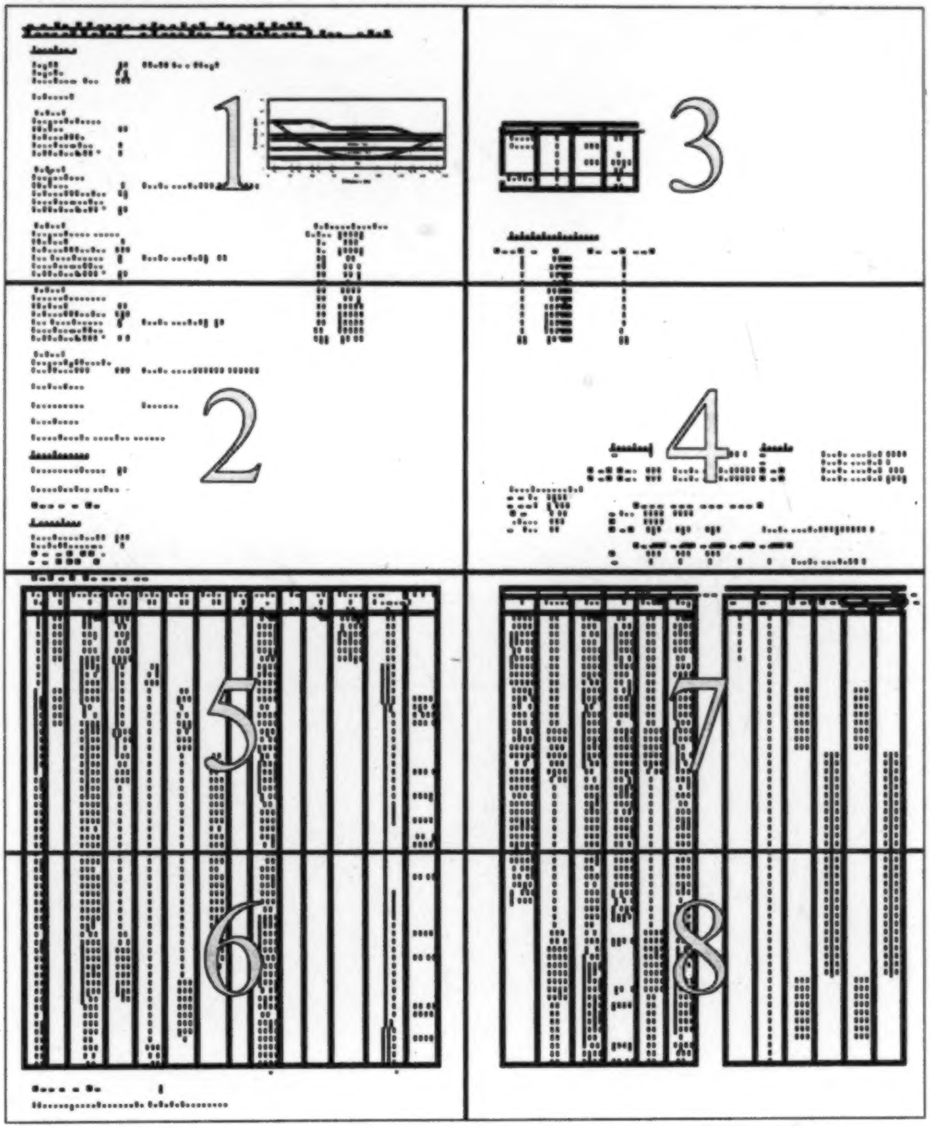

Spreadsheet Layout

JAMES BAY HYDROELECTRIC CASE STUDY - DESIGN 1 (H=12m)

PROPOSED PROBABILISTIC SLOPE ANALYSIS METHODOLOGY (BISHOP'S METHOD)

1-	**Slope Geometry**		
	Height, H (m)	12.0	With a 56m berm at mid height
	Slope "h : v"	3.0 : 1.0	
	Slope Angle, θ (deg.)	18.4	
2-	**Soil Stratigraphy**		
	Soil Type 1		
	Description : Cohesionless fill		
	Thickness, t_m (m)	12.0	
	Cohesion, C_m (kPa)	0.0	
	Friction Angle, ϕ_m (deg.)	30.0	
	Bulk Unit Weight, γ_m (kN/m^3)	20.0	
	Soil Type 2		
	Description : Clay crust		
	Thickness, t_{cr} (m)	4.0	Random variable (TN(4,0.48,2.56,5.44))
	Undrained Shear Strength, S_{u-cr} (kPa)	41.0	
	Friction Angle, ϕ_{u-cr} (deg.)	0.0	
	Bulk Unit Weight, γ_{cr} (kN/m^3)	19.0	
	Soil Type 3		
	Description : Sensitive marine clay		
	Thickness, t_M (m)	8.0	
	Undrained Shear Strength, S_{uM} (kPa)	34.5	
	Bjerrum Vane Correction Factor, μ_M	1.00	Random variable (N(1.0,0.075))
	Friction Angle, ϕ_{uM} (deg.)	0.0	
	Bulk Unit Weight, γ_M (kN/m^3)	19.0	

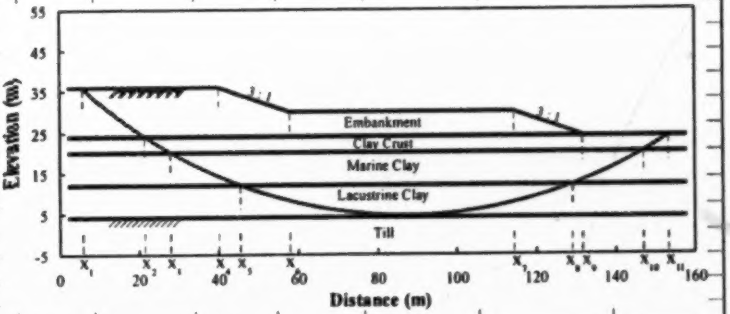
Elevation (m)
55
45
35
25
15
5
-5
0
20
40
60
80
100
120
140
160
Distance (m)
3:1
3:1
Embankment
Clay Crust
Marine Clay
Lacustrine Clay
Till
X_1
X_2
X_3
X_4
X_5
X_6
X_7
X_8
X_9
X_{10}
X_{11}

Slip Surface Control Points

Radius, R	122.81	
Xo	85.90	Centre of slip circle
Yo	128.31	
X1	4.90	
X2	21.08	
X3	28.01	

				X4	40.00
	Soil Type 4			X5	46.48
	Description : Lacustrine clay			X6	58.01
	Thickness, t_L (m)	6.5		X7	114.43
	Undrained Shear Strength, S_{uL} (kPa)	31.2		X8	125.32
	Bjerrum Vane Correction Factor, μ_L	1.00	Random variable {N(1.0,0.15)}	X9	132.43
	Friction Angle, ϕ_{uL} (deg.)	0.0		X10	143.79
	Bulk Unit Weight, γ_L (kN/m^3)	20.5		X11	150.72
	Soil Type 5				
	Description : Till (rigid boundary)				
	Depth below G.S., D_{ts} (m)	18.5	Random variate {TN(18.5,1.0,15.5,21.5)}		
3-	Pore Water Pressure				
	Pore pressure ratio, r_u	0.00	Total stress analysis		
4-	Failure Surfcae				
	Circular; obtained from a series of deterministic analyses				
5-	Spatial Averaging				
	Autocorrelation distance; r_o (m)	15			
6-	Factor of Safety (Deterministic Analysis)				
	Factor of Safety (FS) =	**1.456**			
7-	Simulation Output				
	Mean Factor of Safety, E[FS] =	**1.464**			
	Standard Deviation, σ[FS] =	**0.20**			
	P_u = P (FS<=1.0) =	**0.47%**			
	β = (E[FS] - 1)/σ[FS]	**2.32**			

Category	Line No.	Slope	Intercept
Ground	1	0.000	36.000
Surface	2	-0.333	49.333
	3	0.000	30.000
	4	-0.333	68.140
	5	0.000	24.000
Sub-Layers	6	0.000	20.000
	5	0.000	12.000

Table For Ranking X values

Rank in list	X		Desired rank
1	4.90		1
2	21.08		2
3	28.01		3

4	40.00		4									
5	46.48		5									
6	58.01		6									
7	114.43		7									
9	132.43		8									
8	125.32		9									
10	143.79		10									
11	150.72		11									
			Spatial Variability					Statistical Error				
			ϕ_{fill}	30.00	Random variable {N(30,1.0)}			ϕ_{fill}	0.00	Random variable {N(0,1.732)}		
								γ_{fill}	0.00	Random variable {N(0,1.0)}		
			$S_{uM\ Zone\ 1}$	34.50	Random variable {TN(34.5,8.142,0,80)}			S_{uM}	0.00	Random variable {N(0,0.951)}		
			$S_{uM\ Zone\ 2}$	34.50	Random variable {TN(34.5,8.142,0,80)}			S_{uL}	0.00	Random variable {N(0,1.731)}		
Spatial Averaging (S_{uL})												
ψ_o (deg.)	71.28											
ψ_{end} (deg.)	108.72			Zone 1	Zone 2	Zone 3	Zone 4					
Arc (m)	80.27		ψ_i (deg.)	85.27	99.27	108.72	108.72					
# of Zones	2.68		X limits	75.78	105.68	125.32	125.32					
ψ_r (deg.)	14.00		S_{uL}	31.20	31.20	31.20		Random variables {TN(31.2,8.649,0,80)}				
				Zone 1	Zone 2	Zone 3	Zone 4	Zone 5				
			X limits	34.90	64.90	94.90	124.90	132.43				
			γ_{fill}	20.00	20.00	20.00	20.00	20.00	Random variables {N(20,1.0)}			

Table of Calculations

Slice	Width	Total Height	Ht. in Soil#1	Ht. in Soil#2	Ht. in Soil#3	Ht. in Soil#4	Weight	Base Angle	W sin α	c'b	$W(1-r_u)\tan\phi'$	$\frac{\sec\alpha}{1+(\tan\phi'.\tan\alpha/F)}$ (*)	("2"+"3")."4"
No.	b	h	h_1	h_2	h_3	h_4	W	α		"2"	"3"		
	(m)	(m)	(m)	(m)	(m)	(m)	(kN)	(deg.)	(kN)	(kN/m)	(kN)	"4"	
1	2.70	1.17	1.17	0.00	0.00	0.00	62.88	40.44	40.79	0.00	36.31	0.98	35.656
2	2.70	3.40	3.40	0.00	0.00	0.00	183.28	38.81	114.86	0.00	105.82	0.97	102.966
3	2.70	5.51	5.51	0.00	0.00	0.00	296.93	37.21	179.56	0.00	171.43	0.97	165.449
4	2.70	7.50	7.50	0.00	0.00	0.00	404.25	35.65	235.58	0.00	233.39	0.96	223.629
5	2.70	9.37	9.37	0.00	0.00	0.00	505.62	34.11	283.55	0.00	291.92	0.95	277.946
6	2.70	11.15	11.15	0.00	0.00	0.00	601.36	32.60	324.04	0.00	347.19	0.95	328.773
7	2.31	12.71	12.00	0.71	0.00	0.00	585.58	31.23	303.59	94.72	0.00	1.17	110.768
8	2.31	14.08	12.00	2.08	0.00	0.00	645.55	29.98	322.53	94.72	0.00	1.15	109.346
9	2.31	15.37	12.00	3.37	0.00	0.00	702.58	28.74	337.81	94.72	0.00	1.14	108.026
10	2.40	16.63	12.00	4.00	0.63	0.00	786.79	27.49	363.22	82.75	0.00	1.13	93.289
11	2.40	17.85	12.00	4.00	1.85	0.00	842.17	26.24	372.33	82.75	0.00	1.11	92.260
12	2.40	19.00	12.00	4.00	3.00	0.00	894.58	25.00	378.03	82.75	0.00	1.10	91.306
13	2.40	20.08	12.00	4.00	4.08	0.00	944.12	23.77	380.52	82.75	0.00	1.09	90.423
14	2.40	21.11	12.00	4.00	5.11	0.00	990.88	22.55	380.02	82.75	0.00	1.08	89.605
15	2.16	21.67	11.64	4.00	6.03	0.00	913.40	21.40	333.35	74.43	0.00	1.07	79.945
16	2.16	21.77	10.92	4.00	6.85	0.00	916.08	20.33	318.24	74.43	0.00	1.07	79.374
17	2.16	21.83	10.20	4.00	7.63	0.00	916.88	19.26	302.40	74.43	0.00	1.06	78.842
18	2.88	21.84	9.36	4.00	8.00	0.48	1225.20	18.02	378.97	89.94	0.00	1.05	94.581
19	2.88	21.78	8.40	4.00	8.00	1.38	1222.90	16.61	349.55	89.94	0.00	1.04	93.859
20	2.88	21.64	7.44	4.00	8.00	2.20	1216.06	15.21	319.05	89.94	0.00	1.04	93.208
21	2.88	21.43	6.48	4.00	8.00	2.94	1204.77	13.82	287.81	89.94	0.00	1.03	92.624
22	3.13	21.64	6.00	4.00	8.00	3.64	1325.13	12.38	284.10	97.82	0.00	1.02	100.146
23	3.13	22.29	6.00	4.00	8.00	4.29	1366.60	10.89	258.10	97.82	0.00	1.02	99.610
24	3.13	22.85	6.00	4.00	8.00	4.85	1402.64	9.40	229.10	97.82	0.00	1.01	99.149
25	3.13	23.33	6.00	4.00	8.00	5.33	1433.32	7.92	197.53	97.82	0.00	1.01	98.759
26	3.13	23.72	6.00	4.00	8.00	5.72	1458.71	6.45	163.79	97.82	0.00	1.01	98.440
27	3.13	24.04	6.00	4.00	8.00	6.04	1478.86	4.98	128.30	97.82	0.00	1.00	98.187
28	3.13	24.27	6.00	4.00	8.00	6.27	1493.80	3.51	91.46	97.82	0.00	1.00	98.001

	29	3.13	24.42	6.00	4.00	8.00	6.42	1503.58	2.05	53.67	97.82	0.00	1.00	97.880
	30	3.13	24.49	6.00	4.00	8.00	6.49	1508.20	0.58	15.34	97.82	0.00	1.00	97.822
	31	3.13	24.49	6.00	4.00	8.00	6.49	1507.67	-0.88	-23.16	97.82	0.00	1.00	97.829
	32	3.13	24.40	6.00	4.00	8.00	6.40	1502.01	-2.34	-61.41	97.82	0.00	1.00	97.899
	33	3.13	24.23	6.00	4.00	8.00	6.23	1491.18	-3.81	-99.04	97.82	0.00	1.00	98.034
	34	3.13	23.98	6.00	4.00	8.00	5.98	1475.18	-5.28	-135.63	97.82	0.00	1.00	98.233
	35	3.13	23.65	6.00	4.00	8.00	5.65	1453.97	-6.75	-170.80	97.82	0.00	1.01	98.499
	36	3.13	23.24	6.00	4.00	8.00	5.24	1427.51	-8.22	-204.13	97.82	0.00	1.01	98.833
	37	3.13	22.74	6.00	4.00	8.00	4.74	1395.75	-9.70	-235.22	97.82	0.00	1.01	99.237
	38	3.13	22.17	6.00	4.00	8.00	4.17	1358.61	-11.19	-263.64	97.82	0.00	1.02	99.713
	39	3.13	21.50	6.00	4.00	8.00	3.50	1316.03	-12.68	-288.98	97.82	0.00	1.03	100.264
	40	1.82	20.62	5.70	4.00	8.00	2.92	729.42	-13.87	-174.86	56.65	0.00	1.03	58.350
	41	1.82	19.55	5.09	4.00	8.00	2.46	690.22	-14.74	-175.67	56.65	0.00	1.03	58.577
	42	1.82	18.45	4.49	4.00	8.00	1.96	649.92	-15.62	-175.02	56.65	0.00	1.04	58.821
	43	1.82	17.32	3.88	4.00	8.00	1.44	608.50	-16.50	-172.86	56.65	0.00	1.04	59.082
	44	1.82	16.16	3.28	4.00	8.00	0.89	565.94	-17.39	-169.14	56.65	0.00	1.05	59.361
	45	1.82	14.98	2.67	4.00	8.00	0.30	522.24	-18.28	-163.79	56.65	0.00	1.05	59.658
	46	2.37	13.57	1.97	4.00	7.59	0.00	615.51	-19.31	-203.54	81.76	0.00	1.06	86.632
	47	2.37	11.92	1.18	4.00	6.73	0.00	539.45	-20.49	-188.80	81.76	0.00	1.07	87.278
	48	2.37	10.22	0.39	4.00	5.82	0.00	460.89	-21.67	-170.20	81.76	0.00	1.08	87.976
	49	2.27	8.87	0.00	4.00	4.87	0.00	382.81	-22.84	-148.60	78.36	0.00	1.09	85.024
	50	2.27	7.89	0.00	4.00	3.89	0.00	340.36	-24.00	-138.42	78.36	0.00	1.09	85.770
	51	2.27	6.85	0.00	4.00	2.85	0.00	295.53	-25.16	-125.65	78.36	0.00	1.10	86.571
	52	2.27	5.75	0.00	4.00	1.75	0.00	248.26	-26.34	-110.15	78.36	0.00	1.12	87.433
	53	2.27	4.60	0.00	4.00	0.60	0.00	198.47	-27.53	-91.73	78.36	0.00	1.13	88.360
	54	2.31	3.37	0.00	3.37	0.00	0.00	148.13	-28.74	-71.22	94.72	0.00	1.14	108.026
	55	2.31	2.08	0.00	2.08	0.00	0.00	91.09	-29.98	-45.51	94.72	0.00	1.15	109.346
	56	2.31	0.71	0.00	0.71	0.00	0.00	31.12	-31.23	-16.13	94.72	0.00	1.17	110.768
									Σ =	3903.91			Σ =	5685.441
	Factor of Safety "FS" =			**1.456**										

(*) The iterative process for the value of "F" is embeded in the calculations

Centre of Slice			Right Edge of Slice				Input Variables for Each Slice Taking Spatial Variability Into Account					
"X"	"Y" at slope	"Y" at slip surface	"X"	"Y" at slope	"Y" at slip surface		ϕ_{fill}	γ_{fill}	S_{uM}	S_{uL}	Truncated variables (>0)	
											S_{uM}	S_{uL}
6.248	36.00	34.83	7.60	36.00	33.70		30.00	20.00	0.00	0.00	0.00	0.00
8.945	36.00	32.60	10.29	36.00	31.53		30.00	20.00	0.00	0.00	0.00	0.00
11.642	36.00	30.49	12.99	36.00	29.49		30.00	20.00	0.00	0.00	0.00	0.00
14.338	36.00	28.50	15.69	36.00	27.55		30.00	20.00	0.00	0.00	0.00	0.00
17.035	36.00	26.63	18.38	36.00	25.72		30.00	20.00	0.00	0.00	0.00	0.00
19.732	36.00	24.85	21.08	36.00	24.00		30.00	20.00	0.00	0.00	0.00	0.00
22.235	36.00	23.29	23.39	36.00	22.60		0.00	20.00	0.00	0.00	0.00	0.00
24.545	36.00	21.92	25.70	36.00	21.27		0.00	20.00	0.00	0.00	0.00	0.00
26.856	36.00	20.63	28.01	36.00	20.00		0.00	20.00	0.00	0.00	0.00	0.00
29.210	36.00	19.37	30.41	36.00	18.75		0.00	20.00	34.50	0.00	34.50	0.00
31.609	36.00	18.15	32.81	36.00	17.57		0.00	20.00	34.50	0.00	34.50	0.00
34.007	36.00	17.00	35.21	36.00	16.45		0.00	20.00	34.50	0.00	34.50	0.00
36.406	36.00	15.92	37.61	36.00	15.39		0.00	20.00	34.50	0.00	34.50	0.00
38.805	36.00	14.89	40.00	36.00	14.40		0.00	20.00	34.50	0.00	34.50	0.00
41.083	35.64	13.97	42.16	35.28	13.55		0.00	20.00	34.50	0.00	34.50	0.00
43.240	34.92	13.15	44.32	34.56	12.75		0.00	20.00	34.50	0.00	34.50	0.00
45.397	34.20	12.37	46.48	33.84	12.00		0.00	20.00	34.50	0.00	34.50	0.00
47.917	33.36	11.52	49.36	32.88	11.06		0.00	20.00	0.00	31.20	0.00	31.20
50.800	32.40	10.62	52.24	31.92	10.20		0.00	20.00	0.00	31.20	0.00	31.20
53.682	31.44	9.80	55.12	30.96	9.42		0.00	20.00	0.00	31.20	0.00	31.20
56.564	30.48	9.06	58.01	30.00	8.71		0.00	20.00	0.00	31.20	0.00	31.20
59.573	30.00	8.36	61.14	30.00	8.02		0.00	20.00	0.00	31.20	0.00	31.20
62.708	30.00	7.71	64.28	30.00	7.42		0.00	20.00	0.00	31.20	0.00	31.20
65.843	30.00	7.15	67.41	30.00	6.90		0.00	20.00	0.00	31.20	0.00	31.20
68.977	30.00	6.67	70.54	30.00	6.46		0.00	20.00	0.00	31.20	0.00	31.20
72.112	30.00	6.28	73.68	30.00	6.11		0.00	20.00	0.00	31.20	0.00	31.20
75.247	30.00	5.96	76.81	30.00	5.84		0.00	20.00	0.00	31.20	0.00	31.20
78.382	30.00	5.73	79.95	30.00	5.64		0.00	20.00	0.00	31.20	0.00	31.20

81.516	30.00	5.58	83.08	30.00	5.53		0.00	20.00	0.00	31.20	0.00	31.20
84.651	30.00	5.51	86.22	30.00	5.50		0.00	20.00	0.00	31.20	0.00	31.20
87.786	30.00	5.51	89.35	30.00	5.55		0.00	20.00	0.00	31.20	0.00	31.20
90.921	30.00	5.60	92.49	30.00	5.68		0.00	20.00	0.00	31.20	0.00	31.20
94.055	30.00	5.77	95.62	30.00	5.89		0.00	20.00	0.00	31.20	0.00	31.20
97.190	30.00	6.02	98.76	30.00	6.17		0.00	20.00	0.00	31.20	0.00	31.20
100.325	30.00	6.35	101.89	30.00	6.55		0.00	20.00	0.00	31.20	0.00	31.20
103.460	30.00	6.76	105.03	30.00	7.00		0.00	20.00	0.00	31.20	0.00	31.20
106.595	30.00	7.26	108.16	30.00	7.53		0.00	20.00	0.00	31.20	0.00	31.20
109.729	30.00	7.83	111.30	30.00	8.15		0.00	20.00	0.00	31.20	0.00	31.20
112.864	30.00	8.50	114.43	30.00	8.86		0.00	20.00	0.00	31.20	0.00	31.20
115.339	29.70	9.08	116.25	29.39	9.31		0.00	20.00	0.00	31.20	0.00	31.20
117.155	29.09	9.54	118.06	28.79	9.79		0.00	20.00	0.00	31.20	0.00	31.20
118.970	28.49	10.04	119.88	28.18	10.29		0.00	20.00	0.00	31.20	0.00	31.20
120.785	27.88	10.56	121.69	27.58	10.83		0.00	20.00	0.00	31.20	0.00	31.20
122.601	27.28	11.11	123.51	26.97	11.40		0.00	20.00	0.00	31.20	0.00	31.20
124.416	26.67	11.70	125.32	26.37	12.00		0.00	20.00	0.00	31.20	0.00	31.20
126.509	25.97	12.41	127.69	25.58	12.83		0.00	20.00	34.50	0.00	34.50	0.00
128.879	25.18	13.27	130.06	24.79	13.72		0.00	20.00	34.50	0.00	34.50	0.00
131.248	24.39	14.18	132.43	24.00	14.66		0.00	20.00	34.50	0.00	34.50	0.00
133.569	24.00	15.13	134.70	24.00	15.61		0.00	20.00	34.50	0.00	34.50	0.00
135.840	24.00	16.11	136.98	24.00	16.63		0.00	20.00	34.50	0.00	34.50	0.00
138.111	24.00	17.15	139.25	24.00	17.69		0.00	20.00	34.50	0.00	34.50	0.00
140.382	24.00	18.25	141.52	24.00	18.82		0.00	20.00	34.50	0.00	34.50	0.00
142.654	24.00	19.40	143.79	24.00	20.00		0.00	20.00	34.50	0.00	34.50	0.00
144.944	24.00	20.63	146.10	24.00	21.27		0.00	20.00	0.00	0.00	0.00	0.00
147.255	24.00	21.92	148.41	24.00	22.60		0.00	20.00	0.00	0.00	0.00	0.00
149.565	24.00	23.29	150.72	24.00	24.00		0.00	20.00	0.00	0.00	0.00	0.00